Significance of small molecules in control of quiescence and resuscitation in *Synechocystis sp.* PCC 6803

Dissertation

der Mathematisch-Naturwissenschaftlichen Fakultät

der Eberhard Karls Universität Tübingen

zur Erlangung des Grades eines

Doktors der Naturwissenschaften

(Dr. rer. nat.)

vorgelegt von

Markus Burkhardt

aus Nürtingen

Tübingen

2023

Gedruckt mit Genehmigung der Mathematisch-Naturwissenschaftlichen Fakultät der Eberhard Karls Universität Tübingen.

Tag der mündlichen Qualifikation:	29.02.2024
Dekan:	Prof. Dr. Thilo Stehle
1. Berichterstatter/-in:	Prof. Dr. Karl Forchhammer
2. Berichterstatter/-in:	Dr. Evi Stegmann

Erklärung

Ich erkläre hiermit, dass ich die zur Promotion eingereichte Arbeit selbständig verfasst, nur die angegebenen Quellen und Hilfsmittel benutzt und Stellen, die wörtlich oder inhaltlich nach den Werken anderer Autoren entnommen sind, als solche gekennzeichnet habe. Eine detaillierte Abgrenzung meiner eigenen Leistungen von den Beiträgen meiner Kooperationspartner habe ich in „Declaration of author contribution“ vorgenommen.

Tübingen, den 07.11.2023 _____

Markus Burkhardt

Contents

Abbreviations

2-OG – 2-Oxoglutarate

3PG – Glycerate-3-phopshate

ADP – Adenosine Diphosphate

AMP – Adenosine Monophosphate

ARTO – Alternative Respiratory Terminal Oxidase

ATP – Adenosine Triphosphate

BCECF – 2′, 7′-bis-(2carboxyethyl)-5-(and-6)-carboxyfluorescein

cAMP – Cyclic Adenosine Monophosphate

CBB – Calvin-Benson-Bassham cycle

CCM – Carbon Concentrating Mechanism

Cda – Cyclic di-AMP Synthase

c-di-AMP – Cyclic di-Adenosine Monophosphate

COX – *aa3*-type Cytochrome c Oxidase

CP – Cyanophycin

Cyd – Cytochrome *bd*-type Oxidase

DacA – Diadenylate Cyclase A

DiBAC - Bis-(1,3-Dibutylbarbituric Acid)-Trimethine Axonol

DisA – DNA Integrity Scanning Protein A

ED – Entner-Duodoroff pathway

EMP – Embden-Meyerhoff-Parnas pathway

ETC – Electron Transport Chain

GDH – Glutamate Dehydrogenase

GlgB – Glycogen Branching Enzyme

GOGAT – Glutamate Synthase

GS – Glutamine Synthetase

K_d – Dissoziation constant

NAD^+/NADH – Nicotinamide Adenine Dinucleotide

$NADP^+$/NADPH – Nictoinamide Adenine Dinucleotide Phosphate

NhaS – Sodium Proton Antiporter

OPP – Oxidative Pentose Phosphate pathway

PBS – Phycobilisome

PCR – Polymerase Chain Reaction

PDE – Phosphodiesterase

PEP – Phosphoenolpyruvate

PGM – Phosphoglucomutase

PGAM – Phosphoglycerate Mutase

PHB – Polyhydroxybutyrate

ppGpp/pppGpp – Guanosine tetraphosphate/pentaphosphate

PQ/PQH_2 – Plastoquinone/ Plastoquinole

PS – Photosystem

RTO – Respiratory Terminal Oxidase

RuBisCO – Ribulose-1,5-bisphosphate Carboxylase/Oxygenase

SbtB – Sodium Bicarbonate Transporter B

SDH – Succinate Dehydrogenase

Synechocystis – *Synechocystis sp.* PCC 6803

TCA – Tricarboxylic acid cycle

WT – Wildtype

I. Zusammenfassung

Bakterielle Dormanz ist einer der am weitesten verbreiteten Überlebensmechanismen. Sie reicht von einer kurzen Phase, wie dem Nachtschlaf, bis hin zu einer langfristigen Phase, wie der Sporenbildung. Parallel zum streng regulierten Eintritt in die Dormanz ist ein ebenso regulierter Wiedererweckungsprozess, wie die Keimung, erforderlich. Cyanobakterien, eines der ursprünglichsten und am weitesten verbreiteten bakteriellen Phyla, nutzen Dormanz ebenfalls, um unterschiedliche Stresssituationen zu überstehen. Ein Mitglied dieses Phylum, *Synechocystis sp.* PCC 6803, ist nicht in der Lage, Stickstoff zu fixieren und reagiert auf den Mangel an kombinierten Stickstoffquellen mit metabolischer Ruhe. Dieser gut strukturierte Prozess führt zum Abbau von Phycobilisomen und Thylakoidmembranen, zur Ansammlung von Glykogen, zur Proteinsynthese als Vorbereitung auf das Erwachen und zur Verringerung der Energie, sodass die Zellen längere Hungerperioden überleben können. Um in Gegenwart von kombiniertem Stickstoff wieder zu erwachen, wird Glykogen abgebaut, um den Zellstoffwechsel wieder aufzubauen. In dieser Arbeit untersuchten wir die Bedeutung von Natrium und c-di-AMP bei der Regulierung des Eintritts in und des Austritts aus dem Ruhezustand.

Vegetative Zellen erzeugen ihre Energie mithilfe eines durch Photosynthese erzeugten, elektrochemischen H^+-Gradienten an den Thylakoidmembranen. Ruhende Zellen verfügen nur über eine reduzierte Menge an Thylakoidmembranen, was die Fähigkeit zur Energiegewinnung verringert. In dieser Arbeit beschreiben wir den elektrochemischen Na^+-Gradienten an der Cytoplasmamembran, der die Energiesynthese sicherstellt. Während der Wiederbelebung wird Natrium dann für die pH-Kontrolle und die Abschwächung von osmotischem Stress benötigt.

Der Sekundärbotenstoff c-di-AMP beeinflusst in Cyanobakterien die Nachtruhe und die Reaktion auf osmotischen Stress. Diese Studie ergab, dass der Einfluss von c-di-AMP auf die Glykogensynthese ein entscheidender Faktor für das nächtliche Überleben ist. Darüber hinaus ist c-di-AMP auch für die durch Stickstoffmangel induzierte Dormanz wichtig. Die beobachteten Auswirkungen sind global und beeinflussen erneut die Glykogenakkumulation, wenn auch über einen anderen Mechanismus als für die Nachtruhe. Die zugrundeliegenden Mechanismen und Anforderungen an c-di-AMP für die metabolische Dormanz sind Gegenstand weiterer Forschung.

II. Summary

Bacterial dormancy is one of the most widespread survival mechanisms, ranging from short, like nocturnal sleep, to long term, like spores. Concomitant to a tightly regulated entry into dormancy, a just as regulated resuscitation process, like germination, is necessary. Dormancy is a ubiquitous response also present in the ubiquitous phylum of cyanobacteria. One member thereof, *Synechocystis sp.* PCC 6803, is unable to fix nitrogen and responds to deprivation of combined nitrogen sources with metabolic quiescence. This well-structured process leads to a degradation of phycobilisomes and thylakoid membranes, accumulation of glycogen, protein synthesis in preparation for recovery and reduction of energy, enabling cells to survive prolonged periods of starvation. To resuscitate in presence of combined nitrogen, glycogen is degraded to fuel re-establishment of the cell metabolism. In this work, we studied the significance of sodium and c-di-AMP in regulation of entry into and exit out of metabolic dormancy.

Vegetative cells produce their energy through a photosynthesis-based, electrochemical H^+ gradient at the thylakoid membranes. Dormant cells only keep reduced amounts of thylakoid membranes, reducing the capability of energy production. In this study, we describe the electrochemical Na^+ gradient established on the cytoplasmic membrane, which secures energy synthesis. During resuscitation, sodium is then required for pH control and mitigation of osmotic stress.

The second messenger c-di-AMP has been previously reported to influence night-time survival and osmotic stress response in cyanobacteria. This study revealed the influence of c-di-AMP on glycogen synthesis to be the pivotal factor in night-time survival. Furthermore, c-di-AMP is also essential for nitrogen starvation induced dormancy. The observed effects are global, once more influencing the accumulation of glycogen, though through a different mechanism than in diurnal rhythm. the underlying mechanisms and requirements for c-di-AMP in dormancy are subject of ongoing research.

III. Publications

Accepted Publications:

Publication 1: Research Article

> **Doello, S**, Burkhardt, M, Forchhammer, K (2021). The essential role of sodium bioenergetics and ATP homeostasis in the developmental transitions of a cyanobacterium. *Curr. Biol.* 31, 1-10

Publication 2: Research Article

> **Selim, K, Haffner, M,** Burkhardt, M, Mantovani, O, Neumann, N, Albrecht, R, Seifert, R, Krüger, L, Stülke, J, Hartmann, M, Hagemann, M, Forchhammer, K (2021). Diurnal metabolic control in cyanobacteria requires perception of second messenger signaling molecule c-di-AMP by the carbon control protein SbtB. *Sci. Adv.* 7, eabk0568

Publication 3: Research Article

> **Burkhardt, M**, Rapp, J, Menzel, C, Link, H, Forchhammer, K (2023). The Global Influence of Sodium on Cyanobacteria in Resuscitation from Nitrogen Starvation. *Biology* **2023**, 12, 159

Manuscripts in preparation:

Publication 4: Research Article

> **Burkhardt, M**, Haffner, M, D, L, Menzel, C, Mantovani, O, Hagemann, M, Forchhammer, K. Working Title: The significance of c-di-AMP in metabolic dormancy.

Personal contributions:

Publication 1: “The essential role of sodium bioenergetics and ATP homeostasis in the developmental transitions of a cyanobacterium”

I performed the physiological measurements of the optical density of the cultures, the glycogen determination and the oxygen evolution.

Publication 2: “Diurnal metabolic control in cyanobacteria requires perception of second messenger singaling molecule c-di-AMP by the carbon control protein SbtB”

I constructed the Δ*dacA* mutant strain and measured the c-di-AMP concentrations in all conditions in cooperation with Roland Seifert.

Publication 3: “The Global Influence of Sodium on Cyanobacteria in Resuscitation from Nitrogen Starvation”

I designed and performed all experiments except for the transmission electron microscopy and the metabolite measurement. I prepared all figures and wrote the manuscript under the supervision of Prof. Karl Forchhammer.

Publication 4: “Working Title: The significance of c-di-AMP in metabolic dormancy.”

I designed and performed all experiments except for the transmission electron microscopy and the metabolite measurement. I prepared all figures and wrote the manuscript under the supervision of Prof. Karl Forchhammer.

IV. Introduction

1. Cyanobacteria

Cyanobacteria are one of the most primordial groups of bacteria known today [1]. They are gram negative and evolved oxygenic photosynthesis, giving them a unique niche in the primordial biosphere and giving rise to the great oxidation event [2,3]. This highlights the role of cyanobacteria in the foundation of modern life. Photosynthesis enabled cyanobacteria to settle all over the planet, from the phototrophic layer of the ocean to arctic and arid deserts [4–6]. The ability to inhabit almost all illuminated habitats gave rise to the radiation of cyanobacteria, resulting in unprecedented morphological diversity of cyanobacteria. Based on their appearance, they have been classified into five sections [7]. Sections I and II are unicellular, with members of section I dividing by binary fission, like *Synechocystis sp.* PCC 6803 or *Synechococcus elongatus* PCC 7942, while members of section II, like *Pleurocapsa sp.*, perform reductive division in baeocytes [8], large gelatinous membranes which bloat with cells until they rupture. Section III to V are filamentous [7], with section III lacking and section IV and V having developed cell differentiation [9], making members of section IV and V multicellular organisms. Typical specialised cells are heterocysts, to fix nitrogen from the surrounding air [7,10], akinetes, spore-like cells to endure environmental stress [7,10,11], and hormogonia, short motile filaments to spread and colonise new areas [7,10]. Section IV, like *Anabaena variabilis* ATCC 29413, grow in one plane, while members of Section V, like *Nostoc punctiforme*, can branch out and grow in multiple planes [7]. A major distinction to be made is whether the culture is diazotrophic (gr. di = two, azo = nitrogen, troph = pertaining to food or nourishment) or not. Diazotrophs synthesise the enzyme nitrogenase to fix nitrogen from the surrounding air [12], but the enzyme is oxygen-sensitive and requires special protection, especially in photosynthetic organisms. Unicellular and some filamentous cyanobacteria protect the nitrogenase by temporal separation of nitrogen fixation and photosynthetic activity [13], evolving oxygen in the day and fixing nitrogen in the night. Filamentous diazotrophic cyanobacteria of sections IV and V perform spatial separation, fixing nitrogen using heterocysts and performing oxygenic photosynthesis in vegetative cells [14]. Non-diazotrophs, on the other hand, are dependent on fixed nitrogen sources like nitrate, ammonium and urea [15].

1.1. *Synechocystis* sp. PCC 6803

Synechocystis sp. PCC 6803 (hereafter *Synechocystis*) is a section I cyanobacterium. It has been isolated in 1968 from a freshwater lake in Berkeley, CA, USA [16]. It gained a status as model organism because it was the first completely sequenced phototrophic organism and it is naturally competent, being able to import exogenous DNA [17]. This enabled the development of different mutagenic tools, yielding *Synechocystis* mutant strains with relative ease. Many cyanobacterial species are obligate phototrophs, but *Synechocystis* is able to survive mixotrophically [18]. Though it was found in a freshwater lake, it is also able to survive in brackish water [19], indicating the ability to survive in a rapidly changing saline environment. *Synechocystis* is a non-diazotrophic strain, dependent on fixed nitrogen sources. Nitrogen is a macronutrient in high demand, thus, *Synechocystis* developed an adaptation process to nitrogen starvation by turning metabolically quiescent [15,20,21]. These properties of *Synechocystis* made it a promising target to investigate photosynthesis, CO_2 fixation, bacterial dormancy and persistence. It is also of interest to biotechnology, due to its ease in genetic engineering and because *Synechocystis* produces different types of carbon polymers from CO_2, namely glycogen [20,22] polyhydroxybutyrate (PHB) [23]. The different aspects of metabolism and stress responses of *Synechocystis* will be explained in more detail in the following chapters.

1.2. 1.2 Carbon Metabolism of *Synechocystis*

Synechocystis is able to assimilate most of the required carbon in the form of CO_2 or bicarbonate (HCO_3^-) [24]. Using the energy and reduction equivalents produced in the photosynthetic light-reaction, these carbon sources are fixed by the following dark reaction. Excess fixed carbohydrates can be stored in different polymers, as mentioned above.

1.3. Carbon assimilation

Carbon fixation is a major part of phototrophic life, as the so-called dark reaction of photosynthesis is solely committed to it. The reactions thereof are mostly found in the Calvin-Benson-Basham (CBB) cycle. The key member of the CBB is the enzyme ribulose-1,5-bisphosphate carboxylase/oxygenase (RuBisCO) which carboxylates ribulose-1,5-phosphate to glycerate-3-phosphate (3PG) or, in the presence of O_2, forms the toxic glycolate-2-phosphate (G2P) [25]. 3PG can be immediately incorporated into the cell metabolism while G2P needs to be converted first through photorespiration [26]. Thus, the carboxylase reaction is preferable for cells and to

ensure it consistently, cyanobacteria evolved the carbon concentrating mechanism (CCM) [27,28]. Carbon import can happen through diffusion in the case of CO_2 or through active import. *Synechocystis* contains several inorganic carbon (Ci) uptake systems. The bulk of HCO_3^- import is done by SbtA and BicA, Na^+/HCO_3^- symporters [24,29,30], while the high affinity BCT1 system is only expressed under carbon limitation [31]. Inside the cell, CO_2 is converted to HCO_3^- by the thylakoid membrane bound NDH-1 complex and then enters the carboxysome, a special microcompartment encapsulating the RuBisCo [28]. There, carbonic anhydrases convert it to CO_2 which will then be used by the RuBisCO in its carboxylase reaction to produce 3PG [25]. 3PG is then exported into the cytoplasm. There the majority of 3PG is used to regenerate ribulose-1,3-bisphosphate while small amounts can be either processed by phosphoglycerate mutase (PGAM) to reach the Krebs cycle or be used in gluconeogenesis and further, to produce the carbon storage polymer glycogen [32].

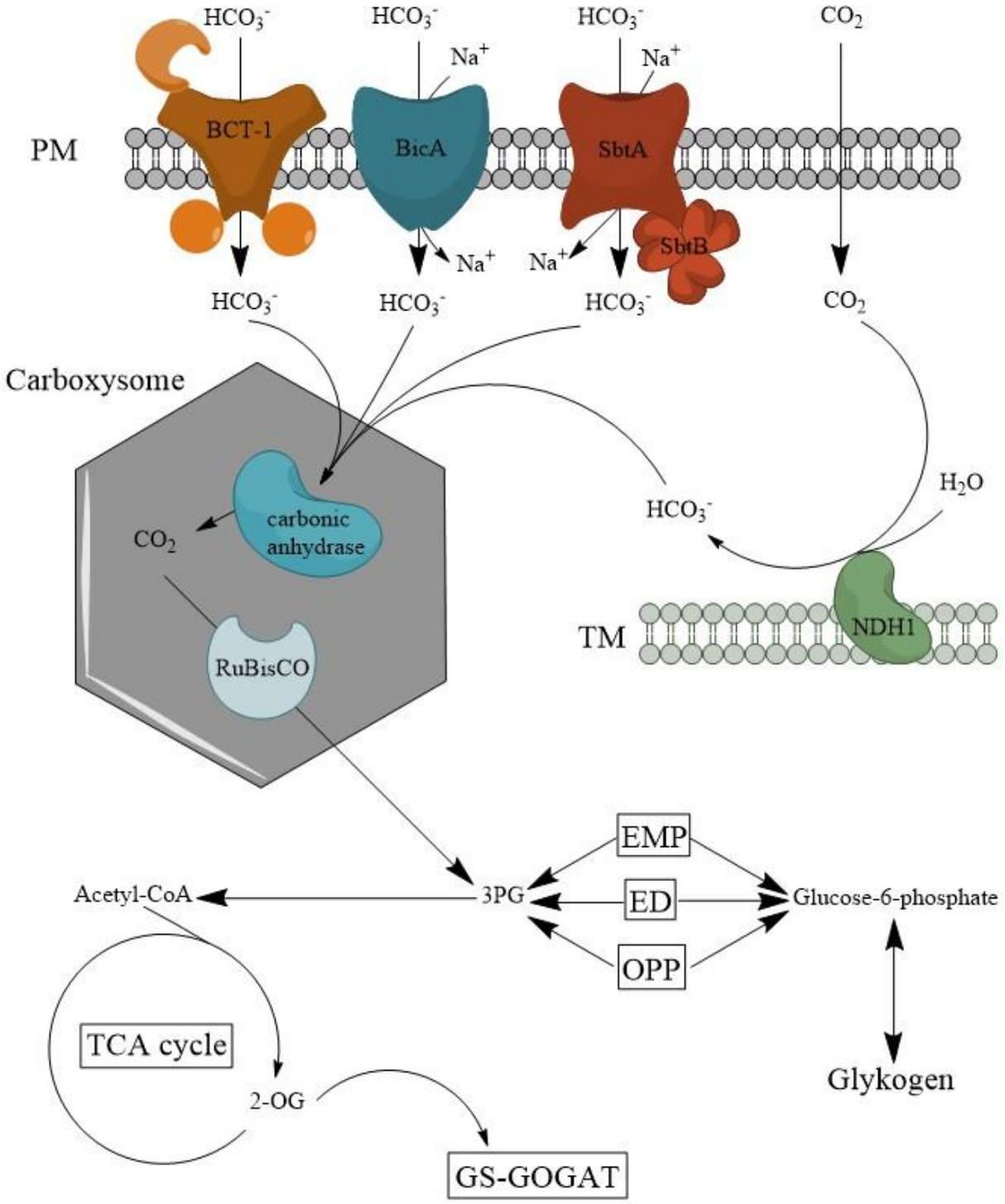

Figure 1: schematic overview of carbon fixation in *Synechocystis*.

1.4. Carbon sensing signal transduction Protein SbtB

Genetically co-localised to *sbtA* is the *slr1513* gene in the same transcriptional unit. Due to the proximity to *sbtA*, the encoded protein was termed SbtB. Structural analysis identified it as a PII-like protein, similar in structure and also forming homo-trimers, and biochemical studies revealed interaction with adenosine monophosphate (AMP), adenosine diphosphate (ADP), adenosine triphosphate (ATP) and cyclic AMP (cAMP).

The binding of cAMP allows SbtB to sense the carbon levels and regulate SbtA activity accordingly [33].

1.5. Carbon Storage

In excess of carbon, *Synechocystis* will diverge fructose-6-phosphate from the CBB for gluconeogenesis, transform it to glucose-1-phosphate using the phosphoglucomutase PGM [34] and synthesises glycogen thereof [32]. The first step is the reaction of glucose-1-phosphate and ATP to pyrophosphate and ADP-Glucose catalysed by the glucose-1-phosphate adenylyltransferase GlgC [35]. These are then chained together by the glycogen synthase isoforms GlgA1 and GlgA2, forming long α (1-4) glucan chains. These are subsequently branched by the glycogen branching enzyme GlgB. GlgB will cleave a growing α (1-4) glucan chain and attach it at the 1-6 position via an α bond. The new branch can then be built upon by GlgA1/2 [36].

When glycogen is degraded, it starts with the activity of the glycogen phosphorylases GlgP1 and GlgP2 cleaving off glucose-1-phosphate molecules until only 3 – 6 remain in the glucan chain. Then, the glycogen debranching enzymes, GlgX1/2 cut the branch of at the α (1-6) glycosidic bond and transform the remaining small chain into several molecules of glucose-1-phosphate. Glucose-1-phosphate will then be transformed to glucose-6-phosphate by the PGM and thus made available for the different degradation pathways found in *Synechocystis* [22].

1.6. Carbon Catabolism

The degradation of glucose is generally regarded to start with glucose-6-phosphate. When glucose is imported from the environment, it is phosphorylated to remove it from the concentration gradient and the three glycolytic pathways of *Synechocystis* start with glucose-6-phosphate [32]. All three produce energy and reduction equivalents and combine at glyceraldehyde-3-phosphate into the uniform, lower glycolysis. The Embden-Meyerhoff-Parnas (EMP) pathway produces the most ATP of the three pathways and recovers $NADH^{+}+H^{+}$, but does not provide pentose sugars, central carbon structures in cellular metabolism.

The Entner-Duodoroff (ED) pathway, produces lesser energy levels, but requires less proteins and is independent of the CBB cycle, which shares enzymes with the EMP and the oxidative pentose phosphate (OPP) pathway. The OPP produces ribulose-5-phosphate, a precursor to ribulose-1,5-bisphosphate, which is required for CO_2 fixation. Additionally, the OPP generates NADPH and pentose sugars, required for

DNA synthesis [32]. All three pathways congregate at glyceraldehyde-3-phosphate, finishing the upper glycolysis involving 6-carbon sugars, and transitioning to the lower glycolysis, involving 3-carbon sugars.

Lower glycolysis will generate further ATP and reduction equivalents, as well as, phosphoenolpyruvate (PEP) and acetyl-CoA, which then can be fed into the tricarboxylic acid cycle (TCA), also known as Krebs cycle, via the PEP carboxylase PepC or the citrate synthase GltA. The TCA cycle then yields reduction equivalents and precursors for amino acid synthesis and the carbon status sensor metabolite 2-oxoglutarate (2-OG) [32].

2. Energy metabolism of *Synechocystis*

ATP is the universal energy carrier. *Synechocystis* is a facultative mixotroph, being able to grow mostly photoautotrophically but also able to import and use sugars from the environment. Due to the absence of photosynthesis in the dark, cyanobacteria depend on respiration when deprived of light. The adaption to the daily night-time survival caused them to generate the first diurnal rhythm of nature. Interestingly, in most cyanobacteria, the proteins used in the electron transport chain of photosynthesis can also be used for respiration [38].

2.1. Oxygenic photosynthesis

Oxygenic photosynthesis evolved in cyanobacteria and later gave rise to the entire plant kingdom, according to the endosymbiotic theory [39]. It can be divided into the light, oxygen evolving reaction and the dark, CO_2 fixing reaction, which was described above. The light reaction begins by harvesting of light energy in the phycobilisomes (PBS). PBS are membrane attached protein complexes with a hemidiscoidal, tricylindrical core of allophycocyanin and six peripheral rods of allophycocyanin, phycocyanin, phycoerythrin or phycoerythrocyanin [40]. The energy is then transferred to P680 in the reaction centre of photosystem 2 (PSII), exciting an electron to a higher energy level [41]. The excited electron will be transferred to plastoquinone (PQ), reducing it to plastosemiquinone and with a second electron to plastoquinole (PQH_2) [42]. To return to the reduced state, the oxidised P680 then oxidises a nearby tyrosine, which consequently takes an electron from the manganese cluster of the oxygen evolving complex. This complex will regain its electrons, after 4 cylces, by splitting 2 water molecules into di-oxygen gas (O2) and 4 protons (H^+). Meanwhile, 2 PQH_2 transfer 4 electrons into the cytochrome-b_6f complex. The Q cycle, a number of redox

reactions, pumps 4 protons into the thylakoid lumen, 2 electrons are allocated to plastocyanin or the cytochrome c_6 and one PQH_2 is restored [43]. In most cyanobacteria, including *Synechocystis*, plastocyanin is the main redox carrier, which will then reduce an oxidised photosystem I (PSI). Cytochrome c_6 is only expressed in a low copper environment. The transferred electron will substitute one in the P700 of PSI and will be transferred to ferredoxin via an iron-sulfur cluster. Lastly, the electron will be transferred from ferredoxin to $NADP^+$ by the ferredoxin-$NADP^+$ reductase. In total, two electrons are required to generate NADPH, a major reduction equivalent in *Synechocystis* with a large role in carbon fixation [41–43]. Overall, through the electron transport chain in oxygenic photosynthesis, one water molecule is split, one molecule of NADPH produced, and 6 protons are translocated, which can then be used for ATP synthesis.

Synechocystis is also able to perform cyclic electron flow around the PSI. One of the NADPH dehydrogenase complexes, NDH-1 or NDH-2, accepts electrons from the reduced ferredoxin, channelling them into the PQ pool, generating new PQH_2. These will then transfer available electrons to the PSI, completing a cyclic electron flow [44,45].

2.2. Respiration

Cyanobacterial respiration shares several structures with the photosynthetic electron transport chain, namely the PQ pool, the cytochrome b_6f complex, and plastocyanin/cytochrome c_6, as respiration also occurs in large parts in the thylakoid membrane [38]. There are respiratory electron transport chains (ETC) also found in the plasma membrane though, as the energy and gradients can be used for the activity of nutrient uptake systems and ion pumps [46]. It was long thought that the electrons are derived from the reduction of NADPH or oxidation of ferredoxin by NDH-1 and NDH-2 or by the oxidation of succinate to fumarate by the succinate dehydrogenase (SDH) [47]. However, recent research into NDH-1 revealed not only 4 different variants, their respective significance [48], but also how NDH-1 takes relevance in photosynthetic and cyclic electron transfer while an NDH-like complex containing a NADH DH-domain supplying electrons to respiration [45].

The electrons are then transferred to the PQ pool and further to cytochrome b_6f. Instead of PSI, the electron reaches a respiratory terminal oxidase (RTO). They facilitate ATP synthesis through proton pumping by reducing oxygen to water coupled

with electron transfer [46]. *Synechocystis* has three different types of RTOs: an *aa3*-type cytochrome x oxidase (COX), a cytochrome *bd*-type oxidase (Cyd) and an alternative RTO (ARTO), also belonging to the heme-copper oxidase superfamily [49]. The function of ARTO and Cyd is unclear to date. The respiratory chain can work in parallel, as the initialising electron can be obtained from NDH-1, NDH-2 or SDH and Cyd and ARTO can receive electrons directly from the PQ pool, while COX is dependent on the cytochrome c_6 complex. Thus, COX is mostly found in the thylakoid membrane. How no futile cycles occur due to these parallel reactions or the use of those cycles are also unknown. In *Synechocystis*, three NDH2 are known, NdbA, NdbB and NdbC [50], though their significance is still cryptic.

2.3. ATP synthesis

ATP is the universal energy carrier. It is commonly synthesised by F_0F_1-ATP synthases using an electrochemical proton gradient or, less often described, a sodium gradient [51,52]. The energy of this gradient is used to form ATP from adenosine diphosphate (ADP) and inorganic phosphate. The F_0 complex is a membrane bound channel whereas the F_1 complex is a soluble protein where the ATP synthesis occurs [53]. Concomitantly to the proton gradient producing ETCs, ATP synthases in *Synechocystis* are mostly found in the thylakoid membranes, but also in the plasma membrane [54].

The specificity for protons or sodium ions is determined by the c-ring of the F_0 complex. Within the c-ring, the cations are bound by the negative residue of glutamate and the surrounding amino acids determine the specificity. Proton specific c-rings surround the glutamate residues with hydrophobic amino acid residues, while sodium specificity comes with polar groups [51,52,55,56]. Since protons are highly reactive and sodium is the most abundant cation in the environment, this selectivity is significant to prevent salt stress. Though proton ATP synthases are found ubiquitously in modern organisms, the sodium dependent ATP synthases appear to be the evolutionary predecessor, as ancestrous membranes were proton permeable but tight enough for a sodium gradient [57].

3. Nitrogen metabolism of *Synechocystis*

3.1. Nitrogen acquisition

Synechocystis is a non-diazotrophic strain, dependent on combined nitrogen sources. Thus, it has transport systems for ammonium, nitrate, nitrite, urea and different amino acids [32]. In laboratory conditions, cells are typically supplied with ammonium or

nitrate. Ammonium can be imported by three different transporters: Amt 1, Amt 2, and Amt 3 [32,58]. It was recently discovered for the ammonium transporter AmtB of *Escherichia coli* that ammonium is co-transported as ammonia and a proton [59]. It is so far unknown though, whether ammonium is reconstituted after import. When fed with nitrate, cells import it via the NrtABCD uptake system. Nitrate is imported and reduced to nitrite and water by oxidising 2 ferredoxins via the nitrate reductase NarB. Nitrite is then reduced to ammonium by the nitrite reductase NirA using 6 reduced ferredoxins. Urea will be imported by the UrtABCDE uptake system and converted to ammonium by the UreABCDEFG system. Ammonium or ammonia is then integrated into the cell metabolism via the glutamine-synthetase-glutamate-synthase (GS-GOGAT) cycle. The GS reaction aminates glutamate to glutamine while consuming ATP. The GOGAT reaction then transfers the amine residue of glutamine to 2-OG yielding 2 glutamate molecules. Deriving from the carbon metabolism and being a key substrate of the nitrogen metabolism, 2-OG is the key sensor of the C/N homeostasis. The glutamate dehydrogenase (GDH) can directly incorporate ammonium into 2-OG, circumventing the GS reaction, if necessary [60]. If cells have an excess of nitrogen, they can store it in the form of cyanophycin (CP). CP consists of a poly-L-aspartate backbone with arginine sidechains. It is synthesised by the CP synthase CphA, a large, non-ribosomal peptide synthase [61].

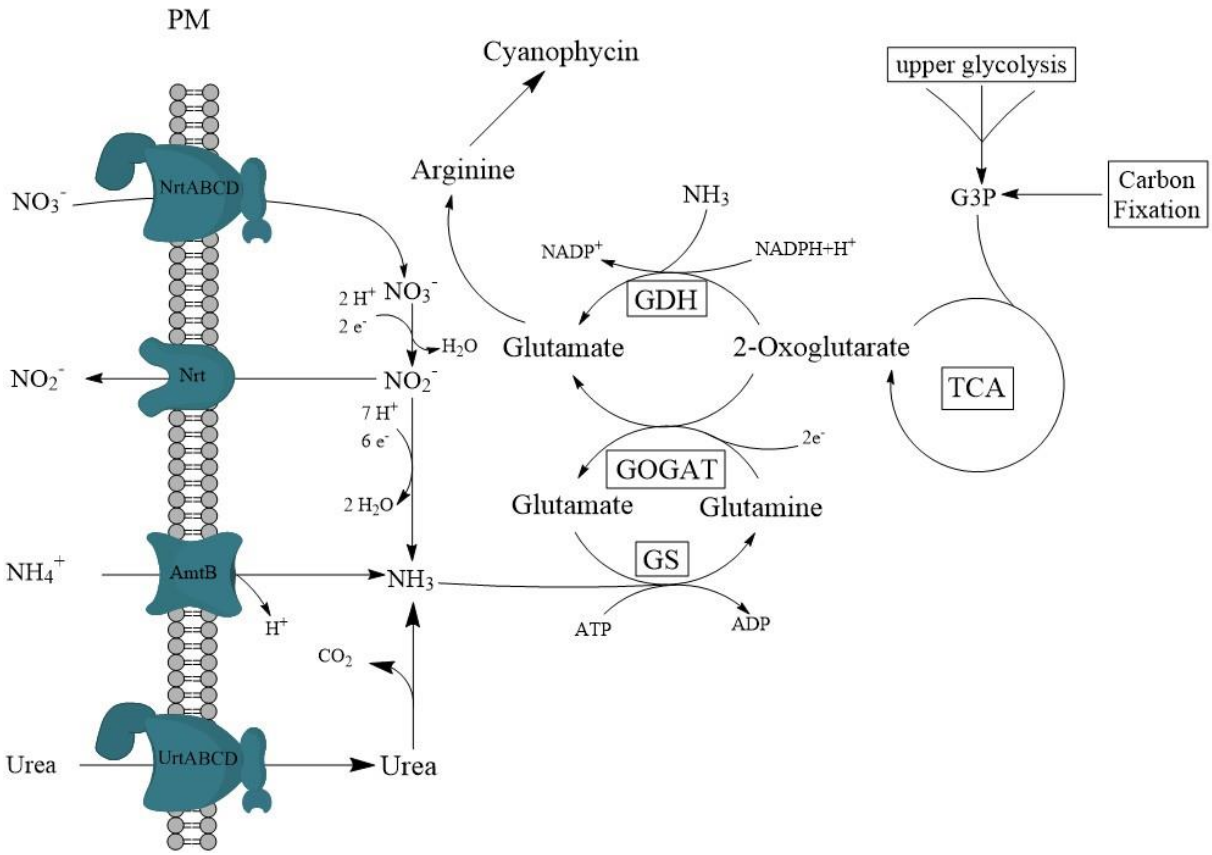

Figure 2: schematic overview of nitrogen assimilation in *Synechocystis*.

3.2. Nitrogen Starvation induced Chlorosis

Nitrogen is one of the most limiting macronutrients in the environment, thus *Synechocystis* requires mechanisms to survive nitrogen starvation. The acclimation to nitrogen starvation is a pre-determined, highly structured program. The immediate consequence of nitrogen starvation is an increase in 2-OG. This then activates transcription dependent on the global nitrogen regulatory protein NtcA, initiating the first phase of chlorosis. The immediate arrest of anabolic pathways requiring nitrogen causes intracellular accumulation of ATP and reduction equivalents. To prevent damage, the photosynthetic apparatus is degraded. This starts with the NtcA dependent increased expression of *nblA*, encoding the PBS degradation protein NblA. The PBS will then be detached from the thylakoid membranes and degraded, reducing photostress and providing resources [62–64]. This degradation leads to a colour change from blue-green to orange-yellow, terming the process chlorosis [64–66].

The accumulation of 2-OG also causes the P_{II}-interacting regulator of carbon metabolism PirC to bind and inhibit the phosphoglycerate mutase PGAM. PGAM catalyses the conversion of 3PG to 2-phosphoglycerate. The 3PG kinase can

otherwise convert 3PG to 1,3-bisphosphoglycerate and begin gluconeogenesis. The binding of PirC to PGAM shifts the carbon flux away from lower glycolysis and towards glycogen synthesis, causing a large accumulation of glycogen [67], peaking at about 60 % of cell dry weight [68]. Glycogen synthesis is essential for survival in chlorosis, due to respiration of the storage providing carbon skeleton and energy for resuscitation and the polymer reducing osmotic stress [22,68].

While the initial steps of chlorosis occur, cells will divide one last time and synthesize the proteins required for resuscitation [15,64,65].

In the second phase of chlorosis, cells reduce their metabolic activity and further degrade the photosynthetic machinery, until only a residual amount of photosynthetic activity remains [15,21]. At that stage, cells have entered the third phase and remain therein, until a new source of fixed nitrogen becomes available. No major metabolic activity is occurring anymore, except for PHB synthesis, but the physiological role of PHB is unknown to date [23].

3.3. Resuscitation from Nitrogen Starvation Chlorosis

Recovery from chlorosis is a multi-levelled process that is as controlled and organised as the entry therein is. When chlorotic cells of *Synechocystis* encounter a fresh source of combined nitrogen, the immediate responses are uptake of this nitrogen compound and an increase in ATP. The levels of ATP almost double in the first 20 minutes after encountering a nitrogen source [22]. It was unclear how this happens. According to one assumption, the remaining thylakoid membranes could become more active with a nitrogen source in the environment, though this would hinder resuscitation in the dark. The first steps of resuscitation are a heterotrophic-like process, depending on the catabolism of glycogen. All remaining photosynthetic activity is stopped, and the residual thylakoid membranes degraded [15,20]. The main energy supply at this point and the carbon skeleton to rebuild the cell metabolism are derived from the respiration of glycogen [22]. In vegetative growth, glycogen degradation is inhibited in the light (Kok effect), but in resuscitation, no such limitation exists. The proteins required for glycogen degradation are synthesised at the start of chlorosis and kept stable, but mostly inactive, until the time resuscitation begins. Then, the glycogen is degraded through the ED and OPP pathway, yielding less ATP than through the EMP pathway, but producing carbon structures essential in rebuilding the cellular metabolism. During this early phase of resuscitation, genes encoding central anabolic proteins, such as

the ribosomes or proteins of nitrogen assimilation, show an increased expression [68]. The photosynthetic activity first vanishes before the expression of the proteins of the photosynthetic machinery proteins increases [20,69]. Thus, for the first day of resuscitation, only respiration occurs [20,22].

After the re-establishment of the central cellular synthesis processes, the metabolically and energetically expensive task of rebuilding the photosynthetic machinery can begin. Expression of the respective genes increases between 12 and 24 hours after start of resuscitation and during this time, photosynthetic parameters, like the amount of chlorophyll, the quantum yield of PSII and an increasing oxygen evolution, are observable [68]. The glycogen storages are still degrading at this stage, rendering the cells in a mixotrophic metabolic state [20,22]. After 48 hours of resuscitation, most cells will have reconstituted their thylakoid membranes and associated proteins and degraded their glycogen storages. At this point in time, they re-enter vegetative growth by a first binary, reductive cell division [20].

4. Bacterial Stress Response and Second Messengers

Nitrogen starvation is a frequent, but not the only environmental stress bacteria must be able to face. Most bacteria are heterotrophs and can frequently face starvation conditions because of the competition for carbohydrates. Desiccation is also an ever-present threat for unicellular organisms outside of water and osmotic homeostasis and stress mitigation is a Sisyphean task. The bacterial responses towards these stress conditions hinges on the efficient signal transmission for which so called second messengers are employed.

4.1. Second messengers

Second messengers are small molecules and ions that transmit environmental and intracellular signals, the so called “first message”, to receptor and effector proteins to tune cellular responses [70]. The receptor receives the signal, altering the receptors confirmation and thus increases the production or acquisition of second messengers. These will then diffuse to the target proteins and adapt their activity to the cellular requirement. The homeostasis of second messengers is tightly controlled, as dysregulation can obstruct the stress response or even lead to cell death. Most bacterial second messengers have been studied in pathogenic bacteria and so their role in cyanobacteria was mostly unknown to date.

Second messengers are separated into 4 different groups: gases and free radicals, which can signal intracellularly and to neighbouring cells, lipid messengers that signal within membranes, and ions and cyclic nucleotides, which both transmit signals intracellularly [70].

Ions regarded as second messengers in bacteria are mostly magnesium and calcium, with the latter being the more researched. It was found that Ca^{2+} signalling modulates motility [71,72], oxygen stress response [72,73], and cell division [72,74]. In cyanobacteria, Ca^{2+} ions have been found to influence the response to low nitrogen in filamentous [75,76] and unicellular [77] strains. In filamentous strains, Ca^{2+} not only influences the cell differentiation for heterocysts, but also for hormogonia [78], thus influencing motility as in heterotrophic bacteria.

Another second messenger strongly associated with nutrient deficiency and starvation is the alarmone guanosin-tetraphosphate ((p)ppGpp). It is involved in the stringent response, a well-studied bacterial stress response to amino acid starvation. Guanosin pentaphopshate is synthesised by pppGpp synthase RelA and converted to ppGpp by the pppGpp phosphohydrolase. Increasing levels of ppGpp will then inhibit protein synthesis and DNA replication, arresting cell growth [79]. In cyanobacteria (p)ppGpp has also been shown to influence the starvation response. Its predominant role is in regulation of the response to changing light conditions in most cyanobacteria [80–82], while also, for example, influencing the response to differing nitrogen supply in filamentous cyanobacteria [83–85].

The most studied class of second messengers in prokaryotes are cyclic nucleotides. They are synthesised by nucleotide cyclases and degraded by phosphodiesterases (PDE) [70]. The most investigated second messenger is 3’, 5’-cyclic adenosine monophosphate (cAMP). Cell metabolism is regulated by cAMP largely through the cAMP receptor protein, which is a transcription regulator influencing carbon utilisation genes to achieve catabolite repression [86] in different heterotrophic bacteria. The role of cAMP in cyanobacteria pertains to light-respondent motility [87], nutrient deficiency [88] and rehydration after desiccation [89].

A to date comparably poorly studied sub-group of cyclic nucleotides are the cyclic di-nucleotides. They are synthesised by di-nucleotide cyclases and degraded by PDEs. The major known types of cyclic di-nucleotides are 3’, 5’ cyclic di-guanosine 5’-

monophosphate, 3', 5' cyclic di-adenosine 5'-monophosphate (c-di-AMP) and 2', 5' cyclic guanosine adenosine monophosphate.

4.2. C-di-AMP

In this work, we focused on the second messenger c-di-AMP. It has been discovered in 2008 in *Bacillus subtilis* as part of the DNA integrity scanning protein A (DisA) taking part in the sporulation process [90]. It has since been an interesting target for investigation, as c-di-AMP is essential in organisms synthesising it and genes encoding c-di-AMP synthesising proteins have been found in a wide range of bacteria and archea, though not in the model organism *Escherichia coli* and neither in eukaryotes [91,92]. Synthesis is catalysed by diadenylate cyclases from 2 ATP, yielding c-di-AMP and 2 pyrophosphates [93,94], and 2 structurally different types of cyclases are known so far: Cda and Dis [90,95]. The degradation to 5'-phosphadenylyl adenosine is catalysed by PDEs. So far, the significance of c-di-AMP has been mostly studied in firmicutes and a large influence of c-di-AMP on ion and osmolyte homeostasis has been discovered [96]. Osmotic stress increases the intracellular c-di-AMP production and higher levels of c-di-AMP will then inhibit the synthesis or activity of K^+ ions importing proteins and increase the export of K^+ [97,98]. At the same time, high concentrations of c-di-AMP will also block the import of osmolytes [96,99]. A PII-like signal transduction protein DarA has also been found to bind c-di-AMP and is assumed to influence the nitrogen metabolism of *L.monocytogenes* [100]. All these data suggest c-di-AMP in a central and global regulatory position.

4.3. c-di-AMP in cyanobacteria

First investigations on the role of c-di-AMP in cyanobacteria yielded interesting results. In *Synechococcus elongatus* PCC 7942, a mutant unable to produce c-di-AMP has shown a severe growth disadvantage in a diurnal rhythm [101]. This mutant produced more than twice as much reactive oxygen species than the WT during the switch from light to dark. Concomitantly, the levels of c-di-AMP start to rise towards dusk in the WT with a significant increase immediately after loss of light.

Investigation of abiotic salt and osmo stress in different cyanobacteria yielded interesting results there as well [102]. While salt stress induced mainly an increase in c-di-GMP levels, though also in c-di-AMP levels, solely osmotic stress through the addition of sorbitol increased the levels of c-di-AMP. Additionally, in *Synehcocystis*, overexpression of the diadenylate cyclase DacA or the PDE Slr0104 yielded mutants sensitive to both salt and osmotic stress.

5. Aim of Research

Bacterial dormancy and persistence came increasingly into the focus of research. The appearance of antibiotic resistances associated with bacterial dormancy is a large medical issue. On the other hand, some quiescent states, like chlorosis in *Synechocystis*, can be used to synthesise products of interest, like PHB. Both entering and recovering from different types of metabolic quiescence have been intensively researched but are not understood completely to date.

Ions are well known to influence the activity of life, as they are omnipresent and used as co-factors in a multitude of different enzymatic reactions. The influence of many an ion has been investigated and documented, but these were focused on rarer ions, whose absence could occur, like Ca^{2+} or Mg^{2+}. In this work, we chose to focus on the ubiquitous cation Na^{+} and investigated, what its primary requirements in the cell metabolism of *Synechocystis* are and how it influences dormancy and resuscitation.

Second messengers are equally well studied, with some ions even being regarded as second messengers. These molecules can cause global responses to whatever stress condition they signal. Dormancy is such a global response and the role of c-di-AMP in this process is unknown. Since this molecule was found in *Bacillus subtilis* in the sporulation process, an active significance for chlorosis can be hypothesised. In this work, the groundwork for future research of c-di-AMP in cyanobacteria, especially regarding quiescence, was laid.

V. Results

1. Vegetative growth

As ubiquitously encountered photoautotrophic organisms, cyanobacteria must be able to survive drastically changing environmental conditions. Changing illumination, macronutrient starvation, changing osmotic and saline conditions, predators, and competitors, just to name a few. The model cyanobacterium *Synechocystis* developed different survival strategies, the knowledge and understanding of which we attempted to deepen in this work.

1.1. Significance of sodium for carbon assimilation

Sodium is the most abundant cation in the environment and ubiquitously present. It has been found to influence different physiological properties in bacteria, like pH control, osmotic stress or acting as a co-factor [103,104]. *Synechocystis* has 6 different sodium-proton antiporter systems, summarised in the NhaS family [105–107]. Additionally, there are two sodium dependent bicarbonate uptake systems, SbtA and BicA, present [24]. We found that cells of *Synechocystis* were unable to survive vegetative growth at ambient air in absence of sodium (Publication 1, figure 5, C). This was reversable by placing the cells in a 2 % CO_2 environment. This seemed to completely alleviate the phenotype, indicating high affinity bicarbonate uptake as the primary requirement for sodium during vegetative growth. An influence on ATP synthesis has been ruled out, as cells treated with the sodium ionophore monensin kept their ATP level constant (Publication 1, figure 5, A).

1.2. Significance of c-di-AMP in diurnal rhythm

The second messenger c-di-AMP has been reported to influence survival in a diurnal rhythm in *Synechococcus elongatus* PCC 7842 [101]. To investigate the significance of c-di-AMP in *Synechocystis*, we performed a pulldown with crude cell extract of *Synechocystis* using c-di-AMP as bait. Several different ion transporter systems were found, but the most abundant protein was the PII-like signal transduction protein SbtB (Publication 2, figure 1, B). This interaction was confirmed and characterised using isothermal titration calorimetry (Publication 2, figure 1, A). Similar to the negative cooperative binding of ATP to the subunits of the PII protein [108], the monomers of SbtB, which forms a trimer as well, bind c-di-AMP. The SbtB protein can bind c-di-AMP with a dissociation constant (K_d) of K_{d1} 2,3 µM for the first, K_{d2} 12,2 µM for the second

and K_{d3} 35,9 µM for the third binding site, comparable to the binding of cAMP to SbtB. The T-loop of SbtB changes conformation upon binding of c-di-AMP, which has been shown through crystallography studies (Publication 2, figure, 1, C to F).

To further investigate the physiological role of c-di-AMP in *Synechocystis*, we created a mutant strain, unable to produce c-di-AMP. This was achieved by inserting a kanamycin resistance cassette into the active center encoding sequence of the gene *dacA* (*sll0505*), which encodes the only diadenylate cyclase of *Synechocystis*. This was done to avoid downstream effects on the following gene (*sll0506*), encoding an undecaprenyl phosphate synthase. The promoter and start sequence of *sll0506* overlap with the 3'-region of *dacA*. To prove the activity of DacA as a diadenylate cyclase, a plasmid expressing a *dacA*-green fluorescent protein (GFP) fusion under control of the T7-promoter was transformed into *E.coli*, as it does not naturally synthesise c-di-AMP. Measurement of the intracellular concentrations of c-di-AMP in these cells after induction of DacA-GFP expression using isopropyl-β-D-thiogalactopyranoside (IPTG) revealed high levels of c-di-AMP, proving DacA activity (Publication 2, supplementary figure S3). Also, the Δ*dacA* mutant synthesised no measurable amount of c-di-AMP (Publication 2, figure 2, A).

To investigate the link between c-di-AMP and SbtB, the Δ*dacA* strain and a previously engineered Δ*sbtB* knockout strain [33] were compared under different physiological conditions. The group of Montgomery previously reported in *Synechocystis* a significance of c-di-AMP on osmotic stress response [109]. Accordingly, when presented with increasing levels of sorbitol, the Δ*dacA* strain grew increasingly slower until it completely arrested growth at 300 mM sorbitol. In comparison, the Δ*sbtB* strain was not affected (Publication 2, supplementary figure S4). Thus, the significance of c-di-AMP for osmotic stress is proven again and shown to be independent of its interaction with SbtB.

Since SbtB plays a large role in the carbon concentrating mechanism [33], the strains were observed under different carbon conditions. The Δ*dacA* mutant was able to adapt to high carbon like the WT (Publication 2, figure 2, B), by lowering the affinity to HCO_3^- in contrast to the Δ*sbtB* strain [33]. When faced with night-time survival, cells need to accumulate glycogen, which will be respired during the night to acquire the energy to survive. The accumulation of glycogen is dependent on succesful on carbon assimilation. The group of Susan Golden previously reported on the significance of c-

di-AMP in the diurnal survival of *Synechococcus elongatus* PCC 7842 [101] and we were able to show this for *Synechocystis* as well. Both, the Δ*dacA* and the Δ*sbtB* strain displayed severe growth impairment in a 12 h light/12 h dark rhythm (Publication 2, figure 2, C and D).

SbtB is a PII-like protein and PII is reported to regulate cell metabolism through direct protein-protein interactions, so we performed SbtB-bait pulldown assays searching for hits relevant in a diurnal rhythm. In coimmunoprecipitation experiments with crude cell extract, several different glycogen metabolism related proteins were identified: a glycogen synthase GlgA2, a glycogen phosphorylase GlgP2, the glycogen branching enzyme GlgB, and a glycogen debranching enzyme GlgX1. To investigate whether these interactions are dependent on c-di-AMP, pulldowns with immobilized, c-terminal His_8- or Strep-tagged SbtB on magnetic Ni^{2+} or streptavidin beads, respectively, were incubated with crude *Synechocystis* cell extract in either presence or absence of c-di-AMP. With both different tags, in the presence of c-di-AMP, GlgB was enriched (Publication 2, figure 3,A; supplementary figure S9B), while incubation with cAMP failed to enrich GlgB (Publication 2, supplementary figure S9, C and D). To prove this interaction, a bacterial two-hybrid assay was performed. Interaction was observable between SbtB and GlgB when GlgB was N-terminally tagged (Publication 2, figure 3, B), while not with C-terminally tagged GlgB or any other identified glycogen metabolism related protein (Publication 2, supplementary figure S10). The interaction between SbtB and GlgB was also proven by microscale thermophoresis, though the addition of c-di-AMP did not alter the binding constant significantly (Publication 2, figure 3, C).

A previously generated Δ*glgB* mutant [110] was checked for survival in a diurnal rhythm. It displayed a comparable phenotype to the Δ*dacA* and Δ*sbtB* strains (Publication 2, figure 3, D). To solidify the involvement of SbtB and c-di-AMP in the glycogen metabolism, the glycogen concentration was measured at midday phase in all three mutants. All of them had significantly lower lewels than the WT (Publication 2, figure 3, E). A complementation of the Δ*sbtB* mutant under control of the *psbA*2 promoter had WT-like levels of glycogen in diurnal growth (Publication 2, supplementary figure S11, C). Since glycogen respiration is vital in the night, oxygen consumption was observed in the Δ*dacA* and Δ*sbtB* strains throughout several days of diurnal growth. Both mutants showed significantly lower levels of oxygen and oxygen evolution rate during the light phase, and both immediately dropped at the onset of

dark, while in the WT a gradual decline throughout the dark phase was observable (Publication 2, figure 3. F and G). The lower oxygen evolution during the day indicated a reduced rate of photosynthesis, which indicates a lower carbon fixation through the CBB cycle (Publication 2, supplementary figure S6, B, C).

Lastly, we measured the intracellular concentration of c-di-AMP throughout 24 hours of diurnal growth in the WT. The levels decreased throughout the night but rapidly increased to almost 3 times as much at the start of the light phase (Publication 2, figure 2, E). This is contradictory to the quantification in *Synechococcus elongatus* PCC 7842, in which the levels increased throughout the night, peaking shortly before dawn, and dropped during the day [101].

Overall, we could show that c-di-AMP in cooperation with SbtB regulates GlgB and thus, the levels of glycogen for night-time survival, emphasising its essentiality in diurnal rhythm.

2. Chlorosis

Synechocystis, being non-diazotrophic, must be able to survive times of nitrogen starvation and does so by entering the metabolic dormancy termed chlorosis. We investigated the significance of sodium and c-di-AMP in this well-established quiescent state.

2.1. Significance of sodium for bioenergetics

During vegetative growth, the primary requirement for sodium is the HCO_3^- uptake through BicA and SbtA (Publication 1, figure 5, C). This could be the main requirement in early chlorosis as well, as the cells accumulate large storages of glycogen in the first days. There could be additional requirements for sodium afterwards, as chlorotic cells have only a residual carbon fixation as sink for the residual photosynthesis. In absence of sodium, cells can't survive chlorosis. They are unable to accumulate large glycogen storages (Publication 1, figure 5, E), as was expected. Still, even when starved of sodium after accumulation of glycogen, these storages begun to be degraded and cells were unable to survive (Publication 1, figure 5, E, blue bars). Keeping the cells in a 2 % CO_2 environment, enabling survival in vegetative growth in absence of sodium, failed to mitigate the lack of Na^+ (Publication 1, figure 5, D). Recovering cells will consume glycogen for energy generation, leading us to believe that sodium could be required during chlorosis for ATP synthesis. This hypothesis was proven, as an

increase in environmental sodium led to an increase of ATP in the cells (Publication 1, figure 2, E). Since chlorotic cells are dormant, they have a reduced requirement of ATP. Recovering cells of *Synechocystis*, on the other hand, begin their process of resuscitation with a significant increase in ATP [22]. Thus, we decided to investigate the influence of sodium on bioenergetics in early resuscitation.

2.2. Significance of c-di-AMP for survival in chlorosis

Since the retarded accumulation of glycogen appears to be the reason why the Δ*dacA* and the Δ*sbtB* mutants fail to maintain diurnal growth (Publication 2, figure 2, C,D), death during nitrogen starvation due to the same reason was expected. In fact, the Δ*dacA* strain was unable to survive chlorosis, while the Δ*sbtB* mutant did not display a phenotype (Pubilcation 2, supplementary figure S5, B, C). Thus, the missing interaction between the SbtB-c-di-AMP complex and GlgB is not responsible for death of the Δ*dacA* strain in chlorosis. Consequently, the acclimation of the c-di-AMP deficient strain to nitrogen starvation was investigated in more detail.

Intracellular c-di-AMP measurements throughout 14 days of chlorosis revealed increased levels in early chlorosis (Publication 4, figure 1, A), before reducing towards the later stages of chlorosis again. Thus, the part of c-di-AMP in the recalibration of the cellular metabolism in response to nitrogen starvation is significant, for without it, the cells die.. Fitting to this assumption, when the cells were stained with the fluorescent dye Bis-(1,3-Dibutylbarbituric Acid)-trimethine axonol (DiBAC), which enters depolarized cells, around 40 % of Δ*dacA* cells appeared fluorescent after one day (Publication 4, figure 1, D). Fluorescence indicates cell death and after 14 days, the culture was visibly white, another indication, and approximately 60 % of cells appeared stained, further increasing towards day 21 (Publication 4, figure 1, B – D). The cells appeared dead, but the cell density, measured via the optical density at 750 nm, did not decrease. Furthermore, the mutant cells were unable to perform the last cell division at the start of chlorosis (Publication 4, figure 1, E). The degradation of the photosynthetic machinery occurs as in the WT though (Publication 4, figure 1, F and G), even if the mutant has already a lower quantum yield of PSII in vegetative growth. A large difference between mutant and WT was visible in the levels of ATP and glycogen (Publication 4, figure 1, H, I). The levels of ATP reduced significantly at the start of chlorosis in the WT, while in the mutant, they increased to approximately 150

% of vegetative level in the first 2 days before dropping down again. The levels of glycogen increased rapidly in early chlorosis in the WT, as expected. Meanwhile, the mutant failed to accumulate large amounts of glycogen and remained at about 50 % of the WT level. This resembles to the phenotype in diurnal rhythm, but since the Δ*sbtB* mutant did not display this phenotype, indicating that the reduced glycogen synthesis in the Δ*dacA* strain is not mediated by c-di-AMP sensing of SbtB. Concerning the influence of c-di-AMP on osmotic stress response, transmission electron microscope pictures of cells after 21 days of chlorosis showed a heterogenous Δ*dacA* culture with cells displaying different stages of plasmolysis (Publication 4, figure 1, J).

Since we were unable to clearly pinpoint the role of c-di-AMP in chlorosis, we performed untargeted metabolomic analysis (Publication 4, figure 2). In the WT, different profiles of amino acid level changes were observed. They either peaked in early chlorosis, visible in case of lysine (Publication 4, figure 2, B), remained constant, visible for glutamine (Publication 4, figure 2, A), or declined gradually, as visible for glutamate (Publication 4, figure 2, A). In the Δ*dacA* strain, various amino acids showed either increased or decreased levels as compared to the WT. Glutamate, the primary pivot point of nitrogen metabolism dropped rapidly in the WT while in the mutant, it did increase. This was highly unexpected, as the cells were starved of fixed nitrogen, so the supply should have dropped. Levels of proline (Publication 4, figure 2, A), aspartate, methionine (Publication 4, figure 2, B) and tryptophane (Publication 4, figure 2, C) increased within early chlorosis in the mutant. The levels of proline stayed high, which could be due to its function as osmolyte, attempting to mitigate osmotic stress. Another interesting increase is that of methionine (Publication 4, figure 2, B), As it is the initiating amino acid of protein translation and precursor of the methyl-group donor S-adenosine-L-methionine, this could indicate a disturbance in protein synthesis and possibly also in DNA-methylation.

3. Resuscitation

When faced with a new source of fixed nitrogen, cells will start a multi-levelled, highly organised resuscitation process. During this process, the entire cellular metabolism is restructured and rebuilt.

3.1. Significance of sodium for pH control, bioenergetics, and GS activity

When chlorotic cells are supplied with a new nitrogen source, the ATP levels increase very rapidly, but the mechanism behind this response was unknown [22]. The energy

could derive from the two known energy producing systems in *Synechocystis*, respiration or photosynthesis. To investigate this, cells of the Δ*glgP1/2* mutant, which is unable to degrade glycogen, were recovered and their ATP content measured. The cells were still able to increase their ATP levels like WT (Publication 1, figure 1, A). Next, we attempted to recover chlorotic cells in the dark, so they are incapable of photosynthesis, or in presence of the inhibitor 3-(3,4-dichlorophenyl)-1,1-dimethylurea, which blocks the electron transfer from PSII to PQ. Cells were still able to rapidly synthesise new ATP (Publication 1, figure 1, B and C). Lastly, we added either dibromthymochinon or antimycin A to inhibit the electron flow to cytochrome b_6f, neither inhibited ATP synthesis. Thus, neither respiration nor photosynthesis are required for the immediate ATP increase in the first minutes of resuscitation.

Sodium has been suggested to influence the ATP synthesis in chlorosis and possibly also resuscitation earlier in this work (see 2.2.1 sodium in chlorosis). First, it had to be proven that protons are not necessary for ATP synthesis. To achieve this, we recovered cells in presence of the protonophores carbonyl cyanide m-chlorophenyl and 2,3-dinitrophenol. In both conditions, ATP synthesis upon addition of $NaNO_3$ was unhindered (Publication 1, figure 2 A, B). When recovering cells with KNO_3 in presence of 5 mM sodium, a reduced increase in ATP was observable (Publication 1, figure 2, C) and when recovering in absence of sodium, no increase was detectable at all (Publication 1, figure 2, D). This clearly indicated the importance of sodium for bioenergetics. However, it was unclear whether this was a combined effect of sodium and the supplied nitrogen source. To investigate this, we sequentially added first NaCl and second KNO_3 to chlorotic cultures. Both caused separate increases in ATP and when the experiment was repeated in presence of the GS inhibitor L-methionine sulfoximine, only the sodium increase was measurable (Publication 1, figure 2, E). On the other hand, when cells were incubated with the sodium ionophore monensin and recovered, only a small increase was observable (Publication 1, figure 2, F). Strikingly, when recovered in presence of ethyl-isopropyl amiloride, which blocks sodium channels and proton-sodium antiporters, no increase in ATP was measurable. All these results consolidate the role of sodium in bioenergetics.

To identify whether there are additional requirements for sodium in resuscitation, further investigation was carried out. To observe the significance of sodium for carbon fixation in resuscitation, recovery in a 2 % CO_2 environment was performed. Cells were

unable to recover (Publication 3, figure 1). As the increase in ATP could be seperated in a sodium dependent and nitrogen dependent, we investigated whether sodium is also influencing the nitrogen acquisition. When cells were recovered in absence of sodium, ammonium was imported at a rate comparable to standard conditions (Publication 3, figure 2, B). In contrast, nitrate was imported in absence of sodium only transiently while the levels of nitrite in the medium increased (Publication 3, figure 2, C, D). This indicates a requirement for sodium in the assimilation of nitrate. The reduction of nitrate to nitrite requires 2 protons and the further reduction to ammonia requires 6 additional protons. Apparently, the cells imported some nitrate, reduced it to nitrite but failed to reduce it further. Likely, they were lacking protons, which would be provided by the activity of H^+/Na^+ antiporters, like the members of the NhaS-family. Cells recovering with nitrate and sodium turned the media more alkaline, indicating proton uptake, while the pH remained constant in the absence of sodium (Publication 3, figure 2, E). The intracellular pH was measured using the fluorescent indicator 2′, 7′-bis-(2carboxyethyl)-5-(and-6)-carboxyfluorescein (BCECF) and became more alkaline in early recovery with nitrate and acidic with ammonium. Throughout resuscitation, when recovered with ammonium or in presence of sodium with nitrate, the pH returned to approximately 7,5, whereas when recovered with nitrate in the absence of sodium, the intracellular pH stayed alkaline at approximately 8,25 (Publication 3, figure 2, F). This shows that there are additional effects to the sodium dependent ATP synthesis, here, pH control and nitrogen acquisition.

Since sodium starvation has a global effect, we also investigated the metabolome of cells resuscitating with nitrate in presence and absence of sodium. We investigated the first 12 hours, when photosynthesis is yet inactive, excluding secondary effects due to incapability of carbon fixation. Under standard resuscitation conditions, many amino acids remained constant (Publication 3, figure 3). The levels of glutamate increased rapidly and consistently (Publication 3, figure 3, A). This was expected, as it is the primary entry point of new nitrogen into the cell metabolism. In the absence of sodium, there was a smaller increase and only to approximately 50 % of the standard condition level. In contrast to glutamate, the levels of glutamine remained almost constant. This indicates that the newly synthesised glutamine molecules are immediately turned over by the GOGAT reaction. In the absence of sodium, the glutamine levels were lower than during recovery in presence of sodium, indicating a delay and dysregulation of the GS-GOGAT cycle (Publication 3, figure 3, A). Arginine shows a similar pattern to

glutamine, as the levels remained almost constant in the presence of sodium, while sinking in absence of sodium (Publication 3, figure 3, A). This could be caused by the high demand for the limited amount of glutamate, which can serve as a substrate in arginine synthesis [111,112]. Proline showed a unique pattern, as the levels increased significantly in absence of sodium, in contrast to the constant levels in presence thereof (Publication 3, figure 3, A). Proline can function as an osmolyte [113], so increasing levels could compensate for missing protein and molecule biosynthesis in absence of sodium.

Another interesting pattern was observed for two of the aromatic amino acids, tyrosine and phenylalanine. Tyrosine showed decreasing levels in standard resuscitation, fitting to the observation that increased levels are found in chlorosis [63]. Both aromatic amino acids showed an intermediary increase in absence of sodium (Publication 3, figure 3, C).A possible reason except missing protein synthesis is not known.

Lastly, some intermediates of the TCA cycle were observable. Increased levels of succinate were observed during recovery in absence of sodium (Publication 3, figure 2, E). Succinate is produced in the modified TCA cycle of cyanobacteria from 2-OG and is reduced by the SDH to fumarate. As the GS-GOGAT cycle seems impaired in the absence of sodium, further processing of 2-OG to succinate could serve as a sink.

As the levels of ammonium in the medium decreased even in the absence of sodium, we questioned whether cells accumulate more of the nitrogen storage molecule cyanophycin in absence of sodium. It has been reported that recovering cells accumulate some CP as safeguard to reoccurring chlorosis [114]. Staining with the Sakaguchi method and observation of the cells revealed a missing or reduced CP production in absence of sodium with either nitrate or ammonium as nitrogen source, respectively (Publication 3, figure 4). This indicates an alternative, yet to be identified sink of ammonium in absence of sodium.

As to gain further insights why cells need sodium for proper resuscitation , transmission electron microscopic pictures of recovering cells in presence and absence of sodium were made. During recovery in the absence of sodium, the intracellular structures degrade over time until cells appeared ghost like (Publication 3, figure 5).

3.2. Significance of c-di-AMP due to changing metabolism and appearance of adapted strains

The expression and protein levels of DacA peak in early resuscitation [68,69]. To investigate whether the protein is also active, we measured the intracellular concentrations of c-di-AMP throughout two days of resuscitation. The levels peaked within 8 hours after addition of fixed nitrogen before dropping again (Publication 4, figure 3, A). When Δ*dacA* cells were recovered, the ATP levels increased less than in the WT and dropped back to chlorotic levels after 48 hours (Publication 4, figure 3, B). Additionally, the switch to mixotrophic and photoautotrophic growth appeared delayed, as PSII quantum yield was only measurable after 48 hours, a day later than in the WT (Publication 4, figure 3, C). In a drop plate recovery assay, the mutant lacked behind the WT by 2 orders of magnitude (Publication 4, figure 3, D). This appears reasonable, as only a quarter of cells survived chlorosis, as shown earlier (Publication 4, figure 1, C and D). As c-di-AMP deficient mutants have been reported to develop suppressor mutations in different organisms [115–120], we investigated whether the severe stress conditions of chlorosis and resuscitation would cause similar effects in *Synechocystis*. A colony PCR of the recovered mutant cells revealed a restored *dacA* gene (Publication 4, figure 3, E) and an intracellular c-di-AMP measurement showed that the revertant produced even more of the second messenger than the WT (Publication 4, figure 3, F). This indicates that the surviving cells have undergone genomic adaptions and therefore could survive chlorosis and resuscitation. To investigate this, we starved the adapted strain of nitrogen a second time. The c-di-AMP deficient phenotype was completely alleviated (Publication 4, figure 3, G – H). It appears that the cells removed the kanamycin resistance cassette from the intended location and inserted it into the chromosome somewhere else. This new location has not been found in this work.

VI. Discussion

1. Requirement for sodium in *Synechocystis*

Sodium is as ubiquitous as cyanobacteria are and the latter have learned to live with the former. As life likely originated in a potassium rich environment [57], sodium is typically more bane than boon, but still, cells find use for it.

1.1. Carbon fixation and bioenergetics in vegetative growth

During vegetative growth, an absence of sodium can be compensated by increased levels of CO_2 (Publication 1, figure 5, C). This clearly signifies that the primary requirement for sodium in vegetative growth is the import of HCO_3^- through the sodium dependent HCO_3^- transporters SbtA and BicA. Almost all ATP synthesis during vegetative growth occurs at the thylakoid membranes, powered by photosynthesis. Thus, bioenergetics are largely independent of sodium.

1.2. Sodium bioenergetics in chlorosis

With the onset of nitrogen starvation chlorosis, the levels of ATP drop significantly [22]. There are multiple possible reasons for this, for example glycogen synthesis is ATP consuming [121]. Additionally, ATP has been reported to act as a hydrotrope [122], meaning reduction of the ATP levels will turn the cytoplasm more crystalline, slowing molecule movement speed in the cytoplasm and thus, slowing the speed in metabolic networks.

As the thylakoid membranes degrade largely during chlorosis, an additional energy source is required. The results presented in this work suggest that sodium motive force is used to synthesise ATP at the plasma membrane. The proposed mechanism is a reduction of NAD(P)H to NAD(P), likely by the NAD-reductase NDH-II, as it was found in the plasmamembrane. The electrons will then be transported to the alternative respiratory terminal oxidase (ARTO), which will export protons. These would be immediately reimported through a Na^+/H^+ antiporter, likely of the NhaS-family. The Na^+ ions would then, following the concentration gradient, try to re-enter the cells, which is channelled through the ATPase, synthesising new ATP. Cyanobacteria can turn their environment more alkaline when feeding on nitrate or nitrite sources. This compromises the proton motif force, while a sodium motif can easily be maintained.

1.3. Sodium bioenergetics, pH control and nitrogen incorporation in resuscitation

In resuscitation, the first measurable response to a new source of fixed nitrogen is an immediate and drastic increase in ATP. This is required to fuel the anabolic reactions to rebuild the cell metabolism. The GS-GOGAT cycle is pivotal, as through its nitrogen assimilation activity, cells sense the availability of a new nitrogen source.. This has been proven by blocking the GS-GOGAT cycle with inhibitors and the concomitant lack of ATP increase [22]. The earlier postulated mechanism for sodium bioenergetics still applies here. To compensate the incorporation of free protons, Na^+/H^+ antiporter activity is essential for nitrogen assimilation and buffering of the cytoplasmic pH. Typically, the cytoplasm is buffered by K^+ ions and glutamate [123], but in the absence of sodium, GS activity is likely compromised due to lower levels of ATP and inhibited nitrite reduction. Due to sodium depletion, missing sodium-proton antiport causes the cytoplasm to become more alkaline and the pH of the medium to remain constant (Publication 3, figure 2, E).

Proline can act as an osmolyte and it can also derive from arginine catabolism [112]. The N-terminal domain of ArgZ has an arginine dihydrolase activity, splitting arginine into ornithine, ammonia and CO_2. Ornithine, as an arginine substrate, can then re-enter arginine synthesis or be converted to proline by an ornithine cyclodeaminase. The C-terminal part of ArgZ is presumed to have such an activity [112]. Because the absence of sodium hinders the nitrogen assimilation, the nitrogen-containing substrates for arginine synthesis (carbamoyl-phosphate) are lacking and therefore, ornithine could preferentially be converted into proline. The subsequent osmoprotection could be a secondary effect, though a necessary one, as cells recovering without sodium appear to degrade all their cellular structures (Publication 3, figure 5). The expression of *argZ* and protein levels of ArgZ increase in early resuscitation [68,69], which also indicates the turnover of ornithine to proline. The drop in tyrosine in standard resuscitation is likely caused by de-novo protein synthesis. The increase in absence of sodium remains enigmatic. It has been reported to act as radical quencher in specific enzymes [124,125], but whether free tyrosine can function the same way is so far unknown.

2. Requirement for c-di-AMP in *Synechocystis*

The second messenger c-di-AMP has been the focus of much research since its discovery in 2008 [90]. It has been reported to be of significance in cyanobacteria for survival in diurnal growth [101] and for osmotic stress response [102]. In this work, we

further investigated the significance of c-di-AMP for night-time and metabolic dormancy.

2.1. Osmoregulation through c-di-AMP in *Synechocystis*

In firmicutes, c-di-AMP is mainly involved in osmoregulation and ion homeostasis, the latter largely focused on K^+ [100,115,118,119]. For *Synechocystis*, it has also been reported though without description of a mechanism [102]. In different c-di-AMP based pulldown assays, we identified several different cation transporters as interaction partners, mainly of Na^+, K^+, and Mg^{2+} ions. The interaction of c-di-AMP with any of these transporters has still to be confirmed. In follow-up work in our laboratory, an interaction between c-di-AMP and the Na^+/H^+ antiporter NhaS5 has been observable and indicates a significance of c-di-AMP for Na^+ homeostasis.

2.2. Glycogen accumulation for night-time survival

Night-time survival is essential for photoautotrophic organisms, like cyanobacteria. The metabolism switches from the purely phototrophic to a heterotrophic-like mode, for which tight control is required. We have discovered here an interaction between c-di-AMP and the signal transduction protein SbtB. This complex will then increase the activity of GlgB and enable branched glycogen molecules. The branching of glycogen is pivotal for its subsequent rapid degradation, which is necessary to survive in a diurnal rhythm.

2.3. Global requirement for chlorosis and resuscitation

As shown in this work, c-di-AMP is essential in chlorosis. Cells lacking c-di-AMP appear to be unable to enter chlorosis. Levels of c-di-AMP peak in early chlorosis (Publication 4, figure 1, A) and deficient cells fail to divide or accumulate glycogen (Publication 4, figure 1 E, I) and within the first 2 days, already approximately 40 % of Δ*dacA* cells show a signal, dependent on a lack of membrane potential (Publication 4, figure 1, C – D), a clear indication of cell death. The mutant cells which do not emit a fluorescent signal when stained with DiBAC are still viable. Among these, adapted cells were able to recover.

Throughout chlorosis, a constant requirement for c-di-AMP is also osmotic regulation, observable in the cytoplasmic shrinkage of deficient cells in late chlorosis (Publication 4, figure 1, J). The phenomenon of cytoplasmic reduction has been previously reported as an answer to starvation conditions [126]. This is an unobserved behaviour in *Synechocystis* and thus, likely occurring due to the absence of c-di-AMP.

The metabolome is greatly disturbed in absence of c-di-AMP (Publication 4, figure 2), which implements it further, as a central second messenger.

2.4. Adaptation process

Mutants deficient in c-di-AMP production have been established in different bacteria as well as suppressor mutations reported in those mutants. These suppressor mutations have been largely focused on proteins connected to osmoregulation [96,100,117,119]. In this work, the adapted mutant removed the antibiotic resistance cassette from the gene locus (Publication 4, figure 3). This was possible, because the mutant was generated via insertion mutation of the antibiotic resistance cassette into the active centre encoding region of *sll0505*. This was necessary to circumvent downstream effects on *sll0506*, an undecaprenyl phosphate synthase encoding gene, whose 5'-end is overlapping with the 3'-end of *sll0505*. Still, there are likely additional suppressor mutations, whose discovery could further the understanding of the significance of c-di-AMP.

3. Conclusion

This work helps elucidating the global mechanisms of entry into metabolic quiescence and awakening thereof in *Synechocystis*. The ubiquitous cation Na^+ is used for maintaining an energised membrane during bacterial dormancy, a subject of interest regarding biodiversity, pathogenic persistence, and generation of antibiotic resistances. For the awakening process, it is also employed for nitrogen acquisition, pH control and osmoregulation, signifying the central role of this ubiquitous ion can have. However, it is still unclear how widespread these properties are in the bacterial world. Another small molecule with a global impact on *Synechocystis* is c-di-AMP, which we have shown to be essential in glycogen synthesis to survive nocturnal dormancy. Additionally, c-di-AMP is of great importance for entry and exit of metabolic quiescence, thought the underlying mechanisms are so far unknown, necessitating further research.

VII. References

1. Demoulin, C.F.; Lara, Y.J.; Cornet, L.; François, C.; Baurain, D.; Wilmotte, A.; Javaux, E.J. Cyanobacteria Evolution: Insight from the Fossil Record. *Free Radic. Biol. Med.* **2019**, *140*, 206–223, doi:10.1016/j.freeradbiomed.2019.05.007.
2. Bekker, A.; Holland, H.D.; Wang, P.-L.; Rumble, D.; Stein, H.J.; Hannah, J.L.; Coetzee, L.L.; Beukes, N.J. Dating the Rise of Atmospheric Oxygen. *Nature* **2004**, *427*, 117–120, doi:10.1038/nature02260.
3. Hannah, J.L.; Bekker, A.; Stein, H.J.; Markey, R.J.; Holland, H.D. Primitive Os and 2316 Ma Age for Marine Shale: Implications for Paleoproterozoic Glacial Events and the Rise of Atmospheric Oxygen. *Earth Planet. Sci. Lett.* **2004**, *225*, 43–52, doi:10.1016/j.epsl.2004.06.013.
4. Garcia-Pichel, F.; Pringault, O. Cyanobacteria Track Water in Desert Soils. *Nature* **2001**, *413*, 380–381, doi:10.1038/35096640.
5. Pandey, K.D.; Shukla, S.P.; Shukla, P.N.; Giri, D.D.; Singh, J.S.; Singh, P.; Kashyap, A.K. Cyanobacteria in Antarctica: Ecology, Physiology and Cold Adaptation. *Cell. Mol. Biol. Noisy--Gd. Fr.* **2004**, *50*, 575–584.
6. Palinska, K.A. Cyanobacteria. In *Encyclopedia of Life Sciences*; John Wiley & Sons, Ltd, Ed.; John Wiley & Sons, Ltd: Chichester, UK, 2008 ISBN 978-0-470-01617-6.
7. Rippka, R.; Deruelles, J.; Waterbury, J.B.; Herdman, M.; Stanier, R.Y. Generic Assignments, Strain Histories and Properties of Pure Cultures of Cyanobacteria. *Microbiology,* **1979**, *111*, 1–61, doi:10.1099/00221287-111-1-1.
8. Pinevich, A.V.; Averina, S.G.; Gavrilova, O.V.; Migunova, A.V. [Baeocytes in the cyanobacterium Pleurocapsa sp.: characterization of the differentiated cells produced by multiple fission]. *Mikrobiologiia* **2008**, *77*, 71–78.
9. Schirrmeister, B.E.; Antonelli, A.; Bagheri, H.C. The Origin of Multicellularity in Cyanobacteria. *BMC Evol. Biol.* **2011**, *11*, 45, doi:10.1186/1471-2148-11-45.
10. Flores, E.; Herrero, A. Compartmentalized Function through Cell Differentiation in Filamentous Cyanobacteria. *Nat. Rev. Microbiol.* **2010**, *8*, 39–50, doi:10.1038/nrmicro2242.
11. Kaplan-Levy, R.N.; Hadas, O.; Summers, M.L.; Rücker, J.; Sukenik, A. Akinetes: Dormant Cells of Cyanobacteria. In *Dormancy and Resistance in Harsh Environments*; Lubzens, E., Cerda, J., Clark, M., Eds.; Topics in Current Genetics; Springer: Berlin, Heidelberg, 2010; pp. 5–27 ISBN 978-3-642-12422-8.
12. Gaikwad, Dr.R. Nitrogenase Enzyme: A Review. *Pharm. Sin.* **2010**, *1*.
13. Falcón, L.I.; Cipriano, F.; Chistoserdov, A.Y.; Carpenter, E.J. Diversity of Diazotrophic Unicellular Cyanobacteria in the Tropical North Atlantic Ocean. *Appl. Environ. Microbiol.* **2002**, *68*, 5760–5764, doi:10.1128/AEM.68.11.5760-5764.2002.
14. Adams, D.G.; Carr, N.G.; Wilcox, M. The Developmental Biology of Heterocyst and Akinete Formation in Cyanobacteria. *CRC Crit. Rev. Microbiol.* **1981**, *9*, 45–100, doi:10.3109/10408418109104486.
15. Sauer, J.; Schreiber, U.; Schmid, R.; Völker, U.; Forchhammer, K. Nitrogen Starvation-Induced Chlorosis in Synechococcus Pcc 7942. Low-Level Photosynthesis as a Mechanism of Long-Term Survival. *Plant Physiol.* **2001**, *126*, 233–243.
16. Stanier, R.Y.; Kunisawa, R.; Mandel, M.; Cohen-Bazire, G. Purification and Properties of Unicellular Blue-Green Algae (Order Chroococcales). *Bacteriol. Rev.* **1971**, *35*, 171–205.
17. Ikeuchi, M.; Tabata, S. Synechocystis Sp. PCC 6803 — a Useful Tool in the Study of the Genetics of Cyanobacteria. *Photosynth. Res.* **2001**, *70*, 73–83, doi:10.1023/A:1013887908680.
18. Wang, Y.; Li, Y.; Shi, D.; Shen, G.; Ru, B.; Zhang, S. Characteristics of Mixotrophic Growth of Synechocystis Sp. in an Enclosed Photobioreactor. *Biotechnol. Lett.* **2002**, *24*, 1593–1597, doi:10.1023/A:1020384029168.

19. Iijima, H.; Nakaya, Y.; Kuwahara, A.; Hirai, M.Y.; Osanai, T. Seawater Cultivation of Freshwater Cyanobacterium Synechocystis Sp. PCC 6803 Drastically Alters Amino Acid Composition and Glycogen Metabolism. *Front. Microbiol.* **2015**, *6*.
20. Klotz, A.; Reinhold, E.; Doello, S.; Forchhammer, K. Nitrogen Starvation Acclimation in Synechococcus Elongatus: Redox-Control and the Role of Nitrate Reduction as an Electron Sink. *Life* **2015**, *5*, 888–904, doi:10.3390/life5010888.
21. Forchhammer, K.; Schwarz, R. Nitrogen Chlorosis in Unicellular Cyanobacteria – a Developmental Program for Surviving Nitrogen Deprivation. *Environ. Microbiol.* **2019**, *21*, 1173–1184, doi:10.1111/1462-2920.14447.
22. Doello, S.; Klotz, A.; Makowka, A.; Gutekunst, K.; Forchhammer, K. A Specific Glycogen Mobilization Strategy Enables Rapid Awakening of Dormant Cyanobacteria from Chlorosis. *Plant Physiol.* **2018**, *177*, 594–603, doi:10.1104/pp.18.00297.
23. Koch, M.; Doello, S.; Gutekunst, K.; Forchhammer, K. PHB Is Produced from Glycogen Turn-over during Nitrogen Starvation in Synechocystis Sp. PCC 6803. *Int. J. Mol. Sci.* **2019**, *20*, 1942, doi:10.3390/ijms20081942.
24. Shibata, M.; Katoh, H.; Sonoda, M.; Ohkawa, H.; Shimoyama, M.; Fukuzawa, H.; Kaplan, A.; Ogawa, T. Genes Essential to Sodium-Dependent Bicarbonate Transport in Cyanobacteria FUNCTION AND PHYLOGENETIC ANALYSIS. *J. Biol. Chem.* **2002**, *277*, 18658–18664, doi:10.1074/jbc.M112468200.
25. Erb, T.J.; Zarzycki, J. A Short History of RubisCO: The Rise and Fall (?) Of Nature's Predominant CO2 Fixing Enzyme. *Curr. Opin. Biotechnol.* **2018**, *49*, 100–107, doi:10.1016/j.copbio.2017.07.017.
26. Orf, I.; Timm, S.; Bauwe, H.; Fernie, A.; Hagemann, M.; Kopka, J.; Nikoloski, Z. Can Cyanobacteria Serve as a Model of Plant Photorespiration? - A Comparative Meta-Analysis of Metabolite Profiles. *J. Exp. Bot.* **2016**, *67*, doi:10.1093/jxb/erw068.
27. Burnap, R.L.; Nambudiri, R.; Holland, S. Regulation of the Carbon-Concentrating Mechanism in the Cyanobacterium Synechocystis Sp. PCC6803 in Response to Changing Light Intensity and Inorganic Carbon Availability. *Photosynth. Res.* **2013**, *118*, 115–124, doi:10.1007/s11120-013-9912-4.
28. Burnap, R.; Hagemann, M.; Kaplan, A. Regulation of CO2 Concentrating Mechanism in Cyanobacteria. *Life* **2015**, *5*, 348–371, doi:10.3390/life5010348.
29. Price, G.D.; Howitt, S.M. The Cyanobacterial Bicarbonate Transporter BicA: Its Physiological Role and the Implications of Structural Similarities with Human SLC26 Transporters. *Biochem. Cell Biol. Biochim. Biol. Cell.* **2011**, *89*, 178–188, doi:10.1139/o10-136.
30. Kaplan, A.; Volokita, M.; Zenvirth, D.; Reinhold, L. An Essential Role for Sodium in the Bicarbonate Transporting System of the Cyanobacterium Anabaena Variabilis. *FEBS Lett.* **1984**, *176*, 166–168, doi:10.1016/0014-5793(84)80933-3.
31. Omata, T.; Takahashi, Y.; Yamaguchi, O.; Nishimura, T. Structure, Function and Regulation of the Cyanobacterial High-Affinity Bicarbonate Transporter, BCT1. *Funct. Plant Biol. FPB* **2002**, *29*, 151–159, doi:10.1071/PP01215.
32. Mills, L.A.; McCormick, A.J.; Lea-Smith, D.J. Current Knowledge and Recent Advances in Understanding Metabolism of the Model Cyanobacterium Synechocystis Sp. PCC 6803. *Biosci. Rep.* **2020**, *40*, doi:10.1042/BSR20193325.
33. Selim, K.A.; Haase, F.; Hartmann, M.D.; Hagemann, M.; Forchhammer, K. PII-like Signaling Protein SbtB Links cAMP Sensing with Cyanobacterial Inorganic Carbon Response. *Proc. Natl. Acad. Sci.* **2018**, 201803790, doi:10.1073/pnas.1803790115.
34. Jablonsky, J.; Papacek, S.; Hagemann, M. Different Strategies of Metabolic Regulation in Cyanobacteria: From Transcriptional to Biochemical Control. *Sci. Rep.* **2016**, *6*, 33024, doi:10.1038/srep33024.
35. Glycogen: A Dynamic Cellular Sink and Reservoir for Carbon Available online: https://www.caister.com/hsp/abstracts/cyano2/08.html (accessed on 15 June 2023).

36. Preiss, J.; Romeo, T. Molecular Biology and Regulatory Aspects of Glycogen Biosynthesis in Bacteria. *Prog. Nucleic Acid Res. Mol. Biol.* **1994**, *47*, 299–329, doi:10.1016/s0079-6603(08)60255-x.
37. Doello, S.; Mokowka, A.; Gutekunst, K.; Forchhammer, K. A Specific Glycogen Mobilization Strategy Enables Awakening of Dormant Cyanobacteria from Chlorosis. *J. Plant Physiol.*
38. Westermark, S.; Steuer, R. Toward Multiscale Models of Cyanobacterial Growth: A Modular Approach. *Front. Bioeng. Biotechnol.* **2016**, *4*.
39. Deusch, O.; Landan, G.; Roettger, M.; Gruenheit, N.; Kowallik, K.V.; Allen, J.F.; Martin, W.; Dagan, T. Genes of Cyanobacterial Origin in Plant Nuclear Genomes Point to a Heterocyst-Forming Plastid Ancestor. *Mol. Biol. Evol.* **2008**, *25*, 748–761, doi:10.1093/molbev/msn022.
40. Singh, N.K.; Sonani, R.R.; Rastogi, R.P.; Madamwar, D. The Phycobilisomes: An Early Requisite for Efficient Photosynthesis in Cyanobacteria. *EXCLI J.* **2015**, *14*, 268–289, doi:10.17179/excli2014-723.
41. Shevela, D.; Björn, L.; Govindjee, G. *Photosynthesis: Solar Energy for Life*; 2019; ISBN 978-981-322-310-3.
42. Hervás, M.; Navarro, J.A.; De La Rosa, M.A. Electron Transfer between Membrane Complexes and Soluble Proteins in Photosynthesis. *Acc. Chem. Res.* **2003**, *36*, 798–805, doi:10.1021/ar020084b.
43. Lea-Smith, D.J.; Bombelli, P.; Vasudevan, R.; Howe, C.J. Photosynthetic, Respiratory and Extracellular Electron Transport Pathways in Cyanobacteria. *Biochim. Biophys. Acta BBA - Bioenerg.* **2016**, *1857*, 247–255, doi:10.1016/j.bbabio.2015.10.007.
44. Yamori, W.; Makino, A.; Shikanai, T. A Physiological Role of Cyclic Electron Transport around Photosystem I in Sustaining Photosynthesis under Fluctuating Light in Rice. *Sci. Rep.* **2016**, *6*, 20147, doi:10.1038/srep20147.
45. Miller, N.T.; Vaughn, M.D.; Burnap, R.L. Electron Flow through NDH-1 Complexes Is the Major Driver of Cyclic Electron Flow-Dependent Proton Pumping in Cyanobacteria. *Biochim. Biophys. Acta BBA - Bioenerg.* **2021**, *1862*, 148354, doi:10.1016/j.bbabio.2020.148354.
46. Hart, S.E.; Schlarb-Ridley, B.G.; Bendall, D.S.; Howe, C.J. Terminal Oxidases of Cyanobacteria. *Biochem. Soc. Trans.* **2005**, *33*, 832–835, doi:10.1042/BST0330832.
47. Shimakawa, G.; Kohara, A.; Miyake, C. Characterization of Light-Enhanced Respiration in Cyanobacteria. *Int. J. Mol. Sci.* **2020**, *22*, 342, doi:10.3390/ijms22010342.
48. Zhang, C.; Shuai, J.; Ran, Z.; Zhao, J.; Wu, Z.; Liao, R.; Wu, J.; Ma, W.; Lei, M. Structural Insights into NDH-1 Mediated Cyclic Electron Transfer. *Nat. Commun.* **2020**, *11*, 888, doi:10.1038/s41467-020-14732-z.
49. Pils, D.; Schmetterer, G. Characterization of Three Bioenergetically Active Respiratory Terminal Oxidases in the Cyanobacterium Synechocystis Sp. Strain PCC 6803. *FEMS Microbiol. Lett.* **2001**, *203*, 217–222, doi:10.1111/j.1574-6968.2001.tb10844.x.
50. Huokko, T.; Muth-Pawlak, D.; Aro, E.-M. Thylakoid Localized Type 2 NAD(P)H Dehydrogenase NdbA Optimizes Light-Activated Heterotrophic Growth of Synechocystis Sp. PCC 6803. *Plant Cell Physiol.* **2019**, *60*, 1386–1399, doi:10.1093/pcp/pcz044.
51. Dimroth, P.; Cook, G.M. Bacterial Na+- or H+-Coupled ATP Synthases Operating at Low Electrochemical Potential. In *Advances in Microbial Physiology*; Academic Press, 2004; Vol. 49, pp. 175–218.
52. Schulz, S.; Iglesias-Cans, M.; Krah, A.; Yildiz, Ö.; Leone, V.; Matthies, D.; Cook, G.M.; Faraldo-Gómez, J.D.; Meier, T. A New Type of Na+-Driven ATP Synthase Membrane Rotor with a Two-Carboxylate Ion-Coupling Motif. *PLOS Biol.* **2013**, *11*, e1001596, doi:10.1371/journal.pbio.1001596.
53. The ATP Synthase: The Understood, the Uncertain and the Unknown | Biochemical Society Transactions | Portland Press Available online: https://portlandpress.com/biochemsoctrans/article-abstract/41/1/1/68090/The-ATP-synthase-the-understood-the-uncertain-and (accessed on 19 June 2023).

54. Huang, F.; Parmryd, I.; Nilsson, F.; Persson, A.L.; Pakrasi, H.B.; Andersson, B.; Norling, B. Proteomics of Synechocystis Sp. Strain PCC 6803: Identification of Plasma Membrane Proteins. *Mol. Cell. Proteomics MCP* **2002**, *1*, 956–966, doi:10.1074/mcp.m200043-mcp200.
55. Leone, V.; Pogoryelov, D.; Meier, T.; Faraldo-Gómez, J.D. On the Principle of Ion Selectivity in Na+/H+-Coupled Membrane Proteins: Experimental and Theoretical Studies of an ATP Synthase Rotor. *Proc. Natl. Acad. Sci. U. S. A.* **2015**, *112*, E1057-1066, doi:10.1073/pnas.1421202112.
56. Schlegel, K.; Leone, V.; Faraldo-Gómez, J.D.; Müller, V. Promiscuous Archaeal ATP Synthase Concurrently Coupled to Na+ and H+ Translocation. *Proc. Natl. Acad. Sci. U. S. A.* **2012**, *109*, 947–952, doi:10.1073/pnas.1115796109.
57. Mulkidjanian, A.Y.; Dibrov, P.; Galperin, M.Y. The Past and Present of the Sodium Energetics: May the Sodium-Motive Force Be with You. *Biochim. Biophys. Acta* **2008**, *1777*, 985–992, doi:10.1016/j.bbabio.2008.04.028.
58. Montesinos, M.L.; Muro-Pastor, A.M.; Herrero, A.; Flores, E. Ammonium/Methylammonium Permeases of a Cyanobacterium: IDENTIFICATION AND ANALYSIS OF THREE NITROGEN-REGULATEDamt GENES IN SYNECHOCYSTIS Sp. PCC 6803 *. *J. Biol. Chem.* **1998**, *273*, 31463–31470, doi:10.1074/jbc.273.47.31463.
59. Zheng, L.; Kostrewa, D.; Bernèche, S.; Winkler, F.K.; Li, X.-D. The Mechanism of Ammonia Transport Based on the Crystal Structure of AmtB of Escherichia Coli. *Proc. Natl. Acad. Sci.* **2004**, *101*, 17090–17095, doi:10.1073/pnas.0406475101.
60. Chávez, S.; Lucena, J.M.; Reyes, J.C.; Florencio, F.J.; Candau, P. The Presence of Glutamate Dehydrogenase Is a Selective Advantage for the Cyanobacterium Synechocystis Sp. Strain PCC 6803 under Nonexponential Growth Conditions. *J. Bacteriol.* **1999**, *181*, 808–813, doi:10.1128/jb.181.3.808-813.1999.
61. Sharon, I.; Haque, A.S.; Grogg, M.; Lahiri, I.; Seebach, D.; Leschziner, A.E.; Hilvert, D.; Schmeing, T.M. Structures and Function of the Amino Acid Polymerase Cyanophycin Synthetase. *Nat. Chem. Biol.* **2021**, *17*, 1101–1110, doi:10.1038/s41589-021-00854-y.
62. Baier, K.; Nicklisch, S.; Grundner, C.; Reinecke, J.; Lockau, W. Expression of Two nblA-Homologous Genes Is Required for Phycobilisome Degradation in Nitrogen-Starved Synechocystis Sp. PCC6803. *FEMS Microbiol. Lett.* **2001**, *195*, 35–39.
63. Krauspe, V.; Fahrner, M.; Spät, P.; Steglich, C.; Frankenberg-Dinkel, N.; Maček, B.; Schilling, O.; Hess, W.R. Discovery of a Small Protein Factor Involved in the Coordinated Degradation of Phycobilisomes in Cyanobacteria. *Proc. Natl. Acad. Sci.* **2021**, *118*, e2012277118, doi:10.1073/pnas.2012277118.
64. Allen, M.M.; Smith, A.J. Nitrogen Chlorosis in Blue-Green Algae. *Arch. Für Mikrobiol.* **1969**, *69*, 114–120, doi:10.1007/BF00409755.
65. Görl, M.; Sauer, J.; Baier, T.; Forchhammer, K. Nitrogen-Starvation-Induced Chlorosis in Synechococcus PCC 7942: Adaptation to Long-Term Survival. *Microbiology* **1998**, *144*, 2449–2458.
66. Chlorosis Induced by Nutrient Deprivation in Synechococcus Sp. Strain PCC 7942: Not All Bleaching Is the Same | Journal of Bacteriology Available online: https://journals.asm.org/doi/abs/10.1128/jb.174.14.4718-4726.1992 (accessed on 19 June 2023).
67. Orthwein, T.; Scholl, J.; Spät, P.; Lucius, S.; Koch, M.; Macek, B.; Hagemann, M.; Forchhammer, K. The Novel PII-Interactor PirC Identifies Phosphoglycerate Mutase as Key Control Point of Carbon Storage Metabolism in Cyanobacteria. *Proc. Natl. Acad. Sci.* **2021**, *118*, doi:10.1073/pnas.2019988118.
68. Klotz, A.; Georg, J.; Bučinská, L.; Watanabe, S.; Reimann, V.; Januszewski, W.; Sobotka, R.; Jendrossek, D.; Hess, W.R.; Forchhammer, K. Awakening of a Dormant Cyanobacterium from Nitrogen Chlorosis Reveals a Genetically Determined Program. *Curr. Biol.* **2016**, *26*, 2862–2872, doi:10.1016/j.cub.2016.08.054.

69. Spät, P.; Klotz, A.; Rexroth, S.; Maček, B.; Forchhammer, K. Chlorosis as a Developmental Program in Cyanobacteria: The Proteomic Fundament for Survival and Awakening. *Mol. Cell. Proteomics* **2018**, mcp.RA118.000699, doi:10.1074/mcp.RA118.000699.
70. Newton, A.C.; Bootman, M.D.; Scott, J.D. Second Messengers. *Cold Spring Harb. Perspect. Biol.* **2016**, *8*, a005926, doi:10.1101/cshperspect.a005926.
71. Tisa, L.S.; Adler, J. Chemotactic Properties of Escherichia Coli Mutants Having Abnormal Ca2+ Content. *J. Bacteriol.* **1995**, *177*, 7112–7118, doi:10.1128/jb.177.24.7112-7118.1995.
72. Dominguez, D.C. Calcium Signalling in Bacteria. *Mol. Microbiol.* **2004**, *54*, 291–297, doi:10.1111/j.1365-2958.2004.04276.x.
73. Herbaud, M.L.; Guiseppi, A.; Denizot, F.; Haiech, J.; Kilhoffer, M.C. Calcium Signalling in Bacillus Subtilis. *Biochim. Biophys. Acta* **1998**, *1448*, 212–226, doi:10.1016/s0167-4889(98)00145-1.
74. Addinall, S.G.; Holland, B. The Tubulin Ancester, FtsZ, Draughtsman, Designer and Driving Force for Bacterial Cytokinesis. *J. Mol. Biol.* **2002**, *318*, 219–236, doi:10.1016/S0022-2836(02)00024-4.
75. Hu, Y.; Zhang, X.; Shi, Y.; Zhou, Y.; Zhang, W.; Su, X.-D.; Xia, B.; Zhao, J.; Jin, C. Structures of Anabaena Calcium-Binding Protein CcbP: INSIGHTS INTO CA2+ SIGNALING DURING HETEROCYST DIFFERENTIATION *. *J. Biol. Chem.* **2011**, *286*, 12381–12388, doi:10.1074/jbc.M110.201186.
76. Zhao, Y.; Shi, Y.; Zhao, W.; Huang, X.; Wang, D.; Brown, N.; Brand, J.; Zhao, J. CcbP, a Calcium-Binding Protein from Anabaena Sp. PCC 7120, Provides Evidence That Calcium Ions Regulate Heterocyst Differentiation. *Proc. Natl. Acad. Sci.* **2005**, *102*, 5744–5748, doi:10.1073/pnas.0501782102.
77. Leganés, F.; Forchhammer, K.; Fernández-Piñas, F. Role of Calcium in Acclimation of the Cyanobacterium Synechococcus Elongatus PCC 7942 to Nitrogen Starvation. *Microbiology* **2009**, *155*, 25–34, doi:10.1099/mic.0.022251-0.
78. Agostoni, M.; Montgomery, B. Survival Strategies in the Aquatic and Terrestrial World: The Impact of Second Messengers on Cyanobacterial Processes. *Life* **2014**, *4*, 745–769, doi:10.3390/life4040745.
79. Bange, G.; Brodersen, D.E.; Liuzzi, A.; Steinchen, W. Two P or Not Two P: Understanding Regulation by the Bacterial Second Messengers (p)ppGpp. *Annu. Rev. Microbiol.* **2021**, *75*, 383–406, doi:10.1146/annurev-micro-042621-122343.
80. Mann, N.; Carr, N.G.; Midgley, J.E. RNA Synthesis and the Accumulation of Guanine Nucleotides during Growth Shift down in the Blue-Green Alga Anacystis Nidulans. *Biochim. Biophys. Acta* **1975**, *402*, 41–50, doi:10.1016/0005-2787(75)90368-8.
81. Hood, R.D.; Higgins, S.A.; Flamholz, A.; Nichols, R.J.; Savage, D.F. The Stringent Response Regulates Adaptation to Darkness in the Cyanobacterium Synechococcus Elongatus. *Proc. Natl. Acad. Sci. U. S. A.* **2016**, *113*, E4867-4876, doi:10.1073/pnas.1524915113.
82. Puszynska, A.M.; O'Shea, E.K. ppGpp Controls Global Gene Expression in Light and in Darkness in S. Elongatus. *Cell Rep.* **2017**, *21*, 3155–3165, doi:10.1016/j.celrep.2017.11.067.
83. Wood, N.B.; Haselkorn, R. Control of Phycobiliprotein Proteolysis and Heterocyst Differentiation in Anabaena. *J. Bacteriol.* **1980**, *141*, 1375–1385, doi:10.1128/jb.141.3.1375-1385.1980.
84. Friga, G.M.; Borbély, G.; Farkas, G.L. Accumulation of Guanosine Tetraphosphate (ppGpp) under Nitrogen Starvation in Anacystis Nidulans, a Cyanobacterium. *Arch. Microbiol.* **1981**, *129*, 341–343, doi:10.1007/BF00406458.
85. Zhang, S.-R.; Lin, G.-M.; Chen, W.-L.; Wang, L.; Zhang, C.-C. ppGpp Metabolism Is Involved in Heterocyst Development in the Cyanobacterium Anabaena Sp. Strain PCC 7120. *J. Bacteriol.* **2013**, *195*, 4536–4544, doi:10.1128/JB.00724-13.
86. Görke, B.; Stülke, J. Carbon Catabolite Repression in Bacteria: Many Ways to Make the Most out of Nutrients. *Nat. Rev. Microbiol.* **2008**, *6*, 613–624, doi:10.1038/nrmicro1932.
87. Ohmori, M.; Okamoto, S. Photoresponsive cAMP Signal Transduction in Cyanobacteria. *Photochem. Photobiol. Sci.* **2004**, *3*, 503–511.
88. Francko, D.A.; Wetzel, R.G. Dynamics of Cellular and Extracellular cAmp in Anabaena Flos-Aquae (Cyanophyta): Intrinsic Culture Variability and Correlation with Metabolic Variables. *J Phycol U. S.* **1981**, *17*, doi:10.1111/j.0022-3646.1981.00129.x.

89. Imashimizu, M.; Yoshimura, H.; Katoh, H.; Ehira, S.; Ohmori, M. NaCl Enhances Cellular cAMP and Upregulates Genes Related to Heterocyst Development in the Cyanobacterium, *Anabaena* Sp. Strain PCC 7120. *FEMS Microbiol. Lett.* **2005**, *252*, 97–103, doi:10.1016/j.femsle.2005.08.035.
90. Witte, G.; Hartung, S.; Büttner, K.; Hopfner, K.-P. Structural Biochemistry of a Bacterial Checkpoint Protein Reveals Diadenylate Cyclase Activity Regulated by DNA Recombination Intermediates. *Mol. Cell* **2008**, *30*, 167–178, doi:10.1016/j.molcel.2008.02.020.
91. Corrigan, R.M.; Gründling, A. Cyclic Di-AMP: Another Second Messenger Enters the Fray. *Nat. Rev. Microbiol.* **2013**, *11*, 513–524, doi:10.1038/nrmicro3069.
92. Braun, F.; Thomalla, L.; van der Does, C.; Quax, T.E.F.; Allers, T.; Kaever, V.; Albers, S.-V. Cyclic Nucleotides in Archaea: Cyclic Di-AMP in the Archaeon Haloferax Volcanii and Its Putative Role. *MicrobiologyOpen* **2019**, *0*, e829, doi:10.1002/mbo3.829.
93. Pham, T.H.; Liang, Z.-X.; Marcellin, E.; Turner, M.S. Replenishing the Cyclic-Di-AMP Pool: Regulation of Diadenylate Cyclase Activity in Bacteria. *Curr. Genet.* **2016**, *62*, 731–738, doi:10.1007/s00294-016-0600-8.
94. Commichau, F.M.; Heidemann, J.L.; Ficner, R.; Stülke, J. Making and Breaking of an Essential Poison: The Cyclases and Phosphodiesterases That Produce and Degrade the Essential Second Messenger Cyclic Di-AMP in Bacteria. *J. Bacteriol.* **2018**, doi:10.1128/JB.00462-18.
95. Heidemann, J.L.; Neumann, P.; Dickmanns, A.; Ficner, R. Crystal Structures of the C-Di-AMP Synthesizing Enzyme CdaA. *J. Biol. Chem.* **2019**, doi:10.1074/jbc.RA119.009246.
96. Commichau, F.M.; Gibhardt, J.; Halbedel, S.; Gundlach, J.; Stülke, J. A Delicate Connection: C-Di-AMP Affects Cell Integrity by Controlling Osmolyte Transport. *Trends Microbiol.* **2018**, *26*, 175–185, doi:10.1016/j.tim.2017.09.003.
97. Bai, Y.; Yang, J.; Zarrella, T.M.; Zhang, Y.; Metzger, D.W.; Bai, G. Cyclic Di-AMP Impairs Potassium Uptake Mediated by a Cyclic Di-AMP Binding Protein in Streptococcus Pneumoniae. *J. Bacteriol.* **2014**, *196*, 614–623, doi:10.1128/JB.01041-13.
98. Commichau, F.M.; Dickmanns, A.; Gundlach, J.; Ficner, R.; Stülke, J. A Jack of All Trades: The Multiple Roles of the Unique Essential Second Messenger Cyclic Di-AMP. *Mol. Microbiol.* **2015**, *97*, 189–204, doi:10.1111/mmi.13026.
99. Huynh, T.N.; Choi, P.H.; Sureka, K.; Ledvina, H.E.; Campillo, J.; Tong, L.; Woodward, J.J. Cyclic Di-AMP Targets the Cystathionine Beta-Synthase Domain of the Osmolyte Transporter OpuC. *Mol. Microbiol.* **2016**, *102*, 233–243, doi:10.1111/mmi.13456.
100. Whiteley, A.T.; Garelis, N.E.; Peterson, B.N.; Choi, P.H.; Tong, L.; Woodward, J.J.; Portnoy, D.A. C-Di-AMP Modulates Listeria Monocytogenes Central Metabolism to Regulate Growth, Antibiotic Resistance, and Osmoregulation. *Mol. Microbiol.* **2017**, *104*, 212–233, doi:10.1111/mmi.13622.
101. Rubin, B.E.; Huynh, T.N.; Welkie, D.G.; Diamond, S.; Simkovsky, R.; Pierce, E.C.; Taton, A.; Lowe, L.C.; Lee, J.J.; Rifkin, S.A.; et al. High-Throughput Interaction Screens Illuminate the Role of c-Di-AMP in Cyanobacterial Nighttime Survival. *PLOS Genet.* **2018**, *14*, e1007301, doi:10.1371/journal.pgen.1007301.
102. Agostoni, M.; Logan-Jackson, A.R.; Heinz, E.R.; Severin, G.B.; Bruger, E.L.; Waters, C.M.; Montgomery, B.L. Homeostasis of Second Messenger Cyclic-Di-AMP Is Critical for Cyanobacterial Fitness and Acclimation to Abiotic Stress. *Front. Microbiol.* **2018**, *9*, doi:10.3389/fmicb.2018.01121.
103. Dimroth, P. Sodium Ion Transport Decarboxylases and Other Aspects of Sodium Ion Cycling in Bacteria. *Microbiol. Rev.* **1987**, *51*, 320–340.
104. Häse, C.C.; Fedorova, N.D.; Galperin, M.Y.; Dibrov, P.A. Sodium Ion Cycle in Bacterial Pathogens: Evidence from Cross-Genome Comparisons. *Microbiol. Mol. Biol. Rev.* **2001**, *65*, 353–370, doi:10.1128/mmbr.65.3.353-370.2001.
105. Elanskaya, I.V.; Karandashova, I.V.; Bogachev, A.V.; Hagemann, M. Functional Analysis of the Na+/H+ Antiporter Encoding Genes of the Cyanobacterium Synechocystis PCC 6803. *Biochem. Biokhimiia* **2002**, *67*, 432–440, doi:10.1023/a:1015281906254.

106. Inaba, M.; Sakamoto, A.; Murata, N. Functional Expression in Escherichia Coli of Low-Affinity and High-Affinity Na+(Li+)/H+ Antiporters of Synechocystis. *J. Bacteriol.* **2001**, *183*, 1376–1384, doi:10.1128/JB.183.4.1376-1384.2001.
107. Tsunekawa, K.; Shijuku, T.; Hayashimoto, M.; Kojima, Y.; Onai, K.; Morishita, M.; Ishiura, M.; Kuroda, T.; Nakamura, T.; Kobayashi, H.; et al. Identification and Characterization of the Na+/H+ Antiporter NhaS3 from the Thylakoid Membrane of Synechocystis Sp. PCC 6803*. *J. Biol. Chem.* **2009**, *284*, 16513–16521, doi:10.1074/jbc.M109.001875.
108. Forchhammer, K. Global Carbon/Nitrogen Control by PII Signal Transduction in Cyanobacteria: From Signals to Targets. *FEMS Microbiol. Rev.* **2004**, *28*, 319–333, doi:10.1016/j.femsre.2003.11.001.
109. Agostoni, M.; Waters, C.M.; Montgomery, B.L. Regulation of Biofilm Formation and Cellular Buoyancy through Modulating Intracellular Cyclic di-GMP Levels in Engineered Cyanobacteria. *Biotechnol. Bioeng.* **2016**, *113*, 311–319, doi:10.1002/bit.25712.
110. Gründel, M.; Scheunemann, R.; Lockau, W.; Zilliges, Y. Impaired Glycogen Synthesis Causes Metabolic Overflow Reactions and Affects Stress Responses in the Cyanobacterium Synechocystis Sp. PCC 6803. *Microbiol. Read. Engl.* **2012**, *158*, 3032–3043, doi:10.1099/mic.0.062950-0.
111. Flores, E.; Arévalo, S.; Burnat, M. Cyanophycin and Arginine Metabolism in Cyanobacteria. *Algal Res.* **2019**, *42*, 101577, doi:10.1016/j.algal.2019.101577.
112. Flores, E. Studies on the Regulation of Arginine Metabolism in Cyanobacteria Should Include Mixotrophic Conditions. *mBio* **2021**, *12*, e01433-21, doi:10.1128/mBio.01433-21.
113. Götz, F.; Longnecker, K.; Soule, M.C.K.; Becker, K.W.; McNichol, J.; Kujawinski, E.B.; Sievert, S.M. Targeted Metabolomics Reveals Proline as a Major Osmolyte in the Chemolithoautotroph Sulfurimonas Denitrificans. *MicrobiologyOpen* **2018**, *7*, doi:10.1002/mbo3.586.
114. Watzer, B.; Forchhammer, K. Cyanophycin Synthesis Optimizes Nitrogen Utilization in the Unicellular Cyanobacterium Synechocystis Sp. Strain PCC 6803. *Appl. Environ. Microbiol.* **2018**, *84*, e01298-18, doi:10.1128/AEM.01298-18.
115. Gundlach, J.; Herzberg, C.; Kaever, V.; Gunka, K.; Hoffmann, T.; Weiß, M.; Gibhardt, J.; Thürmer, A.; Hertel, D.; Daniel, R.; et al. Control of Potassium Homeostasis Is an Essential Function of the Second Messenger Cyclic Di-AMP in *Bacillus Subtilis*. *Sci. Signal.* **2017**, *10*, eaal3011, doi:10.1126/scisignal.aal3011.
116. Whiteley, A.T.; Pollock, A.J.; Portnoy, D.A. The PAMP C-Di-AMP Is Essential for Listeria Monocytogenes Growth in Rich but Not Minimal Media Due to a Toxic Increase in (p)ppGpp. *Cell Host Microbe* **2015**, *17*, 788–798, doi:10.1016/j.chom.2015.05.006.
117. Zeden, M.S.; Schuster, C.F.; Bowman, L.; Zhong, Q.; Williams, H.D.; Gründling, A. Cyclic Di-Adenosine Monophosphate (c-Di-AMP) Is Required for Osmotic Regulation in Staphylococcus Aureus but Dispensable for Viability in Anaerobic Conditions. *J. Biol. Chem.* **2018**, *293*, 3180–3200, doi:10.1074/jbc.M117.818716.
118. Gundlach, J.; Krüger, L.; Herzberg, C.; Turdiev, A.; Poehlein, A.; Tascón, I.; Weiß, M.; Hertel, D.; Daniel, R.; Hänelt, I.; et al. Sustained Sensing in Potassium Homeostasis: Cyclic Di-AMP Controls Potassium Uptake by KimA at the Levels of Expression and Activity. *J. Biol. Chem.* **2019**, doi:10.1074/jbc.RA119.008774.
119. Pham, H.T.; Nhiep, N.T.H.; Vu, T.N.M.; Huynh, T.N.; Zhu, Y.; Huynh, A.L.D.; Chakrabortti, A.; Marcellin, E.; Lo, R.; Howard, C.B.; et al. Enhanced Uptake of Potassium or Glycine Betaine or Export of Cyclic-Di-AMP Restores Osmoresistance in a High Cyclic-Di-AMP Lactococcus Lactis Mutant. *PLoS Genet.* **2018**, *14*, e1007574, doi:10.1371/journal.pgen.1007574.
120. Quintana, I.M.; Gibhardt, J.; Turdiev, A.; Hammer, E.; Commichau, F.M.; Lee, V.T.; Magni, C.; Stülke, J. The KupA and KupB Proteins of Lactococcus Lactis IL1403 Are Novel C-Di-AMP Receptor Proteins Responsible for Potassium Uptake. *J. Bacteriol.* **2019**, JB.00028-19, doi:10.1128/JB.00028-19.
121. Klotz, A.; Forchhammer, K. Glycogen, a Major Player for Bacterial Survival and Awakening from Dormancy. *Future Microbiol.* **2017**, *12*, 101–104, doi:10.2217/fmb-2016-0218.

122. Patel, A.; Malinovska, L.; Saha, S.; Wang, J.; Alberti, S.; Krishnan, Y.; Hyman, A.A. ATP as a Biological Hydrotrope. *Science* **2017**, *356*, 753–756.
123. Booth, I.R.; Higgins, C.F. Enteric Bacteria and Osmotic Stress: Intracellular Potassium Glutamate as a Secondary Signal of Osmotic Stress? *FEMS Microbiol. Rev.* **1990**, *6*, 239–246, doi:10.1111/j.1574-6968.1990.tb04097.x.
124. Ignasiak, M.; Frackowiak, K.; Pedzinski, T.; Davies, M.J.; Marciniak, B. Unexpected Light Emission from Tyrosyl Radicals as a Probe for Tyrosine Oxidation. *Free Radic. Biol. Med.* **2020**, *153*, 12–16, doi:10.1016/j.freeradbiomed.2020.03.022.
125. Hoganson, C.W.; Tommos, C. The Function and Characteristics of Tyrosyl Radical Cofactors. *Biochim. Biophys. Acta BBA - Bioenerg.* **2004**, *1655*, 116–122, doi:10.1016/j.bbabio.2003.10.017.
126. Shi, H.; Westfall, C.S.; Kao, J.; Odermatt, P.D.; Anderson, S.E.; Cesar, S.; Sievert, M.; Moore, J.; Gonzalez, C.G.; Zhang, L.; et al. Starvation Induces Shrinkage of the Bacterial Cytoplasm. *Proc. Natl. Acad. Sci.* **2021**, *118*, e2104686118, doi:10.1073/pnas.2104686118.
127. Newton, A.C.; Bootman, M.D.; Scott, J.D. Second Messengers. *Cold Spring Harb. Perspect. Biol.* **2016**, *8*, a005926, doi:10.1101/cshperspect.a005926.
128. Burnap, R.; Hagemann, M.; Kaplan, A. Regulation of CO2 Concentrating Mechanism in Cyanobacteria. *Life* **2015**, *5*, 348–371, doi:10.3390/life5010348.
129. Römling, U. Great Times for Small Molecules: C-Di-AMP, a Second Messenger Candidate in Bacteria and Archaea. *Sci. Signal.* **2008**, *1*, pe39–pe39, doi:10.1126/scisignal.133pe39.
130. Corrigan, R.M.; Gründling, A. Cyclic Di-AMP: Another Second Messenger Enters the Fray. *Nat. Rev. Microbiol.* **2013**, *11*, 513–524, doi:10.1038/nrmicro3069.
131. Braun, F.; Thomalla, L.; van der Does, C.; Quax, T.E.F.; Allers, T.; Kaever, V.; Albers, S.-V. Cyclic Nucleotides in Archaea: Cyclic Di-AMP in the Archaeon Haloferax Volcanii and Its Putative Role. *MicrobiologyOpen* **2019**, *0*, e829, doi:10.1002/mbo3.829.
132. Witte, G.; Hartung, S.; Büttner, K.; Hopfner, K.-P. Structural Biochemistry of a Bacterial Checkpoint Protein Reveals Diadenylate Cyclase Activity Regulated by DNA Recombination Intermediates. *Mol. Cell* **2008**, *30*, 167–178, doi:10.1016/j.molcel.2008.02.020.
133. Stülke, J.; Krüger, L. Cyclic Di-AMP Signaling in Bacteria. *Annu. Rev. Microbiol.* **2020**, *74*, 159–179, doi:10.1146/annurev-micro-020518-115943.
134. Gundlach, J.; Herzberg, C.; Kaever, V.; Gunka, K.; Hoffmann, T.; Weiß, M.; Gibhardt, J.; Thürmer, A.; Hertel, D.; Daniel, R.; et al. Control of Potassium Homeostasis Is an Essential Function of the Second Messenger Cyclic Di-AMP in *Bacillus Subtilis*. *Sci. Signal.* **2017**, *10*, eaal3011, doi:10.1126/scisignal.aal3011.
135. Devaux, L.; Sleiman, D.; Mazzuoli, M.-V.; Gominet, M.; Lanotte, P.; Trieu-Cuot, P.; Kaminski, P.-A.; Firon, A. Cyclic Di-AMP Regulation of Osmotic Homeostasis Is Essential in Group B Streptococcus. *PLoS Genet.* **2018**, *14*, doi:10.1371/journal.pgen.1007342.
136. Gundlach, J.; Mehne, F.M.P.; Herzberg, C.; Kampf, J.; Valerius, O.; Kaever, V.; Stülke, J. An Essential Poison: Synthesis and Degradation of Cyclic Di-AMP in Bacillus Subtilis. *J. Bacteriol.* **2015**, *197*, 3265–3274, doi:10.1128/JB.00564-15.
137. Mehne, F.M.P.; Gunka, K.; Eilers, H.; Herzberg, C.; Kaever, V.; Stülke, J. Cyclic Di-AMP Homeostasis in Bacillus Subtilis. *J. Biol. Chem.* **2013**, *288*, 2004–2017, doi:10.1074/jbc.M112.395491.
138. Huynh, T.N.; Luo, S.; Pensinger, D.; Sauer, J.-D.; Tong, L.; Woodward, J.J. An HD-Domain Phosphodiesterase Mediates Cooperative Hydrolysis of c-Di-AMP to Affect Bacterial Growth and Virulence. *Proc. Natl. Acad. Sci. U. S. A.* **2015**, *112*, E747–E756, doi:10.1073/pnas.1416485112.
139. Gundlach, J.; Krüger, L.; Herzberg, C.; Turdiev, A.; Poehlein, A.; Tascón, I.; Weiß, M.; Hertel, D.; Daniel, R.; Hänelt, I.; et al. Sustained Sensing in Potassium Homeostasis: Cyclic Di-AMP Controls Potassium Uptake by KimA at the Levels of Expression and Activity. *J. Biol. Chem.* **2019**, doi:10.1074/jbc.RA119.008774.
140. Quintana, I.M.; Gibhardt, J.; Turdiev, A.; Hammer, E.; Commichau, F.M.; Lee, V.T.; Magni, C.; Stülke, J. The KupA and KupB Proteins of Lactococcus Lactis IL1403 Are Novel C-Di-AMP

Receptor Proteins Responsible for Potassium Uptake. *J. Bacteriol.* **2019**, JB.00028-19, doi:10.1128/JB.00028-19.
141. Bremer, E.; Krämer, R. Responses of Microorganisms to Osmotic Stress. *Annu. Rev. Microbiol.* **2019**, *73*, 313–334, doi:10.1146/annurev-micro-020518-115504.
142. Wang, X.; Cai, X.; Ma, H.; Yin, W.; Zhu, L.; Li, X.; Lim, H.M.; Chou, S.-H.; He, J. A C-Di-AMP Riboswitch Controlling kdpFABC Operon Transcription Regulates the Potassium Transporter System in Bacillus Thuringiensis. *Commun. Biol.* **2019**, *2*, doi:10.1038/s42003-019-0414-6.
143. Nelson, J.W.; Sudarsan, N.; Furukawa, K.; Weinberg, Z.; Wang, J.X.; Breaker, R.R. Riboswitches in Eubacteria Sense the Second Messenger C-Di-AMP. *Nat. Chem. Biol.* **2013**, *9*, 834–839, doi:10.1038/nchembio.1363.
144. Rubin, B.E.; Huynh, T.N.; Welkie, D.G.; Diamond, S.; Simkovsky, R.; Pierce, E.C.; Taton, A.; Lowe, L.C.; Lee, J.J.; Rifkin, S.A.; et al. High-Throughput Interaction Screens Illuminate the Role of c-Di-AMP in Cyanobacterial Nighttime Survival. *PLOS Genet.* **2018**, *14*, e1007301, doi:10.1371/journal.pgen.1007301.
145. Selim, K.A.; Haffner, M.; Burkhardt, M.; Mantovani, O.; Neumann, N.; Albrecht, R.; Seifert, R.; Krüger, L.; Stülke, J.; Hartmann, M.D.; et al. Diurnal Metabolic Control in Cyanobacteria Requires Perception of Second Messenger Signaling Molecule C-Di-AMP by the Carbon Control Protein SbtB. *Sci. Adv.* **2021**, *7*, eabk0568, doi:10.1126/sciadv.abk0568.
146. Agostoni, M.; Logan-Jackson, A.R.; Heinz, E.R.; Severin, G.B.; Bruger, E.L.; Waters, C.M.; Montgomery, B.L. Homeostasis of Second Messenger Cyclic-Di-AMP Is Critical for Cyanobacterial Fitness and Acclimation to Abiotic Stress. *Front. Microbiol.* **2018**, *9*, doi:10.3389/fmicb.2018.01121.
147. Görl, M.; Sauer, J.; Baier, T.; Forchhammer, K. Nitrogen-Starvation-Induced Chlorosis in Synechococcus PCC 7942: Adaptation to Long-Term Survival. *Microbiology* **1998**, *144*, 2449–2458.
148. Sauer, J.; Schreiber, U.; Schmid, R.; Völker, U.; Forchhammer, K. Nitrogen Starvation-Induced Chlorosis in Synechococcus Pcc 7942. Low-Level Photosynthesis as a Mechanism of Long-Term Survival. *Plant Physiol.* **2001**, *126*, 233–243.
149. Forchhammer, K.; Schwarz, R. Nitrogen Chlorosis in Unicellular Cyanobacteria – a Developmental Program for Surviving Nitrogen Deprivation. *Environ. Microbiol.* **2019**, *21*, 1173–1184, doi:10.1111/1462-2920.14447.
150. Neumann, N.; Doello, S.; Forchhammer, K. Recovery of Unicellular Cyanobacteria from Nitrogen Chlorosis: A Model for Resuscitation of Dormant Bacteria. *Microb. Physiol.* **2021**, *31*, 1–10, doi:10.1159/000515742.
151. Díaz-Troya, S.; Roldán, M.; Mallén-Ponce, M.J.; Ortega-Martínez, P.; Florencio, F.J. Lethality Caused by ADP-Glucose Accumulation Is Suppressed by Salt-Induced Carbon Flux Redirection in Cyanobacteria. *J. Exp. Bot.* **2020**, *71*, 2005–2017, doi:10.1093/jxb/erz559.
152. Spät, P.; Klotz, A.; Rexroth, S.; Maček, B.; Forchhammer, K. Chlorosis as a Developmental Program in Cyanobacteria: The Proteomic Fundament for Survival and Awakening. *Mol. Cell. Proteomics MCP* **2018**, *17*, 1650–1669, doi:10.1074/mcp.RA118.000699.
153. Watzer, B.; Forchhammer, K. Cyanophycin Synthesis Optimizes Nitrogen Utilization in the Unicellular Cyanobacterium Synechocystis Sp. Strain PCC 6803. *Appl. Environ. Microbiol.* **2018**, *84*, e01298-18, doi:10.1128/AEM.01298-18.
154. Burkhardt, M.; Rapp, J.; Menzel, C.; Link, H.; Forchhammer, K. The Global Influence of Sodium on Cyanobacteria in Resuscitation from Nitrogen Starvation. *Biology* **2023**, *12*, 159, doi:10.3390/biology12020159.
155. Doello, S.; Burkhardt, M.; Forchhammer, K. The Essential Role of Sodium Bioenergetics and ATP Homeostasis in the Developmental Transitions of a Cyanobacterium. *Curr. Biol.* **2021**, S0960982221001305, doi:10.1016/j.cub.2021.01.065.
156. Krauspe, V.; Timm, S.; Hagemann, M.; Hess, W.R. Phycobilisome Breakdown Effector NblD Is Required To Maintain Cellular Amino Acid Composition during Nitrogen Starvation. *J. Bacteriol.* **2022**, *204*, e00158-21, doi:10.1128/jb.00158-21.

157. Commichau, F.M.; Stülke, J. Coping with an Essential Poison: A Genetic Suppressor Analysis Corroborates a Key Function of c-Di-AMP in Controlling Potassium Ion Homeostasis in Gram-Positive Bacteria. *J. Bacteriol.* **2018**, JB.00166-18, doi:10.1128/JB.00166-18.
158. Fontecave, M.; Atta, M.; Mulliez, E. S-Adenosylmethionine: Nothing Goes to Waste. *Trends Biochem. Sci.* **2004**, *29*, 243–249, doi:10.1016/j.tibs.2004.03.007.
159. Shi, H.; Westfall, C.S.; Kao, J.; Odermatt, P.D.; Anderson, S.E.; Cesar, S.; Sievert, M.; Moore, J.; Gonzalez, C.G.; Zhang, L.; et al. Starvation Induces Shrinkage of the Bacterial Cytoplasm. *Proc. Natl. Acad. Sci.* **2021**, *118*, e2104686118, doi:10.1073/pnas.2104686118.
160. Schink, S.; Polk, M.; Athaide, E.; Mukherjee, A.; Ammar, C.; Liu, X.; Oh, S.; Chang, Y.-F.; Basan, M. The Energy Requirements of Ion Homeostasis Determine the Lifespan of Starving Bacteria 2022, 2021.11.22.469587.
161. Mantovani, O.; Reimann, V.; Haffner, M.; Herrmann, F.P.; Selim, K.A.; Forchhammer, K.; Hess, W.R.; Hagemann, M. The Impact of the Cyanobacterial Carbon-Regulator Protein SbtB and of the Second Messengers cAMP and c-Di-AMP on CO2-Dependent Gene Expression. *New Phytol.* **2022**, *234*, 1801–1816, doi:10.1111/nph.18094.
162. Cheng, X.; Guinn, E.J.; Buechel, E.; Wong, R.; Sengupta, R.; Shkel, I.A.; Record, M.T. Basis of Protein Stabilization by K Glutamate: Unfavorable Interactions with Carbon, Oxygen Groups. *Biophys. J.* **2016**, *111*, 1854–1865, doi:10.1016/j.bpj.2016.08.050.
163. Wood, J.M.; Bremer, E.; Csonka, L.N.; Kraemer, R.; Poolman, B.; van der Heide, T.; Smith, L.T. Osmosensing and Osmoregulatory Compatible Solute Accumulation by Bacteria. *Comp. Biochem. Physiol. A. Mol. Integr. Physiol.* **2001**, *130*, 437–460, doi:10.1016/S1095-6433(01)00442-1.
164. Götz, F.; Longnecker, K.; Soule, M.C.K.; Becker, K.W.; McNichol, J.; Kujawinski, E.B.; Sievert, S.M. Targeted Metabolomics Reveals Proline as a Major Osmolyte in the Chemolithoautotroph Sulfurimonas Denitrificans. *MicrobiologyOpen* **2018**, *7*, doi:10.1002/mbo3.586.
165. Sleator, R.D.; Hill, C. Bacterial Osmoadaptation: The Role of Osmolytes in Bacterial Stress and Virulence. *FEMS Microbiol. Rev.* **2002**, *26*, 49–71, doi:10.1111/j.1574-6976.2002.tb00598.x.
166. Rittershaus, E.S.C.; Baek, S.; Sassetti, C.M. The Normalcy of Dormancy. *Cell Host Microbe* **2013**, *13*, 643–651, doi:10.1016/j.chom.2013.05.012.

VIII. Appendix

Publication 1 (Accepted)

Research Article

Sofía Doello, Markus Burkhardt, and Karl Forchhammer

The essential role of sodium bioenergetics and ATP homeostasis in the developmental transitions of a cyanobacterium.

2021. *Current Biology.* 20, 31, 1-10

Article

Current Biology

The essential role of sodium bioenergetics and ATP homeostasis in the developmental transitions of a cyanobacterium

Graphical Abstract

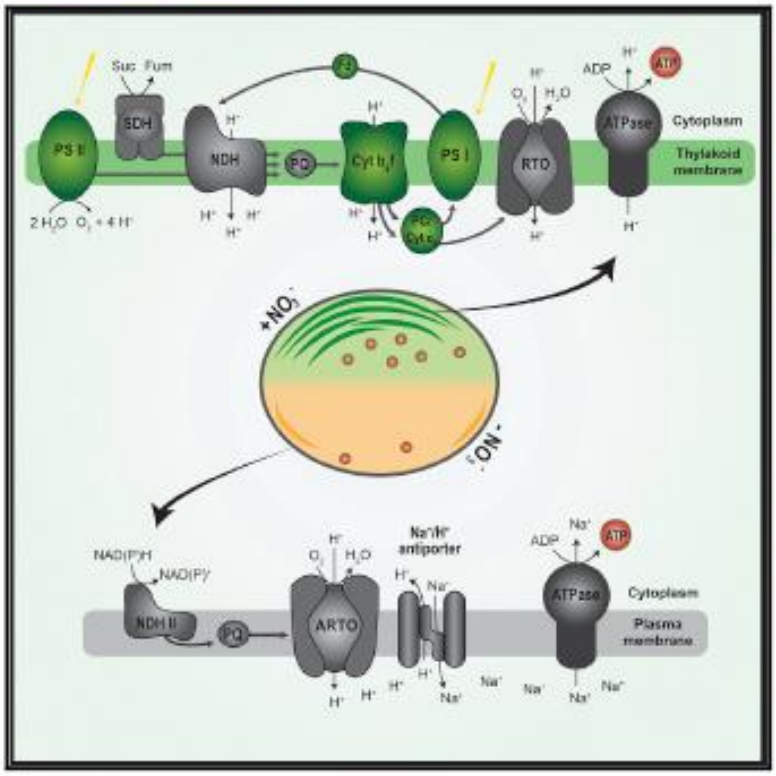

Authors

Sofia Doello, Markus Burkhardt, Karl Forchhammer

Correspondence

karl.forchhammer@uni-tuebingen.de

In Brief

How do dormant cells obtain energy to survive and resume growth after prolonged nutrient starvation? Doello et al. use nitrogen-starved *Synechocystis* cells to investigate the regulation of ATP homeostasis during dormancy and unravel a critical role for sodium bioenergetics and a precise regulation of the energy metabolism in dormant cells.

Highlights

- *Synechocystis* engages sodium bioenergetics during nitrogen starvation
- Sodium-dependent ATP synthesis is only essential during metabolic dormancy
- ATP levels are finely tuned according to the metabolic requirements

Doello et al., 2021, Current Biology *31*, 1606–1615
April 26, 2021 © 2021 The Author(s). Published by Elsevier Inc.
https://doi.org/10.1016/j.cub.2021.01.065

CellPress

CellPress
OPEN ACCESS

Current Biology

Article

The essential role of sodium bioenergetics and ATP homeostasis in the developmental transitions of a cyanobacterium

Sofia Doello,[1] Markus Burkhardt,[1] and Karl Forchhammer[1,2,*]
[1]Interfaculty Institute of Microbiology and Infection Medicine, University of Tübingen, Auf der Morgenstelle 28, 72076 Tübingen, Germany
[2]Lead contact
*Correspondence: karl.forchhammer@uni-tuebingen.de
https://doi.org/10.1016/j.cub.2021.01.065

SUMMARY

The ability to resume growth after a dormant period is an important strategy for the survival and spreading of bacterial populations. Energy homeostasis is critical in the transition into and out of a quiescent state. *Synechocystis* sp. PCC 6803, a non-diazotrophic cyanobacterium, enters metabolic dormancy as a response to nitrogen starvation. We used *Synechocystis* as a model to investigate the regulation of ATP homeostasis during dormancy, and we unraveled a critical role for sodium bioenergetics in dormant cells. During nitrogen starvation, cells reduce their ATP levels and engage sodium bioenergetics to maintain the minimum ATP content required for viability. When nitrogen becomes available, energy requirements rise, and cells immediately increase ATP levels, employing sodium bioenergetics and glycogen catabolism. These processes allow them to restore the photosynthetic machinery and resume photoautotrophic growth. Our work reveals a precise regulation of the energy metabolism essential for bacterial survival during periods of nutrient deprivation.

INTRODUCTION

Dormant micro-organisms are vastly represented in natural environments.[1] Dormancy highly contributes to the survival of bacterial populations, the spreading of pathogens, and the development of antibiotic resistances.[2] The molecular processes that lead bacterial cells into a dormant state are diverse but generally characterized by growth arrest and residual metabolic activity.[3] Despite having a reduced metabolism, dormant cells still require energy for maintenance.[1] In fact, energy homeostasis is critical for the survival of dormant cells.[3] However, how the energy metabolism is regulated when bacterial cells enter and exit periods of dormancy is to date poorly understood.

Cyanobacteria represent a diverse group of prokaryotes endowed with the ability to adapt to changing environmental conditions, which has allowed them to colonize a wide range of ecosystems.[4] One of the most common hurdles cyanobacteria face in natural environments is limitation of combined nitrogen.[5] *Synechocystis* sp. PCC 6803 (*Synechocystis*) is a non-diazotrophic cyanobacterial strain that survives periods of nitrogen starvation by entering metabolic quiescence, thus representing a good model to study fundamental aspects of bacterial dormancy.[6] *Synechocystis* can survive prolonged periods of nitrogen starvation by undergoing nitrogen-chlorosis, a process characterized by the degradation of most of the thylakoid membranes. Cells enter cell cycle arrest and shut down their metabolism. Most of the photosynthetic apparatus is degraded, leaving cells with residual photosynthetic capacity, and energetically costly processes, like anabolic reactions, are halted.[6] In this resting state, the intracellular ATP concentration is about ¼ of the level during vegetative growth.[7] In addition, as cells degrade most of their cellular components, they synthesize reserve polymers, which are essential for exiting dormancy and resuming growth. Glycogen is the main storage molecule during nitrogen starvation: its synthesis and degradation are crucial for cell survival under these conditions.[6–8]

When nitrogen becomes available to dormant cells, they immediately initiate a highly organized resuscitation program.[6,9] During the first stages of the resuscitation process, cells catabolize the accumulated glycogen to obtain energy and metabolic intermediates to restore the previously degraded cellular components. When the photosynthetic machinery is restored, cells switch back to phototrophic metabolism.[6] Upon nitrogen addition, the energy requirement of chlorotic cells suddenly increases due to the initiation of anabolic reactions, such as the glutamine synthetase/glutamate synthase (GS/GOGAT) reaction cycle. Concomitantly with the increased energy demand, the low ATP content of dormant cells rapidly increases to an intermediate level, which represents approximately 50% of the ATP content of a vegetative growing cell.[7] So far, how dormant cells produce this ATP has remained unknown. Intriguingly, we observed a rapid increase in ATP levels also in mutant cells unable to degrade glycogen.[7] This observation prompted us to investigate the source of the rise in ATP content in resuscitating cells. The aim of this study was to reveal how dormant cells maintain the required ATP levels to keep viability and how they obtain the necessary energy to awaken from dormancy.

This is an open access article under the CC BY-NC-ND license (http://creativecommons.org/licenses/by-nc-nd/4.0/).

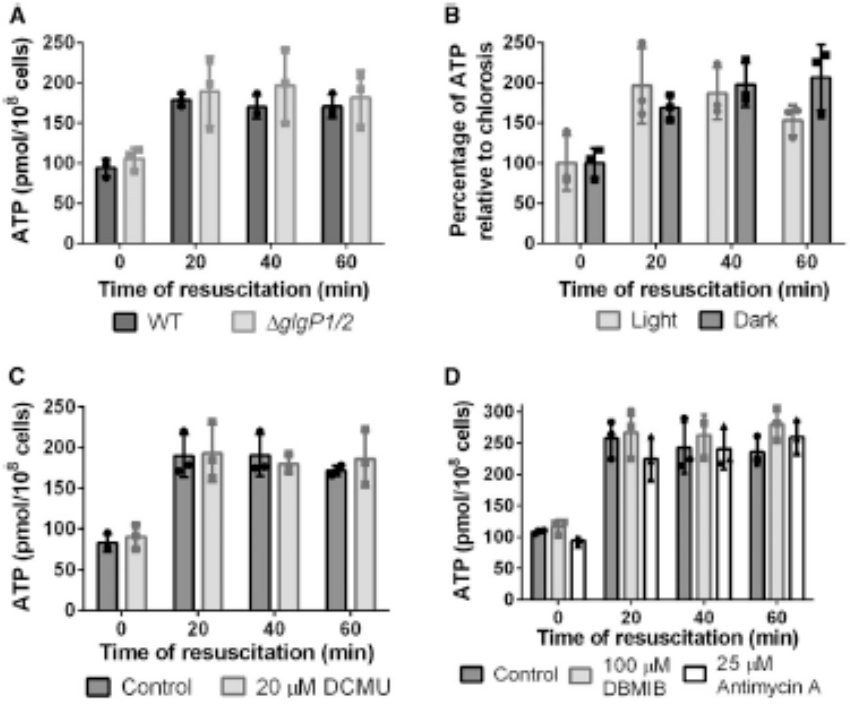

Figure 1. The rapid increase in ATP levels upon $NaNO_3$ addition is independent of glycogen catabolism and photosynthesis

(A) ATP content normalized to 1 × 10^8 cells of WT and Δ*glgP1/2* chlorotic cells after addition of 17 mM $NaNO_3$.

(B) WT chlorotic cells after incubation for 1 h in darkness and addition of 17 mM $NaNO_3$.

(C and D) WT chlorotic cells treated with (C) 20 μM DCMU and (D) 100 μM DBMIB and 25 μM antimycin A. Cells were treated for 5 min before the first measurement (0 min). Resuscitation was then induced by addition of 17 mM $NaNO_3$. At least three biological replicates were measured; error bars represent the SD; asterisks represent the statistical significance.

See also Figures S1 and S2.

RESULTS

The rapid ATP increase in response to nitrogen availability is independent of glycogen degradation and photosynthesis

Upon nitrogen addition, cells start the resuscitation program and their energy demands increase. Cells must then produce ATP to support nitrogen assimilation and biosynthetic processes. We measured the intracellular ATP levels within the first hour of resuscitation and observed an increase of ~100% in the ATP content 20 min after the addition of $NaNO_3$, and these levels were maintained for the first hour of recovery (Figure 1A). This ATP increase constitutes the fastest measured response of chlorotic cells to the presence of nitrogen,[6] but how it is produced is not yet understood.

A rise in the ATP levels might seem an obvious consequence of activating a dormant metabolism and entering a transient phase of heterotrophy. It is tempting to assume that the increased ATP values at the start of resuscitation come from the onset of glycogen catabolism, which is induced soon after the addition of $NaNO_3$ to dormant cells.[6] Previously, we observed that a mutant lacking the glycogen phosphorylases (Δ*glgP1/2*) displayed elevated ATP levels 3 h after $NaNO_3$ addition, but these cells did not further recover. Here, we compared the short-term response in ATP levels between Δ*glgP1/2* and wild type (WT) in more detail and found that $NaNO_3$ triggered a similar rapid ATP increase in the Δ*glgP1/2* mutant as it did in the WT, implying that the onset of ATP synthesis does not depend on glycogen catabolism (Figure 1A). Respiration of other metabolites can be excluded, because Δ*glgP1/2* does not show any oxygen consumption upon addition of $NaNO_3$. In fact, the rise in ATP levels happened before cells perform respiration at full capacity. During nitrogen-chlorosis, cells display residual photosynthetic activity, which is completely repressed after a few hours of resuscitation, when degradation of glycogen is fully operating.[7] Pulse-amplitude modulation (PAM) fluorometry measurements revealed that, 1 h after nitrate addition, much after an ATP increase is measurable, glycogen catabolism has not yet suppressed PSII activity (Figure S1). After 2 h of resuscitation, when cells are fully respirating, the PSII activity disappears and only resumes when cells have partially restored their photosynthetic machinery (~12 h after nitrate addition). Thus, the increase in ATP levels during early resuscitation could depend on photosynthesis instead of respiration. To test this possibility, we measured the ATP content of dark-incubated cells (Figure 1B). Although ATP levels were overall lower in the dark than in the light, addition of $NaNO_3$ caused a similar increase under both conditions. To completely exclude the role of photosynthesis on the rise of ATP levels, we treated chlorotic cells with different photosynthetic inhibitors. Exposure to dichlorophenyl dimethylurea (DCMU), which blocks the electron transfer from PSII to the plastoquinone (PQ) (Figure 1C), dibromthymochinon (DBMIB), which inhibits the electron flow from PQ to the cytochrome b_6f (Cyt b_6f), and antimycin A, which disrupts the Q cycle in Cyt b_6f (Figure 1D), did not affect the cell's ability to produce ATP after addition of $NaNO_3$, although treated cells showed impaired resuscitation from nitrogen starvation (Figure S2).

The ATP increase relies on a sodium motive force

Respiration and photosynthesis are the two main bioenergetic processes that generate an electrochemical proton gradient that can be used by the ATP synthase to power ATP production. When both processes were blocked, nitrogen-starved cells could still increase ATP levels upon addition of $NaNO_3$. To elucidate the contribution of proton motive force (*PMF*) to the ATP increase, chlorotic cells were treated with the protonophores carbonyl cyanide m-chlorophenyl hydrazone (CCCP) and 2,3-dinitrophenol (DNP). Protonophores make membranes permeable to protons, destroying proton gradients. Although treatment with CCCP and DNP prevented resuscitation (Figure S2), it did

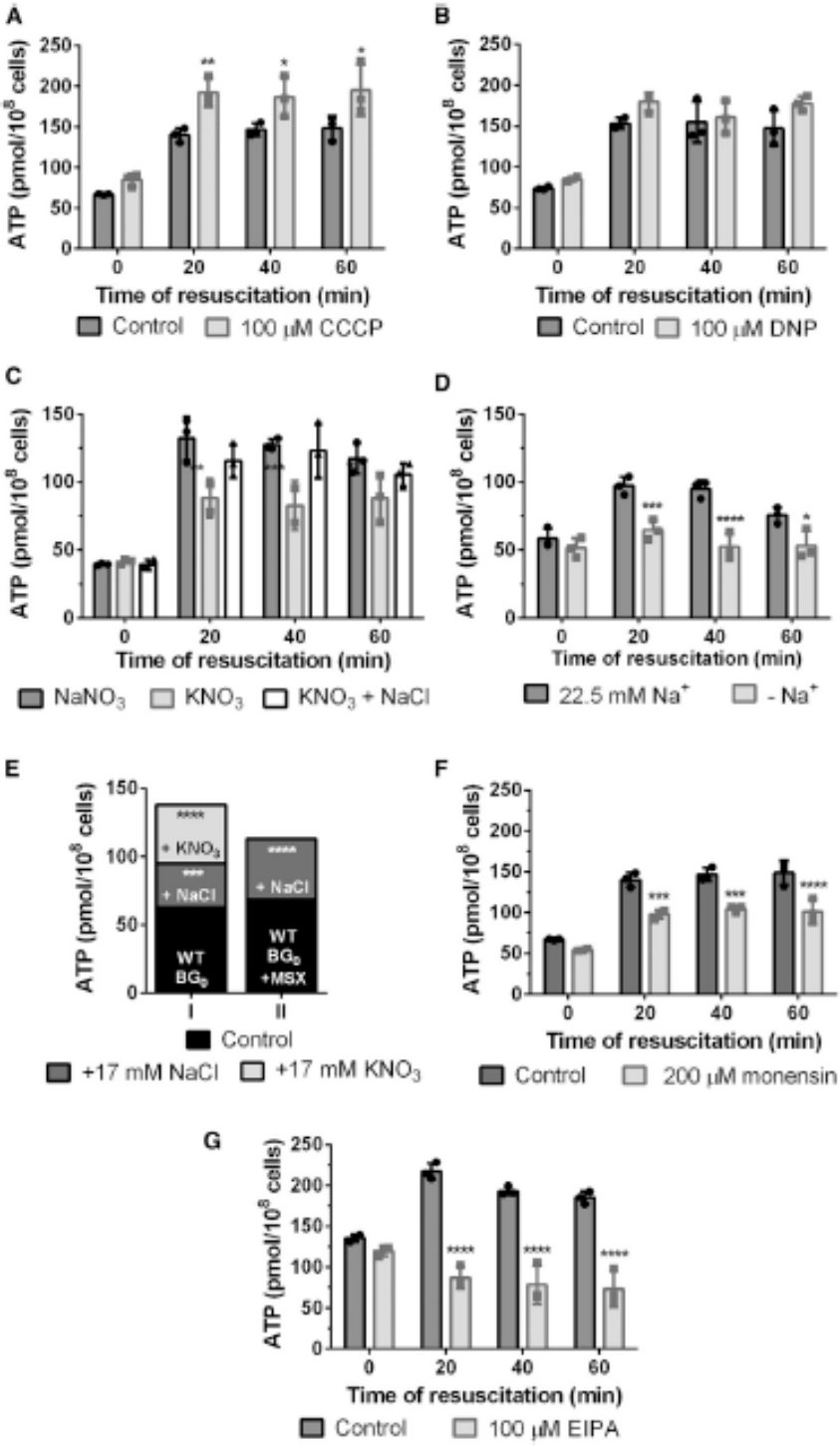

Figure 2. The rise of cellular ATP upon $NaNO_3$ addition does not rely on a proton gradient and is a response to both increased sodium concentrations and nitrogen assimilation

(A and B) ATP content normalized to 1×10^8 cells of WT chlorotic cells treated with (A) 100 µM CCCP and (B) 100 µM DNP. Cells were treated for 5 min before the first measurement (0 min). Resuscitation was then induced by addition of 17 mM $NaNO_3$.

(C) Cells were resuscitated using either 17 mM $NaNO_3$, 17 mM KNO_3, or 17 mM KNO_3 + 17 mM NaCl.

(D) Cells were washed twice with $BG_{11\text{-}0\text{-}Na}$ sodium-free medium and resuscitated with 17 mM KNO_3.

(E) ATP content normalized to 1×10^8 cells of chlorotic cells in $BG_{11\text{-}0}$ (black), after supplementation with 17 mM NaCl (dark gray), and after additional supplementation with 17 mM KNO_3 (light gray). Column I: untreated WT chlorotic cells supplemented with 17 mM NaCl and 17 mM KNO_3 are shown. Column II: WT chlorotic cells treated with 200 µM MSX and supplemented with 17 mM NaCl and 17 mM KNO_3 are shown.

(F) Chlorotic cells treated with 200 µM monensin.

(G) Chlorotic cells treated with 100 µM EIPA.

In (F) and (G), cells were treated for 5 min before the first measurement (0 min) and then resuscitation was induced by addition of 5 mM NH_4Cl + 17 mM NaCl. At least three biological replicates were measured; error bars represent the SD; asterisks represent the statistical significance. See also Figure S2.

not abolish the rise in ATP levels (Figures 2A and 2B). In fact, treatment with CCCP led to a higher ATP production in chlorotic cells after addition of $NaNO_3$, indicating that ATP synthesis does not depend on an electrochemical proton gradient. However, protons are not the only ions that can be used for ATP synthesis, as some ATP synthases can also use a sodium motive force (*SMF*) to power ATP production.[10] Sodium ions are more abundant in the extracellular medium than in the cytoplasm and form a gradient across the plasma membrane that can be utilized by sodium-binding ATP synthases to produce ATP. Besides the thylakoidal ATP synthases, which translocate proton from the thylakoid lumen to the cytoplasm to produce ATP, *Synechocystis* also possesses ATP synthases in the plasma membrane,[11] which might use an *SMF*.

The above experiments were performed by adding 17 mM $NaNO_3$ to chlorotic cells in nitrogen-free $BG_{11\text{-}0}$ medium, increasing the sodium concentration 4-fold. This raised the question whether the rapid increase of intracellular ATP is connected to the sudden rise in sodium levels. To test this, recovery experiments were performed by the addition of 17 mM KNO_3 to cells in $BG_{11\text{-}0}$ (Figure 2C). In this case, the concentration of sodium remained constant. Remarkably, the ATP increase was significantly lower than in the previous experiments with the addition of 17 mM $NaNO_3$. The rapid rise in ATP levels could be restored when 17 mM NaCl was added together with KNO_3 to dormant cells (Figure 2C). When sodium was completely removed from the medium by washing with $BG_{11\text{-}0\text{-}Na}$ (in which sodium salts have been

substituted by potassium salts), addition of KNO_3 triggered almost no increase of ATP levels (Figure 2D). These results demonstrated that sodium plays an important role in ATP synthesis in chlorotic cells. However, whether or not the addition of a nitrogen source also contributes to the rise in ATP levels remained unclear. To address this question, sodium and nitrogen were added to dormant cells sequentially (Figure 2E). The sole addition of 17 mM NaCl to chlorotic cells in BG_{11-0} caused a partial increase of the ATP levels within 20 min, compared to the standard resuscitation experiment. When 20 min after supplementation with NaCl a nitrogen source was added to the cells in the form of KNO_3 (Figure 2E, column I), a further rise in ATP levels was observed after 1 h. This indicates that the rise in ATP levels after addition of $NaNO_3$ to chlorotic cells has two components: one due to the increase in the sodium concentration and another one due to the presence of nitrogen. To distinguish whether cells sense the presence of nitrogen or detect it through initiating assimilation via the GS-GOGAT cycle, cells were treated with the GS inhibitor L-methionine sulfoximine (MSX). This treatment completely abolished the nitrogen-dependent component of the ATP increase (Figure 2E, column II), indicating that activation of nitrogen assimilation is required for the nitrogen-dependent ATP increase.

To corroborate the role of sodium in ATP synthesis during chlorosis, nitrogen-starved cells were treated with monensin, a sodium ionophore, and ethyl-isopropyl amiloride (EIPA), an inhibitor of sodium channels and sodium/proton antiport. To exclude any indirect effects caused by possible interference of the inhibitors with nitrate transport, the effect of monensin and EIPA on the ATP content was measured after adding a combination of NH_4Cl and NaCl to chlorotic cells. Treatment with monensin led to lower ATP levels than the untreated control (Figure 2F). Strikingly, exposure to EIPA completely abolished the ATP increase (Figure 2G), proving the key role of sodium bioenergetics in chlorotic cells.

An increase in the sodium motive force provides a source of free energy for dormant cells

The results above showed that ATP synthesis was stimulated in dormant cells by increasing the concentration of sodium, which contributes to a rise in the *SMF*. The ion motive force (*IMF*) is the electrochemical gradient of an ion across the membrane and depends on the membrane potential and the concentration of the ion at both sides of the membrane. For an ion with charge z, its *IMF* is

$$IMF(mV) = V_m - \frac{RT}{zF} ln \frac{C_{out}}{C_{in}},$$

where V_m is the membrane potential, R the gas constant, F the Faraday constant, C_{in} the concentration of ion inside the cell, and C_{out} the concentration of ion outside the cell.[12] Raising the extracellular sodium concentration from 5.5 mM to 17 mM contributes to the *SMF* with approximately −30 mV, which suggests that, for increasing ATP synthesis, there should already be sufficient V_m in chlorotic cells. To estimate this residual V_m, we used the fluorescent voltage reporter bis-(1,3-dibutylbarbituric acid)-trimethine oxonol (DiBAC4(3)). DiBAC4(3) penetrates depolarized cells, exhibiting enhanced fluorescence in the cytoplasm, but does not enter cells with an intact V_m. As a control, we used cells killed by heat inactivation and vegetative cells. Killed cells showed high permeability to DiBAC4(3), whereas no signs of fluorescence were detected in vegetative cells (Figure 3A). 1-month-chlorotic cells showed a more heterogeneous population: although most cells showed no fluorescence, some were stained by DiBAC4(3). This heterogeneity agrees with the fact that, after a month of nitrogen starvation, not all cells keep viability. However, most chlorotic cells did not show fluorescence, indicating they maintain a similar membrane potential than vegetative cells, which, in addition to the extra voltage obtained after addition of 17 mM NaCl, constitutes sufficient *SMF* to drive ATP synthesis.

To confirm that the ATP increase depends on a rise of the *SMF*, we provided cells with different concentrations of NaCl (Figure 3B). Supplementation with 17 mM NaCl triggered an ~100% increase in ATP levels, whereas addition of 50 mM NaCl led to an ~150% increase, which agrees with the proposed models for ATP yield as a function of the *IMF*.[13,14] To ascertain whether the ATP synthases are responsible for this change in ATP levels, we treated chlorotic cells with N,N'-dicyclohexylcarbodiimide (DCCD), an F-ATPase inhibitor. DCCD-treated cells showed a reduced response to NaCl as compared to untreated cells (Figure 3C), confirming that the non-nitrogen-dependent component of the ATP increase is a purely physico-chemical effect of increasing the concentration of sodium and that it relies on the activity of the ATP synthases.

The nitrogen-dependent component of the ATP increase requires respiration

The metabolically induced ATP increase required activation of the GS-GOGAT cycle, but how initiation of nitrogen assimilation leads to ATP synthesis remained to be addressed. Our previous data showed that addition of a nitrogen source to dormant cells induced glycogen degradation.[6] Glycogen degradation supports ATP synthesis by producing reduction equivalents to support respiration and to a smaller extent by substrate-level phosphorylation. To reveal the contribution of glycogen catabolism on the metabolically induced ATP-level increase, we tested the effect of NaCl and KNO_3 on Δ*glgP1/2*. As the MSX-treated cells, Δ*glgP1/2* only reacted to sodium and did not show the nitrogen-dependent component of the ATP increase (Figure 4, column B), confirming that this second component depends on glycogen degradation. To elucidate whether respiration is required to generate ATP upon nitrate addition, we measured the ATP content of chlorotic cells after treatment with potassium cyanide (KCN), which prevents electron transfer from the terminal oxidases to oxygen, inhibiting the respiratory chain. KCN-treated cells increased their ATP levels after addition of NaCl, but not after supplementation with KNO_3 (Figure 4, column C). This indicated that respiration is essential for the metabolically induced increase of ATP levels during early resuscitation. Interestingly, treatment with DBMIB, which blocks the electron transport chain at the Cyt b_6f, did not inhibit the nitrogen-dependent component of the ATP increase (Figure 4, column D), suggesting that respiration takes place on the plasma membrane, because cytochrome b_6f is a specific component of the thylakoid membranes.[15]

Sodium requirement depends on the cellular growth stage

Hitherto, it remained unclear whether cells engage sodium bioenergetics exclusively during nitrogen-chlorosis or whether

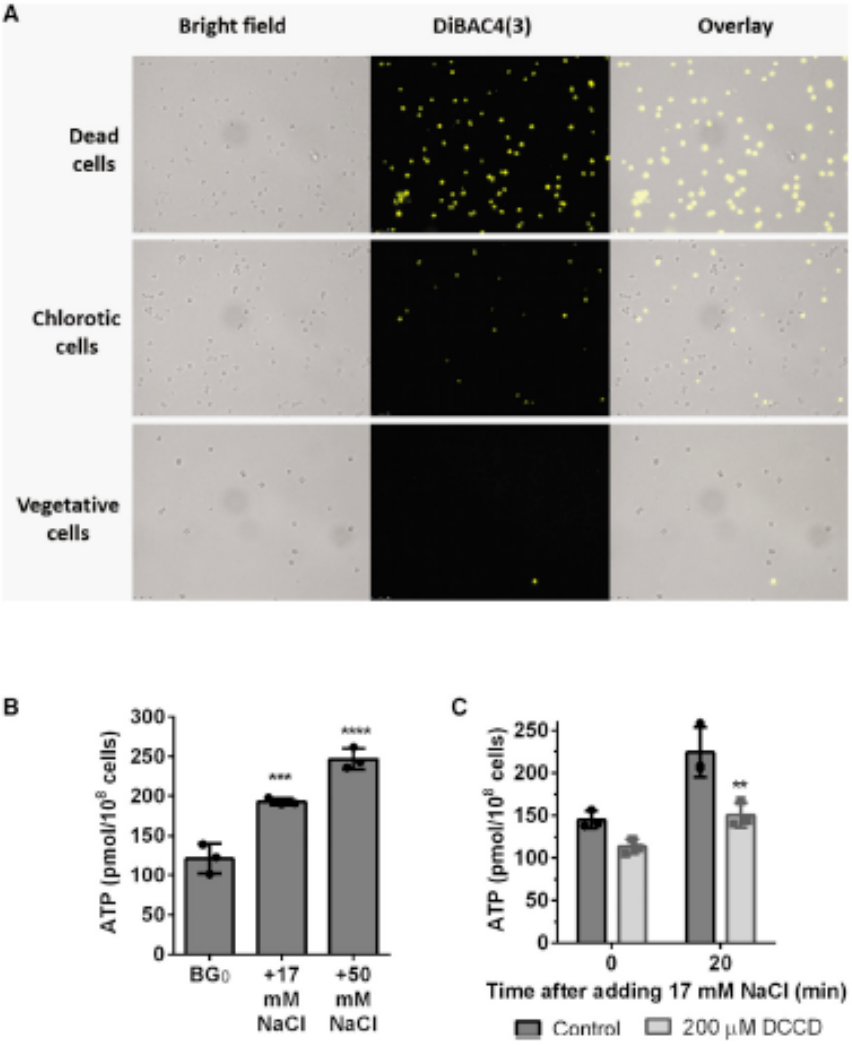

Figure 3. Chlorotic cells maintain a membrane potential, and the amount of ATP produced by the ATP synthases is proportional to the increase in the extracellular concentration of sodium

(A) Microscopic pictures of dead, chlorotic, and vegetative cells stained with DiBAC4(3), which penetrates depolarized cells, showing enhanced fluorescence in the cytoplasm.

(B and C) ATP content normalized to 1×10^8 cells of (B) WT chlorotic cells before and 30 min after addition of 17 mM and 50 mM NaCl and (C) WT chlorotic cells treated with 200 µM DCCD before and 20 min after addition of 17 mM NaCl. Cells were treated for 5 min before the first measurement (0 min). At least three biological replicates were measured; error bars represent the SD; asterisks represent the statistical significance.

sodium-dependent ATP synthesis is a part of *Synechocystis* metabolism in general. To answer this question, vegetative cells were treated with monensin and EIPA. The ATP content of vegetative cells was not affected after treatment with monensin for 30 min (Figure 5A), although EIPA slightly reduced it by 25% (Figure 5B). However, treatment with EIPA also completely inhibited PSII activity (Figure S3), suggesting that the lower ATP levels might be a consequence of inhibition of photosynthesis rather than a direct effect on sodium-dependent ATP synthesis. This indicates that, although sodium bioenergetics plays a key role during nitrogen starvation, vegetative cells do not rely on sodium-dependent ATP synthesis.

To further elucidate the role of sodium on the metabolism of *Synechocystis*, vegetative and nitrogen-starved cells were cultivated in sodium-free medium. Under atmospheric gas conditions in shaking flasks, vegetative cells could not grow in the absence of sodium. However, growth in sodium-free medium could be restored when cells were supplemented with 2% CO_2 (Figure 5C). This is due to the requirement of sodium for bicarbonate uptake through the SbtA and BicA transporters.[16,17] Thus, sodium-dependent bicarbonate transport is essential for growth under atmospheric CO_2 supply, but cells do not require sodium with elevated CO_2 concentrations. Conversely, nitrogen-starved cells showed a decreasing optical density when cultivated in sodium-free medium, even when they were supplemented with 2% CO_2 (Figure 5D), indicating a requirement for sodium beyond the need for inorganic carbon transport.

In the presence of sodium, during the first 24 h of chlorosis, cells synthesize large amounts of glycogen. In sodium-free medium and under atmospheric gas conditions, cells accumulate only ~50% of the amount of glycogen after 2 days of nitrogen starvation as compared to the standard medium, and upon further incubation, glycogen levels decreased (Figure 5E). When cells were nitrogen starved under standard conditions for 24 h, until they reached the maximum glycogen content and were then transferred to sodium-free medium, the glycogen concentration progressively decreased after sodium removal (Figure 5E). This suggests that the absence of sodium triggers glycogen catabolism. When resuscitation of chlorotic cells in sodium-free medium was initiated by the addition of KNO_3 (conditions in which only a low ATP increase was observed), they showed higher respiration rates than cells resuscitating under standard conditions (Figure 5F). However, these cells never re-greened and eventually lost viability, as shown by the complete loss of photosynthetic activity (Figure S1).

ATP levels are rapidly tuned depending on the metabolic requirements

So far, the analysis of sodium requirement in vegetative and chlorotic cells showed that vegetative cells require sodium for bicarbonate transport, whereas chlorotic cells require sodium for ATP synthesis. When cells are nitrogen starved, they are initially photosynthetically competent. To elucidate how ATP levels are affected after transferring vegetative cells to nitrogen-deprived

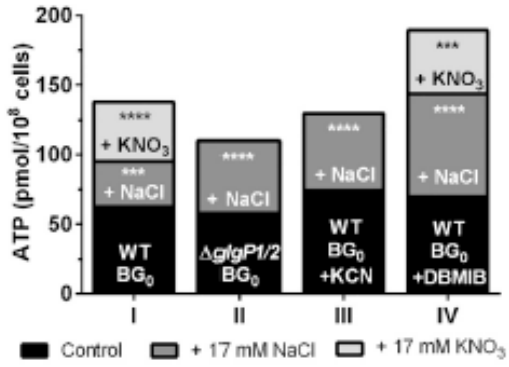

Figure 4. The nitrogen-dependent component of the ATP increase requires respiration of glycogen

ATP content normalized to 1×10^8 cells of chlorotic cells in BG_{11-0} (black), after supplementation with 17 mM NaCl (dark gray), and after additional supplementation with 17 mM KNO_3 (light gray). Column I: WT chlorotic cells are shown. Column II: *ΔglgP1/2* chlorotic cells are shown. Column III: WT chlorotic cells treated with 1 mM KCN cells are shown. Column IV: WT chlorotic cells treated with 200 μM DBMIB are shown. At least three biological replicates were measured; error bars represent the SD; asterisks represent the statistical significance.

conditions at different sodium concentrations, we analyzed the ATP content of vegetative cells after they were transferred either into regular BG_{11-0} (5.5 mM sodium) or into BG_{11-0} supplemented with 17 mM NaCl (22.5 mM). After 30 min shifting to nitrogen-deficient medium, the ATP levels dropped to approximately 1/3 of the initial value, regardless of the sodium concentration. Subsequently, the ATP content was maintained at this low level during long-term chlorosis (Figure 6A). To ensure that the decrease in ATP levels was caused by lowered energy charge and not by reduced levels of adenine nucleotides, we determined the ATP/ADP ratio, which dropped in a similar manner than ATP levels decreased (Figure 6B). This indicates a reduced energy charge rather than a decrease of nitrogen-containing compounds after nitrogen removal and implies that cells adjust ATP levels as a response to the metabolic imbalance caused by nitrogen depletion.

DISCUSSION

Synechocystis engages sodium bioenergetics during nitrogen starvation

During nitrogen-chlorosis, *Synechocystis* re-arranges its metabolism to reach a dormant state that allows cell survival for a prolonged time. This metabolic adaptation includes reduction of energy consumption and production. Thus, chlorotic cells keep ATP at the minimum level to ensure survival (~50–100 pmol/10^8 cells).[7] When a nitrogen source is added to chlorotic cells, the ATP demand dramatically increases due to the ammonium-assimilating GS reaction, which consumes one ATP per reaction, and all the following anabolic processes that are induced at the onset of resuscitation.[6,9] Based on measurements of the glutamine levels on vegetative and chlorotic cells,[18,19] the glutamine content can easily increase around 10 mM upon addition of $NaNO_3$ to dormant cells, which implies that approximately 10^7 molecules of glutamine per cell (considering a cell volume of 2 μm^3) have to be synthesized by the GS-GOGAT cycle, requiring 10^7 molecules of ATP. Cells respond accordingly and increase ATP levels by about ~100% to power the anabolic reactions.

Most of the cellular ATP is produced by the ATP synthases from ADP and inorganic phosphate. In cyanobacteria, this reaction typically requires an electrochemical proton gradient across the thylakoid membrane, which is generated by photosynthetic or respiratory electron transport.[20] However, chlorotic cells could still increase ATP levels within several minutes, even when the two main bioenergetic processes that generate a proton gradient were inhibited. We could identify the nature of this increase in the ATP content and dissect it into two components: one that is purely sodium dependent and a second one that was triggered by ammonium assimilation and supported by glycogen-dependent respiration.

Because chlorotic cells have largely degraded their thylakoids, the space for thylakoidal ATP synthases and proton storage is very limited.[6] Previous studies have reported the presence of ATP synthases in the plasma membrane of *Synechocystis*,[11] which suggests that cells could use an extracellular electrochemical gradient to power ATP synthesis. Although cyanobacteria preferably grow under alkaline conditions, where protons are not abundant, *PMF* is not the only *IMF* that can be coupled to ATP synthesis. The fact that *Synechocystis* uses an *SMF* for other bioenergetic processes (e.g., bicarbonate uptake)[17] suggested that an electrochemical sodium gradient might be involved in ATP synthesis in chlorotic cells.

The first component of the rise in intracellular ATP that was triggered by addition of $NaNO_3$ to chlorotic cells can be explained by an increase in the *SMF*. This first component was prevented by treatment with DCCD, suggesting that the ATP synthases in the plasma membrane of *Synechocystis* can use an electrochemical sodium gradient to power ATP synthesis. The ATP synthase is formed by a membrane complex (F_0), which transports the ions across the membrane, and a cytoplasmic complex (F_1), where ATP is synthesized. Ion specificity is determined in the c-ring in complex F_0. In *Synechocystis*, there is just one gene that encodes for the c subunit that forms the c-ring (AtpH). Whether the c-ring binds protons or sodium ions depends on slight variations in the amino acid sequence around the ion-binding site. Both protons and sodium ions bind a glutamate residue, but sodium-ATPases have polar groups around this glutamate residue, whereas proton-ATPases have hydrophobic groups.[10,21] The balance between hydrophobic and polar groups makes the c-rings more or less selective toward one ion or the other. Proton-ATPases must have high proton selectivity, because usually the concentration of sodium is much higher than the concentration of protons in physiological conditions. Some organisms, like *Methanosarcina acetivorans*, possess proton-specific c-rings that can bind sodium physiologically because their proton specificity is not strong enough to overcome the excess of sodium.[21,22] Figure 7A shows an alignment of the sequence of *Synechocystis'* AtpH with those from *Ilyobacter tartaricus*, *M. acetivorans*, and *Arthrospira platensis*, with weak, medium, and strong proton selectivity, respectively, as well as the AtpH from *Synechococcus elongatus* PCC 7942, a freshwater cyanobacterial strain, and the 2 AtpH homologs from *Synechococcus* sp. PCC 7002, a marine cyanobacterial strain. There are 5 key amino acids around the main ion-binding residue

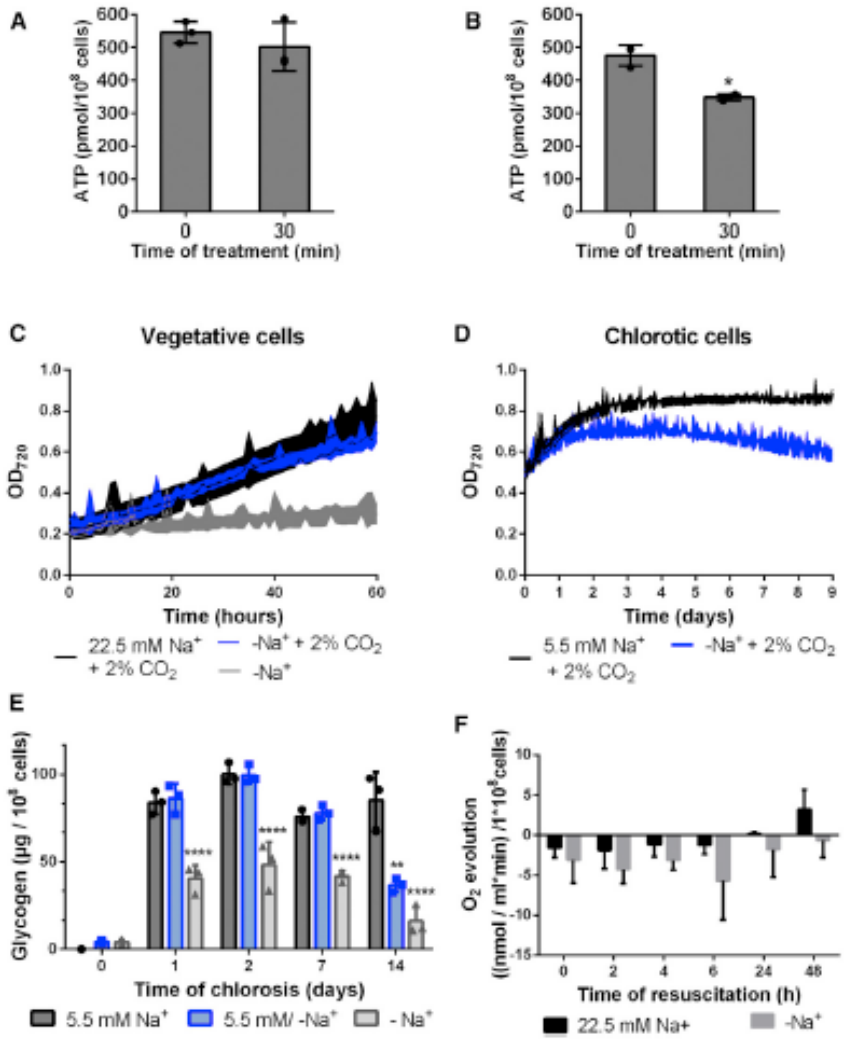

Figure 5. Sodium is required for bicarbonate uptake, but not for ATP synthesis, during vegetative growth

(A) ATP content normalized to 1 × 10^8 cells of vegetative cells treated with 200 µM monensin for 30 min.

(B) ATP content normalized to 1 × 10^8 cells of vegetative cells treated with 100 µM EIPA for 30 min (see also Figure S3).

(C) Optical density at 720 nm of vegetative cells in regular BG_{11} supplemented with 2% CO_2 (black line) and in $BG_{11\text{-}Na}$ sodium-free medium with ambient air (gray line) and 2% CO_2 supplementation (blue line).

(D) Optical density at 720 nm of chlorotic cells in regular $BG_{11\text{-}0}$ supplemented with 2% CO_2 (black line) and in $BG_{11\text{-}0\text{-}Na}$ sodium-free medium supplemented with 2% CO_2 (blue line).

(E) Glycogen content normalized to 1 × 10^8 cells throughout chlorosis of WT cells in medium containing 5.5 mM sodium (black bars, standard conditions), sodium-free medium (gray bars), and cells that were cultivated in standard conditions, i.e., 5.5 mM sodium, for 24 h and then transferred to sodium-free medium (blue bars).

(F) Oxygen evolution of resuscitating WT cells in medium containing 22.5 mM sodium (black bars, standard conditions) and sodium-free medium (gray bars). At least three biological replicates were measured; error bars represent the SD; asterisks represent the statistical significance.

See also Figure S1.

(marked in red) that favor sodium binding: 3 sodium-binding residues (in orange) and 2 residues that bind a stabilizing water molecule (in green). *I. tartaricus* possesses all 5 residues (Figure 7B), although *M. acetivorans* lacks the residues that bind the stabilizing water molecule, which gives the c-ring a higher proton selectivity than the one of *I. tartaricus*. *A. platensis* has hydrophobic amino acids surrounding the glutamate residue, which confers the c-ring high proton selectivity. *Synechocystis*, like *M. acetivorans*, also contains the polar residues that interact with the sodium ion, but not the residues that interact with the stabilizing water molecule, presenting medium proton selectivity. A moderate proton specificity permits the ATP synthases in the thylakoid membranes to bind protons, because the concentration of protons in the thylakoid lumen is high. However, those ATP synthases located in the plasma membrane of dormant cells that live in an alkaline environment are more likely to bind sodium. This enzyme promiscuity allows dormant cells to adapt and survive to an environment where the classical ways to obtain energy are limited. Interestingly, in contrast to *Synechocystis*, which is a brackish water micro-organism and is adapted to high salt concentrations, the fresh-water cyanobacterium *S. elongatus* presents a c-ring with high proton selectivity, although the marine cyanobacterium *Synechococcus* sp. PCC 7002 possesses two AtpH homologs, one with high and one with low proton selectivity. This observation suggests that the switch to sodium bioenergetics under nutrient starvation is likely to be a survival strategy developed only by micro-organisms adapted to high salt concentrations.

The second component of the ATP increase was prevented by treatment with MSX, a specific GS inhibitor, and was absent in a mutant unable to degrade glycogen and when respiration was inhibited by KCN. This suggests that initiation of nitrogen assimilation triggers glycogen catabolism, which contributes to ATP synthesis by supporting respiration. However, inhibition of Cyt b_6f using DBMIB did not prevent the nitrogen-dependent component of the ATP increase. Because Cyt b_6f is only present in the thylakoid membranes, these results suggested that respiration occurs in the plasma membrane during early resuscitation. Previous studies suggested a simpler electron transport chain for the plasma membrane in which electrons are transferred from NAD(P)H dehydrogenases type II (NDH II) to the plastoquinone pool (PQ) and further to an alternative respiratory terminal oxidase (ARTO), without involving Cyt b_6f.[23] Pils and Schmetterer[24] could show that ARTO is energetically active and can energize the plasma membrane in *Synechocystis*. We propose that the

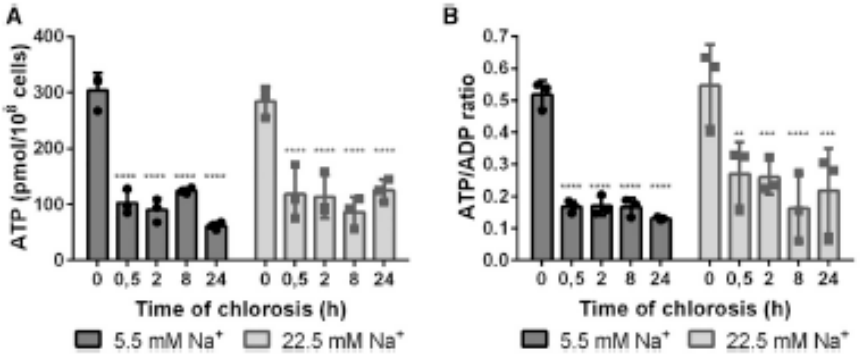

Figure 6. The ATP concentration is rapidly reduced after nitrogen step-down even in the presence of high sodium

(A) ATP content normalized to 1 × 10^8 cells of WT cells after nitrogen deprivation in standard conditions (5.5 mM sodium, black bars) and high-sodium conditions (22.5 mM sodium, gray bars).

(B) ATP/ADP ratio of WT cells after nitrogen deprivation in standard conditions (5.5 mM sodium, black bars) and high-sodium conditions (22.5 mM sodium, gray bars). At least three biological replicates were measured; error bars represent the SD; asterisks represent the statistical significance.

protons transported from the cytoplasm to the periplasmic space by ARTO could be directly used by closely located sodium/protons antiporters to extrude sodium ions from the cytoplasm, immediately converting *PMF* into *SMF*, which can be used for ATP synthesis (Figure 7C). When a proton is translocated across the membrane, its diffusion to the aqueous solution is retarded, because the membrane surface is separated from the bulk aqueous phase by an electrostatic barrier, and proton diffusion between neighboring enzymes occurs in milliseconds.[25] Close cooperation of ARTO and sodium/proton antiporters could avoid protons dissipating into the aqueous solution and would explain the insensitivity of chlorotic cells toward CCCP. In fact, not only did CCCP not prevent a rise in ATP levels in chlorotic cells, but it led to a higher ATP increase than in untreated cells instead. Treatment with CCCP dissipates the proton gradient and allows higher respiration rates, because the proton pumps do not have to work against a gradient,[26] which can lead to an increased sodium-dependent ATP synthesis. In support to this model, NDH II and sodium/proton antiporters are upregulated in chlorotic cells.[9] Interestingly, NdbA (slr0851), one of the three NDH II isoenzymes in *Synechocystis*, is the third most upregulated protein in chlorotic cells. Moreover, this model is in accordance with the extreme sensitivity of chlorotic cells toward the inhibitor of sodium/proton antiport, EIPA. These results show that bioenergetics of chlorotic cells is largely based on sodium, which allows dormant cells to keep the minimum intracellular ATP concentration to maintain cell viability during metabolic quiescence, even in an alkaline environment.

Energy homeostasis in *Synechocystis*

In contrast to chlorotic cells, vegetative cells do not rely on sodium-dependent ATP synthesis but require sodium primarily for sodium-dependent bicarbonate uptake. During vegetative growth, the major ATP synthesis machinery is located in the thylakoid membranes, where photosynthetic and respiratory complexes generate a *PMF* to power ATP synthesis.[20] Upon nitrogen starvation, nitrogen assimilation and most anabolic processes are halted and ATP levels would be expected to increase, because at this point, the ATP synthesis machinery is still intact and the most energy consuming reactions in the cell stop taking place. However, when cells were transferred to nitrogen-free medium, ATP levels rapidly decreased, independently of the concentration of sodium in the medium, suggesting the existence of a powerful yet unexplored regulatory mechanism of tuning ATP levels.

Reduced ATP levels have previously been reported in bacterial cells during metabolic dormancy. In *Mycobacterium tuberculosis*, the ATP content in nutrient-starved cells is maintained at a constant level that is 5-fold lower than in growing cells.[3] However, whether the decreased ATP content is a consequence of a reduced metabolic activity during bacterial dormancy or whether low ATP levels are required to reach this metabolic state has not been elucidated. In *Synechocystis*, mutants unable to synthesize glycogen (Δ*glgA1/2* and Δ*glgC*) present higher ATP levels than the WT and fail to perform a proper acclimation response to nitrogen starvation, which leads to death.[27–29] However, this phenotype is alleviated when synthesis of glucosylglycerol, which is produced from ADP-glucose under conditions of high salt stress, is induced in the Δ*glgA1/2* mutant, showing the importance of an energy dissipation pathway for acclimation to nitrogen starvation.[29] These findings, together with our observation that ATP levels rapidly drop after nitrogen step-down, even in the presence of high sodium, strongly support the idea that a decreased ATP content is important for adaptation of the metabolism to nitrogen starvation. Reduction of the ATP levels may play a role in re-directing the metabolism into dormancy, because some cellular processes that are important for this transition, such as the formation of protein aggregates, are promoted by decreased cellular ATP concentrations.[30] Also, ATP has been shown to act as a biological hydrotrope that influences the fluidity of the cytoplasm.[31] Adaptation of the cytoplasm from a fluid to a glass-like state has important implications on molecular diffusion inside the cells and plays a relevant role in bacterial adaptation to dormancy.[32] Low ATP levels might be a necessary factor for the transition of the cytoplasm into a glass-like state after prolonged exposure to nitrogen-depleted conditions.

We observed that glycogen degradation is induced in the absence of sodium in chlorotic cells, probably in an attempt to maintain the ATP content to a minimum. Similarly, during resuscitation in sodium-free medium, cells respired more (i.e., degraded more glycogen) than in presence of high sodium, most likely to compensate for the lack of sodium-dependent ATP synthesis. These findings support the previously proposed idea that glycogen metabolism is controlled by the intracellular energy charge and plays an important role in energy homeostasis. Nevertheless, the exact molecular mechanism that allows

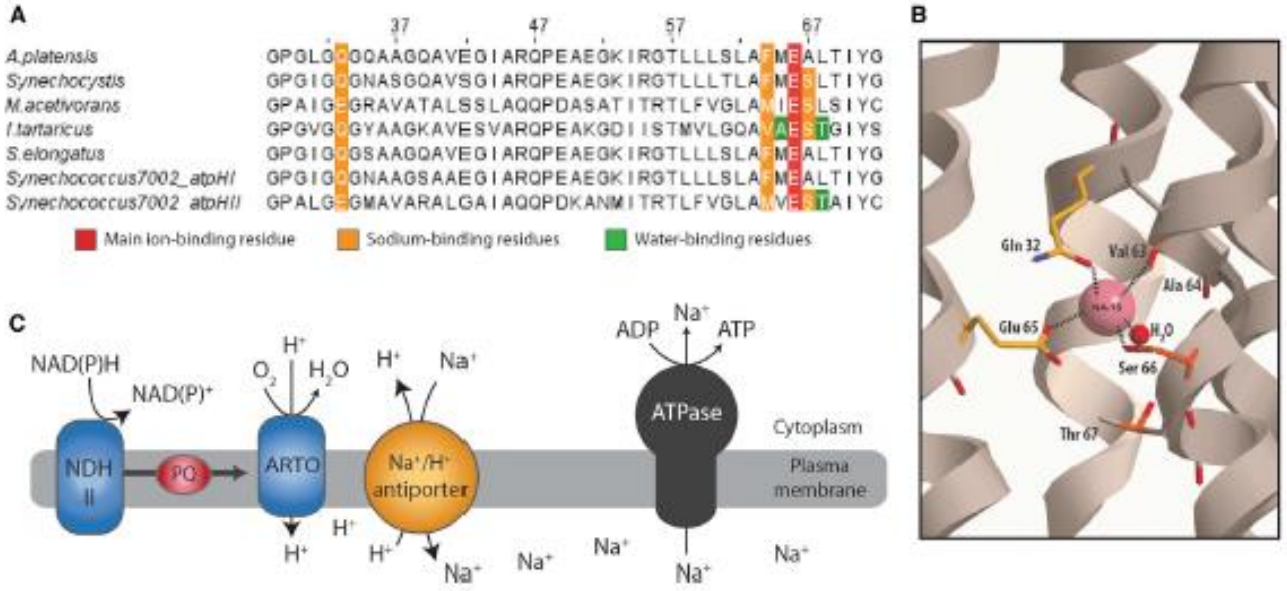

Figure 7. Proposed mechanism of sodium-dependent ATP synthesis in *Synechocystis*

(A) Alignment of the sequence of the ion-binding site of AtpH from *Arthrospira platensis*, *Synechocystis*, *Methanosarcina acetivorans*, *Ilyobacter tartaricus*, *Synechococcus elongatus*, and *Synechococcus* sp. PCC 7002 (AtpH I and AtpH II). Residues involved in Na^+ coordination are indicated in colors.

(B) Na^+ coordination in the c-ring from *I. tartaricus*.

(C) Proposed mechanism for maintaining a Na^+ gradient.

energy dissipation upon nitrogen removal needs yet to be elucidated.[28]

This study sheds light on the regulation of the energy metabolism during bacterial dormancy, which plays a crucial role in the survival and spread of bacterial populations. It remains to be seen how common the phenomenon of engaging sodium bioenergetics to adjust ATP levels to the specific metabolic requirements of each phase of the life cycle is among bacterial species that undergo similar developmental transitions than *Synechocystis*.

STAR★METHODS

Detailed methods are provided in the online version of this paper and include the following:

- KEY RESOURCES TABLE
- RESOURCE AVAILABILITY
  - Lead contact
  - Materials availability
  - Data and code availability
- EXPERIMENTAL MODEL AND SUBJECT DETAILS
- METHOD DETAILS
  - Growth curves
  - ATP determination
  - ADP determination
  - Membrane potential determination
  - Glycogen determination
  - Oxygen evolution measurement
  - Pulse amplification measurement (PAM)
- QUANTIFICATION AND STATISTICAL ANALYSIS

SUPPLEMENTAL INFORMATION

Supplemental Information can be found online at https://doi.org/10.1016/j.cub.2021.01.065.

ACKNOWLEDGMENTS

We thank Dr. Libera Lo Presti for her assistance in writing this manuscript and Armen Mulkidjanian for very helpful discussions. This work was supported by the German Research Council (DFG) FOR 2816 "The Autotrophy-Heterotrophy Switch in Cyanobacteria: Coherent Decision-Making at Multiple Regulatory Layers," GRK 1708 "Molecular Principles of Bacterial Survival Strategies," and EXC 2124 "Controlling Microbes to Fight Infections."

AUTHOR CONTRIBUTIONS

S.D. and K.F. designed the experiments. S.D. and M.B. conducted the experiments. S.D. and K.F. analyzed the data and wrote the manuscript.

DECLARATION OF INTERESTS

The authors declare no competing interests.

Received: September 29, 2020
Revised: November 30, 2020
Accepted: January 19, 2021
Published: February 10, 2021

REFERENCES

1. Greening, C., Grinter, R., and Chiri, E. (2019). Uncovering the metabolic strategies of the dormant microbial majority: towards integrative approaches. mSystems *4*, 1–5.
2. Lewis, K. (2010). Persister cells. Annu. Rev. Microbiol. *64*, 357–372.

3. Rittershaus, E.S., Baek, S.H., and Sassetti, C.M. (2013). The normalcy of dormancy: common themes in microbial quiescence. Cell Host Microbe *13*, 643–651.
4. Houmard, J. (1995). How do cyanobacteria perceive and adjust to their environment? In Molecular Ecology of Aquatic Microbes, I. Joint, ed. (Springer Berlin Heidelberg), pp. 153–170.
5. Vitousek, P.M., and Howarth, R.W. (1991). Nitrogen limitation on land and sea: how can it occur? Biogeochemistry *13*, 87–115.
6. Klotz, A., Georg, J., Bučinská, L., Watanabe, S., Reimann, V., Januszewski, W., Sobotka, R., Jendrossek, D., Hess, W.R., and Forchhammer, K. (2016). Awakening of a dormant cyanobacterium from nitrogen chlorosis reveals a genetically determined program. Curr. Biol. *26*, 2862–2872.
7. Doello, S., Klotz, A., Makowka, A., Gutekunst, K., and Forchhammer, K. (2018). A specific glycogen mobilization strategy enables rapid awakening of dormant cyanobacteria from chlorosis. Plant Physiol. *177*, 594–603.
8. Klotz, A., and Forchhammer, K. (2017). Glycogen, a major player for bacterial survival and awakening from dormancy. Future Microbiol. *12*, 101–104.
9. Spät, P., Klotz, A., Rexroth, S., Maček, B., and Forchhammer, K. (2018). Chlorosis as a developmental program in cyanobacteria: the proteomic fundament for survival and awakening. Mol. Cell. Proteomics *17*, 1650–1669.
10. Schulz, S., Iglesias-Cans, M., Krah, A., Yildiz, O., Leone, V., Matthies, D., Cook, G.M., Faraldo-Gómez, J.D., and Meier, T. (2013). A new type of Na(+)-driven ATP synthase membrane rotor with a two-carboxylate ion-coupling motif. PLoS Biol. *11*, e1001596.
11. Huang, F., Parmryd, I., Nilsson, F., Persson, A.L., Pakrasi, H.B., Andersson, B., and Norling, B. (2002). Proteomics of Synechocystis sp. strain PCC 6803: identification of plasma membrane proteins. Mol. Cell. Proteomics *1*, 956–966.
12. Benarroch, J.M., and Asally, M. (2020). The microbiologist's guide to membrane potential dynamics. Trends Microbiol. *28*, 304–314.
13. Cherepanov, D.A., Mulkidjanian, A.Y., and Junge, W. (1999). Transient accumulation of elastic energy in proton translocating ATP synthase. FEBS Lett. *449*, 1–6.
14. Kaim, G., and Dimroth, P. (1999). ATP synthesis by F-type ATP synthase is obligatorily dependent on the transmembrane voltage. EMBO J. *18*, 4118–4127.
15. Schultze, M., Forberich, B., Rexroth, S., Dyczmons, N.G., Roegner, M., and Appel, J. (2009). Localization of cytochrome b6f complexes implies an incomplete respiratory chain in cytoplasmic membranes of the cyanobacterium Synechocystis sp. PCC 6803. Biochim. Biophys. Acta *1787*, 1479–1485.
16. Shibata, M., Katoh, H., Sonoda, M., Ohkawa, H., Shimoyama, M., Fukuzawa, H., Kaplan, A., and Ogawa, T. (2002). Genes essential to sodium-dependent bicarbonate transport in cyanobacteria: function and phylogenetic analysis. J. Biol. Chem. *277*, 18658–18664.
17. Burnap, R.L., Hagemann, M., and Kaplan, A. (2015). Regulation of CO2 concentrating mechanism in cyanobacteria. Life (Basel) *5*, 348–371.
18. Mérida, A., Candau, P., and Florencio, F.J. (1991). Regulation of glutamine synthetase activity in the unicellular cyanobacterium Synechocystis sp. strain PCC 6803 by the nitrogen source: effect of ammonium. J. Bacteriol. *173*, 4095–4100.
19. Hauf, W., Schlebusch, M., Hüge, J., Kopka, J., Hagemann, M., and Forchhammer, K. (2013). Metabolic changes in Synechocystis PCC6803 upon nitrogen-starvation: Excess NADPH sustains polyhydroxybutyrate accumulation. Metabolites *3*, 101–118.
20. Imashimizu, M., Bernát, G., Sunamura, E., Broekmans, M., Konno, H., Isato, K., Rögner, M., and Hisabori, T. (2011). Regulation of F0F1-ATPase from Synechocystis sp. PCC 6803 by γ and ε subunits is significant for light/dark adaptation. J. Biol. Chem. *286*, 26595–26602.
21. Leone, V., Pogoryelov, D., Meier, T., and Faraldo-Gómez, J.D. (2015). On the principle of ion selectivity in Na+/H+-coupled membrane proteins: experimental and theoretical studies of an ATP synthase rotor. Proc. Natl. Acad. Sci. USA *112*, E1057–E1066.
22. Schlegel, K., Leone, V., Faraldo-Gómez, J.D., and Müller, V. (2012). Promiscuous archaeal ATP synthase concurrently coupled to Na+ and H+ translocation. Proc. Natl. Acad. Sci. USA *109*, 947–952.
23. Baers, L.L., Breckels, L.M., Mills, L.A., Gatto, L., Deery, M.J., Stevens, T.J., Howe, C.J., Lilley, K.S., and Lea-Smith, D.J. (2019). Proteome mapping of a cyanobacterium reveals distinct compartment organization and cell-dispersed metabolism. Plant Physiol. *181*, 1721–1738.
24. Pils, D., and Schmetterer, G. (2001). Characterization of three bioenergetically active respiratory terminal oxidases in the cyanobacterium Synechocystis sp. strain PCC 6803. FEMS Microbiol. Lett. *203*, 217–222.
25. Mulkidjanian, A.Y., Heberle, J., and Cherepanov, D.A. (2006). Protons @ interfaces: implications for biological energy conversion. Biochim. Biophys. Acta *1757*, 913–930.
26. Pansook, S., Incharoensakdi, A., and Phunpruch, S. (2019). Effects of the photosystem II inhibitors CCCP and DCMU on hydrogen production by the unicellular halotolerant cyanobacterium *Aphanothece halophytica*. ScientificWorldJournal *2019*, 1030236.
27. Gründel, M., Scheunemann, R., Lockau, W., and Zilliges, Y. (2012). Impaired glycogen synthesis causes metabolic overflow reactions and affects stress responses in the cyanobacterium Synechocystis sp. PCC 6803. Microbiology (Reading) *158*, 3032–3043.
28. Cano, M., Holland, S.C., Artier, J., Burnap, R.L., Ghirardi, M., Morgan, J.A., and Yu, J. (2018). Glycogen synthesis and metabolite overflow contribute to energy balancing in cyanobacteria. Cell Rep. *23*, 667–672.
29. Díaz-Troya, S., Roldán, M., Mallén-Ponce, M.J., Ortega-Martínez, P., and Florencio, F.J. (2020). Lethality caused by ADP-glucose accumulation is suppressed by salt-induced carbon flux redirection in cyanobacteria. J. Exp. Bot. *71*, 2005–2017.
30. Pu, Y., Li, Y., Jin, X., Tian, T., Ma, Q., Zhao, Z., Lin, S.-Y., Chen, Z., Li, B., Yao, G., et al. (2019). ATP-dependent dynamic protein aggregation regulates bacterial dormancy depth critical for antibiotic tolerance. Mol. Cell *73*, 143–156.e4.
31. Patel, A., Malinovska, L., Saha, S., Wang, J., Alberti, S., Krishnan, Y., and Hyman, A.A. (2017). ATP as a biological hydrotrope. Science *356*, 753–756.
32. Parry, B.R., Surovtsev, I.V., Cabeen, M.T., O'Hern, C.S., Dufresne, E.R., and Jacobs-Wagner, C. (2014). The bacterial cytoplasm has glass-like properties and is fluidized by metabolic activity. Cell *156*, 183–194.
33. Rippka, R., Deruelles, J., Waterbury, J.B., Herdman, M., and Stanier, R.Y. (1979). Generic assignments, strain histories and properties of pure cultures of cyanobacteria. Microbiology *111*, 1–61.
34. Waterhouse, A.M., Procter, J.B., Martin, D.M.A., Clamp, M., and Barton, G.J. (2009). Jalview Version 2–a multiple sequence alignment editor and analysis workbench. Bioinformatics *25*, 1189–1191.
35. Schlebusch, M., and Forchhammer, K. (2010). Requirement of the nitrogen starvation-induced protein Sll0783 for polyhydroxybutyrate accumulation in Synechocystis sp. strain PCC 6803. Appl. Environ. Microbiol. *76*, 6101–6107.
36. Schreiber, U., Endo, T., Mi, H., and Asada, K. (1995). Quenching analysis of chlorophyll fluorescence by the saturation pulse method: Particular aspects relating to the study of eukaryotic algae and cyanobacteria. Plant Cell Physiol. *36*, 873–882.

STAR★METHODS

KEY RESOURCES TABLE

REAGENT or RESOURCE	SOURCE	IDENTIFIER
Experimental models: organisms/strains		
Synechocystis sp. PCC 6803	[33]	PCC 6803
Synechocystis sp. PCC 6803 Δ*glgP1/2*	[7]	N/A
Software and algorithms		
GraphPad PRISM version 6.01	La Jolla, CA, USA	https://www.graphpad.com/
COBALT: Multiple Alignment Tool - NCBI	Bethesda, MD, USA	http://www.ncbi.nlm.nih.gov/projects/cobalt/
Jalview 2	[34]	https://www.jalview.org/
Other		
BG_{11} Medium	[33]	N/A
BG_{11-0} Medium	[35]	N/A
BG_{11} Sodium-free Medium	This study	BG_{11-Na}
BG_{11-0} Sodium-free Medium	This study	$BG_{11-0-Na}$
ATP determination kit	Molecular Probes	A22066
ADP Assay Kit	Sigma-Aldrich	MAK133
Bis-(1,3-Dibutylbarbituric Acid)-trimethine oxonol	AAT Bioquest	21411
Amyloglucosidase	Sigma-Aldrich	10115

RESOURCE AVAILABILITY

Lead contact

Further information and questions or inquiries about data and resources should be directed to and will be fulfilled by the lead author, Karl Forchhammer (karl.forchhammer@uni-tuebingen.de).

Materials availability

No unique reagents were created for this study.

Data and code availability

This study did not generate datasets or code.

EXPERIMENTAL MODEL AND SUBJECT DETAILS

The cyanobacterial strains used in this study are listed in the Key resources table. All strains were grown in BG_{11} supplemented with 5 mM $NaHCO_3$ for vegetative growth, as described previously[33]. The concentration of sodium in standard BG_{11} medium is 22.5 mM. Nitrogen starvation was induced as previously described by a 2-step wash with BG_{11-0} medium supplemented with 5 mM $NaHCO_3$, which contains all BG_{11} components except for $NaNO_3$[6,35]. The concentration of sodium in standard BG_{11-0} medium is 5.5 mM. Resuscitation was induced by addition of 17 mM $NaNO_3$ to cells residing in BG_{11-0} (standard conditions). When indicated, 17 mM $NaNO_3$ was substituted by 17 mM KNO_3 or 5 mM NH_4Cl in recovery experiments, with or without supplementation with 17 mM NaCl, as specified. When stated, cells were transferred to sodium-free (BG_{11-Na} or $BG_{11-0-Na}$) medium, where all sodium salts were replaced by potassium salts. When specified, cells were treated with the inhibitors DCMU (20 μM), DBMIB (100 μM), Antimycin A (25 μM), CCCP (100 μM), DNP (100 μM), MSX (200 μM), monensin (200 μM), EIPA (100 μM) and DCCD (200 μM) for 5 min before the experiment was started unless otherwise indicated. Cultivation was performed with continuous illumination (50 to 60 μmol photons m^{-2} s^{-1}) and shaking (130 to 140 rpm) at 27°C. Δ*glgP1/2* pre-cultures were cultivated with the appropriate concentration of antibiotics[7]. Biological replicates were inoculated with the same pre-cultures, but propagated, nitrogen-starved and resuscitated independently in different flasks under identical conditions.

METHOD DETAILS

Growth curves

Growth curves were generated using a Multi-cultivator OD-1000 with a Gas Mixing System GMS 150 (Photosystems Instruments, Drasov, Czech Republic). Vegetative cells were grown in BG_{11} or BG_{11-Na} medium with and without supplementation with 2%

CO_2. Nitrogen starvation was induced as described above, followed by cultivation in BG_{11-0} or $BG_{11-0-Na}$ medium supplemented with 2% CO_2. The OD was monitored at 720 nm. Three biological replicates per condition were measured.

ATP determination

1 mL aliquots of bacterial cultures were taken and immediately frozen in liquid nitrogen. ATP was extracted by boiling and freezing samples 3 times consecutively (boiling at 100°C, freezing in liquid nitrogen) and spinning them down at 25,000 g for 1 min at 4°C. ATP in the supernatant was quantified with the "ATP determination kit" (Molecular Probes (A22066), Oregon, USA) following the manufacturer's protocol. 50 µl of a reaction mix containing reaction buffer, luciferin, and firefly luciferase were mixed with 10 µl of the samples and the luminescence was quantified in a luminometer (Sirius Luminometer, Berthold Detection Systems). An ATP standard curve was generated and used to calculate ATP content in the collected samples. For every condition, at least three biological replicates were measured.

ADP determination

1 mL aliquots of bacterial cultures were taken and immediately frozen in liquid nitrogen. ATP was extracted by boiling and freezing samples 3 times consecutively (boiling at 100°C, freezing in liquid nitrogen) and spinning them down at 25,000 g for 1 min at 4°C. ATP in the supernatant was quantified with the "ADP Assay Kit" (MAK133, Sigma-Aldrich, Missouri, USA) following the manufacturer's protocol. 90 µl of a reaction mix containing reaction buffer, luciferin, and firefly luciferase were mixed with 10 µl of the samples and the luminescence was quantified in a luminometer to determine the RLU_{ATP}. Subsequently, "ADP enzyme" was added to the samples and the luminescence was measured again after a 2-min incubation to determine the RLU_{ADP}. An ADP standard curve was generated. The luminescence corresponding to ADP was calculated (RLU_{ADP}-RLU_{ATP}) and the ADP content in the samples was determined using the standard curve. For every condition, at least three biological replicates were measured.

Membrane potential determination

The dye Bis-(1,3-Dibutylbarbituric Acid)-trimethine oxonol (DiBAC4(3)) was purchased from AAT Bioquest (Hamburg, Germany; cat. no. 21411). Vegetative, chlorotic and dead cells (killed by boiling at 99°C for 20 min) were stained with 10 µM DiBAC4(3) (dissolved in DMSO) for 30 min in the dark. 10 µL of stained cells were dropped on an agarose-coated microscopy slide. A Leica DM5500 B (Wetzlar, Germany) with an 100x /1.3 oil objective was used to image cells. A yellow fluorescent protein (YFP) filter (excitation: 490-510 nm; emission 520-550 nm) was used to detect DiBAC4(3).

Glycogen determination

Glycogen content was determined as described by Gründel et al.[27] with modifications established by Klotz et al.[6]. 2 mL-samples were collected, span down, and washed with distilled water. Cells were lysed by incubation in 30% KOH at 95°C for 2h. Glycogen was precipitated by addition of cold ethanol to a final concentration of 70% followed by an overnight incubation at −20°C. The precipitated glycogen was pelleted by centrifugation at 15000 g for 10 min and washed with 70% ethanol and 98% absolute ethanol, consecutively. The precipitated glycogen was dried and digested with 35 U of amyloglucosidase (10115, Sigma-Aldrich) in 1 mL of 100 sodium acetate pH 4.5 for 2 h. 200 µl of the samples were mixed with 1 mL of 6% O-toluidine in acetic acid and incubated at 100°C for 10 min. Absorbance was then read at 635 nm. A glucose calibration curve was used to determine the amount of glycogen in the samples. For every condition, at least three biological replicates were measured.

Oxygen evolution measurement

Oxygen evolution was measured *in vivo* using a Clark-type oxygen electrode DW1 (Hansatech, King's Lynn, Norfolk, UK). Light was provided from a high-intensity white light source LS2 (Hansatech). Oxygen evolution of 2 mL recovering cultures at an OD_{750} of 0.5 was measured at room temperature and 50 µmol photons m^{-2} s^{-1}. Three biological replicates per condition were measured.

Pulse amplification measurement (PAM)

PSII activity was analyzed *in vivo* with a WATER-PAM chlorophyll fluorometer (Walz GmbH, Effeltrich, Germany). All samples were dark-adapted for 5 min before measurement. The maximal PSII quantum yield (F_v/F_m) was determined with the saturation pulse method[36]. Cultures were diluted 1:20 before the measurements in a final volume of 2 mL. Three biological and three technical replicates were measured (three measurements of each biological replicate).

QUANTIFICATION AND STATISTICAL ANALYSIS

Statistical details for each experiment can be found in the figure legends. For all experiments, 3 biological replicates were analyzed. Samples taken from cultures that were inoculated with the same pre-cultures, but propagated, nitrogen-starved and resuscitated independently in different flasks under identical conditions were considered different biological replicates. Every measured data point, as well as the mean and SD of the 3 replicates are shown in the graphs. GraphPad PRISM was used to perform paired Student's t tests to determine the statistical significance. Asterisks in the figures were used to symbolize the p value: One asterisk represents $p \leq 0.05$, two asterisks $p \leq 0.01$, three asterisks $p \leq 0.001$, and four asterisks $p \leq 0.0001$.

Current Biology, Volume *31*

Supplemental Information

The essential role of sodium bioenergetics and ATP homeostasis in the developmental transitions of a cyanobacterium

Sofia Doello, Markus Burkhardt, and Karl Forchhammer

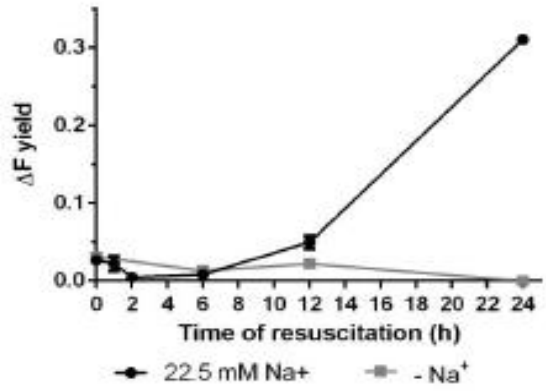

Figure S1. Residual photosynthetic activity is still present during the first hour of resuscitation and it is lost in the absence of sodium. Related to Figures 1 and 5. Photosystem II quantum yield determined by pulse-amplitude-modulation (PAM) fluorometry of WT cells during recovery from chlorosis in the presence and absence of sodium. ΔF yield represents the maximal PSII quantum yield (F_v/F_m). 3 biological and 3 technical replicates were measured.

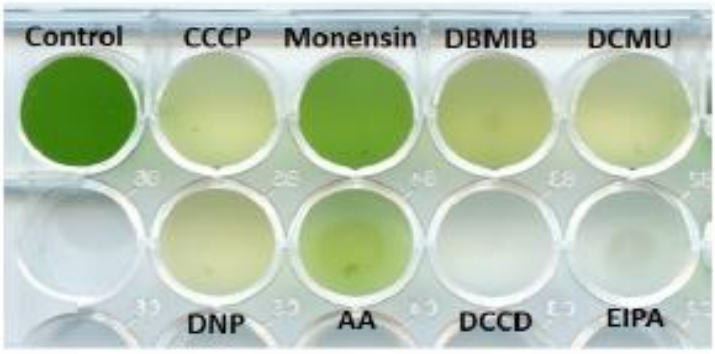

Figure S2. Treatment with ionophores and inhibitors of F-ATPases activity and photosynthetic and respiratory electron transport prevents efficient resuscitation from nitrogen starvation Related to Figures 1 and 2. Effect of 100 µM CCCP, 200 µM monensin, 100 µM DBMIB, 100 µM 20 µM DCMU, 100 µM DNP, 25 µM Antimycin A, 200 µM DCCD and 100 µM EIPA on resuscitation from nitrogen starvation. Chlorotic cells were treated with the inhibitor for 5 min and were then supplemented with 17 mM $NaNO_3$. Picture was taken 2 days after $NaNO_3$ addition.

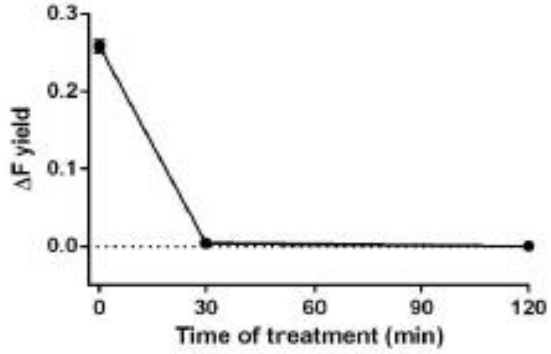

Figure S3. Inhibition of sodium transport blocks photosynthetic activity in vegetative cells. Related to Figure 5. Photosystem II quantum yield determined by pulse-amplitude-modulation (PAM) fluorometry of WT vegetative cells treated with 100 μM EIPA. ΔF yield represents the maximal PSII quantum yield (F_v/F_m). 3 biological and 3 technical replicates were measured.

Publication 2 (Accepted)

Research Article

Selim, K, Haffner, M, Burkhardt, M, Mantovani, O, Neumann, N, Albrecht, R, Seifert, R, Krüger, L, Stülke, J, Hartmann, M, Hagemann, M, Forchhammer, K (2021). Diurnal metabolic control in cyanobacteria requires perception of second messenger signaling molecule c-di-AMP by the carbon control protein SbtB. *Sci. Adv.* 7, eabk0568

SIGNAL TRANSDUCTION

Diurnal metabolic control in cyanobacteria requires perception of second messenger signaling molecule c-di-AMP by the carbon control protein SbtB

Khaled A. Selim[1,2]*†, Michael Haffner[1]†, Markus Burkhardt[1], Oliver Mantovani[3], Niels Neumann[1], Reinhard Albrecht[2], Roland Seifert[4], Larissa Krüger[5], Jörg Stülke[5], Marcus D. Hartmann[2], Martin Hagemann[3], Karl Forchhammer[1]*

Copyright © 2021 The Authors, some rights reserved; exclusive licensee American Association for the Advancement of Science. No claim to original U.S. Government Works. Distributed under a Creative Commons Attribution NonCommercial License 4.0 (CC BY-NC).

Because of their photosynthesis-dependent lifestyle, cyanobacteria evolved sophisticated regulatory mechanisms to adapt to oscillating day-night metabolic changes. How they coordinate the metabolic switch between autotrophic and glycogen-catabolic metabolism in light and darkness is poorly understood. Recently, c-di-AMP has been implicated in diurnal regulation, but its mode of action remains elusive. To unravel the signaling functions of c-di-AMP in cyanobacteria, we isolated c-di-AMP receptor proteins. Thereby, the carbon-sensor protein SbtB was identified as a major c-di-AMP receptor, which we confirmed biochemically and by x-ray crystallography. In search for the c-di-AMP signaling function of SbtB, we found that both SbtB and c-di-AMP cyclase–deficient mutants showed reduced diurnal growth and that c-di-AMP–bound SbtB interacts specifically with the glycogen-branching enzyme GlgB. Accordingly, both mutants displayed impaired glycogen synthesis during the day and impaired nighttime survival. Thus, the pivotal role of c-di-AMP in day-night acclimation can be attributed to SbtB-mediated regulation of glycogen metabolism.

INTRODUCTION

Aerobic life on Earth evolved about 2.7 to 3.2 billion years ago with the evolution of oxygenic photosynthesis by cyanobacteria. Because photosynthesis uses energy provided by sunlight, cyanobacteria have evolved intricate circadian timing machinery to fine-tune photosynthesis and other metabolic activity to successive day-night cycles of different length (*1*). The recent discovery of a true circadian clock in the nonphotosynthetic bacterium *Bacillus subtilis* suggests that circadian rhythms may be widespread among other prokaryotes as well (*2*). All eukaryotic organisms independently evolved a circadian clock to acclimate to different diurnal cycles. In humans, the disruption of circadian timing correlates with diverse health problems including cancer and cardiovascular diseases (*3*).

Photoautotrophic organisms are constantly exposed to alternating day-night light regimes, which requires a permanent metabolic switch between autotrophic CO_2 fixation via Calvin-Benson cycle during the day and heterotrophic-like carbon catabolism during the night. During the day, newly fixed CO_2 is used for anabolic reactions, producing the building blocks for cell growth, and, in addition, for building up organic carbon reserves such as glycogen in cyanobacteria or starch in plants. During the night, glycogen is metabolized mainly using the oxidative pentose-phosphate (OPP) pathway, to provide reduction equivalents for energy conserving respiration (*4*, *5*). The constant switch between autotrophic and heterotrophic metabolism is operated by a sophisticated network of regulatory processes, which we only begin to understand. It involves sensing of the redox, energy, carbon, and nitrogen status as well as a specific timing machinery, the circadian clock (*1*, *3*, *6*). Although it is clear that the diurnal rhythm affects central carbon metabolism, mainly of glycogen anabolism and catabolism (*3*, *7*, *8*), our understanding of the signaling cascades regulating central carbon and nitrogen metabolisms under diurnal growth is still very preliminary.

Recent investigations pointed toward additional regulatory circuits, whose connection to the circadian clock is unclear. For instance, these reports revealed a noncanonical role of the second messengers cyclic di-adenosine monophosphate [3′,5′-c-di–adenosine 5′-monophosphate; hereafter c-di-AMP] and of the alarmone guanosine penta- and tetraphosphate ppGpp(p) in the diurnal photosynthetic lifestyle of cyanobacteria (*9*–*11*). Since its discovery in 2008, the second messenger c-di-AMP came into focus of research, owing to its essentiality in many organisms (*12*–*14*). This cyclic nucleotide has been implicated in regulating several biological processes, mainly related to cell wall and osmotic homeostasis in Firmicutes and, to a lesser extent, in Actinobacteria. In these heterotrophic bacteria, the main c-di-AMP targets are ion and osmolyte transporters, including those of K^+, Na^+, and Mg^{2+} ions, glycine betaine, and amino acids (*12*–*14*). Binding of c-di-AMP has also been demonstrated for a protein of the PII superfamily, termed DarA in *B. subtilis* (*15*) or PstA in *Staphylococcus aureus* (*16*); however, the physiological role of those signaling proteins remains unclear. In cyanobacteria, c-di-AMP has been recently described to be required for nocturnal dormancy of *Synechococcus elongatus*, because mutants of the c-di-AMP cyclase were impaired in nighttime survival. However, the molecular mechanism underlying the function of c-di-AMP in nocturnal dormancy has remained unresolved (*11*). In addition, the analysis of *Synechocystis* sp. mutants in which

[1]Organismic Interactions Department, Interfaculty Institute for Microbiology and Infection Medicine, Cluster of Excellence 'Controlling Microbes to Fight Infections', Tübingen University, Auf der Morgenstelle 28, 72076 Tübingen, Germany. [2]Department of Protein Evolution, Max Planck Institute for Developmental Biology, Tübingen, Germany. [3]Plant Physiology Department, Institute of Biological Sciences, Rostock University, Rostock, Germany. [4]Institute of Pharmacology, Hannover Medical School, Hannover, Germany. [5]Department of General Microbiology, Göttingen Center for Molecular Biosciences (GZMB), Göttingen University, Göttingen, Germany.
*Corresponding author. Email: khaled.selim@uni-tuebingen.de (K.A.S.); karl.forchhammer@uni-tuebingen.de (K.F.)
†These authors shared co-first authorship.

Downloaded from https://www.science.org on July 06, 2023

the c-di-AMP concentration was elevated or reduced implied a role for c-di-AMP in acclimation to abiotic stress and osmotic homeostasis (*17*). These findings agreed with the prediction of c-di-AMP–dependent riboswitches upstream of genes involved in ion homeostasis and osmolyte transport (*18*). Furthermore, expression of the *sll0505* gene, encoding the *Synechocystis* di-adenylate cyclase, showed a strong correlation with the acclimation to long-term nitrogen starvation. Upon resuscitating the chlorotic *Synechocystis* cells from nitrogen starvation, *sll0505* belonged to the strongest early up-regulated genes, implying a role of c-di-AMP in the awakening from dormancy (*19*). Although several c-di-AMP receptor proteins were identified in heterotrophic bacteria (*12*, *14*), the c-di-AMP targets and its signaling role in cyanobacteria remain elusive.

Another second messenger nucleotide that returned into the focus of interest is cyclic AMP (3′,5′-cAMP; hereafter cAMP), as it was revealed as effector molecule for the PII-like signaling protein SbtB. We identified SbtB as a unique component of the cyanobacterial carbon-concentrating mechanism (CCM), required for efficient acclimation to varying inorganic carbon (C_i) regimes (*20*). HCO_3^-/CO_2 metabolism is also strictly regulated by the diurnal metabolic status of the cells, with active C_i accumulation during the autotrophic day mode and arrest of HCO_3^- transport during nocturnal dormancy (*21*). Recently, it has been shown that the diurnal switch of C_i transport activity is regulated via phytochromes involving SbtB (*21*). The *sbtB* gene is located in an operon with the gene for the sodium-dependent bicarbonate transporter SbtA. A similar genetic arrangement is frequently found in proteins of the PII family, which cluster with the transport proteins they regulate. Accordingly, SbtB was proven as a regulator of SbtA transport activity (*20*, *22*, *23*). Similar to canonical PII proteins (*24*, *25*), SbtB perceives energy signals by binding adenosine 5′-triphosphate (5′-ATP) or adenosine 5′-diphosphate (5′-ADP), but unlike canonical PII proteins, SbtB also senses 5′-AMP and preferentially binds the second messenger cAMP (*20*). The cAMP concentration was correlated with the CO_2 supply of the cells, implying an evolutionary conserved role of the second messenger cAMP as an indicator of the cellular carbon status via SbtB signaling (*20*, *26*). Furthermore, structural analysis of SbtB revealed a putative redox-sensitive motif at the C terminus (*20*), suggesting that SbtB may play a role in controlling HCO_3^- transport in response to light/dark-mediated redox stimuli.

The binding of a broad range of adenine nucleotides suggested that SbtB may also bind c-di-AMP. Because our preliminary data confirmed this assumption, we set out to verify the physiological relevance of c-di-AMP binding to SbtB in the cyanobacterial model organism *Synechocystis* sp. PCC 6803 (hereafter *Synechocystis*). The c-di-AMP pull-down experiment to fish in vivo c-di-AMP receptors notably retrieved SbtB as the most enriched protein. The SbtB-c-di-AMP complex could pull down another target of central carbon metabolism, the glycogen-branching enzyme GlgB. C-di-AMP signaling via SbtB turned out to be pivotal for the diurnal lifestyle of *Synechocystis* through regulation of glycogen metabolism via GlgB.

RESULTS

SbtB is the major c-di-AMP receptor protein in *Synechocystis*

The SbtB signaling proteins are highly conserved in cyanobacteria and act as C_i-sensing module using energy and carbon signal inputs through binding of the adenine nucleotides ATP, ADP, and AMP as well as cAMP (*20*, *23*, *27*). This unique ability of SbtB to bind a wide variety of adenine-based nucleotides made it likely that SbtB could also bind the second messenger c-di-AMP. Using isothermal titration calorimetry (ITC), we tested the ability of recombinant SbtB protein from *Synechocystis* (*Sc*SbtB) to bind c-di-AMP. The trimeric *Sc*SbtB was able to bind with high affinity to c-di-AMP (Fig. 1A) with dissociation constant (K_d) values (K_{d1} of 2.3 μM, K_{d2} of 12.2 μM, and K_{d3} of 35.9 μM for the first, second, and third binding site of trimeric *Sc*SbtB, respectively) comparable to that of cAMP but stronger than that of ATP, ADP, and AMP (*20*). Moreover, the binding enthalpy for c-di-AMP was almost equivalent or higher than that of ATP, ADP, and AMP at a lower concentration of c-di-AMP (fig. S1), which indicates preferential binding to c-di-AMP over standard adenine nucleotides. To test whether binding to c-di-AMP is a common trait among SbtB proteins in cyanobacteria, we examined the ability of the SbtB protein from the filamentous cyanobacterium *Nostoc* sp. PCC 7120 (*Ns*SbtB) to bind c-di-AMP. Similar to *Sc*SbtB protein, ITC analysis revealed that *Ns*SbtB is able to bind c-di-AMP as well.

To reveal whether c-di-AMP binding to SbtB proteins is of physiological relevance, we performed a pull-down experiment with a crude cell extract from *Synechocystis* using immobilized c-di-AMP as a bait and searched for protein preys that specifically bound to c-di-AMP (Fig. 1B). The *Sc*SbtB protein, encoded by *slr1513*, was the highest enriched protein in the pull-down fraction (Fig. 1B), confirming that *Sc*SbtB is a real target of c-di-AMP signaling. In addition to *Sc*SbtB, we identified several transporters, among them the major potassium transporters in *Synechocystis* KtrA (*sll0493*), TrkA (*slr0773*), and MthK (*sll0993*). Moreover, the magnesium transporter MgtE (*slr1216*), the sodium/H^+ antiporters NhaS2 and NhaS5 (*sll0273* and *slr0415*, respectively), and the glutamate-Na^+ symporter (*slr0625*) were identified as c-di-AMP–binding proteins. In addition to SbtB, the identification of these potential c-di-AMP–dependent transporters implied that c-di-AMP may play a major role in regulating ionic and osmotic homeostasis of *Synechocystis*. KtrA, TrkA, and MgtE are also well-known c-di-AMP target proteins in Gram-positive bacteria (*12*, *14*, *28*); their successful identification here validated our pull-down assay. None of the c-di-AMP target proteins was identified in the negative control experiment.

Collectively, these results established SbtB as yet another PII-like protein interacting with c-di-AMP. Because the function of c-di-AMP sensing by this protein family remains obscure, we focused our investigation on the detailed characterization of the SbtB:c-di-AMP molecular interaction and its physiological consequences.

Structural basis of c-di-AMP binding to SbtB

To gain deeper insight into the structural basis of c-di-AMP binding by *Sc*SbtB, we aimed to obtain the crystal structure of the *Sc*SbtB:c-di-AMP complex. To this end, we used crystals that we previously obtained in different ligandation states from several cocrystallization trials of *Sc*SbtB (*20*). These crystals contain one *Sc*SbtB trimer in the asymmetric unit in space group $P3_2$, such that the three monomers and the three ligand binding sites, which are situated between the subunits, are involved in different crystal contacts (*20*). We now used apo crystals of this form in soaking experiments with c-di-AMP, resulting in a 2.0 Å crystal structure of the *Sc*SbtB:c-di-AMP complex (Fig. 1, C to F). However, only two of the binding sites turned out to be occupied by c-di-AMP (Fig. 1C), both with clear electron density for c-di-AMP in full occupancy (Fig. 1D). In these two sites,

Downloaded from https://www.science.org on July 06, 2023

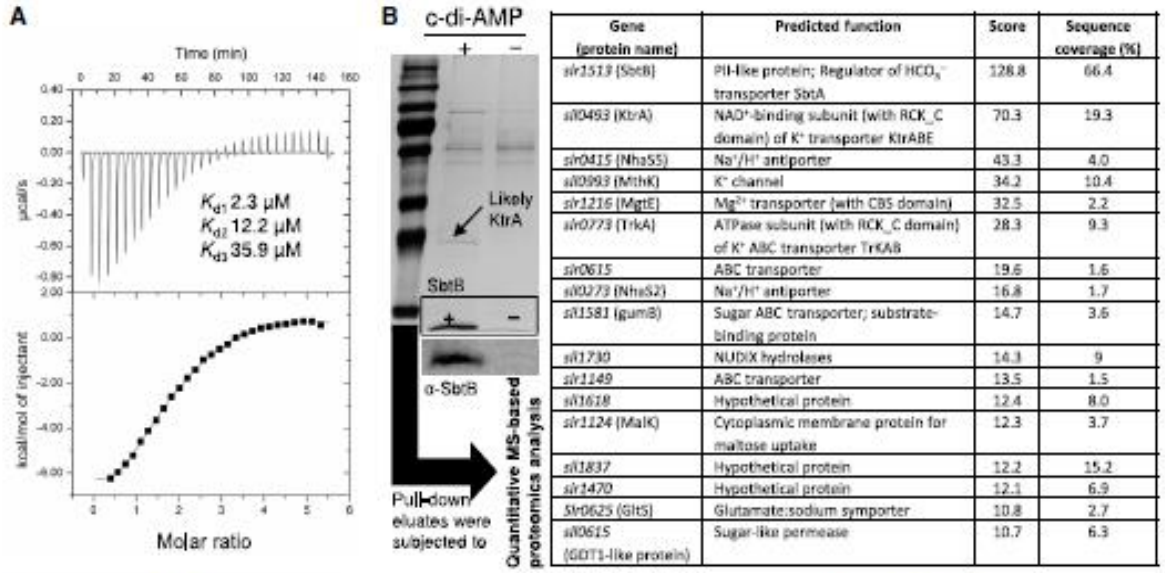

Gene (protein name)	Predicted function	Score	Sequence coverage (%)
slr1513 (SbtB)	PII-like protein; Regulator of HCO_3^- transporter SbtA	128.8	66.4
sll0493 (KtrA)	NAD^+-binding subunit (with RCK_C domain) of K^+ transporter KtrABE	70.3	19.3
slr0415 (NhaS5)	Na^+/H^+ antiporter	43.3	4.0
sll0993 (MthK)	K^+ channel	34.2	10.4
slr1216 (MgtE)	Mg^{2+} transporter (with CBS domain)	32.5	2.2
slr0773 (TrkA)	ATPase subunit (with RCK_C domain) of K^+ ABC transporter TrKAB	28.3	9.3
slr0615	ABC transporter	19.6	1.6
sll0273 (NhaS2)	Na^+/H^+ antiporter	16.8	1.7
sll1581 (gumB)	Sugar ABC transporter; substrate-binding protein	14.7	3.6
sll1730	NUDIX hydrolases	14.3	9
slr1149	ABC transporter	13.5	1.5
sll1618	Hypothetical protein	12.4	8.0
slr1124 (MalK)	Cytoplasmic membrane protein for maltose uptake	12.3	3.7
sll1837	Hypothetical protein	12.2	15.2
slr1470	Hypothetical protein	12.1	6.9
Slr0625 (GltS)	Glutamate:sodium symporter	10.8	2.7
sll0615 (GDT1-like protein)	Sugar-like permease	10.7	6.3

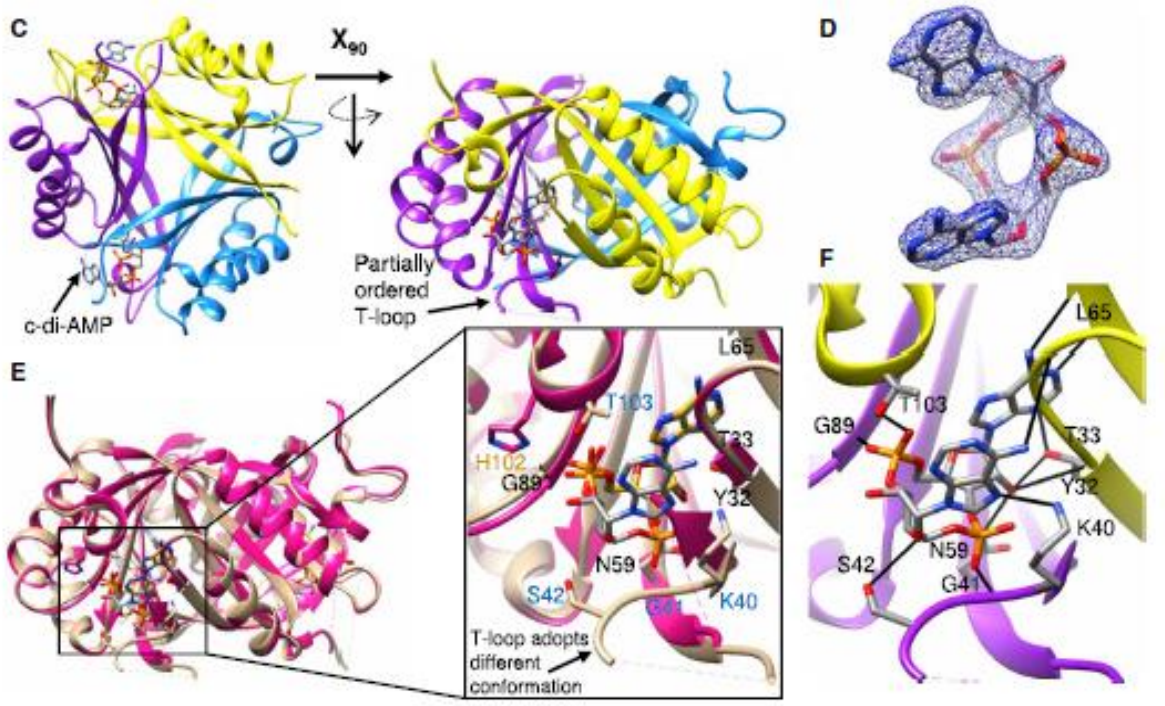

Fig. 1. Identification of SbtB as a major c-di-AMP receptor protein in cyanobacteria. (**A**) ITC analysis shows that SbtB binds c-di-AMP in an anticooperative manner with K_d values as indicated. Top: The raw ITC data in the form of the heat produced during the titration of 33.3 µM SbtB (trimeric concentration) with 0.5 mM c-di-AMP. Bottom: The binding isotherms and the best-fit curves according to the three sequential binding site model. (**B**) SDS–polyacrylamide gel electrophoresis analysis of c-di-AMP pull-down elution fraction and Western blot detection of SbtB, using α-SbtB antibodies. Samples were analyzed with quantitative MS-based proteomics analysis. Identified proteins are sorted by their scores. NAD^+, nicotinamide adenine dinucleotide; ATPase, adenosine triphosphatase; ABC, ATP-binding cassette; NUDIX hydrolases cleave nucleoside diphosphates linked to any ("x") moiety. (**C** to **F**) Structural and binding properties of the *Sc*SbtB protein. (C) Overall architecture of the trimeric SbtB:c-di-AMP complex with nucleotide-binding pockets located in the intersubunit clefts and shown in ribbon representation with different color for each monomer. (D) The electron density of c-di-AMP is shown as an F_o-F_c omit map contoured at 2.5 σ. (E) Superposition of *Sc*SbtB:c-di-AMP (brown) with *Sc*SbtB:AMP (pink; PDB: 5O3R), yielding an root mean square deviation of 0.33 Å and showing that the T-loop in the SbtB:c-di-AMP complex is partially ordered and adopts a different conformation than in the SbtB:AMP structure. (F) Close-up of the c-di-AMP binding site with relevant residues for nucleotide binding shown as sticks, and H bonds indicated by thin lines. (*E*) Inset: Highlighting the superposition of the nucleotide binding sites, with residues specific for c-di-AMP binding labeled in blue and those for AMP in orange.

as compared to the AMP- or cAMP-bound complexes, the base of the T-loop was found in a different conformation (Fig. 1E), forming additional interactions with the ligand (Fig. 1F), while the third site remained in apo-state due to limitations of the crystal packing. To exclude that also the folding of the T-loop or other binding-induced conformational changes were possibly restrained by crystal contacts during the soaking experiment, we also performed cocrystallization trials with c-di-AMP. Unexpectedly, these again yielded the same

Downloaded from https://www.science.org on July 06, 2023

crystal form resulting in a dataset of similar resolution, with the same two sites occupied and no noticeable structural differences.

All three subunits of the *Sc*SbtB:c-di-AMP complex are essentially in the same conformation as in the apo-*Sc*SbtB coordinates, and the whole *Sc*SbtB:c-di-AMP complex superimposes with a Cα–root mean square deviation value of 0.26 Å on the apo-*Sc*SbtB trimer [Protein Data Bank (PDB): 5O3P] (fig. S2). While there were no major differences between the *Sc*SbtB:c-di-AMP complex and apo-*Sc*SbtB, a comparison with the AMP- or cAMP-bound complexes revealed several additional unique interactions between c-di-AMP and the base of the T-loop (Fig. 1, E and F, and fig. S2), which caused a partial ordering and restructuring of the loop (Fig. 1, C to F). Structural alteration of the T-loop is a characteristic mechanism by which effector molecules modulate the interaction of canonical PII proteins with their receptors (*25*, *29*). The effect of c-di-AMP binding on the T-loop conformation strengthened the above results on the specificity of c-di-AMP binding to SbtB and suggested that c-di-AMP signaling via SbtB is functionally relevant and affects SbtB interaction with diverse interaction partners.

Physiological role of SbtB as a c-di-AMP receptor protein

Next, to search for a functional link between SbtB as a c-di-AMP receptor protein and c-di-AMP signaling cascade, we aimed to compare the phenotype of a *sbtB*-deficient mutant (encoded by *slr1513*) with a mutant deficient in *dacA*, which encodes for the only identified di-adenylate cyclase A (DacA; encoded by *sll0505*) in *Synechocystis*. To create a c-di-AMP free mutant, we first attempted the generation of a deletion or insertion Δ*dacA* mutant in a glucose-sensitive background (GS-strain). The insertion attempt aimed to avoid a polar effect on the expression of the downstream gene *sll0506* (encoding for undecaprenyl phosphate synthetase), because the *sll0505* gene overlaps with *sll0506* and is predicted to contain a possible promoter region for *sll0506* (*17*). However, we only achieved partial segregation by both attempts (fig. S3). In contrast, complete segregation was obtained in the background of glucose-tolerant *Synechocystis* strain (GT-strain), as revealed by the absence of the wild-type (WT) gene fragment through polymerase chain reaction (PCR) amplification (fig. S3). This implies that DacA is not essential for the viability of the GT-*Synechocystis* under standard, glucose-free conditions but it is, for unknown reasons, essential for the lifestyle of GS-*Synechocystis*. Unless mentioned otherwise, the following results were generated using the fully segregated Δ*dacA* insertion mutant in GT-*Synechocystis* background. However, we were able to reproduce all these results using the Δ*dacA* deletion mutant in GT-*Synechocystis* as well.

Measurements of the intracellular c-di-AMP concentration confirmed that the completely segregated Δ*dacA* mutant was free of c-di-AMP, while the WT cells contained around 4.6 μmol per cell of c-di-AMP under photoautotrophic growth conditions (Fig. 2A). To further confirm that *dacA* gene (*sll0505*) encodes an active di-adenylate cyclase able to synthesize c-di-AMP, *Escherichia coli*, which does not synthesize c-di-AMP naturally, was transformed with a plasmid expressing a *sll0505*–green fluorescent protein (GFP) fusion protein under the control of the isopropyl-β-D-thiogalactopyranoside (IPTG)–inducible T7 promoter. High concentration of c-di-AMP was detected in *E. coli* cells upon induction as compared to uninduced cells (fig. S3), confirming the annotation of DacA.

In cyanobacteria, c-di-AMP signaling was previously linked to osmoregulation, to the resuscitation from long-term chlorosis under nitrogen starvation condition, and to day-night rhythms (*11*, *17*, *19*), whereas SbtB was shown to be important for C_i acclimation (*20*). It was therefore obvious to assume that c-di-AMP perception by SbtB could be involved in one or more of those c-di-AMP–linked processes by comparing the phenotypes of the mutants Δ*dacA* and Δ*sbtB* under different growth conditions.

First, *Synechocystis* WT, Δ*dacA*, and Δ*sbtB* mutants were subjected to osmotic stress by treating them with increasing concentrations of sorbitol (50 to 600 mM) (fig. S4). In agreement with a previous study (*17*), the growth of Δ*dacA* was strongly impaired in the presence of high osmolyte concentrations, with 300 mM sorbitol completely preventing growth. By contrast, the Δ*sbtB* mutant was not affected by osmotic stress (fig. S4), implying that c-di-AMP sensing by SbtB is not involved in osmoregulation. This clear phenotype of Δ*dacA* supports the notion that c-di-AMP has a key role in osmoregulation and maintenance of the intracellular turgor pressure within cyanobacteria. Moreover, this phenotype agrees with the identification of several ion and osmolyte transporters in the c-di-AMP pull-down experiment, including those for K^+, Na^+, and Mg^{2+} ions, glutamate, and maltose (Fig. 1B).

Second, the recovery from nitrogen starvation–induced chlorosis of the mutant strains was tested by resupplementation with a nitrogen source. The Δ*dacA* mutant was neither able to properly enter chlorosis nor to recover from chlorosis nearly as efficiently as the WT cells, which is consistent with high expression of the *dacA* gene under resuscitation conditions (fig. S5) (*19*). In contrast, the Δ*sbtB* mutant did not show any phenotypic difference to WT during these treatments (fig. S5). This suggests that SbtB is not required for entering and exiting from chlorosis, whereas c-di-AMP plays an important role in this process perhaps due to interaction with as yet unknown receptor protein.

Third, we wanted to test whether c-di-AMP might be involved in primary C_i acquisition, because our previous study revealed that Δ*sbtB* is impaired in proper C_i acclimation (*20*). Therefore, the photosynthetic HCO_3^--dependent oxygen evolution of the Δ*dacA* mutant was compared to WT in high C_i (HC)– and low C_i (LC)–acclimated cells (Fig. 2B and fig. S6). Both WT and Δ*dacA* cells showed the expected acclimation to HC conditions by lowering affinity for HCO_3^- as estimated by an increase of HCO_3^- K_m to about 300 μM (Fig. 2B). Under LC conditions, the affinity toward HCO_3^- increased markedly in both Δ*dacA* mutant and WT cells (Fig. 2B). Although the initial rise of the photosynthetic activity at low C_i concentrations was similar, the maximal photosynthetic rates (V_{max}) in the Δ*dacA* mutant was lower than in WT cells under LC-acclimated condition. The decreased V_{max} indicates a lower activity of the Calvin-Benson cycle (fig. S6), at saturating C_i amounts. Despite this difference, this experiment indicated that, in contrast to the Δ*sbtB* mutant, operation of the CCM was not affected in the Δ*dacA* mutant (*20*).

Last, we investigated the involvement of DacA and SbtB in diurnal growth by exposing the cells to 12-hour light/12-hour dark cycles. Similar to *S. elongatus* (*11*), the *Synechocystis* Δ*dacA* mutant showed a strong growth defect under day-night conditions (Fig. 2, C and D, and fig. S7). Unexpectedly, the Δ*sbtB* mutant showed a similar diurnal growth impairment (Fig. 2, C and D, and fig. S7). SbtB is known to regulate the HCO_3^- transporter SbtA through direct protein-protein interaction in response to the energy state of the cell and the second messenger cAMP (*20*, *22*, *23*, *27*), raising several questions of either an involvement of SbtA or cAMP in impaired

Downloaded from https://www.science.org on July 06, 2023

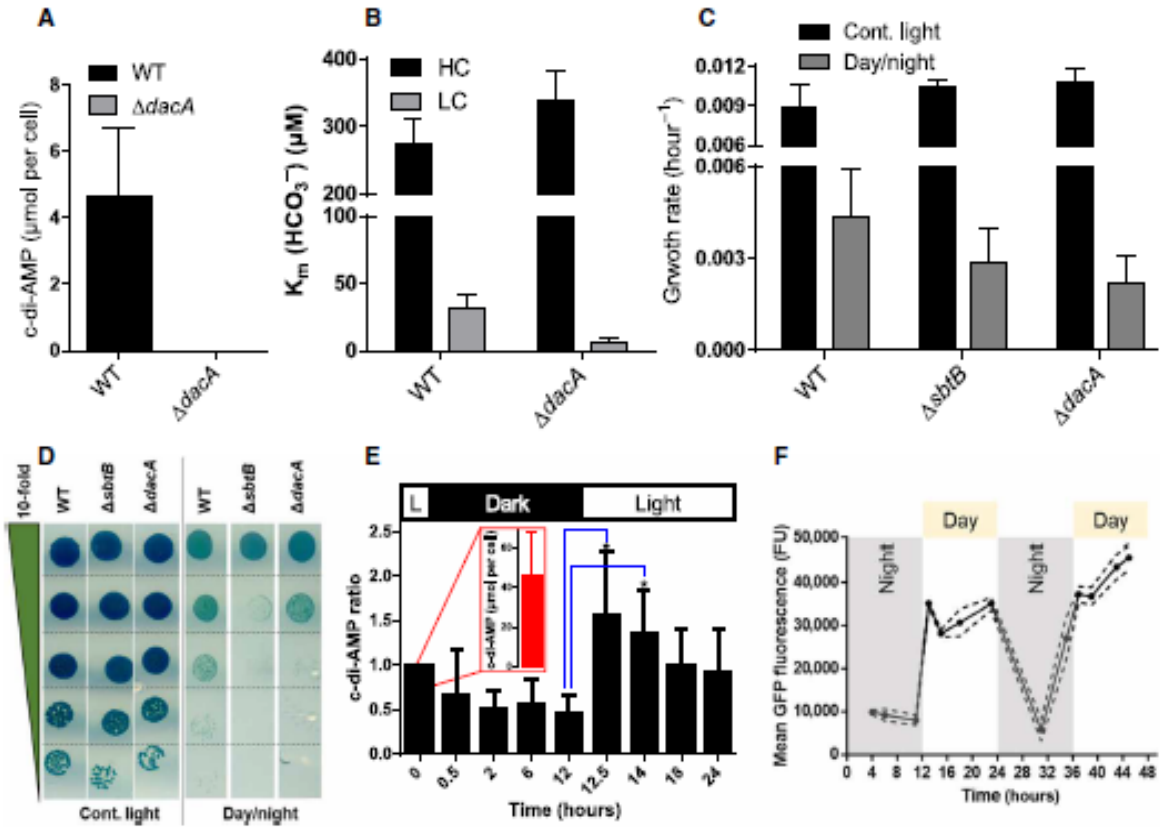

Fig. 2. Physiological characterization of Δ*sbtB* and Δ*dacA* mutants. (**A**) c-di-AMP concentration shown in µmol per cell within vegetative photoautotrophic growing *Synechocystis* sp. PCC 6803 WT (black bar) and the di-adenylate cyclase deficient mutant Δ*dacA* (gray bar; undetectable). (**B**) Bicarbonate affinity represented by the K_m (HCO_3^-) values of *Synechocystis* WT and the Δ*dacA* mutant under either high carbon (HC; black bars) or low carbon (LC; gray bars) regimes. (**C**) Specific growth rate of *Synechocystis* WT, Δ*sbtB*, and Δ*dacA* cells under either continuous light (black bars) or a 12-hour diurnal rhythm (gray bars). (**D**) Growth test by drop plate assay of *Synechocystis* WT, Δ*sbtB*, and Δ*dacA* cells as indicated under either continuous light (left) or a 12-hour diurnal rhythm (right). Cells were normalized to an optical density at 750 nm (OD_{750}) of 1.0 and serial diluted in 10-fold steps (top to bottom; depicted by a green triangle). (**E**) Relative c-di-AMP concentration within *Synechocystis* WT cells throughout a 12-hour diurnal rhythm. Statistically significant differences ($P < 0.05$) are indicated by asterisk (*) for the transition from the end of the night phase (12 hours) to early day-phase (12.5 and 14 hours). Values are means ± SD; $n = 5$ to 6 independent measurements. The c-di-AMP was not detectable within Δ*dacA* cells. The *x* axis shows the time in hours; the *y* axis shows the relative amount of c-di-AMP normalized to the first time point at the end of the day phase (indicated by 0.0 hours). (E) Inset: c-di-AMP concentration shown in micromoles per cell for the first measurable time point (0.0 hours). (**F**) Mean of in vivo SbtB-sfGFP expression throughout a 12-hour diurnal rhythm, as indicated. The *x* axis shows the time in hours; the *y* axis shows the mean GFP fluorescence in fluorescence units (FU).

diurnal growth. However, the Δ*sbtA* and Δ*cya1* (encodes for the major cAMP cyclase in *Synechocystis*) mutants grew almost like WT cells under 13 successive day-night cycles (fig. S7D). Together, these results indicated that the common growth defect of the Δ*sbtB* and Δ*dacA* mutants under diurnal cycles (Fig. 2, C and D) was not mediated by neither cAMP nor by a defect in primary C_i acquisition via SbtA (Figs. 2B and figs. S6 and S7). Rather, it pointed toward a specific/unidentified c-di-AMP–controlled process, involving signal perception by SbtB.

Diurnal cycling of c-di-AMP correlates with SbtB

To gain insight into the mechanism that makes c-di-AMP and SbtB indispensable for diurnal growth, we first looked for *sbtB* (*slr1513*) and *dacA* (*sll0505*) expression in the transcriptome dataset of diurnally grown *Synechocystis* cells (*30*). Both *sbtB* and *dacA* transcripts showed a diurnal dynamic, with a sharp increase at the beginning of the day and a decline in the dark phase (fig. S8). To reveal whether the changes in *dacA* transcript levels correlated with the c-di-AMP levels, the intracellular concentration of c-di-AMP was determined in WT *Synechocystis* cells under diurnal growth at different time points during day-night cycles. The first sampling point was taken at the end of the light phase, and four samples were taken during the following 12 hours of dark phase and four samples in the following 12 hours of light phase (Fig. 2E). While the c-di-AMP concentration dropped during the dark period, a rapid two to fourfold increase in c-di-AMP concentration was observed 30 min after onset of light (Fig. 2E). The maximum c-di-AMP concentration was reached in the early light phase and then declined throughout the remaining light phase (Fig. 2E), correlating well with the expression pattern of *dacA* (fig. S8). Because SbtB is known to bind the second messenger cAMP as well and to further exclude any possible role for cAMP in day-night metabolism (fig. S7E), we checked for intracellular concentration of cAMP under the same cycling condition in the WT and Δ*dacA* cells. The intracellular concentration of cAMP did not change markedly between day-night cycle within both of WT and Δ*dacA* cells (fig. S8C), which further supports the specificity of c-di-AMP in regulating *Synechocystis* diurnal metabolism. Moreover, we monitored SbtB expression using as a reporter the fluorescently

Downloaded from https://www.science.org on July 06, 2023

labeled fusion protein SbtB–super-folded GFP (sfGFP) (*20*). The SbtB-sfGFP fluorescence showed the same cycling pattern as the c-di-AMP concentration, dropping during the dark phase and peaking during the day (Fig. 2F). Last, to examine whether there might be a regulatory connection between *sbtB* and *dacA* at the level of transcription, we checked for the expression profile of *sbtB* (*slr1513*) in Δ*dacA* and for *dacA* (*sll0505*) in Δ*sbtB* mutant in comparison to WT cells using microarray technology (fig. S8, D and E). The *sbtB* mutation had negligible effect on the expression of *dacA*, while the *dacA* mutation led to partial down-regulation of *sbtB*, which could explain the inability of *dacA* mutant to fully activate the Calvin-Benson cycle (fig. S6), consistent with the proposed role for SbtB in regulating the entire CCM (*20*). Notably, the expression of the genes situated upstream (*sll0504*) and downstream (*sll0506*) of *dacA* was similar in both the Δ*dacA* and Δ*sbtB* mutants and very close to that of the WT cells, which confirmed that *dacA* mutation has no polar effects on the transcription of neighboring genes.

SbtB regulates glycogen metabolism via interaction with the glycogen-branching enzyme GlgB

Because the proteins of the PII superfamily, to which SbtB belongs, are known to exert their regulatory functions via direct protein-protein interaction (*29*), we hypothesized that SbtB binds to yet unknown target(s) in a c-di-AMP–dependent manner, thereby affecting diurnal growth.

To identify potential SbtB interaction partners, we characterized the global SbtB interactome using several mass spectrometry-based pull-down approaches and screened for hits that could be involved in day-night acclimation. First, coimmunoprecipitation (CoIP) experiments were performed with WT *Synechocystis* crude cell extracts using α-SbtB–specific antibodies. As negative control, we used crude cell extracts from Δ*sbtB* cells. Compared to the negative control, the immunoprecipitate contained five to ninefold enriched enzymes related to glycogen metabolism (fig. S9A). In particular, we identified glycogen synthase (GlgA2, *sll1393*), glycogen phosphorylase (GlgP2, *slr1367*), glycogen-branching enzyme (GlgB, *sll0158*), and glycogen-debranching enzyme (GlgX1, *slr0237*) as potential SbtB interacting partners. Because glycogen metabolism is of primary importance for day-night acclimation in cyanobacteria (*3*, *8*), the observed enrichment of glycogen metabolic enzymes would fit into the proposed c-di-AMP–related function of SbtB in diurnal growth.

To further elucidate c-di-AMP–dependent SbtB interactions, we performed several pull-down assays by immobilizing recombinant C-terminal His_8- or strep-tagged *Sc*SbtB protein on Ni^{2+} magnetic beads or streptavidin magnetic beads, respectively, and incubating them with *Synechocystis* crude cell extracts either in the presence or absence of c-di-AMP, followed by successive washes to remove the unbound proteins. In several pull-down experiments, the known SbtB-target SbtA was identified, which validated the procedure. With the His_8-tagged *Sc*SbtB protein on Ni^{2+} magnetic beads, in addition to SbtA, we identified again GlgA2, GlgP2, GlgB, GlgX, and furthermore the second glycogen-debranching enzyme (GlgX2, *slr1857*) and glucose-1-phosphate adenylyltransferase (GlgC, *slr1176*). Notably, GlgB and GlgA2 were more than 20-fold enriched in the presence of c-di-AMP (fig. S9B), implying that they could be of particular importance. When strep-tagged *Sc*SbtB protein was used as affinity bait, a cleaner pull-down with a low background due to higher specificity of streptavidin beads was obtained. Using this attempt, only the glycogen-branching enzyme GlgB was enriched as specific interaction partner (Fig. 3A and fig. S9, C and D). In the presence of c-di-AMP, GlgB was 14 times more abundant as compared to the pull-down in the absence of effector molecules (Fig. 3A). This enrichment was specific for c-di-AMP and not observed in the presence of cAMP (fig. S9, C and D). GlgB was not identified in the negative control (empty streptavidin beads) as well.

To further validate the specificity of SbtB-GlgB interaction and examine possible interactions with other glycogen-related enzymes by an independent method, we carried out interaction assays using the bacterial adenylate cyclase two-hybrid (BACTH) system. The BACTH system relies on the reconstitution of a functional adenylate cyclase (Cya) upon positive interaction of the proteins of interest fused to the T25 and T18 subunits of Cya, which can be detected by color change on X-Gal reporter plates. Here, we fused the T25 subunit of Cya N-terminally to SbtB, while the T18 subunit of Cya was fused either N- or C-terminally to the glycogen-related enzymes GlgA1, GlgA2, GlgP1, GlgP2, GlgB, and GlgC (fig. S10). The T25-SbtB fusion with an empty pUT18 vector was used as negative control, while the leucine zipper interaction was used as positive control. A clear interaction was observed only between T25-SbtB and GlgB N-terminally tagged with a T18 subunit (Fig. 3B), whereas no interaction was obtained with C-terminally tagged GlgB and the other glycogen metabolic enzymes (fig. S10). This result strongly indicated that SbtB is a specific interactor of GlgB.

To gain further insights into SbtB-GlgB complex formation, we studied the SbtB-GlgB interaction using microscale thermophoresis (MST). We titrated SbtB against labeled GlgB in the presence or absence of c-di-AMP. SbtB was able to bind GlgB with a K_d of 0.22 ± 0.07 μM (Fig. 3C); however, the presence of c-di-AMP (100 μM) did not change the binding constant markedly (K_d of 0.43 ± 0.10 μM).

Molecular basis for diurnal, c-di-AMP–dependent control of GlgB by SbtB

The photosynthetic synthesis of glycogen as carbohydrate reserve during the day is crucial for cyanobacterial survival in the night (*3*, *7*, *31*). To confirm the involvement of GlgB in this process, we tested diurnal growth of a Δ*glgB* mutant. The Δ*glgB* mutant was impaired in diurnal growth in a similar manner to the Δ*sbtB* and Δ*dacA* mutants (Fig. 3D), confirming the importance of glycogen metabolism and GlgB in diurnal growth. To obtain further evidence of a functional link between SbtB and the regulation of glycogen metabolism via GlgB in a c-di-AMP–dependent manner, we determined the intracellular glycogen concentration at the mid of the day phase. As compared to *Synechocystis* WT cells, glycogen levels were significantly reduced in all three mutants (Δ*sbtB*, Δ*dacA*, and Δ*glgB*) (Fig. 3E), with Δ*dacA* showing the lowest amount of glycogen with about 14.7%, Δ*sbtB* with 28.2%, and Δ*glgB* with 26.7% (Fig. 3E). Complementation of Δ*sbtB* by introducing copy of *slr1513* under the control of the *psbA2* promoter restored the growth of the mutant under day-night rhythm and restored the glycogen content to the levels of WT cells (fig. S11, A and B). Moreover, addition of glucose to BG_{11} medium rescued the diurnal growth defect of Δ*sbtB* (fig. S11C).

Because glycogen catabolism is the major source for respiration in the dark, supporting a heterotrophic mode of metabolism (*32*), we measured oxygen evolution and respiration during three successive day-night cycles. During the day, both Δ*sbtB* and Δ*dacA* mutants showed 50% less oxygen evolution than WT cells (Fig. 3F), in agreement with the inability of both mutants to fully activate the

Downloaded from https://www.science.org on July 06, 2023

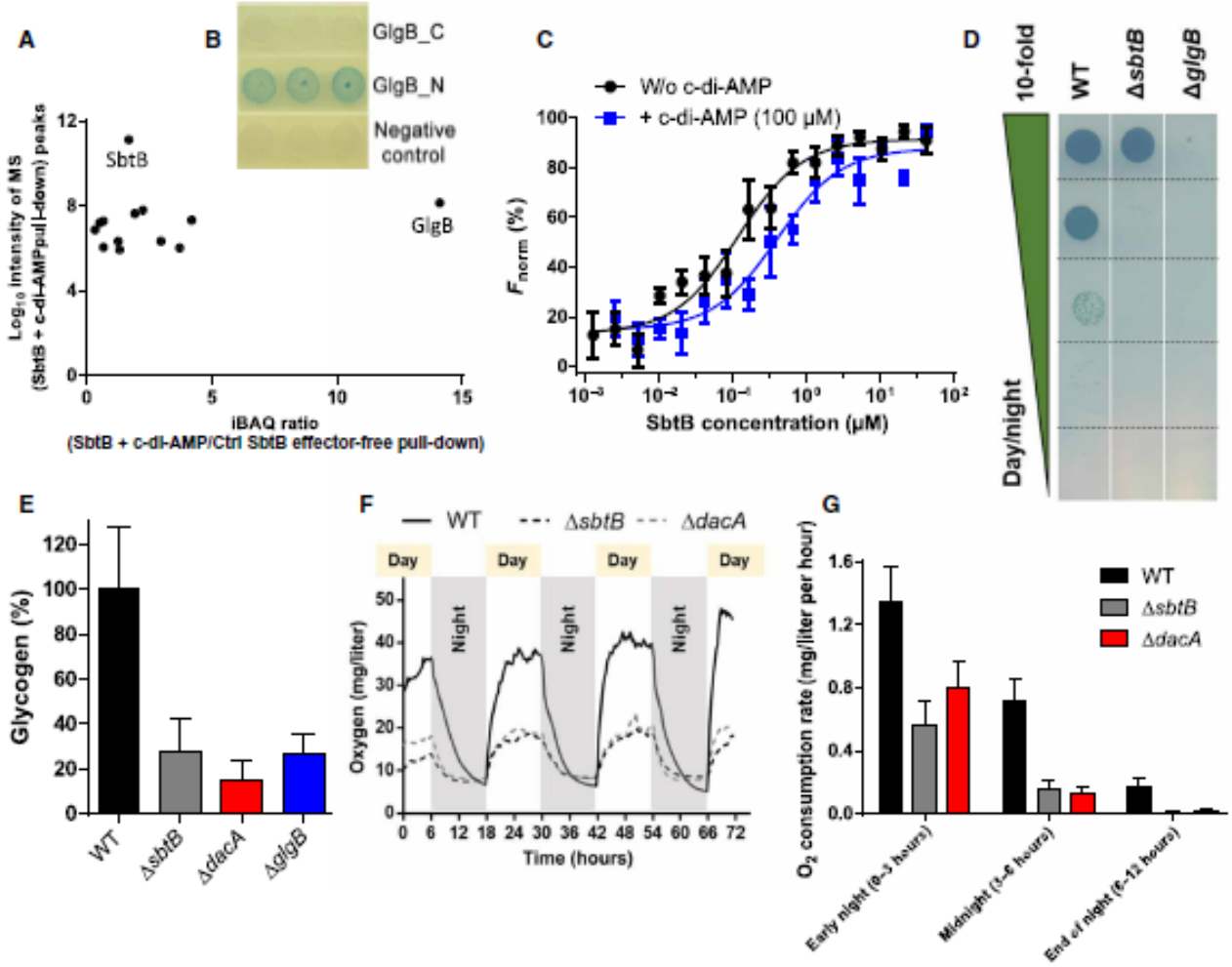

Fig. 3. Regulation of glycogen metabolism via c-di-AMP dependent SbtB signaling. (**A**) Streptavidin magnetic bead-based pull-downs using strep-tagged *Sc*SbtB protein in the absence or presence of c-di-AMP. The c-di-AMP enriched SbtB-GlgB interaction. (**B**) BACTH assay was performed using *E. coli* cells expressing T25-SbtB fusion together with either C-terminal (GlgB_C) or N-terminal (GlgB_N) T18-GlgB fusion, or empty Cya-T18 (negative control). SbtB-GlgB interaction is evidenced by appearance of a blue color on X-Gal reporter plates (middle). (**C**) MST analysis of the SbtB-GlgB interaction in either presence (blue line) or absence (black line) of 100 µM c-di-AMP, as indicated. The *y* axis shows the relative, normalized fluorescence units. (**D**) Growth test by drop plate assay of *Synechocystis* WT, Δ*sbtB*, and Δ*glgB* cells, as indicated in a 12-hour diurnal rhythm. Cells were normalized to an OD_{750} of 1.0 and serial diluted in 10-fold steps (up to down). (**E**) Relative glycogen levels of *Synechocystis* WT (black bar), Δ*sbtB* (gray bar), Δ*dacA* (red bar), and Δ*glgB* (blue bar) cells in the midday of a 12-hour diurnal rhythm. The glycogen content was normalized to 100% of WT cells. (**F**) Photosynthetic oxygen production and respiration of *Synechocystis* WT (black line) in comparison to Δ*sbtB* (black, dashed line) and Δ*dacA* (gray, dashed line) throughout a 12-hour diurnal rhythm for 72 hours, as indicated. The *y* axis shows the oxygen levels in parts per million (milligrams per liter). (**G**) Oxygen consumption rates in milligrams per liter per hour based on the data from (F). Oxygen consumption rates for WT (black bars), Δ*sbtB* (gray bars), and Δ*dacA* (red bars) were calculated for the early night (first 3 hours), midnight (next 3 to 6 hours), and the end of the night (last 6 to 12 hours).

Calvin-Benson cycle (fig. S6) (*20*). Upon onset of darkness, all strains started respiration, with WT cells displaying approximately twofold higher oxygen consumption than the mutants. Whereas WT cells kept on the respiration process for the whole night (12 hours), the Δ*sbtB* and Δ*dacA* cells ceased respiration after 6 hours (fig. 3FG). This result suggests that both mutants were unable to maintain respiration throughout a 12-hour night period and, therefore, were impaired in diurnal growth. To confirm this assumption, we determined the viability of the mutants compared to the WT cells during a prolonged dark incubation for 5 days. As revealed by drop plate assay, both mutants showed a marked loss of viability after 2 days of darkness. After 5 days of darkness, Δ*sbtB* cells were completely unviable (fig. S11D). Moreover, all strains retained a comparable efficiency of photosystem II (PSII) and photosynthetic pigmentations over 3 days of darkness, implying that the loss of viability of the mutants was not due to an alteration in the photosynthetic machinery (fig. S11, E and F). Again, all of those results indicate that the low glycogen levels in both mutants are the main cause of the growth defect under the day-night rhythm. However, it should be mentioned that Δ*dacA* cells showed about 25% reduction of apparent PSII quantum yield [determined by pulse-amplitude modulation (PAM) fluorescence] in the absence of actinic light as compared to WT cells (fig. S11E).

DISCUSSION

Here, we revealed that the PII-like signaling protein SbtB binds the second messenger c-di-AMP in addition to the standard adenine

Downloaded from https://www.science.org on July 06, 2023

nucleotides (AMP, ADP, and ATP) and to the carbon status reporting second messenger nucleotide cAMP. To our knowledge, this is the first signaling protein known to interact with both cAMP and c-di-AMP. This highlights the central role of SbtB as a switch point in cyanobacterial cell physiology, integrating not only signals from the energy state and carbon supply through adenine nucleotide and cAMP binding (*20*, *23*, *27*), respectively, but also from the diurnal state by binding to c-di-AMP. We were able to confirm the ability of SbtB to bind c-di-AMP from two distinct cyanobacterial species of unicellular *Synechocystis* sp. PCC 6803 and filamentous filamentous *Nostoc* sp. PCC 7120, which emphasizes a general role for c-di-AMP signaling via SbtB. In Gram-positive bacteria, c-di-AMP synthesis is related to cell wall homeostasis, potassium homeostasis, and osmotic control (*12*–*14*). Previous data indicated that, in cyanobacteria too, c-di-AMP might also control osmoregulation (*17*), which we were able to confirm in our study as well (Fig. 1B). We linked the c-di-AMP signaling with cyanobacterial osmoregulation by identifying several c-di-AMP target transporters in the c-di-AMP–dependent pull-down experiment, including transporters for K^+, Na^+, and Mg^{2+} ions, glutamate, and maltose. Furthermore, a link between c-di-AMP and nighttime survival was reported in *S. elongatus* as suggested by loss of viability of the Δ*dacA* mutant under dark conditions by a cryptic mechanism (*11*). Here, we revealed the exact mechanism by which c-di-AMP contributes to the regulation of the day-night rhythm in cyanobacteria.

Our data indicate that binding of c-di-AMP to SbtB modulates the interaction of SbtB with enzymes of glycogen synthesis, particularly with the glycogen-branching enzyme GlgB (Fig. 4), which we were able to confirm by different independent methods. In the *sbtB*-deficient mutant, the accumulation of glycogen during daytime is severely diminished and to a similar degree in the Δ*dacA* or Δ*glgB* mutants, which are unable to synthesize c-di-AMP or branched glycogen, respectively. Further support for a correlation between c-di-AMP concentration and glycogen synthesis comes from the diurnal cycling of c-di-AMP concentration, high during the day, when glycogen is synthesized, and low in the night, when glycogen is consumed. In *Synechocystis*, the daily c-di-AMP cycling levels correlate well with the expression of the diadenylate cyclase-encoding gene *sll0505* (*dacA*) under day-night cycles. In agreement, the SbtB-encoding gene *slr1513* was found to follow the same expression pattern as *sll0505* (*30*). Furthermore, the interaction between SbtB and GlgB was enriched in the presence of c-di-AMP, at least in the in vivo pull-down experiments; however, such influence was not observed using the recombinant purified proteins from *E. coli* in the in vitro MST experiment. The reason for that is presently ambiguous, but one possibility is that other components in the *Synechocystis* crude extract contribute to enhancing the affinity of SbtB for GlgB, perhaps other components of the glycogen metabolic enzymes, such as GlgA2 and/or GlgP2. Of note, GlgA2 and GlgP2 were enriched in the CoIP and His-tag SbtB pull-downs; however,

Downloaded from https://www.science.org on July 06, 2023

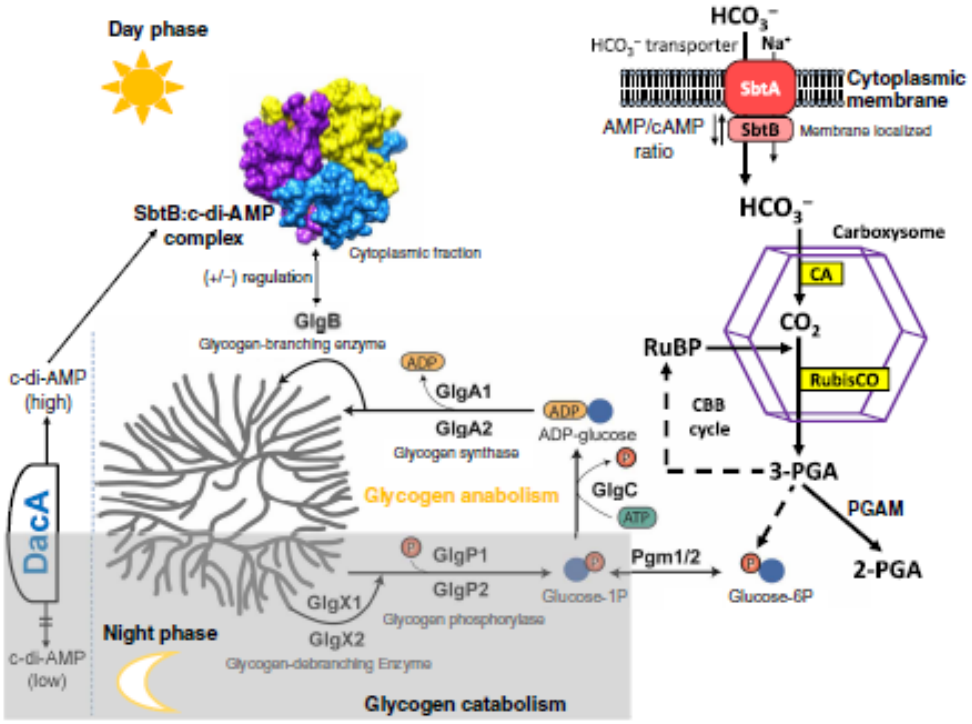

Fig. 4. Model of regulation of day-night switch of glycogen metabolism via c-di-AMP sensing by SbtB. During the day, cyanobacteria use an active carbon concentrating mechanism, which composes of several C_i uptake systems (among them the HCO_3^- transporter SbtA), and the carboxysome, where HCO_3^- is dehydrated to CO_2 by carbonic anhydrase (CA) and then CO_2 fixation occurs by RubisCO. Via the activity of Calvin-Benson (CBB) cycle, a part of the newly fixed carbon is redirected toward synthesis of carbon storage compound (glycogen). Simultaneously, the concentration of the second messenger nucleotide c-di-AMP increases in the day due to di-adenylate cyclase (DacA) activity. The soluble fraction of SbtB protein, not sequestered by SbtA, interacts with c-di-AMP and promotes glycogen synthesis by interacting with the glycogen-branching enzyme GlgB. After nightfall, c-di-AMP concentration decreases, and the catabolism of glycogen, which produced in the day, is the resource for nighttime survival.

we were not able to confirm such interaction with BACTH, implying that they could be indirectly involved in modulating SbtB-GlgB interaction. Nevertheless, a genome-wide fitness assessment of *S. elongatus* revealed that mutations in genes encoding for GlgB (*Synpcc7942_1085*) and SbtB (*Synpcc7942_1476*) and, to a less extent, for DacA (*Synpcc7942_0263*) cause a strong decrease in the bacterium fitness under diurnal rhythms (*3*) but not for SbtA (*Synpcc7942_1475*) or the putative cAMP synthases (*Synpcc7942_2195* or *Synpcc7942_0663*), which further support the specificity notion of SbtB and c-di-AMP signaling for the fitness of cyanobacterial diurnal metabolism.

However, c-di-AMP concentration oscillated in the opposite direction in *S. elongatus*, with high concentration in the night and low concentration during the day (*11*). The reasons for the discrepancy are now unclear, although both strains show a clear phenotypic defect under diurnal rhythm in the absence of the c-di-AMP cyclase, confirming the essentiality of c-di-AMP for cyanobacterial growth under day-night rhythm. It is known that *S. elongatus* uses a precisely operating circadian clock machinery to tune metabolism in a diurnal manner (*1*, *3*, *8*). Although components of this clock are conserved in *Synechocystis*, the overall process appears to be distinct owing to the emergence of multiple paralogs of the oscillator proteins (*6*, *33*). However, to comprehensively understand the control of the diurnal cycling of SbtB and c-di-AMP concentration, detailed analysis of the clock influence on SbtB and on c-di-AMP specific cyclase and phosphodiesterase activities is required. Notably, *sbtB* expression was strongly deregulated in the mutant of the circadian clock output regulator RpaA (*6*), which cannot survive the day-night rhythm as well (*8*).

In contrast to Δ*sbtB* (Fig. 3E), the Δ*rpaA* mutant is not impaired in glycogen synthesis during daytime (*8*, *34*). In this case, the inability of Δ*rpaA* to grow under day-night regime is due to the failure of this mutant to activate, in the night, carbon catabolic genes, including components of the OPP pathway, glycolysis, and glycogen degradation via GlgP (*1*, *6*, *8*, *34*). Apparently, SbtB and RpaA are working in opposite directions on glycogen anabolism and catabolism, respectively. Nevertheless, it appears that RpaA is involved in regulation of *sbtB*-gene expression in the day phase by yet unknown mechanism (*6*).

In addition to a role in regulating glycogen synthesis, c-di-AMP appears to regulate numerous ion transporters and osmotic responses, as deduced from the identification of several K^+ transporters, including KtrA (*sll0493*), TrkA (*slr0773*), and MthK (*sll0993*) as c-di-AMP targets. This highlights a conserved role for c-di-AMP in controlling osmotic homeostasis and K^+ transport (*12*–*14*), which is of particular importance, since K^+ is the major inorganic cation in the cytoplasm, acting as counter-ion of glutamate. In agreement with our identification of KtrA as a potential c-di-AMP target, the Na^+-dependent K^+ uptake system KtrABE was previously shown to be required for regulation of cell turgor and the adaptation to hyperosmotic stress elicited by either sorbitol or NaCl (*35*, *36*). However, osmotic control by c-di-AMP appears to act independently of SbtB, because the Δ*sbtB* mutant was not impaired in its responses to osmotic stress conditions like Δ*dacA* (fig. S4). Moreover, it seems also that the Mg^{2+} transporter MgtE is a conserved c-di-AMP target among different bacterial phyla (*12*, *14*, *28*). Of note, Mg^{2+} is of particular importance for the photosynthetic lifestyle of cyanobacteria as it is the central ion in the chlorophylls and required for the maintenance of the thylakoid membranes (*37*).

Cross-talk between second messenger nucleotides is perhaps a more common phenomenon than so far realized. Recently, it was found that the second messengers c-di-GMP and (p)ppGpp reciprocally control *Caulobacter crescentus* growth by competitive binding to a metabolic switch protein, SmbA (*38*). With this in mind, SbtB might play a similar role in cyanobacterial physiology. As is typical for signaling proteins of the PII family (*29*, *39*), SbtB seems to simultaneously perform multiple tasks in controlling cyanobacterial carbon metabolism: controlling bicarbonate uptake via SbtA interaction in response to cAMP and energy state of the cell (*20*, *22*, *23*, *27*) and controlling glycogen synthesis via interaction with glycogen-branching enzyme GlgB in response to c-di-AMP. Accordingly, SbtB would link the control of glycogen synthesis to bicarbonate availability. Under low carbon conditions, SbtB was preferentially found associated to the membrane fraction, presumably due to binding to SbtA (*20*, *23*). Thereby, less SbtB would be available for activation of glycogen synthesis, which takes place in the cytoplasmic space. More SbtB would become available under elevated C_i conditions, when SbtB is enriched in the soluble fraction (*20*). This hypothesis agrees with the fact that the glycogen levels in cells grown under atmospheric CO_2 concentration are low but increase at elevated C_i conditions (*40*, *41*). But, apparently, SbtB integrates the cellular information of both second messengers c-di-AMP and cAMP independently of each other, in agreement with distinct phenotype of Δ*dacA* and Δ*cya1* mutants (fig. S7). Whereas, cAMP acts as an indicator for cellular carbon status (*20*, *26*) and c-di-AMP is a specific indicator of day-night transition (Fig. 2E), and possibly they compete for SbtB available sites. The fact that c-di-AMP binding to SbtB affects the conformation of the T-loop is in perfect agreement with this scenario. The T-loop represents the major protein-interaction motif of PII signaling proteins (*39*). In complex with c-di-AMP, we have found the T-loop in a new conformation that is distinct from the cAMP or linear adenine nucleotide complex forms (Fig. 1E and fig. S2), a conformation that is seemingly driving the interaction with the newly identified GlgB and possibly yet to be identified receptors. The precise structural and regulatory mechanisms of these interactions, especially between SbtB:c-di-AMP and GlgB, await further biochemical and structural elucidation.

MATERIALS AND METHODS

Generation and purification of recombinant proteins

All the plasmids and primers used in this study are listed in (table S1). The recombinant C-terminal StrepII-tagged *Sc*SbtB was expressed and purified as previously described (*20*). Recombinant C-terminal StrepII-tagged SbtB protein from the filamentous *NsSbtB* was constructed as described in (*20*) using the primer pairs compatible for *Ns*SbtB. For generation of recombinant C-terminal His_8-tagged *Sc*SbtB, the SbtB encoding gene *slr1513* was amplified from *Synechocystis* sp. PCC 6803 and inserted via Gibson cloning in linearized pET28a vector. For generation of recombinant N-terminal His_6-tagged GlgB, the GlgB encoding gene *sll0158* was amplified from *Synechocystis* sp. PCC 6803 and inserted via Gibson cloning in linearized pET15b vector. The recombinant StrepII-tagged proteins were purified as previously described (*20*, *24*), while the His-tagged proteins were purified as described previously (*24*, *42*). For the recombinant C-terminal GFP-tagged DacA, which was used for quantification of c-di-AMP in *E. coli*, the DacA encoding gene

Downloaded from https://www.science.org on July 06, 2023

sll0505 was amplified from *Synechocystis* sp. PCC 6803 and inserted via Gibson cloning in linearized pET28a-eGFP–based vector.

Crystallization, crystal handling, data collection, and structure elucidation

For soaking experiments, crystals of the trigonal apo crystal form were reproduced as described previously (*20*). These crystals were grown with a reservoir solution composed of 0.1 M phosphate-citrate (pH 4.2) and 40% (w/v) polyethylene glycol (PEG) 300 and were soaked in a droplet of reservoir solution supplemented with 0.33 mM c-di-AMP (cyclic di-3′,5′-adenylate sodium salt; catalog no. C088, BioLoG, Germany) for 4 hours. For cocrystallization, 2.5 mM c-di-AMP was added to the protein solution, and crystallization trials were performed as described (*20*). Cocrystals were grown with a reservoir solution of 0.1 M tris-sodium citrate (pH 5.6), 10% (w/v) PEG 4000, and 10% (w/v) isopropanol, and 20% PEG 400 was used for cryo-protection. All crystals were flash-cooled in liquid nitrogen, and diffraction data were collected at 100 K on a PILATUS 6M-F detector at beamline X10SA of the Swiss Light Source (PSI, Villigen, Switzerland). All data were indexed, integrated, and scaled using the XDS software package (*43*). The structures were solved using difference Fourier methods based on the trigonal apo-*Sc*SbtB structure (PDB: 5O3P). After initial rigid body refinement with REFMAC5 (*44*), it became apparent that the cocrystal structure was essentially identical to the costructure obtained by soaking and not regarded further. The structure of the *Sc*SbtB:c-di-AMP complex was rebuilt and completed by cyclic manual modeling with Coot program and refinement with REFMAC5 based on the data obtained from the soaking experiment. Data collection and refinement statistics are shown in (table S2). Structural representations were prepared using UCSF Chimera.

Generation of mutants

The nonmotile unicellular, freshwater cyanobacterium *Synechocystis sp.* PCC 6803 (glucose-tolerant Tübingen substrain; called here GT-strain) was used as a reference WT strain in this study. Our laboratory "Tübingen" substrain of the glucose-tolerant WT *Synechocystis sp.* PCC 6803 is originally derived from the parental strain *Synechocystis sp.* PCC-M (*45*). While the glucose-sensitive strain of *Synechocystis* sp. PCC 6803 (called here GS-strain) was obtained from Rostock cyanobacterial culture collection and adapted to grow under our standard cultivation conditions in Tübingen for almost 14 years. All constructs used in this study were generated via Gibson assembly, unless specified otherwise. All knockout mutants were generated with homolog recombination using the natural competence of *Synechocystis* sp. PCC 6803, as described previously (*20*). All plasmids and primers used in this study are listed in (table S1).

For generation of knockout deletion mutants in either GT-strain or GS-strain, the mutants were constructed by deleting the ORFs *slr1513*, *sll0505*, and *sll0158* (designated *sbtB*, *dacA*, and *glgB*, respectively) and replaced with the erythromycin, spectinomycin, and chloramphenicol resistance cassette, respectively. The cAMP-free mutant was created by knocking out *slr1991* (designated Δ*cya1*), which encodes the soluble adenylyl cyclase in *Synechocystis sp.*, as described previously (*20*). For the generation of the *sbtA* knockout mutant, the *sbtA* upstream sequence was obtained using the primer combination SbtAB_Apa5 and DelSbtA_Bam5, whereas the *sbtA* downstream sequence was obtained using the primer combination SbtAB_Sac3 and DelSbtA_Bam3. First, the two fragments were cloned each in a single pGEMT vector (Promega), and then, the two fragments were combined into one vector by transferring the downstream fragment as Sac I/Bam HI fragment into the vector containing the upstream fragment. Into the central Bam HI restriction site, either a kanamycin or a streptomycin resistance cassette was inserted. The Δ*dacA* insertion mutant was generated by inserting a kanamycin resistance cassette into the region encoding for the active center of DacA. All the plasmids used to generate the mutants were verified by sequencing and then transformed in *Synechocystis* sp. PCC6803, as described (*20*). All mutants were selected on BG_{11} plates supplemented with proper antibiotics and verified by PCR.

For complementation, SbtB-sfGFP strain was generated by introducing the *sbtB* gene (*slr1513*) fused to the gene encoding sfGFP under the control of the native promoter of *sbtB* gene into Δ*sbtB* backgrounds using the self-replicating plasmid pVZ322, as described previously (*20*). For inducible complementation of Δ*sbtB*, the *sbtB* gene (*slr1513*) was reinserted in the genome under the control of the light inducible promotor *psbA2*.

Cultivation conditions

All cyanobacterial growth experiments were performed in nitrate supplemented BG_{11} medium (BG_{11}^{n}) with addition of 5 mM $NaHCO_3$ to avoid C_i limitation. Precultures were grown in shaking conditions at 28°C under continuous light (~50 μE) until mid of logarithmic growth phase before each experiment started. Cells were always normalized to their optical density at 750 nm using a Helios Gamma UV-Vis Spectrophotometer (Thermo Fisher Scientific). Experiments in day-night conditions were performed in a separate day-night chamber, providing 12-hour light phase (~50 μE) followed by a 12-hour darkness phase.

Nitrogen starvation was induced by shifting the cells to nitrogen-free BG_{11} medium (BG_{11}^{0}) with an initial optical density at 750 nm (OD_{750}) of 0.5 and kept under constant light of 50 to 100 μE. For resuscitation assays, samples were taken after 7 and 14 days of nitrogen starvation, and the resuscitation was induced by shifting the cultures back to BG_{11}^{n}, as described previously (*19*, *46*). The osmotic stress was generated by addition of 50 to 600 mM sorbitol to BG_{11}^{n}, as indicated.

To generate long dark conditions, cultures were inoculated to a final OD_{750} of 0.4 and covered from light immediately using dark aluminum foil for 5 days and kept shaking at 28°C. To determine the recovery after prolonged darkness, samples were taken directly before shift to darkness (T_{zero}) and after 1, 2, 3, and 5 days of dark treatment and were recovered by shifting to 50 μE of white continuous light.

The agar drop assays were performed on BG_{11} agar plates containing 1.5% Bacto Agar (Thermo Fisher Scientific) in serial dilutions of OD_{750} ranging from 10^{0} to 10^{-4}, as described previously (*46*). To protect the freshly dropped cells from the photoinhibition, the agar plates were covered with white tissues for 24 hours after dropping, before they were exposed to the required conditions.

Oxygen measurements

To estimate oxygen levels in liquid cultures during 24 hours of diurnal rhythm, cultures were inoculated to a final OD_{750} of 0.4. Oxygen levels were measured in those cultures each 15 min using an Oxy-1 SMA (PreSens GmbH, Regensburg, Germany) device in combination with SP-PSt3-NAU-D5-YOP Oxygen Sensor Spots (PreSens GmbH). In contrast, the rate of C_i-dependent oxygen

Downloaded from https://www.science.org on July 06, 2023

evolution (oxygenic photosynthesis) as a function of increasing HCO_3^- concentration was determined using a Clark-type oxygen electrode (Hansatech), as previously described (*20*). All measurements were performed at least three times.

Estimation of intracellular glycogen concentration

Intracellular glycogen concentration was estimated as previously described (*7*) with modifications from (*19*). Cells were first exposed to two successive day-night cycles, followed by harvest of 40 ml of each culture within the mid of the third day phase.

Measurement of PSII activity by WATER-PAM chlorophyll fluorescence and the whole-cell spectra

On the basis of chlorophyll a fluorescence, PSII activity was determined using PAM fluorometry using a PAM control (Heinz Walz GmbH), as described previously (*20*, *47*), at a wavelength of 650 nm (measuring light). Shortly, the measurements were performed by diluting 20 µl of cells in H_2O to a final volume of 2 ml, followed by measuring every 30 s with the saturating pulse at either zero or 56 µE of actinic light. Samples were normalized to a fluorescence level of unexcited cells (F) that remained between 400 and 500 (*47*). The apparent PSII activity was determined with the saturation pulse method using the F_v/F_m ratio, where F_v defined as $F_m - F_0$.

Whole-cell spectra (320 to 750 nm; 5 nm s^{-1}) were recorded using a SPECORD 205 (Analytik Jena AG). Cultures were diluted 1:5 to a final volume of 1 ml.

Determination of intracellular c-di-AMP concentration

Samples for c-di-AMP measurement were taken throughout 24 hours. The first sample was taken immediately before the dark phase, the second sample 30 min after the onset of darkness, and subsequent samples every 2 hours afterward were harvested. The samples of the day phase were harvested in the same manner as for the night phase. Samples were taken from *Synechocystis sp.* PCC 6803 WT and Δ*dacA* cells. Illumination during light phase was at approximately 40 to 50 µE and during dark below 1 µE. Centrifugation steps were done at 20.800*g*, 4°C, and for 10 min. For sampling, 10 ml of cultures was filtered on a glass fiber prefilter (Merck Millipore Ltd., Cork, Ireland) with a pore size of 1.6 µm. Filters were then put in 2-ml reaction tubes, frozen in liquid nitrogen, and stored at −80°C until further processing. Samples were thawed in 700 µl of ice cold extraction solvent [acetonitrile/methanol/water (2/2/1, v/v/v)] and incubated in ice for 15 min. Afterward, they were heated for 10 min at 95°C, cooled on ice, and centrifuged, and the supernatant was transferred into a new tube. These steps, without the heating, were repeated twice with another 200 µl of extraction solvent. The combination of the supernatants from the three extractions was stored over night at −20°C. The next day, samples were centrifuged once more, supernatants were transferred to new tubes, and liquid were evaporated using a vacuum evaporator (Martin Christ Gefriertrocknungsanlagen GmbH, Osterode am Harz, Germany). The dried samples were resuspended in 200 µl of H_2O of which 40 µl was transferred into mass spectrometry vials filled with 40 µl of H_2O with $^{13}C_{20}{}^{15}N_{10}$-c-di-GMP and $^{13}C_{20}{}^{15}N_{10}$-c-di-AMP (200 ng/ml each). Further dilution, if necessary, was done with a solution of H_2O with $^{13}C_{20}{}^{15}N_{10}$-c-di-GMP and $^{13}C_{20}{}^{15}N_{10}$-c-di-AMP (100 ng/ml each). Calibrator preparation for mass spectrometry measurement was done with either 10 µl of cdiNMP-cGAMP calibrator cdZ0-13 or 10 µl of cdiNMP metabolites calibrator cdM0, 4-13. ddH_2O (40 µl) and ddH_2O (50 µl) with $^{13}C_{20}{}^{15}N_{10}$-c-di-GMP and $^{13}C_{20}{}^{15}N_{10}$-c-di-AMP (200 ng/ml each) were added and vortexed. Samples were heated at 95°C for 10 min, cooled on ice and frozen over night at −20°C. Samples were thawed, centrifuged, and transferred into MS vials with inserts.

Pull-down assays

Cell pellets of logarithmic growing *Synechocystis* WT or Δ*sbtB* cells were resuspended in 1 ml of detergent-free lysis buffer [50 mM tris-HCl, 50 mM NaCl, 50 mM KCl, 1 mM EDTA, 0.5 mM phenylmethylsulfonyl fluoride (pH 7.4)] and transferred into 1.5-ml microtubes containing 0.1 ml of glass beads (0.1 mm). Samples were lysed by using a FastPrep-24 Ribolyser (five cycles; 7.0 m s^{-1}; 30 s per cycle; 5-min break between each cycle; 4°C) and spun down at 10.000*g* and 4°C for 10 min. The supernatant was transferred into a fresh 1.5-ml reaction tube and kept on ice. The cyclic-di-AMP target fishing was performed as described (*48*), by passing the whole crude cell extract from WT *Synechocystis* sp. PCC 6803 cells growing under continuous illumination over 2′-AHC-c-diAMP agarose (catalog no. A183, BioLoG, Germany), while EtOH-NH agarose (catalog no. E010, BioLoG, Germany) was used as a negative control. The detection of SbtB in the c-di-AMP pull-down was confirmed by Western blot analysis using specific *Sc*SbtB-polyclonal antibodies as described previously (*20*).

For the strep-tag pull-down, 10 µM purified strep-tagged *Sc*SbtB was incubated with Δ*sbtB* crude cell extract (normalized to 3 mg of protein) of cells growing under continuous illumination, on 150 µl of MagStrep "type3" XT Beads (IBA GmbH) in the presence of either 2 mM cAMP (3′,5′-cAMP; Sigma-Aldrich, Germany) or 2 mM c-di-AMP (catalog no. C088, BioLoG, Germany) or without effector molecule in 1.5-ml reaction tubes at 28°C for 15 min. As a negative control, the same reaction was performed without purified *Sc*SbtB, to eliminate the proteins which could bind nonspecifically to the Strep beads. After discarding the supernatant, the column was washed three times with 1 ml of washing buffer [100 mM tris-HCl (pH 8.0), 150 mM NaCl, and 1 mM EDTA]. The elution was performed two times with 50 µl of BXT elution buffer (Biotin Elution Buffer, IBA GmbH), and both elution fractions were combined in a fresh 1.5-ml reaction tube. After measuring protein concentration by using a BCA Kit (Thermo Fisher Scientific), the whole sample was sent to liquid chromatography–mass spectrometry.

For the His_8-tag pull-down, 10 µM purified His-tagged SbtB was incubated with WT *Synechocystis* sp. PCC 6803 crude cell extract (normalized to 3 mg of protein) of cells growing under continuous illumination, on 150 µl of Ni-NTA MagBeads (Genaxxion) with either 0.1 mM c-di-AMP or without effector molecules in 1.5-ml reaction tubes at 28°C for 15 min. After discarding the supernatant, the column was washed five times with 1 ml of washing buffer [50 mM Na_2HPO_4 (pH 8.0), 300 mM NaCl, and 10 mM imidazole]. The elution was performed with 20 µl of elution buffer [50 mM Na_2HPO_4 (pH 8.0), 300 mM NaCl, and 250 mM imidazole].

For the SbtB, CoIP cell pellets of 300 ml logarithmic growing *Synechocystis* sp. PCC 6803 WT and Δ*sbtB* cells growing under continuous illumination (day condition) were resuspended in 1 ml of detergent-free lysis buffer [50 mM tris-HCl and 5 mM EDTA (pH 7.4)] and transferred into 1.5-ml microtubes containing 0.1 ml of glass beads (0.1 mm). Samples were lysed by using a FastPrep-24 Ribolyser (five cycles; 7.0 m s^{-1}; 30 s per cycle; 5-min break between

Downloaded from https://www.science.org on July 06, 2023

each cycle; 4°C) and spun down at 16.000*g* and 4°C for 5 min. The supernatant was transferred into a fresh 1.5-ml reaction tube and kept on ice. Aliquots of 150 µl of Protein G magnetic beads (Merck/Millipore PureProteome) were washed twice with 1 ml of lysis buffer and incubated with 60 µl of rabbit *Synechocystis* α-SbtB antiserum for 10 min at room temperature. After three additional washing steps, the beads were incubated under the previous coupling conditions with 3 mg of crude cell extract of either WT or Δ*sbtB*. After another three washing steps, elution was performed in two consecutive steps with each 60 µl of elution buffer (200 mM glycine buffer at pH 2.5). Both fractions were combined, shock-frozen in liquid nitrogen, and stored at −80°C until further analysis. As control for nonspecific binding, WT crude cell extract was incubated with rabbit *B. subtilis* α-TnrA antiserum coupled with Protein G magnetic beads.

For all of pull-down experiments, the eluted protein fractions were first subjected to the short SDS–polyacrylamide gel electrophoresis purification step, where the proteins were migrated into 12% gels for 1.5 cm and then stained with Coomassie blue, followed by in-gel digestion with Trypsin for the stained/isolated pieces of the gel-containing proteins. Trypsin-digested peptides were analyzed by liquid chromatography–tandem mass spectrometry on a Proxeon Easy-nLC coupled to Q Exactive HF, using linear gradient for 60 min. The spectra were searched against *Synechocystis* sp. PCC6803 database (UP000001425_1111708_complete_2019-02-13) and sequences for different versions of SbtB proteins (His-tagged or Strep-tagged). Label-free quantification was used to calculate intensities and iBAQ values that give semiquantitative quantifications of protein enrichment. The number of unique identified peptides/protein, sequence coverage, and score were considered to select proteins of interest.

GFP fluorescence quantification

The total amount of GFP fluorescence in the whole cells was determined as described previously in (*20*) for the Δ*sbtB* strain that expresses sbtB-sfGFP construct under the control of the native promoter of *sbtB* gene in successive day-night cycles. The emission of GFP fluorescence at 525 nm was determined for normalized cells of OD_{750} of 0.1, after excitation at 485 nm, using a Tecan multimode microplate reader (SparK 10M).

BACTH assay

Plasmid construction, cell cultivation, and experimental procedure of BACTH assay were performed as described previously (*49*) only on X-Gal plates supplemented with X-Gal (40 µg/ml), kanamycin (50 µg/ml), ampicillin (100 µg/ml), and IPTG (1 mM). We tested only the N-terminal fusion of T25 subunit of Cya to SbtB, while the T18 subunit of Cya was fused either N- or C-terminally to the glycogen-related enzymes GlgA1, GlgA2, GlgP1, GlgP2, GlgB, and GlgC. Primers used to generate T25-SbtB fusion protein are listed in (table S1). The T25-SbtB fusion with an empty pUT18 vector was used as negative control, while the leucine zipper interaction was used as positive control. The *E. coli* BTH101 (Euromedex) was used for BACTH assays. The BACTH assays were performed at least three-times with three independent *E. coli* colonies to confirm the reproducibility and the specificity of the SbtB-GlgB interaction.

Microscale thermophoresis

MST experiments were carried out as previously described (*20*) using a Monolith NT.115 (NanoTemper Technologies GmbH) with uncoated Monolith NT.115 Capillaries (NanoTemper Technologies GmbH). Primary amines (lysine residues) of His-tagged GlgB were fluorescent labeled using the Monolith Protein Labeling Kit RED-NHS (NanoTemper Technologies GmbH). Titration series of StrepII-tagged *Sc*SbtB in the range of 1.3 nM to 42.5 µM were incubated with 10 nM fluorescent labeled His-tagged GlgB in 50 mM phosphate buffer (pH 8.0). All runs were performed in triplicate with 40% MST power and 60% light-emitting diode power. Single-site fitting was done using the NanoTemper data analysis software.

Isothermal titration calorimetry

ITC experiments were performed as previously described (*20*, *50*) using a VP-ITC microcalorimeter (MicroCal) in 50 mM sodium-potassium phosphate buffer (pH 8.0) supplemented with 0.5 mM EDTA, at 20°C. For determination of binding isotherms of small effector molecules binding to *Sc*SbtB, the protein (33.3 µM trimer concentration) was titrated against 0.5 or 1.0 mM c-di-AMP sodium salt (catalog no. C088, BioLoG, Germany).

SUPPLEMENTARY MATERIALS

Supplementary material for this article is available at https://science.org/doi/10.1126/sciadv.abk0568

View/request a protocol for this paper from *Bio-protocol*.

REFERENCES AND NOTES

1. D. G. Welkie, B. E. Rubin, S. Diamond, R. D. Hood, D. F. Savage, S. S. Golden, A hard day's night: Cyanobacteria in diel cycles. *Trends Microbiol.* **27**, 231–242 (2019).
2. Z. Eelderink-Chen, J. Bosman, F. Sartor, A. N. Dodd, Á. T. Kovács, M. Merrow, A circadian clock in a nonphotosynthetic prokaryote. *Sci. Adv.* **7**, eabe2086 (2021).
3. D. G. Welkie, B. E. Rubin, Y. G. Chang, S. Diamond, S. A. Rifkin, A. LiWanga, S. S. Golden, Genome-wide fitness assessment during diurnal growth reveals an expanded role of the cyanobacterial circadian clock protein KaiA. *Proc. Natl. Acad. Sci. U.S.A.* **115**, E7174–E7183 (2018).
4. N. Wan, D. M. DeLorenzo, L. He, L. You, C. M. Immethun, G. Wang, E. E. K. Baidoo, W. Hollinshead, J. D. Keasling, T. S. Moon, Y. J. Tang, Cyanobacterial carbon metabolism: Fluxome plasticity and oxygen dependence. *Biotechnol. Bioeng.* **114**, 1593–1602 (2017).
5. A. Makowka, L. Nichelmann, D. Schulze, K. Spengler, C. Wittmann, K. Forchhammer, K. Gutekunst, Glycolytic Shunts Replenish the Calvin–Benson–Bassham Cycle as Anaplerotic Reactions in Cyanobacteria. *Mol. Plant* **13**, 471–482 (2020).
6. C. Köbler, S. J. Schultz, D. Kopp, K. Voigt, A. Wilde, The role of the *Synechocystis* sp. PCC 6803 homolog of the circadian clock output regulator RpaA in day–night transitions. *Mol. Microbiol.* **110**, 847–861 (2018).
7. M. Gründel, R. Scheunemann, W. Lockau, Y. Zilliges, Impaired glycogen synthesis causes metabolic overflow reactions and affects stress responses in the cyanobacterium *Synechocystis* sp. PCC 6803. *Microbiology* **158**, 3032–3043 (2012).
8. S. Diamond, D. Jun, B. E. Rubin, S. S. Golden, The circadian oscillator in *Synechococcus elongatus* controls metabolite partitioning during diurnal growth. *Proc. Natl. Acad. Sci. U.S.A.* **112**, E1916–E1925 (2015).
9. R. D. Hood, S. A. Higgins, A. Flamholz, R. J. Nichols, D. F. Savage, The stringent response regulates adaptation to darkness in the cyanobacterium *Synechococcus elongatus*. *Proc. Natl. Acad. Sci. U.S.A.* **113**, E4867–E4876 (2016).
10. A. M. Puszynska, E. K. O'Shea, ppGpp controls global gene expression in light and in darkness in *S. elongatus*. *Cell Rep.* **21**, 3155–3165 (2017).
11. B. E. Rubin, T. N. Huynh, D. G. Welkie, S. Diamond, R. Simkovsky, E. C. Pierce, A. Taton, L. C. Lowe, J. J. Lee, S. A. Rifkin, J. J. Woodward, S. S. Golden, High-throughput interaction screens illuminate the role of c-di-AMP in cyanobacterial nighttime survival. *PLOS Genet.* **14**, e1007301 (2018).
12. J. He, W. Yin, M. Y. Galperin, S. H. Chou, Cyclic di-AMP, a second messenger of primary importance: Tertiary structures and binding mechanisms. *Nucleic Acids Res.* **48**, 2807–2829 (2020).
13. W. Yin, X. Cai, H. Ma, L. Zhu, Y. Zhang, S. H. Chou, M. Y. Galperin, J. He, A decade of research on the second messenger c-di-AMP. *FEMS Microbiol. Rev.* **44**, 701–724 (2020).
14. J. Stülke, L. Krüger, Cyclic di-AMP Signaling in Bacteria. *Annu. Rev. Microbiol.* **74**, 159–179 (2020).
15. J. Gundlach, A. Dickmanns, K. Schröder-Tittmann, P. Neumann, J. Kaesler, J. Kampf, C. Herzberg, E. Hamemr, F. Schwede, V. Kaever, K. Tittmann, J. Stülke, R. Ficner,

Downloaded from https://www.science.org on July 06, 2023

Identification, characterization, and structure analysis of the cyclic di-AMP-binding PII-like signal transduction protein DarA. *J. Biol. Chem.* **290**, 3069–3080 (2015).
16. I. Campeotto, Y. Zhang, M. G. Mladenov, P. S. Freemont, A. Gründling, Complex structure and biochemical characterization of the staphylococcus aureus Cyclic Diadenylate Monophosphate (c-di-AMP)-binding Protein PstA, the Founding Member of a New Signal Transduction Protein Family. *J. Biol. Chem.* **290**, 2888–2901 (2015).
17. M. Agostoni, A. R. Logan-Jackson, E. R. Heinz, G. B. Severin, E. L. Bruger, C. M. Waters, B. L. Montgomery, Homeostasis of Second Messenger Cyclic-di-AMP Is Critical for Cyanobacterial Fitness and Acclimation to Abiotic Stress. *Front. Microbiol.* **9**, 1121 (2018).
18. J. W. Nelson, N. Sudarsan, K. Furukawa, Z. Weinberg, J. X. Wang, R. R. Breaker, Riboswitches in eubacteria sense the second messenger c-di-AMP. *Nat. Chem. Biol.* **9**, 834–839 (2013).
19. A. Klotz, J. Georg, L. Bučinská, S. Watanabe, V. Reimann, W. Januszewski, R. Sobotka, D. Jendrossek, W. R. Hess, K. Forchhammer, Awakening of a Dormant Cyanobacterium from Nitrogen Chlorosis Reveals a Genetically Determined Program. *Curr. Biol.* **26**, 2862–2872 (2016).
20. K. A. Selim, F. Haase, M. D. Hartmann, M. Hagemann, K. Forchhammer, PII-like signaling protein SbtB links cAMP sensing with cyanobacterial inorganic carbon response. *Proc. Natl. Acad. Sci. U.S.A.* **115**, 4861–4869 (2018).
21. N. Oren, S. Timm, M. Frank, O. Mantovani, O. Murik, M. Hagemann, Red/far-red light signals regulate the activity of the carbon-concentrating mechanism in cyanobacteria. *Sci. Adv.* **7**, eabg0435 (2021).
22. J. Du, B. Förster, L. Rourke, S. M. Howitt, G. D. Price, Characterisation of Cyanobacterial Bicarbonate Transporters in *E. coli* Shows that SbtA Homologs Are Functional in This Heterologous Expression System. *PLOS ONE* **9**, 12 (2014).
23. S. Fang, X. Huang, X. Zhang, M. Zhang, Y. Hao, H. Guo, L. N. Liu, F. Yu, P. Zhang, Molecular mechanism underlying transport and allosteric inhibition of bicarbonate transporter SbtA. *Proc. Natl. Acad. Sci. U.S.A.* **118**, e2101632118 (2021).
24. T. Lapina, K. A. Selim, K. Forchhammer, E. Ermilova, The PII signaling protein from red algae represents an evolutionary link between cyanobacterial and Chloroplastida PII proteins. *Sci. Rep.* **8**, 790 (2018).
25. K. A. Selim, E. Ermilova, K. Forchhammer, From cyanobacteria to Archaeplastida: New evolutionary insights into PII signalling in the plant kingdom. *New Phytol.* **227**, 722–731 (2020).
26. Y. Chen, M. J. Cann, T. N. Litvin, V. Iourgenko, M. L. Sinclair, L. R. Levin, J. Buck, Soluble adenylyl cyclase as an evolutionarily conserved bicarbonate sensor. *Science* **289**, 625–628 (2000).
27. J. A. Kaczmarski, N. S. Hong, B. Mukherjee, L. T. Wey, L. Rourke, B. Förster, T. S. Peat, G. D. Price, C. J. Jackson, Structural Basis for the Allosteric Regulation of the SbtA Bicarbonate Transporter by the PII-like Protein, SbtB, from *Cyanobium* sp. PCC7001. *Biochemistry* **58**, 5030–5039 (2019).
28. J. Gundlach, L. Krüger, C. Herzberg, A. Turdiev, A. Poehlein, I. Tascón, M. Weiss, D. Hertel, R. Daniel, I. Hänelt, V. T. Lee, J. Stülke, Sustained sensing in potassium homeostasis: Cyclic di-AMP controls potassium uptake by KimA at the levels of expression and activity. *J. Biol. Chem.* **294**, 9605–9614 (2019).
29. K. Forchhammer, K. A. Selim, Carbon/nitrogen homeostasis control in cyanobacteria. *FEMS Microbiol. Rev.* **44**, 33–53 (2020).
30. R. Saha, D. Liu, A. Hoynes-O'Connor, M. Liberton, J. Yu, M. Bhattacharyya-Pakrasi, A. Balassy, F. Zhang, T. Seok Moon, C. D. Maranas, H. B. Pakrasi, Diurnal regulation of cellular processes in the cyanobacterium *Synechocystis* sp. Strain PCC 6803: Insights from transcriptomic, fluxomic, and physiological analyses. *MBio* **7**, e00464-16 (2016).
31. E. Suzuki, H. Ohkawa, K. Moriya, T. Matsubara, Y. Nagaike, I. Iwasaki, S. Fujiwara, M. Tsuzuki, Y. Nakamura, Carbohydrate metabolism in mutants of the cyanobacterium *Synechococcus elongatus* PCC 7942 defective in glycogen synthesis. *Appl. Environ. Microbiol.* **76**, 3153–3159 (2010).
32. S. Doello, A. Klotz, A. Makowka, K. Gutekunst, K. Forchhammer, A specific glycogen mobilization strategy enables rapid awakening of dormant cyanobacteria from chlorosis. *Plant Physiol.* **177**, 594–603 (2018).
33. A. Wiegard, C. Köbler, K. Oyama, A. K. Dörrich, C. Azai, K. Terauchi, A. Wilde, I. M. Axmann, *Synechocystis* KaiC3 displays temperature- and KaiB-dependent ATPase activity and is important for growth in darkness. *J. Bacteriol.* **202**, e00478-19 (2020).
34. H. Iijima, T. Shirai, M. Okamoto, A. Kondo, M. Y. Hirai, T. Osanai, Changes in primary metabolism under light and dark conditions in response to overproduction of a response regulator RpaA in the unicellular cyanobacterium *Synechocystis* sp. PCC 6803. *Front. Microbiol.* **6**, 888 (2015).
35. S. Berry, B. Esper, I. Karandashova, M. Teuber, I. Elanskaya, M. Rögner, M. Hagemann, Potassium uptake in the unicellular cyanobacterium *Synechocystis* sp. strain PCC 6803 mainly depends on a Ktr-like system encoded by slr1509 (ntpJ). *FEBS Lett.* **548**, 53–58 (2003).
36. N. Matsuda, H. Kobayashi, H. Katoh, T. Ogawa, L. Futatsugi, T. Nakamura, E. P. Bakker, N. Uozumi, Na^+-dependent K^+ Uptake Ktr System from the Cyanobacterium *Synechocystis* sp. PCC 6803 and Its Role in the Early Phases of Cell Adaptation to Hyperosmotic Shock. *J. Biol. Chem.* **279**, 54952–54962 (2004).
37. A. C. Pohland, D. Schneider, D, Mg^{2+} homeostasis and transport in cyanobacteria - at the crossroads of bacterial and chloroplast Mg^{2+} import. *Biol. Chem.* **400**, 1289–1301 (2019).
38. V. Shyp, B. N. Dubey, R. Böhm, J. Hartl, J. Nesper, J. A. Vorholt, S. Hiller, T. Schirmer, U. Jenal, Reciprocal growth control by competitive binding of nucleotide second messengers to a metabolic switch in *Caulobacter crescentus*. *Nat. Microbiol.* **6**, 59–72 (2021).
39. K. Forchhammer, J. Lüddecke, Sensory properties of the PII signalling protein family. *FEBS J.* **283**, 425–437 (2016).
40. M. Eisenhut, E. A. von Wobeser, L. Jonas, H. Schubert, B. W. Ibelings, H. Bauwe, H. C. Matthijs, M. Hagemann, Long-term response toward inorganic carbon limitation in wild type and glycolate turnover mutants of the cyanobacterium *Synechocystis* sp. strain PCC 6803. *Plant Physiol.* **144**, 1946–1959 (2007).
41. J. K. Gupta, P. Rai, K. K. Jain, S. Srivastava, Overexpression of bicarbonate transporters in the marine cyanobacterium *Synechococcus* sp. PCC 7002 increases growth rate and glycogen accumulation. *Biotechnol. Biofuels* **13**, 17 (2020).
42. K. A. Selim, L. Tremiño, C. Marco-Marín, V. Alva, J. Espinosa, A. Contreras, M. D. Hartmann, K. Forchhammer, V. Rubio, Functional and structural characterization of PII-like protein CutA does not support involvement in heavy metal tolerance and hints at a small-molecule carrying/signaling role. *FEBS J.* **288**, 1142–1162 (2021).
43. W. Kabsch, XDS. *Acta Crystallogr. D Biol. Crystallogr.* **66**, 125–132 (2010).
44. G. N. Murshudov, P. Skubák, A. A. Lebedev, N. S. Pannu, R. A. Steiner, R. A. Nicholls, M. D. Winn, F. Long, A. A. Vagin, REFMAC5 for the refinement of macromolecular crystal structures. *Acta Crystallogr. D Biol. Crystallogr.* **67**, 355–367 (2011).
45. D. Trautmann, B. Voss, A. Wilde, S. Al-Babili, W. R. Hess, Microevolution in cyanobacteria: Re-sequencing a motile substrain of Synechocystis sp. PCC 6803. *DNA Res.* **19**, 435–448 (2012).
46. K. A. Selim, M. Haffner, Heavy Metal Stress Alters the Response of the Unicellular Cyanobacterium *Synechococcus elongatus* PCC 7942 to Nitrogen Starvation. *Life* **10**, 275 (2020).
47. A. M. Acuna, J. J. Snellenburg, M. Gwizdala, D. Kirilovsky, R. Van Grondelle, I. H. M. Van Stokkum, Resolving the contribution of the uncoupled phycobilisomes to cyanobacterial pulse-amplitude modulated (PAM) fluorometry signals. *Photosynth. Res.* **127**, 91–102 (2016).
48. J. Kampf, J. Gundlach, C. Herzberg, K. Treffon, J. Stülke, Identification of c-di-AMP-Binding Proteins Using Magnetic Beads, in *c-di-GMP Signaling: Methods and Protocols. Methods in Molecular Biology* (Springer, Science+Business Media LLC, Berlin, 2017), pp. 347–359.
49. B. Watzer, P. Spät, N. Neumann, M. Koch, R. Sobotka, B. Macek, O. Hennrich, K. Forchhammer, The signal transduction protein P_{II} controls ammonium, nitrate and urea uptake in cyanobacteria. *Front. Microbiol.* **10**, 1428 (2019).
50. K. A. Selim, M. Haffner, B. Watzer, K. Forchhammer, Tuning the *in vitro* sensing and signaling properties of cyanobacterial PII protein by mutation of key residues. *Sci. Rep.* **9**, 18985 (2019).

Acknowledgments: We are grateful to A. Klotz and H. Grenzendorf (IMIT, Tübingen University) for the excellent assistance, the staff of beamline X10SA/SLS, the Proteome Center (Tübingen University), W. R. Hess (Freiburg University) for the microarray data, and L. Lo-Presti for critical scientific and linguistic editing of the manuscript. Furthermore, we would like to acknowledge the infrastructural support by the Cluster of Excellence "Controlling Microbes to Fight Infections" (EXC 2124–390838134) of the DFG. K.A.S. would like to dedicate this research to the memory of A. Selim, a distinguished father and medical doctor, for the continued support. **Funding:** This work was supported by the German research foundation (DFG) within the priority program SPP1879 to (K.F., M.Hag., M.Haf., and O.M.) and by institutional funds of the Max Planck Society. DFG-Cluster of Excellence (EXC 2124) "Controlling Microbes to Fight Infections" to (K.A.S.). **Author contributions:** K.A.S. and K.F. conceived, initiated, and supervised the whole project. K.A.S. designed the experiments. M.Haf. and K.A.S. performed most of the physiological and biochemical experiments, except for c-di-AMP quantification by M.B. with help of R.S., photosynthetic HCO_3^--dependent oxygen evolution by O.M. under supervision of M.Hag., and BACTH by N.N. L.K. and J.S. helped M.Haf. for performing c-di-AMP pull-down. R.A. performed crystallographic sample preparation and diffraction data collection, K.A.S. solved the crystal structure, and M.D.H. supervised the structural analysis. K.A.S. evaluated and interpreted the results, prepared the figures, and wrote the manuscript. K.A.S., M.D.H., M.Hag., and K.F. commented and edited on the manuscript. All authors approved the final version of the manuscript. **Competing interests:** The authors declare that they have no competing interests. **Data and materials availability:** Crystallography, atomic coordinates, and structure factors have been deposited in the Protein Data Bank, www.wwpdb.org (PDB ID code: 7OBJ).

Submitted 18 June 2021
Accepted 18 October 2021
Published 8 December 2021
10.1126/sciadv.abk0568

Downloaded from https://www.science.org on July 06, 2023

Science Advances
AAAS

Supplementary Materials for

Diurnal metabolic control in cyanobacteria requires perception of second messenger signaling molecule c-di-AMP by the carbon control protein SbtB

Khaled A. Selim*, Michael Haffner, Markus Burkhardt, Oliver Mantovani, Niels Neumann, Reinhard Albrecht, Roland Seifert, Larissa Kruger, Jorg Stulke, Marcus D. Hartmann, Martin Hagemann, Karl Forchhammer*

*Corresponding author. Email: khaled.selim@uni-tuebingen.de (K.A.S.); karl.forchhammer@uni-tuebingen.de (K.F.)

Published 8 December 2021, *Sci. Adv.* **7**, eabk0568 (2021)
DOI: 10.1126/sciadv.abk0568

This PDF file includes:

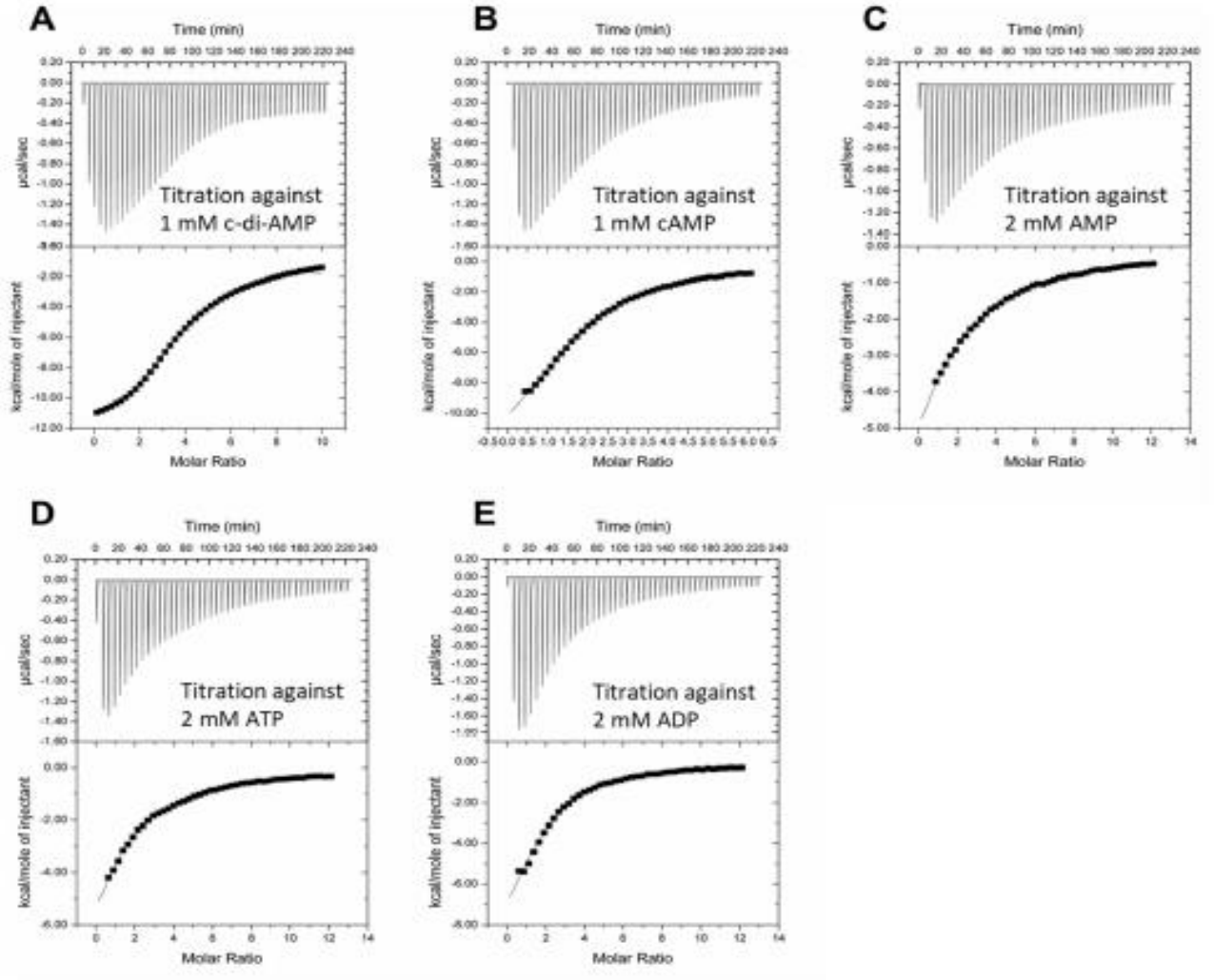

Fig. S1. ITC analysis of ligand binding properties of the *Sc*SbtB protein. Binding of various adenosine nucleotides to the *Sc*SbtB protein with strong binding isotherm. ITC titration against (A) 1 mM c-di-AMP, (B) 1 mM cAMP, (C) 2 mM AMP, (D) 2 mM ATP, and (E) 2 mM ADP. The binding enthalpy for c-di-AMP was almost equivalent or higher than that of AMP, ATP, ADP and cAMP at a lower concentration of c-di-AMP. Upper panels show the raw ITC data in the form of the heat produced during the titration of 33.3 µM SbtB (trimeric concentration) with different effector molecules; lower panels show the binding isotherms and the best-fit curves according to the three sequential binding site models for trimeric SbtB.

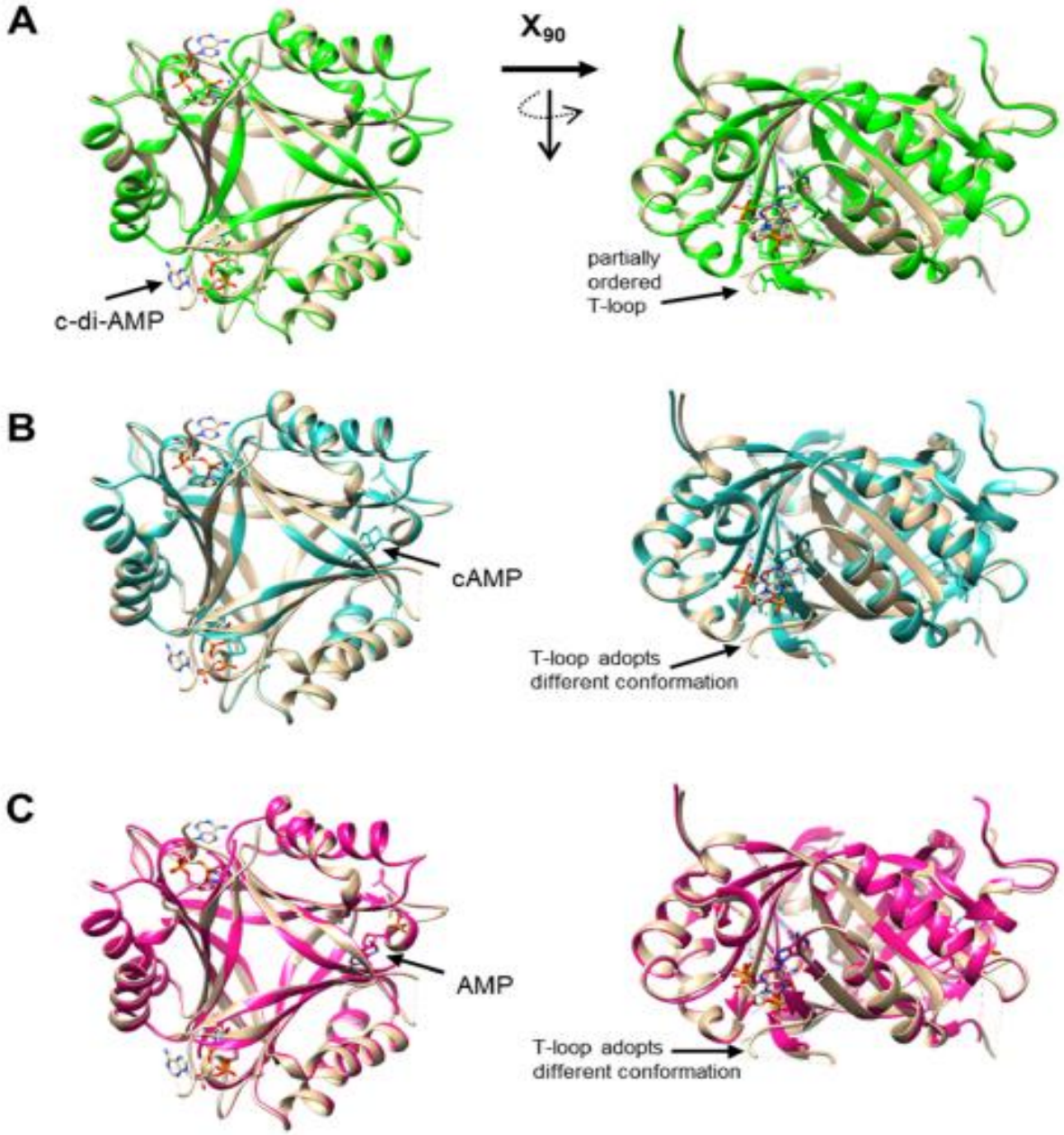

Fig. S2. Structural superpositions of *Sc*SbtB:c-di-AMP complex with different *Sc*SbtB structures. Superposition of *Sc*SbtB:c-di-AMP complex (brown) with (A) apo-*Sc*SbtB trimer (green; PDB: 5O3P), (B) *Sc*SbtB:cAMP complex (blue; PDB: 5O3Q), and *Sc*SbtB:AMP complex (pink; PDB: 5O3R), yielded RMSD values of 0.26 Å, 0.31 Å and 0.33 Å, respectively. Structural representations were prepared using UCSF Chimera (http://www.rbvi.ucsf.edu/chimera).

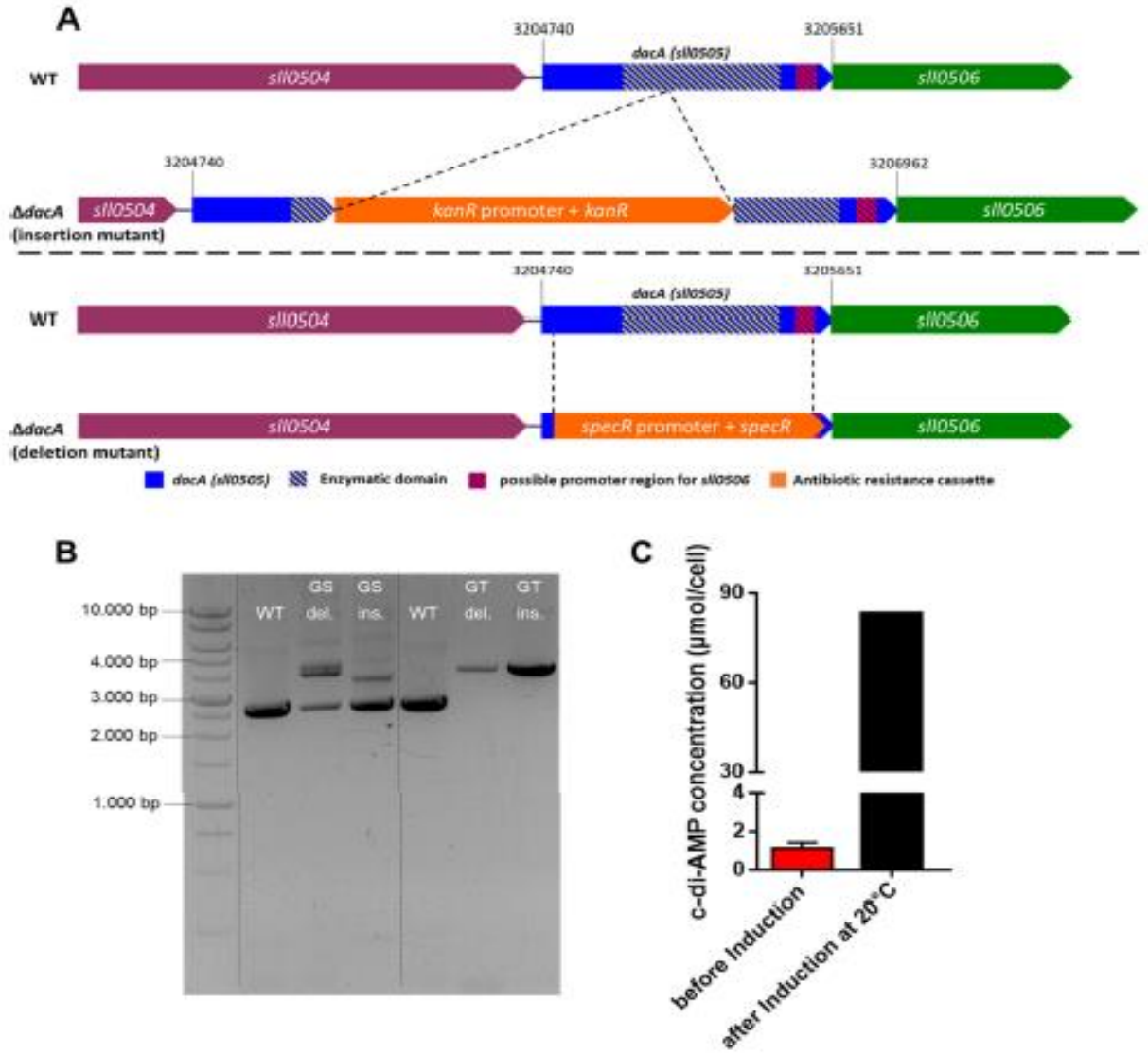

Fig. S3. Generation of the Δ*dacA* mutant in glucose tolerant (GT) and glucose sensitive *Synechocystis* sp. PCC 6803 wild-type cells. (A) Schematic overview of the strategies to generate a Δ*dacA* mutant either by inserting a kanamycin resistance cassette in the enzymatic domain-encoding region of the *sll0505* gene (Δ*dacA* insertion mutant); or by deleting almost the entire *sll0505* gene using a spectinomycin resistance cassette (Δ*dacA* deletion mutant), as indicated. Notably, cyanobacteria show a conserved operon organization for DacA encoding-gene (*sll0505*), where the diaminopimelate decarboxylase (*lysA; sll0504*) and the undecaprenyl pyrophosphate synthase (*uppS; sll0506*) encoding-genes are constantly up- and down-stream of the *sll0505* gene, respectively. (B) segregation level of either Δ*dacA* insertion mutant or the Δ*dacA* deletion mutant in both glucose tolerant (GT) and glucose sensitive (GS) *Synechocystis* backgrounds. (C) c-di-AMP concentration in *E. coli* cells before and after induction of the DacA encoding gene with 0.1 mM IPTG.

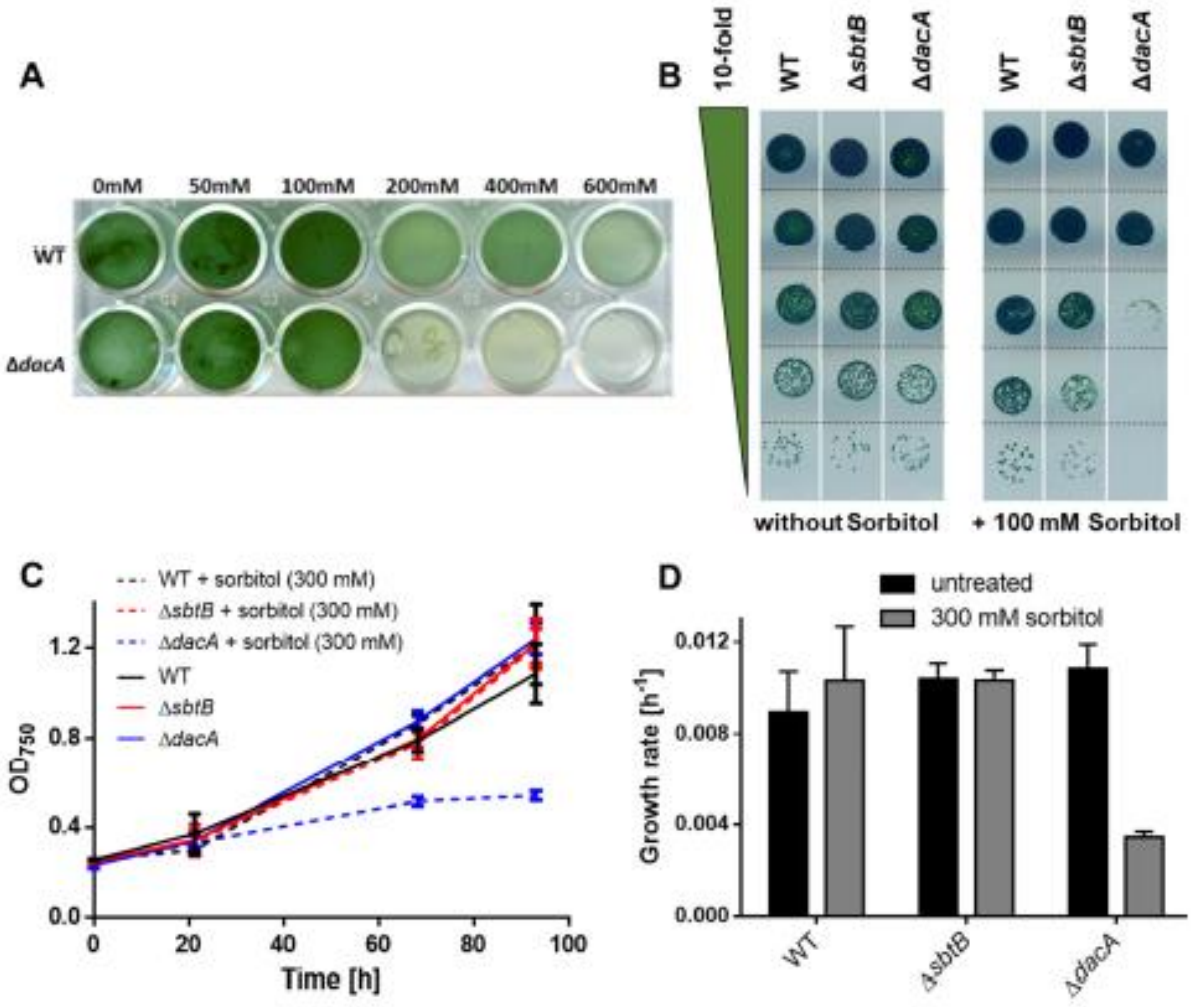

Fig. S4. Sensitivity of the Δ*dacA* mutant to osmotic stress. (A) *Synechocystis* WT and Δ*dacA* cells were exposed to osmotic stress generated by increasing concentrations of sorbitol (ranging from 0 mM – 600 mM). Cells were inoculated to a final OD_{750} of 0.25, and pictures were taken 6 days after inoculation. (B) Growth test by drop-plate assay of *Synechocystis* WT, Δ*dacA*, and Δ*sbtB* cells on BG_{11} agar (left) and BG_{11} agar supplemented with 100 mM sorbitol (right). Cells were normalized to an OD_{750} of 1.0 and serial diluted to an OD_{750} of 1 x 10^{-4} (from top to down). (C and D) Growth curves and rates of *Synechocystis* WT, Δ*dacA*, and Δ*sbtB* cells in the presence and absence of 300 mM sorbitol, as indicated. Notably, the osmotic stress effect of sorbitol was more pronounced in the BG_{11} agar plats in (B) than in liquid culture (A) due to the limitation of gas-exchange and therefore the cells on BG_{11} agar plats are strictly C_i-dependent (i.e. low carbon acclimated).

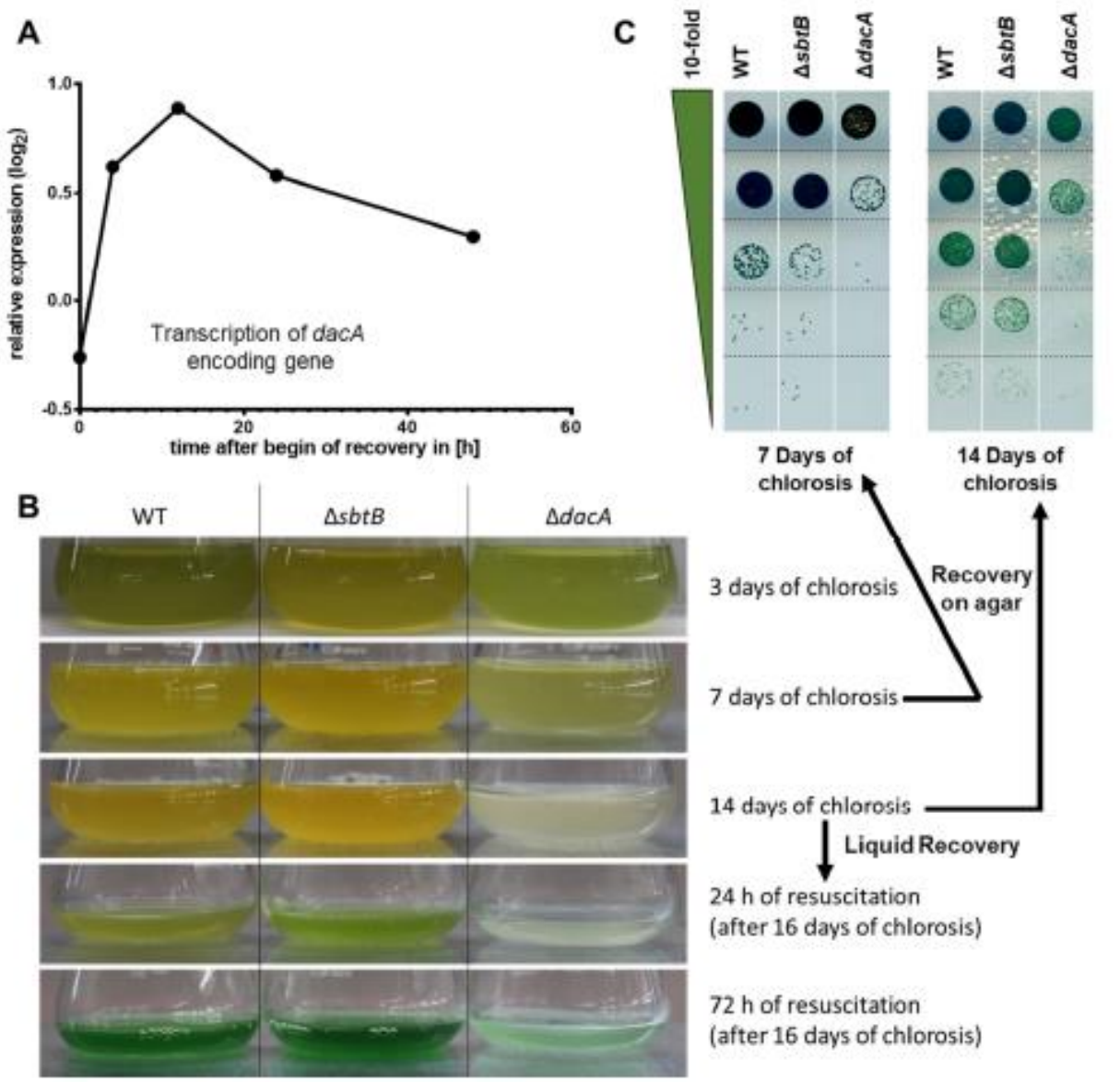

Fig. S5. Characterization of the Δ*sbtB* and Δ*dacA* mutants during recovery from nitrogen starvation. (A) Transcription levels of *sll0505* (encoding for DacA) during 48 hours of resuscitation from nitrogen chlorosis. The expression levels of *sll0505* was extracted from our previous microarray data; published previously in (*19*). X-axis shows the time in hours after the addition of combined nitrogen sources to the media; Y-axis shows the relative gene expression in a logarithmic scale. (B) Nitrogen chlorosis and resuscitation of *Synechocystis* WT, Δ*sbtB* and Δ*dacA* cells as indicated. Pictures were taken after 3, 7, and 14 days of chlorosis (first three pictures; up to down) and at 24 hours as well as 72 hours of resuscitation (last two pictures; up to down). (C) Resuscitation test by drop-plate assay of WT, Δ*sbtB* and Δ*dacA* cells that had been nitrogen starved for 7 and 14 days (samples from [B]). Cells were normalized to an OD_{750} of 1 and serial diluted in 10-fold steps (up to down; depicted by a green triangle).

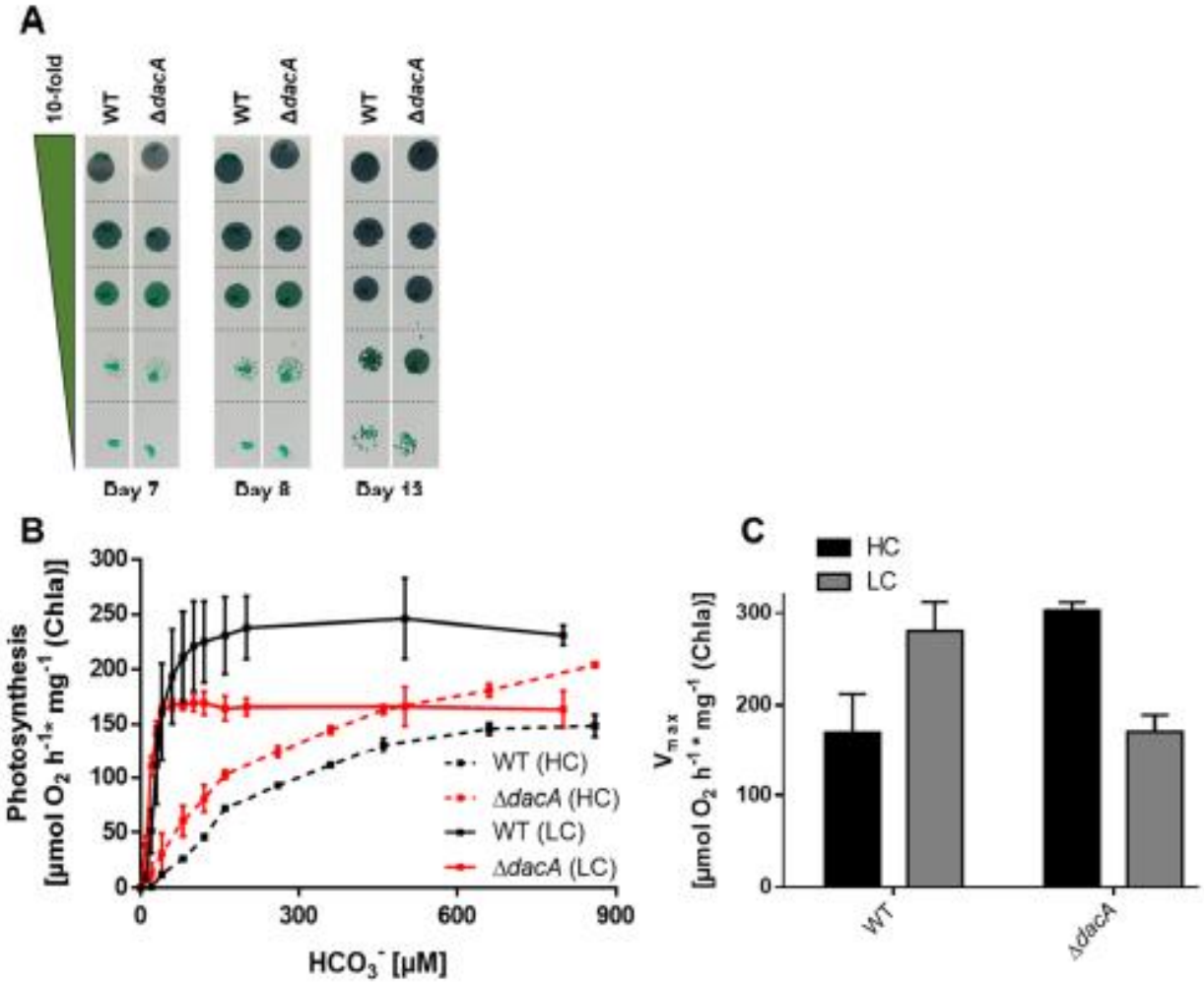

Fig. S6. Characterization of the Δ*dacA* mutant under low carbon conditions. (A) Growth test by drop-plate assay of *Synechocystis* WT and Δ*dacA* cells on carbon-free BG_{11} plates (pH 8.0). Cells were normalized to an OD_{750} of 1 and serial diluted in 10-fold steps (up to down; depicted by a green triangle). (B) *In vivo* bicarbonate uptake (as indicated by oxygen evolution) of *Synechocystis* WT (black lines) and Δ*dacA* (red lines) cells adapted either to high carbon (HC; dashed lines) or to low carbon (LC; solid lines) conditions. X-axis shows bicarbonate dependent oxygen evolution in µmol O_2/h per mg chlorophyll a. Y-axis shows increasing concentrations of bicarbonate in µM. (C) Calculated V_{max} values of bicarbonate uptake in *Synechocystis* WT and Δ*dacA* cells adapted either to high carbon conditions (HC; black bars) or to low carbon conditions (LC; grey bars), based on the data shown in (B).

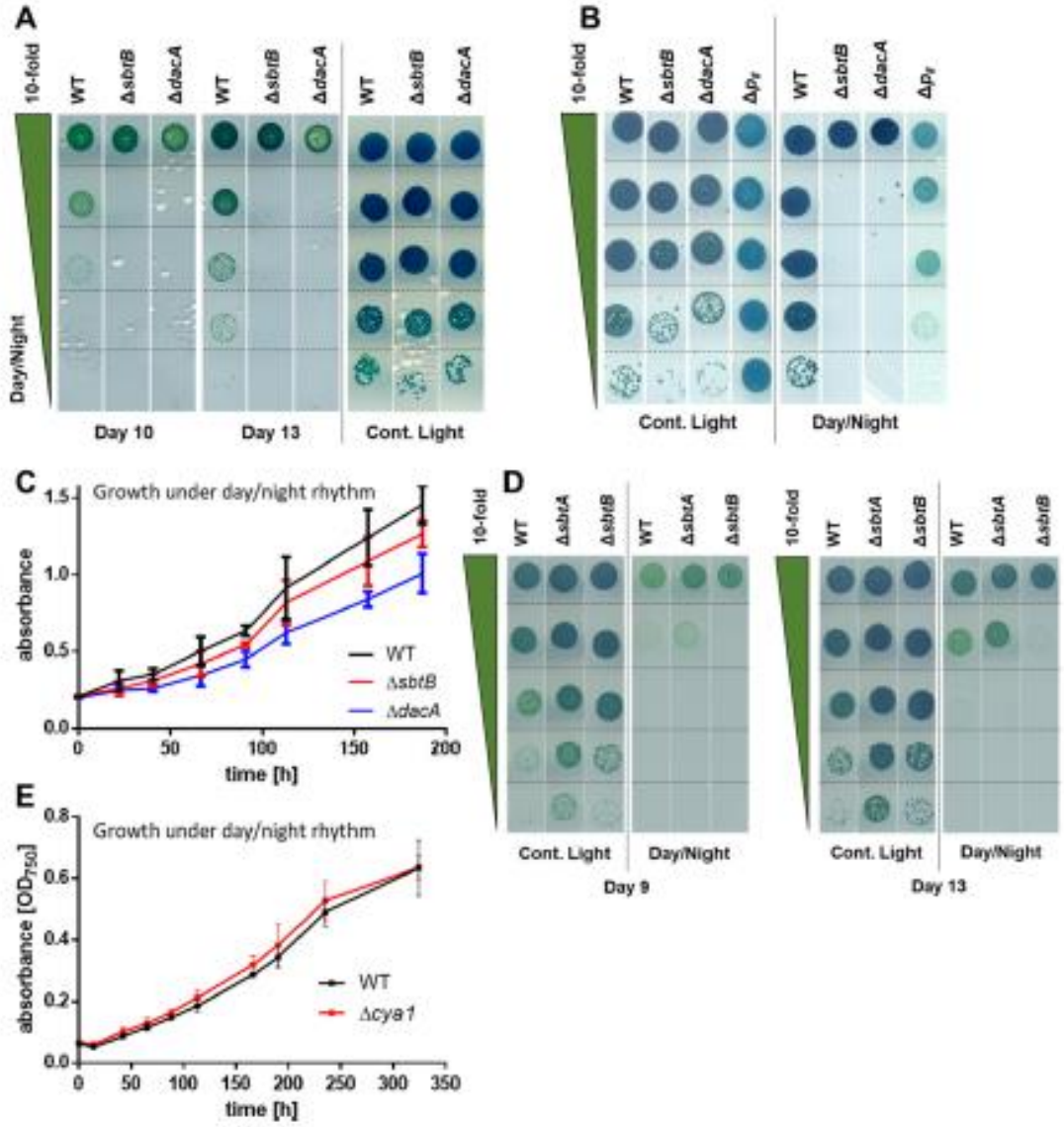

Fig. S7. Characterization of the Δ*sbtB* and Δ*dacA* mutants under diurnal rhythm. (A) Growth test by drop-plate assay of *Synechocystis* WT, Δ*sbtB* and Δ*dacA* (insertion mutant) cells under either continuous light (left) or a 12 h diurnal rhythm (right). (B) Growth test by drop-plate assay of *Synechocystis* WT, Δ*sbtB*, Δ*dacA* (deletion mutant), and Δ*glnB* (Δp_{II}; which encodes for canonical PII protein was used as a negative control) cells under either continuous light (left picture) or a 12 h diurnal rhythm (right picture). (C) Growth curve of *Synechocystis* WT (black line), Δ*sbtB* (red line) and Δ*dacA* (blue line) cells throughout a 12 h diurnal rhythm. (D) Growth test by drop-plate assay of *Synechocystis* WT, Δ*sbtA* and Δ*sbtB* cells under either continuous light or a 12 h diurnal rhythm, as indicated, for 9 and 13 days. (E) Growth curve of *Synechocystis* WT (black line) and Δ*cya1* (red line) cells throughout a 12 h diurnal rhythm. For (A, B and D), the cells were normalized to an OD_{750} of 1.0 and serial diluted in 10-fold steps (up to down; depicted by a green triangle). For (C, E) X-axis shows the time in hours; Y-axis shows the absorbance at 750 nm.

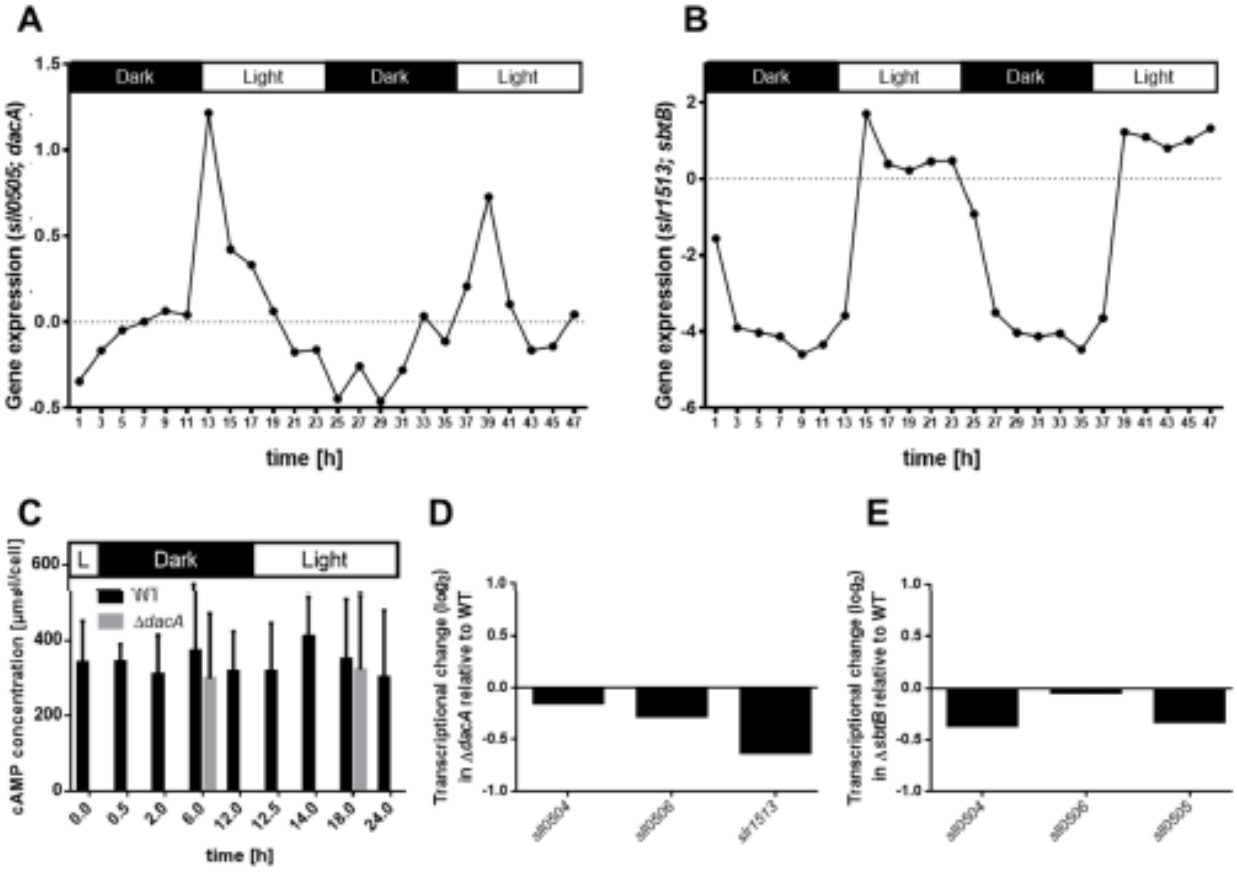

Fig. S8. *dacA* and *sbtB* expression profile and intracellular levels of cAMP. Gene expression profile of (A) *dacA* (*sll0505*) and (B) *sbtB* (*slr1513*) in *Synechocystis* WT throughout a 12 h diurnal rhythm; published previously in (*30*). For (A, B) X-axis shows the time in hours; Y-axis shows the relative gene expression. (C) cAMP concentration throughout a 12 h diurnal rhythm within *Synechocystis* WT (black bars) and Δ*dacA* cells (gray bars), as indicated. X-axis shows the time in hours; Y-axis shows the intracellular concentrations of cAMP. For (A, B, and C) The night phases are depicted by black bars; the day phases are depicted by white bars. (D, E) Expression of the genes situated up- (*sll0504*) or down-stream (*sll0506*) of *dacA* (*sll0505*), and for the SbtB encoding gene (*slr1513*) in Δ*dacA* mutant (D) and for the *dacA* encoding operon (*sll0504-sll0505-sll0506*) in Δ*sbtB* mutant (E), relative to their expression in WT cells under standard cultivation conditions.

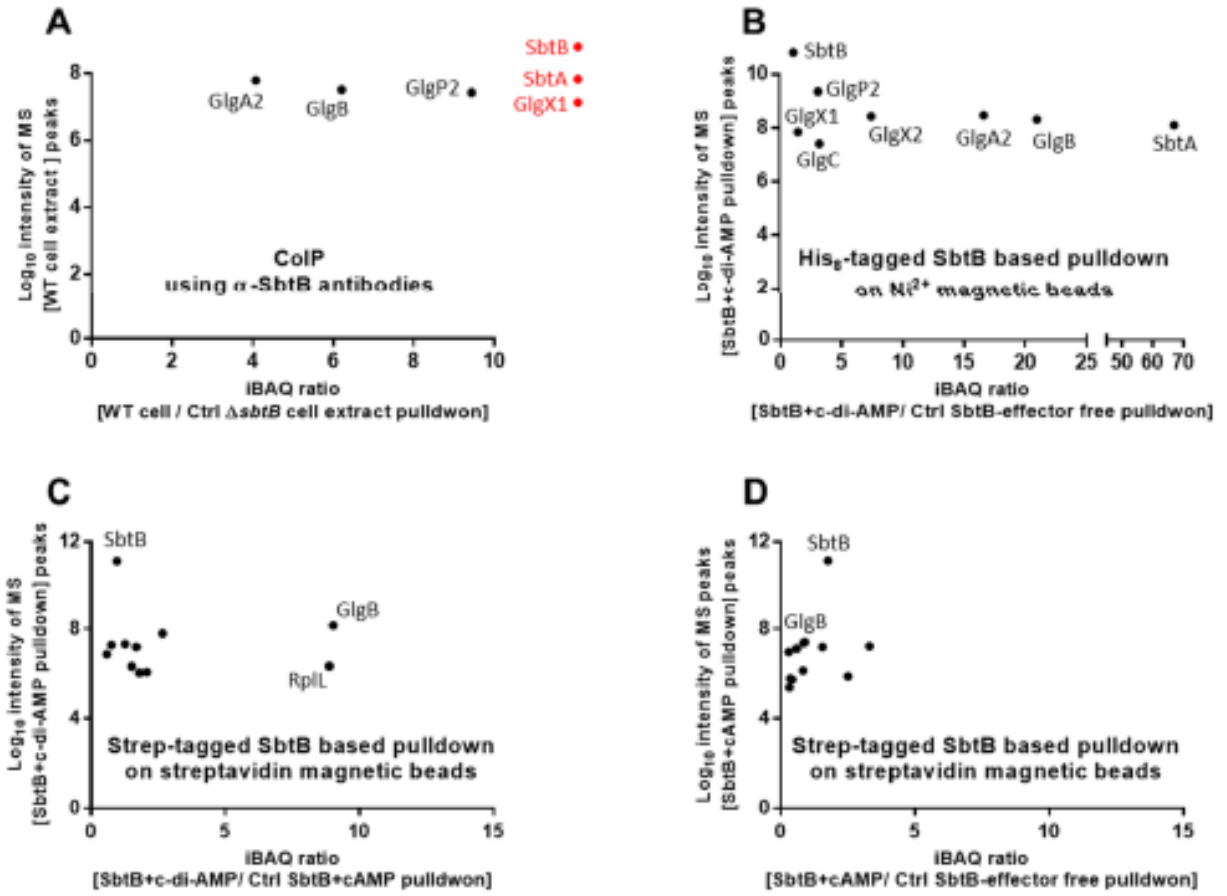

Fig. S9. SbtB interactome and proteins enrichment in different SbtB-based pull-downs. (A) CoIP pull-down using α-SbtB specific antibodies from crude cell extracts from WT cells and Δ*sbtB* mutant (as a control). The red dots were not identified in the Δ*sbtB*-based pull-down. (B) Ni^{2+} magnetic beads-based pull-down using His_8-tagged *St*SbtB protein. The pull-downs were done either in presence or absence of c-di-AMP (0.1 mM). Incubation of SbtB with c-di-AMP enriched the co-elution of glycogen-associated enzymes, in practically GlgB. (C-D) Streptavidin magnetic beads-based pull-downs using strep-tagged *St*SbtB protein. The pull-downs were done either in absence or presence of 2 mM effector molecules (c-di-AMP or cAMP). In contrast to cAMP, the presence of c-di-AMP enriched GlgB interaction with SbtB (compare Fig. 3A with S9C and S9C with S9D). (A-C) Eluates were analyzed by high accuracy LC-MS/MS to calculate protein enrichment ratios. The identified proteins were sorted by score and refined manually to remove unspecific binning proteins. Significantly enriched proteins were calculated based on iBAQ values and plotted against the intensity of MS peaks of the identified/defined peptides. The known SbtB-interacting partner SbtA was identified in (A) and (B), which validated our pull-down approach in general.

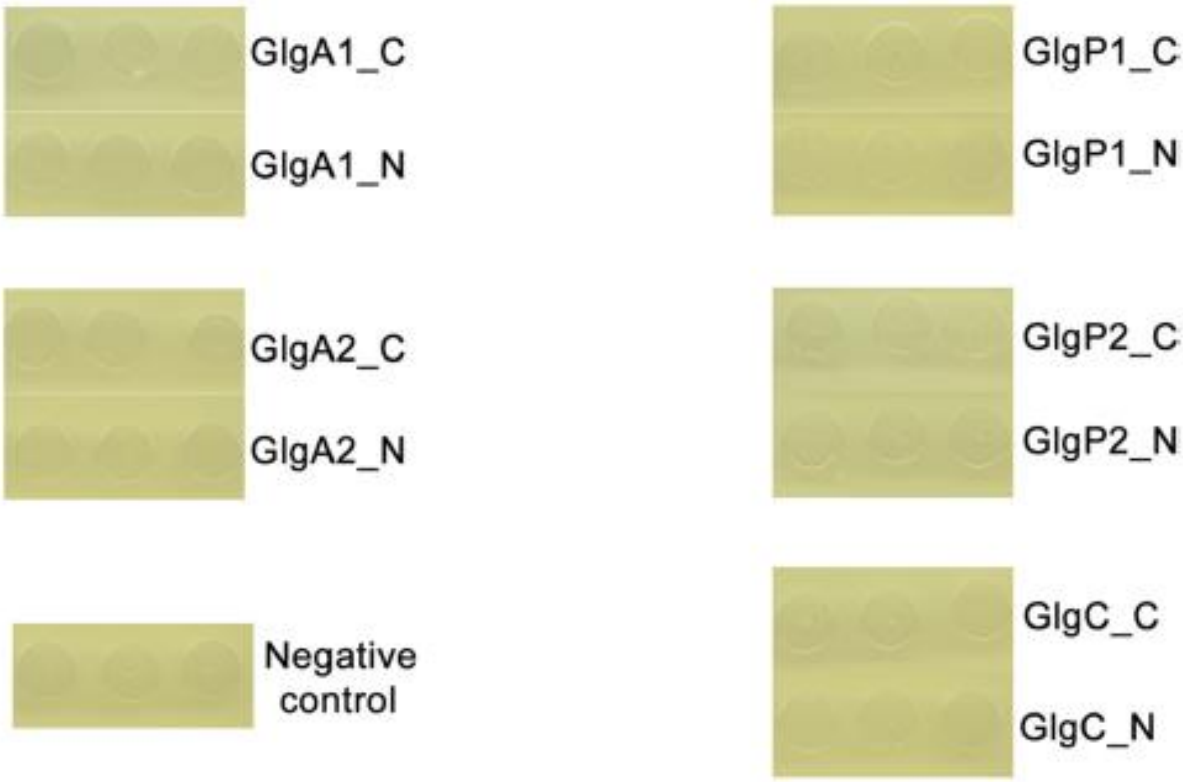

Fig. S10. Analysis of the interaction between glycogen-related enzymes and SbtB via bacterial two hybrid assay. The assay was performed using *E. coli* cells expressing N-terminally fusion of Cya-T25 subunit with SbtB (SbtB_N) together with GlgA1 (left, top), GlgA2 (left, middle), GlgP1 (right, top), GlgP2 (right, middle) or GlgC (right, bottom). Each glycogen related enzyme was either C-terminally (depicted by "_C") or N-terminally (depicted by "_N") fusion of Cya-T18 subunit to the enzyme. Empty Cya-T18 was used as a negative control (left, bottom). No interaction was observed between for GlgA1, GlgA2, GlgP1, GlgP2, and GlgC with SbtB. The assay was done using 3-independent/freshly transformed *E. coli* cells.

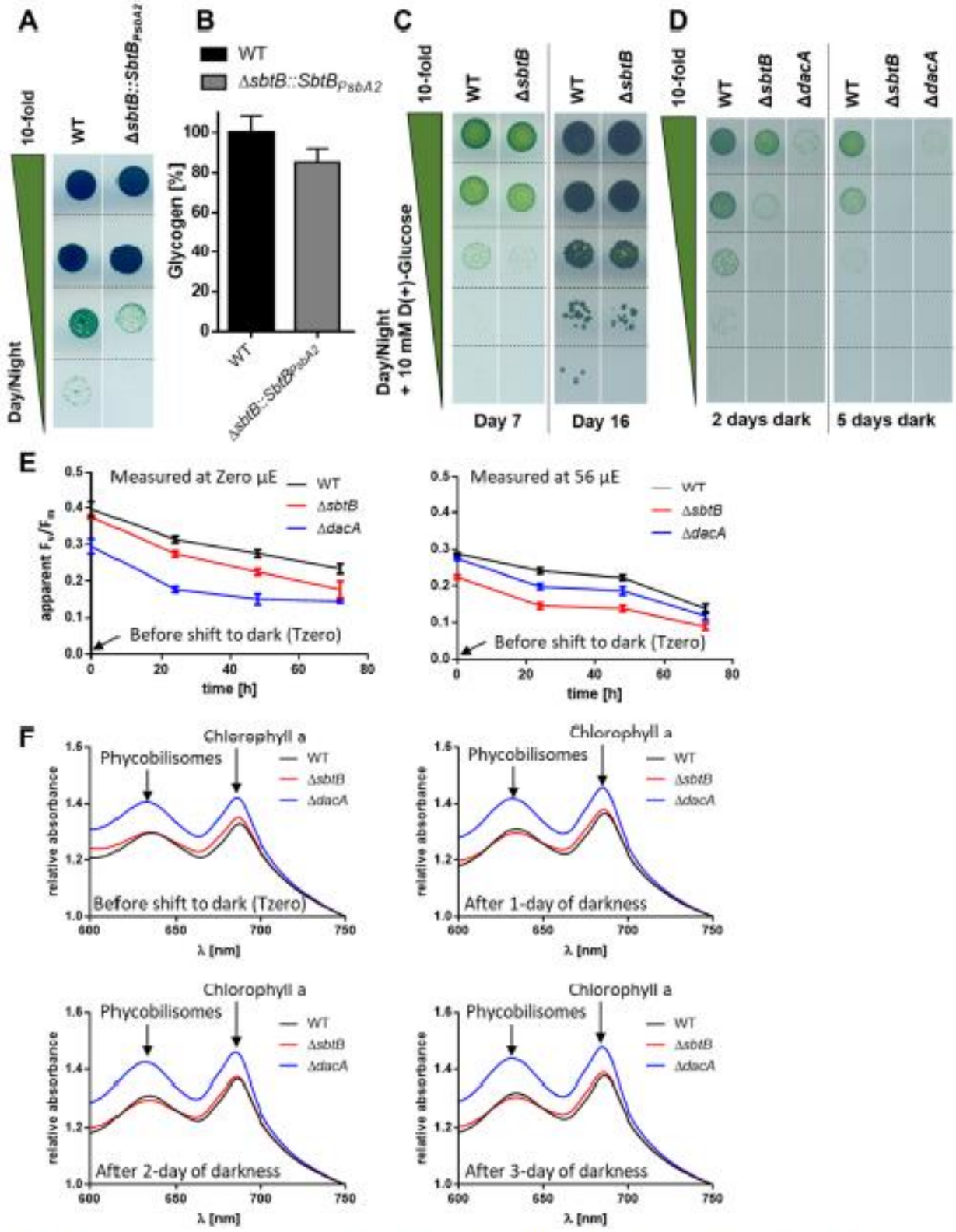

Fig. S11. Complementation and growth defect under prolonged dark conditions of the Δ*sbtB* mutant. (A) Growth test by drop-plate assay of *Synechocystis* WT and complemented Δ*sbtB*:SbtB$_{PsbA2}$ (right) cells

throughout a 12 h diurnal rhythm. The Δ*sbtB* complementation strain Δ*sbtB*::$SbtB_{PnbA}$ complements the phenotype of Δ*sbtB* that is shown in figures 2D and S6. (B) Glycogen levels of the complemented Δ*sbtB*::$SbtB_{PnbA2}$ cells (grey bar) relative to WT (black bar) at midday of a 12 h diurnal rhythm. The Δ*sbtB*::$SbtB_{PnbA2}$ regained almost wild-type levels of glycogen when compared to the Δ*sbtB* that is shown in figure 3D. (C) Complementation of Δ*sbtB* mutant by addition of 10 mM D(+)-glucose under a 12 h diurnal rhythm, as indicated. Pictures were taken after 7 (left) and 16 (right) days of growth. (D) Viability test using the drop-plate assay of *Synechocystis* WT, Δ*sbtB* and Δ*dacA* cells after 2 (left) and 5 (right) days of incubation in complete darkness, as indicated. Cells were normalized to an OD_{750} of 1.0 and serial diluted in 10-fold steps (top to bottom; depicted by a green triangle). Pictures were taken after 7 days of incubation in continuous light. (E) Pulse-amplitude modulation (PAM) fluorometry of *Synechocystis* WT (black line) in comparison to Δ*sbtB* (red line) and Δ*dacA* (blue line) cells before and after 1, 2, and 3 days of prolonged dark treatment. PAM fluorometry was either measured in absence (left; zero μE) or at constant 56 μE of actinic light (right). (F) Whole cell spectra of *Synechocystis* WT (black line) in comparison to Δ*sbtB* (red line) and Δ*dacA* (blue line) before (top, left) and after 1 (top, right), 2 (bottom, left), and 3 (bottom, right) days of dark treatment. The peak representing phycobilisomes at 620 nm as well as the peak representing chlorophyll a at 680 nm are depicted by black arrows. Cultures were mathematically normalized to similar OD_{750}.

Table S1. List of plasmids and primers used in this study

Primers/ amplification	Sequence (5′→3′)	Note/ Ref.
Creation of Δ*dacA* insertion mutant (pUC19-DacA_ins. plasmid)		
Downstream of *slr0505*	FW_Down-slr0505 ATATGTGATGGGTTAAAAAGGATCGATCCTCTAGCTAGAGGACGTAAATTTCGGCGTAGG	This study
	RV_Down-slr0505 TAGCTATAAATTATTTAATAAGTAAGTTAAGGGATGCAGGTACTCAG GCGTTTGCTTTGG	This study
Upstream of *slr0505*	FW_Up-slr0505 TGCACGGATCTGCCCTGGCTTCAGGAGATCGGAAGACCTCGAAAGC CCGACATGGGTAAG	This study
	RV_Up-slr0505 CACTTCATCCGGGGTCAGCACCACCGGCAAGCGCCGCGACTACCAA AGGCTTGACCTACG	This study
Kanamycin resistance cassette	KanRpVZ_0505down_fw ATGCTCGATGAGTTTTTCTAACGCCCTCATGGTGATGGAAG	This study
	KanRpVZ_0505_up_rv GCTCGAATTGACATAAGCCTGTTCCCAATCCGATTTTGGGACAGTTCC	This study
	0505up_KanRpVZ_fw CTGTCCCAAAATCGGATTGGGAACAGGCTTATGTCAATTCGAGCTCG	This study
	0505down_KanRpVZ_rv CATCACCATGAGGGCGTTAGAAAAACTCATCGAGCATCAAATGAAAC TGC	This study
Up- and downstream of *slr0505* + KanR	pUC19_05up_fw CAATTTCACACAGGAAACAGCTATGACCATGATTACGCCAATGTCGG GCTTTCCCCC	This study
	pUC19_0505down_rv TTTTCCCAGTCACGACGTTGTAAAACGACGGCCAGTGAATTTCATTTT TTGTCGTTTTGGGCAGTTGAG	This study
Creation of Δ*dacA* deletion mutant (pUC19-DacA_del. plasmid)		
Upstream of *slr0505*	1670: Fw_Up-slr0505-DacA TGCACGGATCTGCCCTGGCTTCAGGAGATCGGAAGACCTCGAAAGCCCGACATGGGTAAG	This study
	1671: Rv_Up-slr0505-DacA CACTTCATCCGGGGTCAGCACCACCGGCAAGCGCCGCGACTACCAAAGGCTTGACCTACG	This study
Downstream of *slr0505*	1672: Fw_Down-slr0505-DacA ATATGTGATGGGTTAAAAAGGATCGATCCTCTAGCTAGAGGACGTAAATTTCGGCGTAGG	This study
	1673: Rv_Down-slr0505-DacA TAGCTATAAATTATTTAATAAGTAAGTTAAGGGATGCAGGTACTCAGGCGTTTGCTTTGG	This study
Up- and downstream of *slr0505* + spectinomycin resistance cassette	1777: Fw_Down-slr0505-DacA_pUC19 TGTAAAACGACGGCCAGTGAATTCGAGCTCGGTACCCGGGGACGTAAATTTCGGCGTAGG	This study
	1778: Rv_Up-slr0505-DacA_pUC19 ATGACCATGATTACGCCAAGCTTGCATGCCTGCAGGTCGATACCAAAGGCTTGACCTACG	This study
Creation of Δ*sbtB* deletion mutant (pRL270-SbtB_del. plasmid)		
Upstream of *slr1513*	1275_Fw: GAATAAATAAATCCTGGTGTCCCTGTTGATACCGGGAAGCCATCAA CAATAACTAGGCTTGTTTC	(20)
	1276_Rv:CCATATTGGCCACGTTTAAATCAAAACTGGTGAAACTCACCGGCCA TCATCGAAGTGGAAG	(20)
Downstream of *slr1513*	1277_Fw:AGGTATATGTGATGGGTTAAAAAGGATCGATCCTCTAGAGCTGCTG CTGCTAGTATTGAG	(20)
	1278_Rv: TAGCTATAAATTATTTAATAAGTAAGTTAAGGGATGCAGGTTTGTT TATCTCCTAGAAGTATGTAAG	(20)
Creation of Δ*glgB* deletion mutant (pUC19-GlgB_del. plasmid)		
Upstream of *slr0158*	glgB_US_fw: GACCATGATTACGCCAAGCTTGCATGCCTGCAGGTCGACTAACCCCCGTCATTGGCATCAAT ATC	This study
	glgB_US_rev: GGATTTATTTATTCTGCGAATCGGCTATGGTGATTTTTTG	This study
Downstream of *slr0158*	glgB_DS_fw: ATCAGCAGGGAAGAAATTGGTTATAACTGAGTTAGCGATAATTTTC	This study
	glgB_DS_rev: CGGCCAGTGAATTCGAGCTCGGTACCCGGGGATCCTCTAGGACGATCAACCAGCCCAGGAG	This study
Cm resistance cassette	CmR_fw: CAAAAAATCACCATAGCCGATTCGCAGAATAAATAAATCC	This study
	CmR_rev: GAAAATTATCGCTAACTCAGTTATGAGTTTGTAGAAACGCAAAAAG	This study

Creation of Δ*sbtA* deletion mutant (pUC19-SbtA_del. plasmid)		
Downstream of *slr1512*	SbtAB_Apa5 GGGCCCTTTCATCCCGCTCAATCAGG	This study
	SbtAB_Sac3 GAGCTCTCAAACCGGCCAGTATTGAC	This study
Upstream of *slr1512*	DelSbtA_Bam_5 GGATCCGGACAAAAAATCCATAATG	This study
	DelSbtA_Bam_3 GGATCCCCAATAGTTTATGGTC	This study
Complementation of Δ*sbtB* by re-introducing *slr1513* under the control of *psbA2* promoter (pFLAG-SbtB_psbA2 plasmid)		
	FW_pFLAG-SbtB CAATCTGAACATCGACAAATACATAAGGAATTATAACCATATGGCTAA ACCAGCGAACAAG	This study
	RV_pFLAG-SbtB GTTGAATAAATCGAACTTTTGCTGAGTTGAAGGAAGATCTTTAACAGC CCTCAGGGCCA	This study
Generation of SbtB-sfGFP under the native promotor of *slr1513* (pVZ322-SbtB-sfGFP)		
SbtB-sfGFP	pVZ-Seq_Fw: CAGCTCCATAGGCCGCTTTC	(20)
	pVZ-Seq_Rv: GCTGCCCGGATTACAGATC	(20)
Recombinant proteins		
StrepII-tagged *S.*SbtB (*slr1513*); (pASK-*S.*SbtB-strep plasmid)	1256_Fw: GTGAAATGAATAGTTCGACAAAAATCTAGATAACGAGGGCAAAAAATG GCTAAACCAGCGAACAAGCTCG	(20)
	1257_Rv: AAGCTTATTATTTTTCGAACTGCGGGTGGCTCCAAGCGCTACAGCCCT CAGGGCCACAGAAAG	(20)
StrepII-tagged *N.*SbtB (*all2133*); (pASK-*N.*SbtB-strep plasmid)	1664: Fw_all2133_CT strep GTGAAATGAATAGTTCGACAAAAATCTAGATAACGAGGGCAAAAAATGGCCAAGCCAGCCA AAAAG	This study
	1665: Rv_all2133_CT strep CAAGCTTATTATTTTTCGAACTGCGGGTGGCTCCAAGCGCTACAGCCGTCTGGTCCGC	This study
His6-tagged *S.*SbtB (*slr1513*); (pET28a-*S.*SbtB-His6 plasmid)	FW_pET28a-SbtB CTAGAAATAATTTTGTTTAACTTTAAGAAGGAGATATACCATGG CTAAACCAGCGAACAA	This study
	RV_pET28a-SbtB CAGCCGGATCTCAGTGGTGGTGGTGGTGGTGGTGGTGCGAACA GCCCTCAGGGCCACAG	This study
His6-tagged GlgB (*all0158*); (pET15b-GlgB-His6 plasmid)	Fw_GlgB-N-His ATCATCATCACAGCAGCGGCCTGGTGCCGCGCGGCAGCCATATGAC CTACACCATCAACGC	This study
	Rv_GlgB-N-His TCAGCTTCCTTTCGGGCTTTGTTAGCAGCCGGATCCTCGAGCTAAGCT ATGTTGCTAGCCTCTTC	This study
DacA-GFP (sll0505); (pET28a-DacA-eGFP plasmid)	1762: Fw_DacA-eGFP CTAGAAATAATTTTGTTTAACTTTAAGAAGGAGACTCGAGATGTCGGGCTTTCCCCCG	This study
	1763: RV_DacA-eGFP CTCCTTTGCTGAATTGACCCTGGAAGTACAGGTTTTCGGATTTTTTGTCGTTTTGGGCAGTT GAGG	This study
BACTH constructs		
SbtB-BACTH; (pKT25_SbtB plasmid)	pKT25_sbtb_fw: CGATTACCTGGCGCGCACGCGGCGGGCTGCAGGGTCGACTATGGCTAAACCAGCGAACAA G	This study
	pKT25_sbtb_rev: GGCCGAATTCTTAGTTACTTAGGTACCCGGGGATCCTCTAGTTAACAGCCCTCAGGGCCAC	This study
GlgB-N (*all0158_N*); (pUT18_GlgB_N plasmid)	pUT18 glgB sll0158 fw GACCATGATTACGCCAAGCTTGCATGCCTGCAGGTCGACTATGACCTACACCATCAACG	This study
	pUT18 glgB sll0158 rev CCTCGCTGGCGGCTGAATTCGAGCTCGGTACCCGGGGATCAGCTATGTTGCTAGCCTCTTC	This study
GlgB-C (*all0158_C*); (pUT18_GlgB_C plasmid)	pUT18c glgB sll0158 fw GCCGTCGCTGGGCGCAGTGGAACGCCACTGCAGGTCGACTATGACCTACACCATCAACG	This study
	pUT18c glgB sll0158 rev TTAGTTATATCGATGAATTCGAGCTCGGTACCCGGGGATCAGCTATGTTGCTAGCCTCTTC	This study

Table S2: Crystallographic data collection and refinement statistics

Structure	*St*SbtB:c-di-AMP complex
PDB code	7OBJ
Data collection	
Space group	$P3_2$
Cell parameters	a = b = 63.2 Å, c = 81.7 Å
Wavelength (Å)	1.00
Resolution limits (Å)[a]	32.74 – 2.00 (2.12 – 2.00)
Unique reflections	24685 (3942)
Completeness (%)	99.7 (98.3)
I/σI	20.61 (1.03)
Redundancy	10.3 (10.1)
R_{merge} (%)	6.4 (223.1)
CC(1/2)	100 (43.1)
Refinement	
Resolution limits (Å)	32.74 – 2.00 (2.05 – 2.00)
R_{cryst}(%)	17.8 (37.6)
R_{free} (%)	21.5 (38.7)
Protein molecules per asymmetric unit cell	3
Mean B value (Å^2)	58.0
Ramachandran statistics	
Core regions (%)	95.0

[a]Values in parentheses refer to the highest-resolution shell.

Publication 3 (Accepted)

Research Article

Burkhardt, M, Rapp, J, Menzel, C, Link, H, Forchhammer, K (2023). The Global Influence of Sodium on Cyanobacteria in Resuscitation from Nitrogen Starvation. *Biology* **2023**, 12, 159

biology

MDPI

Article

The Global Influence of Sodium on Cyanobacteria in Resuscitation from Nitrogen Starvation

Markus Burkhardt [1], Johanna Rapp [2], Claudia Menzel [1], Hannes Link [2] and Karl Forchhammer [1,*]

[1] Interfaculty Institute of Microbiology and Infection Medicine, University of Tübingen, Auf der Morgenstelle 28, 72076 Tübingen, Germany
[2] CMFI, Bacterial Metabolomics, University of Tübingen, Auf der Morgenstelle 24, 72076 Tübingen, Germany
* Correspondence: karl.forchhammer@uni-tuebingen.de

Simple Summary: Dormancy and resuscitation are key processes to bacterial survival. In the absence of combined nitrogen sources, the non-diazotrophic model cyanobacterium *Synechocystis* sp. PCC 6803 turns into a metabolically quiescent state during a process termed chlorosis, enabling long-term survival. When nitrogen sources reappear, the cells resuscitate in a process that follows a highly orchestrated program. Here, we describe the essential role of sodium in the resuscitation process. We show that in addition to its role in the bioenergetics of chlorotic cells, sodium is involved in nitrogen compound assimilation, pH regulation, and the synthesis of key metabolites.

Abstract: Dormancy and resuscitation are key to bacterial survival under fluctuating environmental conditions. In the absence of combined nitrogen sources, the non-diazotrophic model cyanobacterium *Synechocystis* sp. PCC 6803 enters into a metabolically quiescent state during a process termed chlorosis. This state enables the cells to survive until nitrogen sources reappear, whereupon the cells resuscitate in a process that follows a highly orchestrated program. This coincides with a metabolic switch into a heterotrophic-like mode where glycogen catabolism provides the cells with reductant and carbon skeletons for the anabolic reactions that serve to re-establish a photosynthetically active cell. Here we show that the entire resuscitation process requires the presence of sodium, a ubiquitous cation that has a broad impact on bacterial physiology. The requirement for sodium in resuscitating cells persists even at elevated CO_2 levels, a condition that, by contrast, relieves the requirement for sodium ions in vegetative cells. Using a multi-pronged approach, including the first metabolome analysis of *Synechocystis* cells resuscitating from chlorosis, we reveal the involvement of sodium at multiple levels. Not only does sodium play a role in the bioenergetics of chlorotic cells, as previously shown, but it is also involved in nitrogen compound assimilation, pH regulation, and synthesis of key metabolites.

Keywords: cyanobacteria; dormancy; resuscitation; sodium; chlorosis

check for updates

Citation: Burkhardt, M.; Rapp, J.; Menzel, C.; Link, H.; Forchhammer, K. The Global Influence of Sodium on Cyanobacteria in Resuscitation from Nitrogen Starvation. *Biology* **2023**, *12*, 159. https://doi.org/10.3390/biology12020159

Academic Editor: Davide Di Paola

Received: 8 December 2022
Revised: 11 January 2023
Accepted: 17 January 2023
Published: 19 January 2023

Copyright: © 2023 by the authors. Licensee MDPI, Basel, Switzerland. This article is an open access article distributed under the terms and conditions of the Creative Commons Attribution (CC BY) license (https://creativecommons.org/licenses/by/4.0/).

1. Introduction

Dormancy is one of the most widespread survival strategies in life [1]. In general, dormancy serves to endure unfavourable conditions. Those can range from short-term, for example, lack of sun at night, over long-term depletion of resources to endurance of harmful conditions. Bacteria commonly switch into a quiescent state when faced with nutrient limitation. This state of dormancy can range from long-lived, durable spores as found in, for example, *Bacillus subtilis* [2], over spore-like akinetes of some filamentous cyanobacteria [3] to the sole downregulation and reorganization of the cell metabolism, as observed, for example, in nutrient-deprived *Synechocystis* sp. PCC 6803 (hereafter *Synechocystis*) [4,5].

Cyanobacteria are one of the most primordial and ubiquitous groups of bacteria, and this is reflected in their morphological diversity and metabolic versatility, which enables them to adapt to different environmental conditions. One of the most limiting

macronutrients is nitrogen [6,7]. *Synechocystis* is a unicellular, non-diazotrophic freshwater cyanobacterium. It is non-diazotrophic, therefore it is dependent on combined nitrogen sources such as nitrate or ammonium. When no nitrogen source is available, *Synechocystis* turns into a dormant state in a strictly regulated program termed chlorosis [5,8]. Cell growth arrests, the photosynthetic machinery is almost completely degraded, and after initial synthesis of the storage polymer glycogen, metabolic activities are highly reduced [4,5,9].

When a new nitrogen source is available, a genetically encoded and hierarchical resuscitation program begins. The immediate response is a major increase in ATP to revive cell anabolism [10]. During the first day, energy is produced heterotrophically through the degradation and respiration of glycogen. With the catabolism of glycogen, the cell receives reducing equivalents and carbon compounds for anabolic pathways, such as 2-oxoglutarate (2-OG) for the glutamine-synthetase-glutamate-synthase (GS-GOGAT) cycle [10]. The first genes that are expressed during resuscitation encode components of the translational machinery, RNA polymerases, and central metabolic reactions [9,11]. Subsequently, other cellular processes are activated, especially all components of the photosynthetic apparatus, involving a coordinated expression of the tetrapyrrole biosynthesis genes [11,12]. This leads to an intermediate, mixotrophic phase when the glycogen stores are still being degraded while photosynthesis and carbon fixation start again. When tracking the oxygen evolution, this phase is characterised by a gradual increase in light-dependent oxygen evolution, typically occurring between 20 and 30 h after the addition of a nitrogen source. After approximately 48 h, the glycogen storages are consumed, the cell metabolism is reconstituted, and the switch to vegetative growth occurs with the first cell division [11].

During the resuscitation period not all the assimilated nitrogen is used for protein synthesis. A part of the newly assimilated nitrogen is immediately secured in the nitrogen storage compound cyanophycin (CP) [13]. CP is a nitrogen storage polymer made of aspartate and arginine in equimolar amounts. The backbone is composed of poly-L-aspartic acid, with each carboxy side cahin linked to an arginine residue by an isopeptide bond. It is synthesised by the CP synthase CphA, a large, non-ribosomal peptide synthetase [14]. Typically in non-diazotrophic cyanobacteria, CP is synthesised during unbalanced nutritional conditions that limit growth, such as phosphate starvation [15,16]. In resuscitation however, the surplus of assimilated nitrogen, exceeding the anabolic demand, is temporarily stored as CP and may be mobilised during fluctuating nitrogen supply [13].

We previously showed that chlorotic cells have a specific requirement for sodium that differs from the sodium requirement of vegetative cells [17]. Vegetatively growing *Synechocystis* cells require sodium ions (Na^+) primarily for the uptake of inorganic carbon. This can be explained mainly by the requirement for sodium to fuel two major bicarbonate uptake systems, SbtA and BicA [18]. Therefore, in the presence of elevated CO_2 concentration, vegetative cells can grow in the absence of sodium. By contrast, during nitrogen starvation-induced chlorosis, the maintenance of a sodium motive force is required for membrane bioenergetics and ATP synthesis [17]. When chlorotic cells were supplemented with a combined nitrogen source, a rapid increase in ATP levels could be detected within a few minutes, which is the very first response in the resuscitation process. When resuscitation was started by the addition of $NaNO_3$, the increase in ATP levels was higher than if resuscitation was started by the addition of KNO_3. The surplus of ATP could be attributed to an increase in the sodium motive force by the addition of the sodium salt of nitrate. The same increase in ATP levels could also be obtained by just adding the same concentration of NaCl. However, how sodium affects the entire resuscitation program of *Synechocystis* was not clarified. To gain deeper insights into the awakening process of chlorotic *Synechocystis* and the role of sodium herein, we systematically analysed the requirement for sodium salts in the regreening of nitrogen-starved, chlorotic *Synechocystis* cells.

2. Materials and Methods

2.1. Cultivation and Growth Curves

Growth curves were generated in a Multicultivator OD-1000 with a gas mixing system GMS 150 (Photosystems Instruments, Dasov, Czech Republic). Vegetative cells were grown in a BG_{11} medium [19] in ambient air. Nitrogen starvation was induced by washing cells with the BG_{11-0} medium, which contains all BG_{11} components except for $NaNO_3$. Cells were starved of nitrogen for at least 14 days at ~ 70 µE white light. To induce resuscitation, either just 17.5 mM KNO_3 or additionally 17.5 mM NaCl was added to the culture. When comparing recovery with different N-sources, cultures were recovered with 10 mM KNO_3 with or without 10 mM NaCl in comparison to cultures recovering with 10 mM NH_4Cl with or without 10 mM NaCl. Resuscitation was performed in the presence or absence of 2% CO_2 supplementation.

Recovery in ambient air was done in shaking flasks at 28 °C and approximately 70 µE white light. Samples were taken each day and measured in a photometer Helios δ (Thermo Fisher Scientific, Waltham, MA, USA) at OD_{750}. The whole cell spectrum was measured in a spectrophotometer Specord 50 (Analytik Jena GmbH, Jena, Germany).

2.2. Glycogen Measurement

Glycogen amounts were measured using an enzymatic assay according to [20], with modifications established by [21]. Two ml samples were taken, washed with water, and incubated in 30% KOH for 2 h at 95 °C. Then, ice-cold ethanol was added to a final concentration of 75%, and glycogen precipitated overnight at −20 °C. Samples were then washed with 70 and 98% ethanol, spun down, the pellet dried, and the glycogen digested by the addition of a solution of 1 00 mM sodium acetate and 4.4 U/µL amyloglucosidase at pH 4.5 for 2 h. Then, 200 µL of the samples were mixed with 1 mL of 6% O-toluidine in acetic acid and incubated for 10 min at 100 °C. Absorbance was then measured at 635 nm using a Tecan Spark 10M (Tecan, Männerdorf, Switzerland). A glucose calibration curve was used to determine the glycogen amount in the samples. At least three biological replicates were measured for every condition.

2.3. ATP Determination in the Cells

One ml samples were taken from each culture in cultivation conditions and immediately frozen in liquid nitrogen. Samples were then stored at −80 °C until further processing. Cells were lysed by three cycles of cooking at 99 °C and flash freezing in liquid nitrogen. Debris was spun down at 25,000 g at 4 °C for 1 min. The ATP content in the supernatant was measured according to the instructions of the "ATP determination kit" (Molecular Probes (A22066), Eugene, OR, USA). A 50 µL reaction mix containing reaction buffer, luciferin, and firefly luciferase was mixed with a 10 µL sample supernatant and measured in a Sirius Luminometer (Berthold Detection Systems, Bad Wildbad, Germany). An ATP calibration curve was used to determine the ATP amount in the samples. At least three biological replicates were measured for every condition.

2.4. PS2 Yield with Pulse Amplitude Modulation

The yield of Photosystem II (PSII) was measured in vivo using a WATER-PAM chlorophyll fluorometer (Walz GmbH, Effeltrich, Germany). The maximum PSII quantum yield was determined by saturation pulse. At least three biological replicates were measured, and each one in three technical replicates.

2.5. Nitrate/Nitrite Measurement in the Growth Medium

One mililiter of sample was harvested and centrifuged at 13,000× *g* for 5 min. Nitrate and nitrite were quantified by measuring the absorbance at 210 nm in the cell-free medium. The nitrate values were corrected for the presence of nitrate [22]. To measure, nitrite 300 µL of the cell-free sample was added to 300 µL sulfanilamide solution (1% sulfanilamide in 5% phosphoric acid) and incubated for 10 min at room temperature in the dark. Afterwards,

300 µL NED solution (0.1% N-1-napthylethylenediamin dihydrochloride in water) was added and incubated in the dark for 10 min. Then, the absorbance at 530 nm was measured [23].

2.6. Ammonium Measurement in the Growth Medium

A dilution series from 0 to 2 mM NH_4Cl was prepared. Samples of 1 mL of each culture were taken and spun down; the supernatant was moved to a new reaction tube. A nessler reagent of 20 µL (containing $K_2[HgI_4]$) was mixed with 980 µL of the supernatant or the dilution series. The mixture was transferred to a cuvette, and the absorbance was measured at 410 nm [24].

2.7. Metabolome Measurement

Cells were grown to an $OD_{750} > 0.4$. To sample, 10 mL were filtered through pore-size 1.2 µM filters (WHA1822025, cytiva, Marlborough, MA, USA). Filters were put into reaction tubes, frozen in liquid nitrogen, and stored at −80 °C until further use. The filters were thawed in 500 µL acetonitrile:methanol:water (40:40:20) at −20 °C. Filters were incubated in the extraction solvent for 4 h at −20 °C. Metabolites were extracted from the filter by pipetting the solvent up and down, and the supernatant was then moved to a new tube. To ensure cell lysis glass beads were added to the supernatant and ribolysed at 6.5 m/s for 30 s in 2 cycles and a 5 min break in between, centrifuged at >13,000 × *g* for 15 min at −9 °C, and the supernatant transferred to a new tube once more. The samples were then stored at −80 °C until further use. The measurement was done as described in [25]. Metabolomic analysis was performed via LC-MS/MS (Agilent TQ6495, Santa Clara, CA, USA). Relative quantification was performed by adding a 13C internal standard.

2.8. Oxygen Evolution Measurement

Oxygen evolution was measured using a Clark-type oxygen electrode DW1 (Hansatech, King's Lynn, Norfolk, UK) as described in [17].

2.9. PH Measurement

Extracellular pH was measured using a pH electrode (InLab Micro, Mettler-Toledo, Columbus, OH, USA). At least three biological samples were measured during each sampling point.

Intracellular pH was measured using the fluorescent indicator BCECF (2′, 7′-bis-(2-carboxyethyl)-5-(and-6)-carboxyfluorescein) (Invitrogen AG, Waltham, MA, USA). Samples were taken and mixed with BCECF for a final concentration of 0.5 µM and incubated in the dark for 15 min. Measurement was done in a Spark 10M (Tecan, Männerdorf, Switzerland) with BCECF emission at 535 nm and excitation at either 490 nm or 439 nm. Additionally, measurements at the most acidic point and the most alkaline point of the linear phase were required. To detect those, a calibration curve was made by washing cells free of the medium and resuspending them in BG0 10 mM Hepes with a pH ranging from 4 to 10, in 1 pH increments. BCECF was added to a final concentration of 0.5 µM and samples were incubated in the dark for 5 min before adding a CTAB solution to a final concentration of 0.4% and incubated another 10 min in the dark before measurement in the Spark 10M. The ratio between excitation at 490 nm and 439 nm was calculated, and the necessary measurement points are chosen. The intracellular pH was then calculated using the formula:

$$pH = pK_a - log\frac{(R - R_A)}{(R_B - R)} * \frac{F_{A(439\ nm)}}{F_{B(439\ nm)}} \quad (1)$$

With pK_a being the pK of the medium, R being the ratio of signal between excitation at 490 nm and 439 nm, and F the fluorescent signal. A indicates the most acidic point of the linear range, and B is the most basic.

2.10. Sakaguchi Staining and Bright Field Microscopy

CP granules were visualised by using the arginine-selective Sakaguchi staining method, according to [26].

Photographs were taken with a Leica DM2500 microscope, and a Leica DFC420C color camera and Leica Application Suite Software. Microscope slides were covered in dried 1% (*w/v*) agarose solution to immobilise the cells.

2.11. Transmission Electron Microscopy

Samples for TEM were prepared, and images were taken as described by [26].

3. Results and Discussion

3.1. Resuscitation in Absence of Sodium

To investigate the requirement for sodium in the resuscitation process of chlorotic *Synechocystis*, cultures that had been starved of nitrogen for 2 weeks were used. Before starting resuscitation, the cells were washed and resuspended in a sodium-free BG11 medium. Immediately thereafter, either 10 mM KNO_3 or 10 mM NH_4Cl was added, respectively, with or without the addition of 10 mM NaCl. Then, resuscitation was studied for the following 2 to 3 days. The same type of experiment was carried out either at ambient air in flasks or in tubes that were bubbled with air enriched with 2% CO_2. Cells that were incubated in ambient air were unable to regreen and recover in the absence of Na^+ (Figure 1A, top). The lack of reconstitution of photosynthetic pigments is also visible in the spectrum from 600 to 750 nm after 2 days of resuscitation, where in recovered cells, phycocyanin absorbs light at 630 nm and chlorophyll α at 680 nm (Figure 1B). A further indication of a reconstitution of the photosynthetic activity can be obtained by measuring the quantum yield of photosystem (PS) 2 by pulse amplitude modulation (PAM fluorometry and saturation pulse method). During resuscitation at standard conditions, the PAM signal first drops to 0, followed by an increase starting after 20 h [11]. Here, the PAM signal of the cultures in the presence of sodium increased within 24 h when recovered with nitrate and 48 h when recovered with ammonium. By contrast, in the absence of Na^+, no increase in the PAM signal was detectable (Figure 1C, top). This clearly indicated that in the absence of Na^+, the cells were unable to restore the photosynthetic machinery. Energy production during early resuscitation is solely based on the degradation and respiration of glycogen, and as soon as photosynthetic activity appears, oxygen evolution increases gradually [11]. When resuscitation was performed in the absence of sodium, cells had a higher respiration rate and were unable to turn on oxygen evolution (Figure 1D), another indication of the lack of photosynthetic activity. However, the degradation of glycogen was unaffected by the presence or absence of sodium (Figure 1E). The last step of resuscitation is the initiation of cell division indicated by an increase in OD_{750}. This increase was not observable when resuscitation was performed in the absence of sodium, while the OD_{750} started to increase in presence of Na^+ after about 48 h of resuscitation (Figure 1F). Since these first experiments clearly indicated that resuscitation required Na^+ ions, we asked whether we could bypass the requirement for Na^+ by providing the resuscitating cells with 2% CO_2, as observed for vegetative cells [17]. However, the presence of CO_2 did not enable cells to resuscitate successfully, although a slight green colour appeared after 2 days of incubation (Figure 1A, bottom). The PAM signal indicated a slight recovery of PS2 quantum yield towards 48 h of resuscitation (Figure 1C, bottom), although this minute signal PSII activity was not sufficient to enable oxygen evolution (Figure 1D, bottom). The cells remained in this incomplete recovered state after prolonged incubation, indicating that the partial regreening and traces of PSII activity did not support the resuscitation process. Glycogen consumption was comparable to that in ambient air (Figure 1E), indicating that glycogen catabolism and respiration are not dependent on Na^+ supply. The failure of the cells to switch back to vegetative growth in the absence of sodium is also evidenced by the stagnation of OD_{720} (Figure 1F, bottom). All these results indicate that in contrast to

vegetative cells, which require sodium to import carbon, resuscitating cells require sodium for functions other than carbon acquisition.

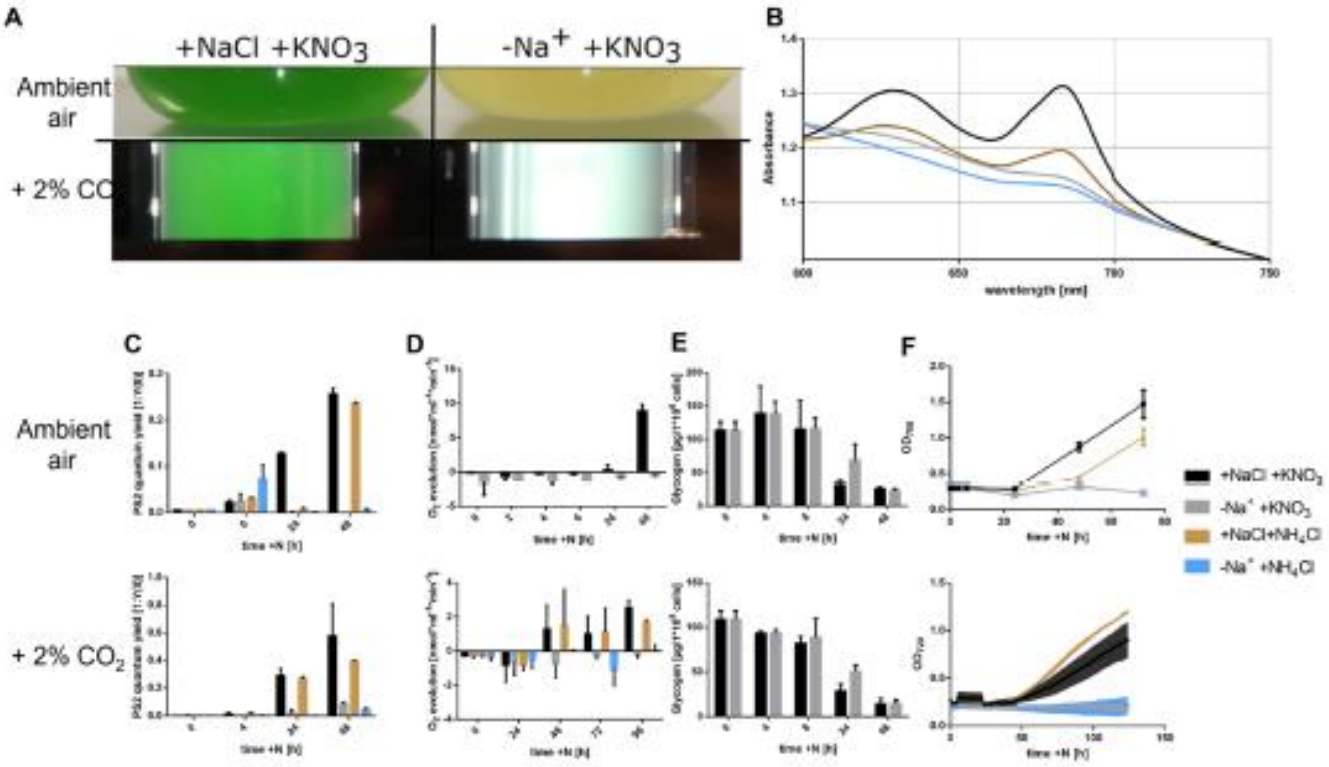

Figure 1. Resuscitation in the absence of Na^+ is impossible. (**A**) shows two cultures after 14 days of chlorosis and two days of resuscitation in ambient air (top) or supplemented with 2% CO_2 (**bottom**), the left in presence of Na^+ and the right in absence thereof. (**B**) shows the absorbance of recovering cultures in ambient air from 600 nm to 750 nm. (**C**) shows the quantum yield of PSII as a measure of photosynthetic activity. (**D**) shows the oxygen evolution during resuscitation. (**E**) shows glycogen consumption. (**F**) shows the OD at 750 nm (top) or 720 nm (bottom) as an indicator of cell mass. (**C**–**E**) top graphs refer to cultures in ambient air, bottom graphs refer to cultures in a 2% CO_2 environment. Samples were taken 0, 4, 6, 24, and 48 h after the addition of 10 mM KNO_3 or 10 mM NH_4Cl, respectively. Each data-point represents measured triplicates. Error bars represent the SD.

We asked ourselves how much sodium is necessary for *Synechocystis* to be able to survive and potentially grow in ambient air. We thus cultivated cells in increasing concentrations of NaCl and discovered that in continuous light, cells require around 100 µM of NaCl in the medium to survive, while in a 12 h day/12 h night cycle, they needed at least 500 µM (Figure S1).

3.2. *Assimilation of Nitrogen Sources and pH*

Based on these results, we next investigated the role of sodium in the acquisition and assimilation of the nitrogen sources during resuscitation from nitrogen chlorosis. Here, we used potassium nitrate or ammonium chloride as nitrogen sources. Since nitrogen is assimilated in the form of ammonium, nitrate must be reduced to nitrite and subsequently to ammonia (Figure 2A). Then, the glutamine synthase (GS) catalyses the incorporation of ammonia into glutamate forming glutamine. Ammonium as an N-source is co-transported across the membrane as ammonia together with a proton and can be immediately incorporated into the GS-GOGAT cycle (Figure 2A). When cells were resuscitated with 1 mM ammonium, its concentration in the medium decreased both in the presence or absence of sodium. However, the levels decreased faster in presence of Na^+, reaching residual levels after 24 h of resuscitation, while in absence of sodium, this took 48 h (Figure 2B). To measure

the consumption of nitrate, cells were recovered with 1 mM KNO_3 either in the presence or absence of sodium, and the extracellular concentrations of nitrate and nitrite were measured over a time period of 48 h. The concentration of nitrate stayed largely unchanged in the first 12 h. Thereafter, in the presence of sodium, extracellular nitrate decreased dramatically and was almost completely consumed after 48 h. By contrast, no significant consumption of nitrate was detected in the absence of sodium (Figure 2C). Nitrite is an intermediate in nitrate reduction and is excreted when nitrate reduction exceeds nitrite reduction [22]. During resuscitation in the presence of sodium, the nitrite levels first increased until 24 h and then dropped again at 48 h, as the cells were nitrogen depleted again. In the absence of Na^+, nitrite levels initially increased even faster than in the presence of sodium until 12 h and then stayed constant until 48 h (Figure 2D). In agreement with the lack of nitrate consumption, no excretion of ammonium could be detected in the sodium-free culture, either (Figure S2). This clearly indicates that the initial uptake of nitrate and nitrate reductase activity is not impaired in the absence of sodium, whereas the reduction to ammonium seems to be impaired.

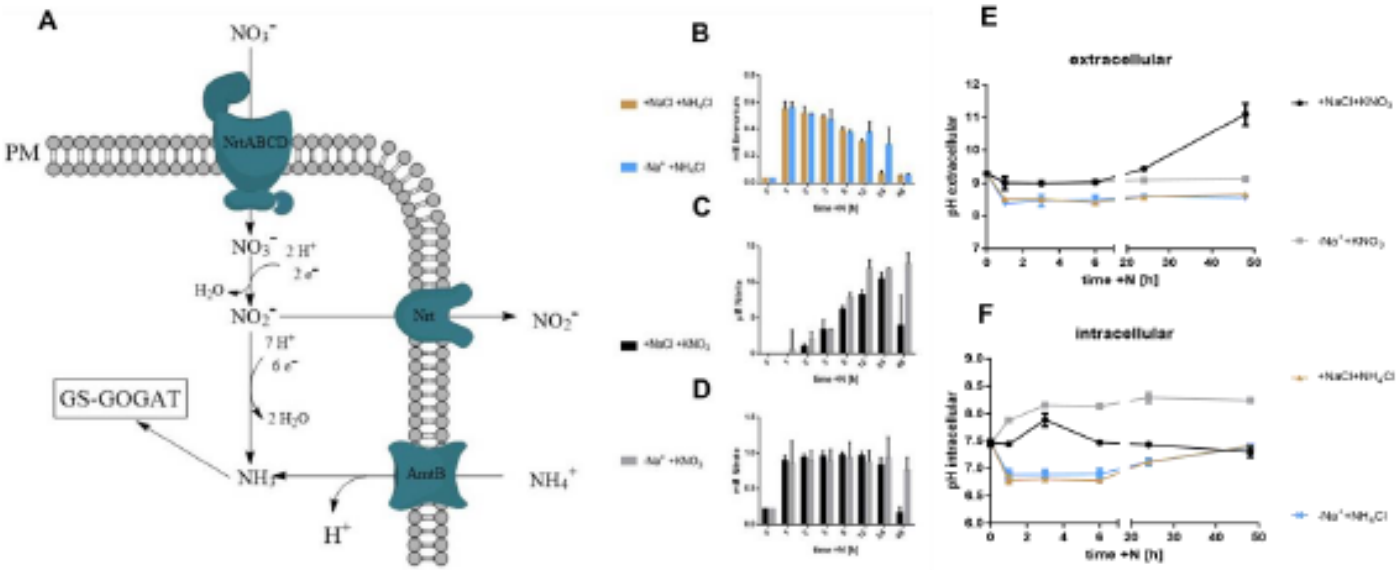

Figure 2. Nitrogen import and incorporation. Time-course analysis of nitrogen compounds and pH during resuscitation. Resuscitation was initiated by the addition of KNO_3 or NH_4Cl to a final concentration of 10 mM. (**A**) depicts a model of the incorporation of combined nitrogen sources into the cell metabolism. GS = Glutamine synthase, GOGAT = Glutamate Oxoglutarate Amidtransferase, PM = Plasmamembrane. Ammonium (**B**) and nitrate (**C**) levels are shown in mM/10^8cells, nitrite levels (**D**) in µM/10^8cells. (**E**) shows the extracellular pH, (**F**) the intracellular. Samples were taken 0, 1, 2, 3, 6, 12, 24, and 48 h after the addition of a combined nitrogen source (KNO_3 or NH_4Cl). Bars represent measurement of biological triplicates. Error bars represent the SD.

The reduction of nitrate to ammonia requires nine protons in total. Given the limited number of available protons in a *Synechocystis* cell [27–29], supplying *Synechocystis* with nitrate as the sole N-source should lead to a cytoplasmic alkalisation unless sufficient protons can be imported. By contrast, when the cells are using ammonium as a nitrogen source, they take up ammonia in co-transport with a proton [30], which delivers new protons into the cytoplasm and should thereby cause its acidification. Therefore, we next measured the extra- and intracellular pH changes during resuscitation to reveal how the presence of sodium affects pH homeostasis. When resuscitation was performed with nitrate in the presence of Na^+, the extracellular pH increased in the second phase of resuscitation (after 20 h). As expected, the extracellular pH remained largely unchanged in the absence of sodium, as no nitrate was consumed (Figure 2E). By contrast, the measurement of intracellular pH using the trapped fluorescent indicator method with BCECF yielded

intriguing results. In the presence of sodium, the intracellular pH transiently increased from pH 7.5 to approximately 7.9, returning to initial levels after 6 h and then remaining constant. By contrast, in the absence of sodium, an immediate increase in intracellular pH occurred which further increased during incubation, reaching a value of 8.3 (Figure 2F). This indicates a lack of intracellular protons, which are generally imported by sodium-dependent antiporters like the Na^+/H^+ antiporter of the NhaS-family [31].

When resuscitation was triggered by the addition of ammonium, transient acidification was measured both in the presence or absence of ammonium (Figure 2F). Likewise, no difference in extracellular pH was observed (Figure 2E). When fed with ammonium, cells appear to regulate the pH independently of the availability of sodium. Nevertheless, also under these conditions, resuscitation in the absence of sodium failed, indicating the existence of further sodium-dependent processes.

3.3. *Metabolome of Resuscitating Cells*

To gain deeper insights into the metabolic changes during resuscitation with nitrate in the presence or absence of sodium, we investigated the metabolome during the first 12 h of resuscitation. In this early phase of resuscitation, no CO_2 fixation takes place, and all cellular carbon is derived from the catabolism of glycogen stores [10]. Therefore, during this heterotrophic phase, sodium should be required for cellular processes other than carbon acquisition. Metabolites were extracted using glass beads to mechanically disrupt the cells in a solvent made of acetonitrile, methanol, and water, and their identity and relative concentration were determined using MS.

The method employed allowed the determination of changes in amino acids and a few central carbon metabolites. This is the first global description of the amino acid steady-state level in the resuscitation of *Synechocystis*, to our knowledge.

The amino acid steady-state levels are the result of amino acid synthesis and its consumption by downstream metabolic pathways and protein synthesis. Overall, for many amino acids, the steady-state level only subtly changed in response to the presence or absence of sodium, although in the absence of sodium, the assimilation of nitrogen was clearly abrogated. This indicates the presence of efficient regulatory mechanisms to keep the steady-state levels of amino acids constant. Therefore, we will focus the analysis of the experiment on examples showing deviations from the standard condition in the absence of sodium.

In the presence of Na^+, glutamate was the amino acid whose cellular concentration increased the most within the first hour of resuscitation (Figure 3A). Thereafter, a further steady increase up to 10 fold was observed after 12 h as compared to the chlorotic cells. This is reasonable since glutamate is the net product of nitrogen assimilation through the GS-GOGAT cycle. In the absence of Na^+, the levels of glutamate also slightly increased, but the steady-state level increased only to about half the concentration. In contrast to glutamate, the concentration of glutamine remained quite constant throughout early resuscitation in the presence of sodium, indicating a thoroughly balanced activity of glutamine synthesis by GS and its consumption by GOGAT. However, in the absence of sodium, glutamine levels dropped and stayed lower, indicating that GS activity lagged behind GOGAT. The imbalanced GS/GOGAT cycle in the absence of sodium could have several reasons. First, the inability to reduce nitrate to ammonia could result in substrate limitation for the GS reaction. Second, the inability to control the intracellular pH could reduce GS enzyme activity. Third, in the absence of sodium, energy metabolism is impaired [17], thus impairing the ATP-dependent GS reaction.

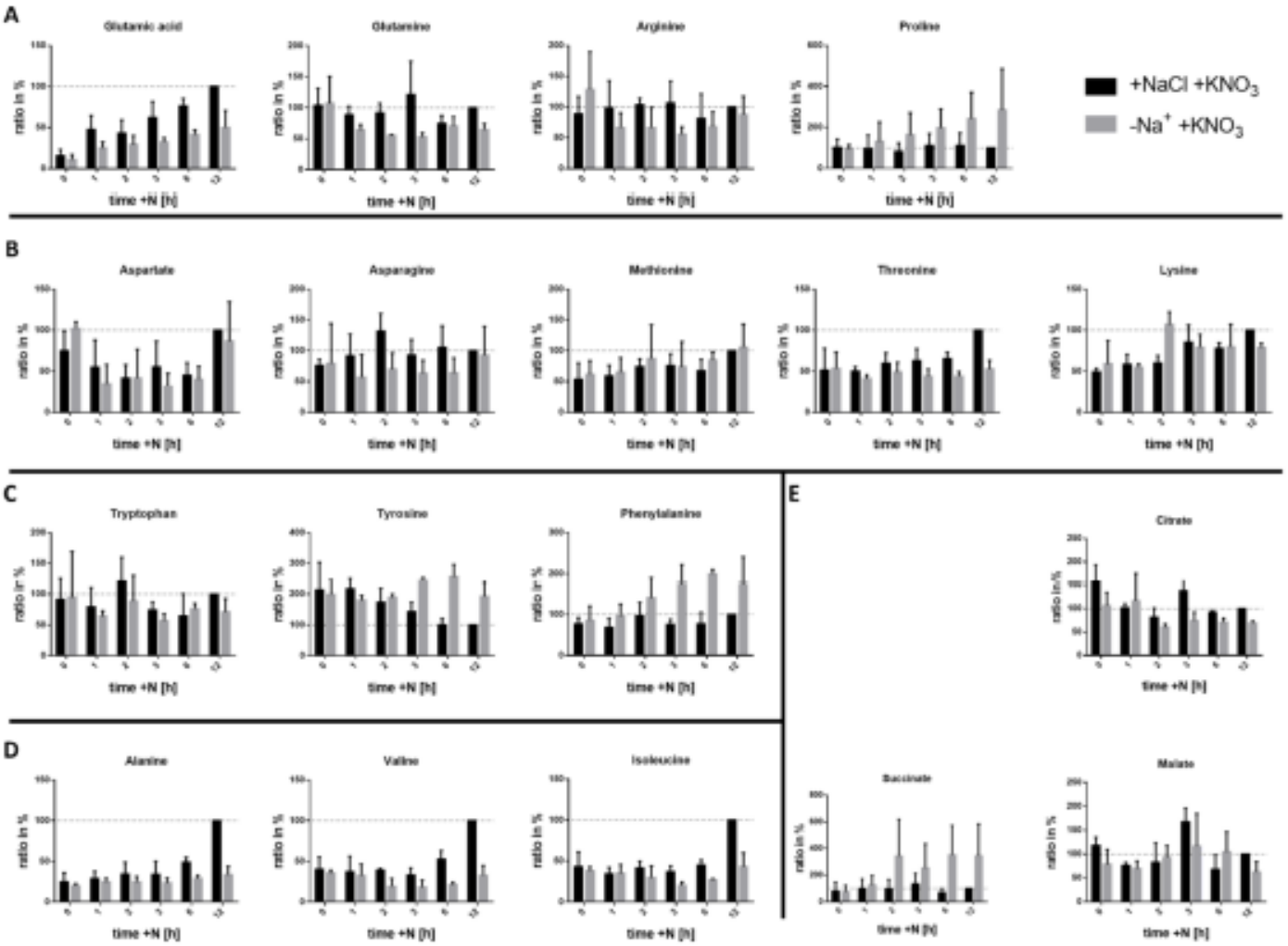

Figure 3. Levels of metabolites during resuscitation in the presence or absence of Na^+. Cells were recovered with 17.5 mM KNO_3 after 2 weeks of nitrogen starvation. (**A**) shows the 2-OG amino acid family, (**B**) the oxaloacetate family, (**C**) the aromatic amino acids and (**D**) the pyruvate family. (**E**) shows intermediates of the TCA cycle. The *y*-axis depicts the ratio in % normalised to 12 h of resuscitation in the presence of sodium, the *x*-axis shows the time after the addition of nitrate in hours. Bars represent measurement of biological triplicates. Error bars represent the SD.

A similar pattern as for glutamine was observed for arginine. Since arginine is derived from glutamate and carbamoyl phosphate, whose synthesis is glutamine derived, the reduced levels of arginine in the absence of sodium could be explained by decreased nitrogen assimilation. A strikingly different pattern was observed for proline, the last member of the oxoglutarate/glutamate-derived amino acid family. Proline levels stayed constant during resuscitation in the presence of sodium, while the levels continuously increased in the absence of Na^+. Proline can be derived from the ArgZ/ArgE catalysed arginine catabolism, which is part of the nitrogen-assimilatory ornithine-ammonia cycle [32]. The N-terminal part of ArgZ displays arginine dihydrolase activity, transforming arginine into ornithine, CO_2, and ammonia. Ornithine can then re-enter arginine synthesis or can be converted by ornithine cyclodeaminase activity into proline, presumably catalysed by the C-terminal domain of ArgZ [33]. The increasing proline levels in the absence of Na^+ indicate that ornithine cyclodeaminase activity exceeds the re-entry of ornithine in the arginine pathway due to impaired nitrogen assimilation. Furthermore, proline is known to function as an osmoprotectant in many bacteria [34–36], and therefore, the increasing proline levels could enhance the protection against osmotic stress.

In the family of oxaloacetate/aspartate amino acids, only subtle differences were observed (Figure 3B). The lower levels of asparagine in the absence of sodium reflect the lower levels of glutamine, which is required for asparagine synthesis.

In the family of aromatic amino acids, tyrosine showed a remarkable pattern. Its levels decreased 2 fold during resuscitation in the presence of sodium, whereas the levels even slightly increased in the absence of sodium (Figure 3C). Increased levels of tyrosine in N-starved *Synechocystis* are in agreement with a recent study reporting a strong accumulation of tyrosine levels when *Synechocystis* cells are subjected to nitrogen deprivation [37]. The levels of phenylalanine also increased during resuscitation in absence of sodium (Figure 3C). No function has been ascribed to free phenylalanine or tyrosine to our knowledge, except in protein synthesis. Thus, we can assume that the drop in tyrosine levels occurring during successful resuscitation reflects its consumption by protein synthesis. The elevated levels in the absence of sodium would then be caused by impaired protein synthesis.

Amino acids from the pyruvate family generally showed lower levels in the absence of Na^+(Figure 3D). For all three, alanine, valine, and isoleucine, a significant increase from 6 to 12 h in resuscitation with sodium was noticeable. This is likely due to the successful re-establishment of the core anabolic reactions, increasing the pool sizes of these amino acids for protein synthesis and further metabolic reactions.

The measured intermediates of the TCA cycle also showed interesting behaviour. The levels of citrate and malate were comparable between the two conditions whereas a large difference was visible for succinate, with a 350% increase at 12 h of resuscitation in the absence of sodium (Figure 3E). Succinate is produced in the modified TCA cycle reactions of cyanobacteria from 2-OG by 2-Oxoglutarate decarboxylase and succinic-semialdehyde dehydrogenase [38]. Since 2-OG can no longer be efficiently converted to glutamate due to the impaired GS-GOGAT cycle in the absence of sodium, the synthesis of succinate is apparently increased under these conditions.

3.4. Consequential Effects on Cyanophycin and the Cytoplasm

Cyanophycin (CP) is a nitrogen storage polymer composed of an aspartate backbone and arginine sidechains. The synthesis of this polymer is an indicator of global nitrogen availability to non-growing cells, as an excess of assimilated nitrogen, not needed for protein synthesis, is stored in this nitrogen-rich polymer. When chlorotic *Synechocystis* cells are resuscitated by nitrate addition, they transiently produce CP during the first day of resuscitation as a nitrogen reservoir to cope with fluctuations in nitrogen supply [13]. To reveal whether this process also depends on Na^+, we assessed CP production using the Sakaguchi reaction, which stains arginine residues. CP granules in cells are visible as red dots [13]. Here, we focused on cultures before and after 12 h of resuscitation. As shown in Figure 4, cells that were resuscitated with nitrate but in the absence of sodium were strongly impaired in CP synthesis, while in the presence of sodium, the expected synthesis of CP could be observed. When cells were resuscitated in the presence of ammonium, a small amount of CP synthesis could be observed.

Since the absence of Na^+ has global consequences for the physiology of the cells, we also investigated cell morphology using transmission electron microscopy. We took samples before the addition of KNO_3 and 24, 48, and 66 h after. During resuscitation in standard conditions, between time points 0 and 24 h +N, the glycogen storages should largely disappear, and ribosomes, CP granules, and an increase in thylakoid membranes should be noticeable. Thereafter, CP granules should disappear again, whereas thylakoid membranes and carboxysomes should appear [11]. These morphological changes were visible in the cultures recovered under standard conditions (Figure 5B). By contrast, the cells that were incubated in the absence of Na^+ appeared to lose intracellular structures (Figure 5A). This indicates that the longer the recovering cells are left without sodium, the more they degrade any intracellular structures to the point of looking like ghost cells.

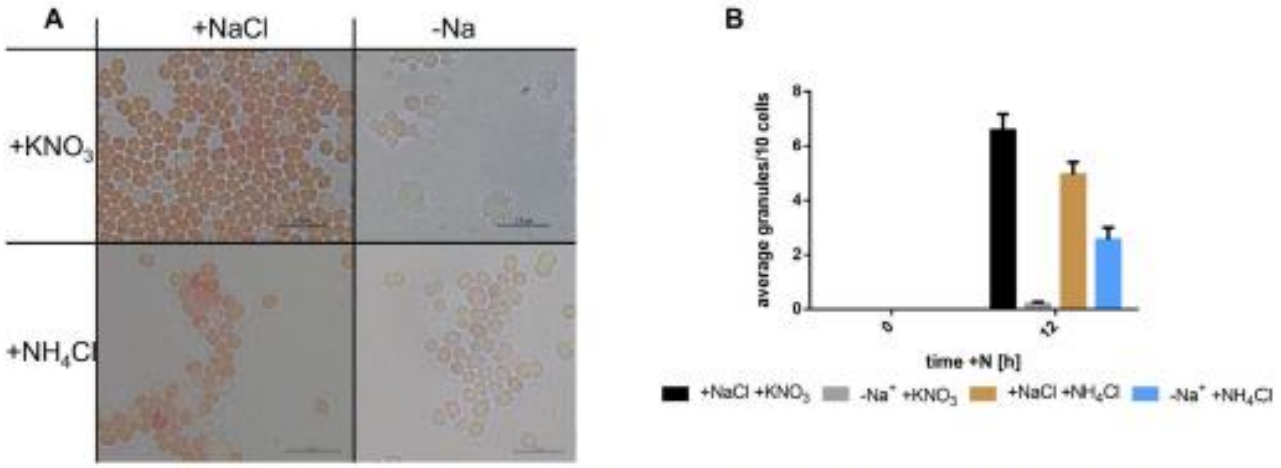

Figure 4. Cyanophycin production in the presence and absence of sodium. (**A**) shows pictures of cells after 12 h of resuscitation with nitrate or ammonium, in the presence or absence of sodium. Cells were stained with the Sakaguchi staining method. Scale bar depicts 7.5 µm in each picture. (**B**) depicts the amount of cyanophycin granules per cell during resuscitation, counted after Sakaguchi staining. Samples were taken before start of resuscitation and 12 h after start. At least 200 cells were counted per sample per time point.

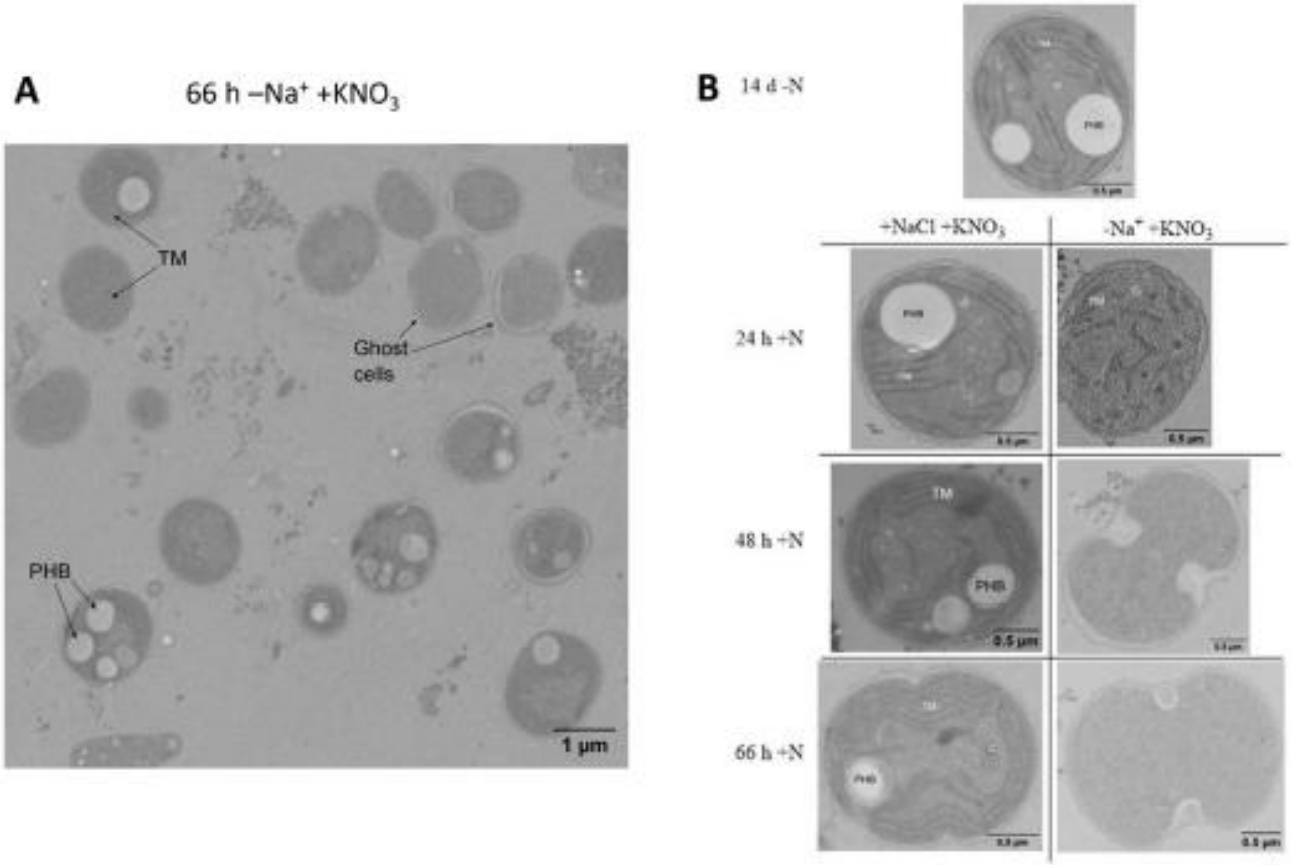

Figure 5. TEM pictures of resuscitating cells in the presence and absence of sodium. (**A**) provides an overview of multiple cells 66 h after the start of resuscitation in the absence of sodium. (**B**) depicts individual cells in resuscitation. On the left side are cells recovering in the presence of sodium, on the right in the absence. Samples were taken before resuscitation (after 14 days of chlorosis) and 24, 48, and 66 h after initiation. TM = thylakoid membrane, PHB = polyhydroxybutyrate, G = glycogen, C = carboxysome. Scale bar in (**A**) represents 1 µm, bars in (**B**) represent 0,5 µm.

4. Conclusions

We have shown in this study that chlorotic cells of *Synechocystis* have a multi-levelled requirement for sodium during resuscitation from nitrogen depletion. Sodium has been previously reported to have a significant role in bioenergetics during the exit from the chlorotic state and in carbon import during vegetative growth [17]. Here we show that throughout resuscitation from nitrogen depletion-induced chlorosis, sodium is required from multiple processes. What are the differences in sodium requirement between vegetatively growing cells and cells resuscitating from chlorosis?

In vegetative cells, the primary requirement for sodium is to enable bicarbonate uptake through the sodium dependence of the major bicarbonate uptake systems SbtA and BicA [18,39,40]. Therefore, at elevated CO_2 levels, which circumvents high-affinity bicarbonate transport, vegetative growth can take place in the absence of sodium. In contrast, in resuscitating cells, supplementation of cells with 2% CO_2, despite enabling synthesis of small amounts of chlorophyll, does not restore full recovery of cells, indicating further requirements for sodium beyond the inorganic carbon supply.

When resuscitation is started by the addition of nitrate, sodium rather helps in the acquisition thereof and the control of intracellular pH. This is because to reduce nitrate to ammonia, cells require nine protons, which requires efficient pH control in the cytoplasm. Na^+/H^+ antiporters can supply the cytoplasm with protons. In the absence of sodium, proton import, and thus, pH control, is impaired leading to the alkalisation of the cytoplasm. Nevertheless, the nitrate reductase reaction, which requires 2 protons, still takes place, and the produced nitrite is now excreted to the medium instead of being further reduced to ammonium. By contrast to nitrate, when fed with ammonia in the absence of sodium, cells are able to take up ammonium but still are unable to incorporate it into proteins or storage compounds like CP. This indicates that central reactions of nitrogen assimilation are also impaired by the absence of sodium.

Metabolite analysis indicated an imbalanced GS/GOGAT cycle in the absence of sodium (see above). The GS reaction appears to be most strongly affected by the lack of sodium, as evidenced by decreasing glutamine levels in sodium-free cells. In addition to the impaired supply of substrate through nitrate reduction, it is likely that the high energy demand of GS cannot be satisfied without the use of sodium bioenergetics, which provides the basis for efficient ATP synthesis in chlorotic cells [17]. This imbalance in one of the most essential metabolic cycles of *Synechocystis* will lead to further problems downstream. The increased levels of proline during resuscitation in absence of sodium, for example, could be derived from arginine catabolism by ArgZ [33]. Supporting this, the expression of *argZ* and the protein levels of ArgZ also increase in early resuscitation [11,12]. Proline would then serve as an osmolyte to stabilise the cytoplasm while the glycogen stores and the intracellular structures are degraded, as witnessed in the TEM analysis. The cells recovering in the absence of sodium degrade their cytoplasmic structures until they appear empty. This is reminiscent of the degradation and recycling processes occurring in lysosomes during the autophagy of eucaryotic cells [41]. It is unclear whether the increased level of tyrosine in chlorotic cells simply reflects the lack of catabolism of free tyrosine during chlorosis or whether it is of functional significance. In specific enzymes, tyrosine residues may act as radical quenchers [42]. Whether free tyrosine could also function as a radical quencher has, to our knowledge, never been demonstrated, but if so, it would provide additional protection to chlorotic cells.

All these results highlight the tight interconnection of cellular processes through the pivotal role of ions such as sodium, protons, and small metabolites. The broad effects of ion homeostasis could be revealed by studying cells in an extreme metabolic situation, with limited possibilities to compensate for external perturbations. In a broader scope, such studies deepen our understanding of the physiology of dormant cells and the reawakening after quiescence.

Supplementary Materials: The following supporting information can be downloaded at: https://www.mdpi.com/article/10.3390/biology12020159/s1, Figure S1: minimal sodium concentration required for vegetative growth, Figure S2: extracellular concentration of nitrogen compounds in recovery; Table S1: metabolome of recovering cells.

Author Contributions: Conceptualization, funding acquisition, project administration, and resources: K.F.; Writing, and data curation: M.B. and KF; Supervision: K.F. and H.L.; Methodology and formal analysis: M.B. and J.R.; Validation and Visualization: M.B.; Investigation; M.B., J.R. and C.M. All authors have read and agreed to the published version of the manuscript.

Funding: This research was funded by the German Research Foundation (DFG) via the research training group GRK 1708 and via the Cluster of Excellence (EXC2124) "Controlling Microbes to Fight Infections".

Institutional Review Board Statement: Not applicable.

Informed Consent Statement: Not applicable.

Data Availability Statement: All data obtained during this work is available from the authors on request.

Acknowledgments: We are grateful to Libera Lo Presti for proofreading and constructive editing of the manuscript and Sofia Doello for helpful discussion and assistance in experimental planning.

Conflicts of Interest: The authors declare no conflict of interest. The funders had no role in the design of the study; in the collection, analyses, or interpretation of data; in the writing of the manuscript, or in the decision to publish the results.

References

1. Rittershaus, E.S.C.; Baek, S.; Sassetti, C.M. The Normalcy of Dormancy. *Cell Host Microbe* **2013**, *13*, 643–651. [CrossRef] [PubMed]
2. Tan, I.S.; Ramamurthi, K.S. Spore Formation in Bacillus Subtilis. *Environ. Microbiol. Rep.* **2014**, *6*, 212–225. [CrossRef]
3. Anderson, J.; Horvath, D.; Chao, W.; Foley, M. Bud Dormancy in Perennial Plants: A Mechanism for Survival. In *Topics in Current Genetics*; Springer: Berlin/Heidelberg, Germany, 1970; Volume 21, pp. 69–90. ISBN 978-3-642-12421-1.
4. Görl, M.; Sauer, J.; Baier, T.; Forchhammer, K. Nitrogen-Starvation-Induced Chlorosis in Synechococcus PCC 7942: Adaptation to Long-Term Survival. *Microbiology* **1998**, *144*, 2449–2458. [CrossRef] [PubMed]
5. Sauer, J.; Schreiber, U.; Schmid, R.; Völker, U.; Forchhammer, K. Nitrogen Starvation-Induced Chlorosis in Synechococcus Pcc 7942. Low-Level Photosynthesis as a Mechanism of Long-Term Survival. *Plant Physiol.* **2001**, *126*, 233–243. [CrossRef] [PubMed]
6. Stanier, R.Y.; Cohen-Bazire, G. Phototrophic Prokaryotes: The Cyanobacteria. *Annu. Rev. Microbiol.* **1977**, *31*, 225–274. [CrossRef] [PubMed]
7. Vitousek, P.M.; Howarth, R.W. Nitrogen Limitation on Land and in the Sea: How Can It Occur? *Biogeochemistry* **1991**, *13*, 87–115. [CrossRef]
8. Schwarz, R.; Forchhammer, K. Acclimation of Unicellular Cyanobacteria to Macronutrient Deficiency: Emergence of a Complex Network of Cellular Responses. *Microbiology* **2005**, *151*, 2503–2514. [CrossRef]
9. Neumann, N.; Doello, S.; Forchhammer, K. Recovery of Unicellular Cyanobacteria from Nitrogen Chlorosis: A Model for Resuscitation of Dormant Bacteria. *Microb. Physiol.* **2021**, *31*, 1–10. [CrossRef]
10. Doello, S.; Klotz, A.; Makowka, A.; Gutekunst, K.; Forchhammer, K. A Specific Glycogen Mobilization Strategy Enables Rapid Awakening of Dormant Cyanobacteria from Chlorosis. *Plant Physiol.* **2018**, *177*, 594–603. [CrossRef]
11. Klotz, A.; Georg, J.; Bučinská, L.; Watanabe, S.; Reimann, V.; Januszewski, W.; Sobotka, R.; Jendrossek, D.; Hess, W.R.; Forchhammer, K. Awakening of a Dormant Cyanobacterium from Nitrogen Chlorosis Reveals a Genetically Determined Program. *Curr. Biol.* **2016**, *26*, 2862–2872. [CrossRef]
12. Spät, P.; Klotz, A.; Rexroth, S.; Maček, B.; Forchhammer, K. Chlorosis as a Developmental Program in Cyanobacteria: The Proteomic Fundament for Survival and Awakening. *Mol. Cell Proteom. MCP* **2018**, *17*, 1650–1669. [CrossRef] [PubMed]
13. Watzer, B.; Forchhammer, K. Cyanophycin Synthesis Optimizes Nitrogen Utilization in the Unicellular Cyanobacterium Synechocystis Sp. Strain PCC 6803. *Appl. Environ. Microbiol.* **2018**, *84*, e01298-18. [CrossRef] [PubMed]
14. Sharon, I.; Haque, A.S.; Grogg, M.; Lahiri, I.; Seebach, D.; Leschziner, A.E.; Hilvert, D.; Schmeing, T.M. Structures and Function of the Amino Acid Polymerase Cyanophycin Synthetase. *Nat. Chem. Biol.* **2021**, *17*, 1101–1110. [CrossRef]
15. Allen, M.M. Inclusions: Cyanophycin. In *Methods in Enzymology*; Cyanobacteria; Academic Press: London, UK, 1988; Volume 167, pp. 207–213.
16. Watzer, B.; Klemke, F.; Forchhammer, K. The Cyanophycin Granule Peptide from Cyanobacteria. In *Bacterial Organelles and Organelle-like Inclusions*; Jendrossek, D., Ed.; Microbiology Monographs; Springer International Publishing: Cham, Switzerland, 2020; pp. 149–175. ISBN 978-3-030-60173-7.
17. Doello, S.; Burkhardt, M.; Forchhammer, K. The Essential Role of Sodium Bioenergetics and ATP Homeostasis in the Developmental Transitions of a Cyanobacterium. *Curr. Biol.* **2021**, *31*, 1606–1615. [CrossRef]

18. Shibata, M.; Katoh, H.; Sonoda, M.; Ohkawa, H.; Shimoyama, M.; Fukuzawa, H.; Kaplan, A.; Ogawa, T. Genes Essential to Sodium-Dependent Bicarbonate Transport in Cyanobacteria: Function and Phylogenetic analysis. *J. Biol. Chem.* **2002**, *277*, 18658–18664. [CrossRef]
19. Rippka, R.; Deruelles, J.; Waterbury, J.B.; Herdman, M.; Stanier, R.Y. Generic Assignments, Strain Histories and Properties of Pure Cultures of Cyanobacteria. *Microbiology* **1979**, *111*, 1–61. [CrossRef]
20. Gründel, M.; Scheunemann, R.; Lockau, W.; Zilliges, Y. Impaired Glycogen Synthesis Causes Metabolic Overflow Reactions and Affects Stress Responses in the Cyanobacterium *Synechocystis* Sp. PCC 6803. *Microbiol. Read. Engl.* **2012**, *158*, 3032–3043. [CrossRef] [PubMed]
21. Klotz, A.; Reinhold, E.; Doello, S.; Forchhammer, K. Nitrogen Starvation Acclimation in Synechococcus Elongatus: Redox-Control and the Role of Nitrate Reduction as an Electron Sink. *Life* **2015**, *5*, 888–904. [CrossRef]
22. Kloft, N.; Forchhammer, K. Signal Transduction Protein PII Phosphatase PphA Is Required for Light-Dependent Control of Nitrate Utilization in Synechocystis Sp. Strain PCC 6803. *J. Bacteriol.* **2005**, *187*, 6683–6690. [CrossRef]
23. Fiddler, R.N. Collaborative Study of Modified AOAC Method of Analysis for Nitrite in Meat and Meat Products. *J. Assoc. Off. Anal. Chem.* **1977**, *60*, 594–599. [CrossRef]
24. Furniss, B.S.; Hannaford, A.J.; Smith, P.W.G.; Tatchell, A.R. *Vogel's Textbook of Practical Organic Chemistry*, 5th ed.; Longman Scientific & Technical: Harlow, UK; John Wiley & Sons, Inc.: New York, NY, USA, 1989.
25. Guder, J.C.; Schramm, T.; Sander, T.; Link, H. Time-Optimized Isotope Ratio LC–MS/MS for High-Throughput Quantification of Primary Metabolites. *Anal. Chem.* **2017**, *89*, 1624–1631. [CrossRef] [PubMed]
26. Watzer, B.; Engelbrecht, A.; Hauf, W.; Stahl, M.; Maldener, I.; Forchhammer, K. Metabolic pathway engineering using the central signal processor PII. *Microb. Cell Fact.* **2015**, *14*, 192–203. [CrossRef] [PubMed]
27. Zavřel, T.; Faizi, M.; Loureiro, C.; Poschmann, G.; Stühler, K.; Sinetova, M.; Zorina, A.; Steuer, R.; Červený, J. Quantitative Insights into the Cyanobacterial Cell Economy. *eLife* **2019**, *8*, e42508. [CrossRef]
28. Kihara, S.; Hartzler, D.A.; Savikhin, S. Oxygen Concentration inside a Functioning Photosynthetic Cell. *Biophys. J.* **2014**, *106*, 1882–1889. [CrossRef]
29. Orij, R.; Brul, S.; Smits, G.J. Intracellular PH Is a Tightly Controlled Signal in Yeast. *Biochim. Biophys. Acta* **2011**, *1810*, 933–944. [CrossRef]
30. Williamson, G.; Tamburrino, G.; Bizior, A.; Boeckstaens, M.; Dias Mirandela, G.; Bage, M.; Pisliakov, A.; Ives, C.; Terras, E.; Hoskisson, P.; et al. A Two-Lane Mechanism for Selective Biological Ammonium Transport. *Biochem. Chem. Biol.* **2020**, *9*, e57183. [CrossRef]
31. Tsunekawa, K.; Shijuku, T.; Hayashimoto, M.; Kojima, Y.; Onai, K.; Morishita, M.; Ishiura, M.; Kuroda, T.; Nakamura, T.; Kobayashi, H.; et al. Identification and Characterization of the Na+/H+ Antiporter NhaS3 from the Thylakoid Membrane of Synechocystis Sp. PCC 6803*. *J. Biol. Chem.* **2009**, *284*, 16513–16521. [CrossRef] [PubMed]
32. Zhang, H.; Liu, Y.; Nie, X.; Liu, L.; Hua, Q.; Zhao, G.-P.; Yang, C. The Cyanobacterial Ornithine–Ammonia Cycle Involves an Arginine Dihydrolase. *Nat. Chem. Biol.* **2018**, *14*, 575–581. [CrossRef] [PubMed]
33. Flores, E. Studies on the Regulation of Arginine Metabolism in Cyanobacteria Should Include Mixotrophic Conditions. *mBio* **2021**, *12*, e01433-21. [CrossRef]
34. Wood, J.M.; Bremer, E.; Csonka, L.N.; Kraemer, R.; Poolman, B.; van der Heide, T.; Smith, L.T. Osmosensing and Osmoregulatory Compatible Solute Accumulation by Bacteria. *Comp. Biochem. Physiol. A. Mol. Integr. Physiol.* **2001**, *130*, 437–460. [CrossRef]
35. Götz, F.; Longnecker, K.; Soule, M.C.K.; Becker, K.W.; McNichol, J.; Kujawinski, E.B.; Sievert, S.M. Targeted Metabolomics Reveals Proline as a Major Osmolyte in the Chemolithoautotroph Sulfurimonas Denitrificans. *MicrobiologyOpen* **2018**, *7*, e00586. [CrossRef] [PubMed]
36. Sleator, R.D.; Hill, C. Bacterial Osmoadaptation: The Role of Osmolytes in Bacterial Stress and Virulence. *FEMS Microbiol. Rev.* **2002**, *26*, 49–71. [CrossRef]
37. Krauspe, V.; Timm, S.; Hagemann, M.; Hess, W.R. Phycobilisome Breakdown Effector NblD Is Required To Maintain Cellular Amino Acid Composition during Nitrogen Starvation. *J. Bacteriol.* **2022**, *204*, e00158-21. [CrossRef]
38. Zhang, S.; Bryant, D. The Tricarboxylic Acid Cycle in Cyanobacteria. *Science* **2011**, *334*, 1551–1553. [CrossRef] [PubMed]
39. Burnap, R.; Hagemann, M.; Kaplan, A. Regulation of CO_2 Concentrating Mechanism in Cyanobacteria. *Life* **2015**, *5*, 348–371. [CrossRef] [PubMed]
40. Price, G.D.; Woodger, F.J.; Badger, M.R.; Howitt, S.M.; Tucker, L. Identification of a SulP-type bicarbonate transporter in marine cyanobnacteria. *Proc. Natl. Acad. Sci. USA* **2004**, *101*, 18228–18233. [CrossRef]
41. Yang, Z.; Klionsky, D.J. An Overview of the Molecular Mechanism of Autophagy. *Curr. Top. Microbiol. Immunol.* **2009**, *335*, 1–32. [CrossRef]
42. Ignasiak, M.; Frackowiak, K.; Pedzinski, T.; Davies, M.J.; Marciniak, B. Unexpected Light Emission from Tyrosyl Radicals as a Probe for Tyrosine Oxidation. *Free Radic. Biol. Med.* **2020**, *153*, 12–16. [CrossRef]

Disclaimer/Publisher's Note: The statements, opinions and data contained in all publications are solely those of the individual author(s) and contributor(s) and not of MDPI and/or the editor(s). MDPI and/or the editor(s) disclaim responsibility for any injury to people or property resulting from any ideas, methods, instructions or products referred to in the content.

Manuscripts in preparation:

Publication 4 (in preparation)

Research Article

Burkhardt, M, Haffner, M, D, L, Menzel, C, Mantovani, O, Hagemann, M, Forchhammer, K. Working Title: Essentiality of c-di-AMP for metabolic quiescence in cyanobacteria.

Working Title: Essentiality of c-di-AMP for metabolic quiescence in cyanobacteria

Markus Burkhardt[1], Michael Haffner[1], Lisa Dengler[2], Claudia Menzel[1], Roland Seifert[3], Martin Hagemann[4], Karl Forchhammer[1]

[1] Interfaculty Institute of Microbiology and Infection Medicine, University of Tübingen, Auf der Morgenstelle 28, 72076 Tübingen, Germany

[2] Interfaculty Institute for Cell Biology, University of Tübingen, Auf der Morgenstelle 15, 72076 Tübingen, Germany

[3] Institute of Pharmacology, Hannover Medical School, Carl-Neuberg-Str. 1, 30625 Hannover, Germany

[4] Institute of Biosciences, Department of Plant Physiology, University of Rostock, 18059 Rostock, Germany

Abstract:

Dormancy is one of the most significant survival mechanisms in bacteria. The entrance and exit from dormancy require tight control. A failure to properly control this process can easily lead to cell death. In the last decade, the second messenger cyclic di-adenosine monophosphate turned out to play key roles in homeostatic regulation of various bacteria. Mostly associated with ion and osmolyte homeostasis, it has also been shown to be essential for survival in cyanobacteria in a diurnal rhythm and indications of its requirement to survive metabolic dormancy in cyanobacteria have also been found. To further investigate the influence of c-di-AMP on metabolic quiescence, the response of a c-di-AMP deficient *Synechocystis sp.* PCC 6803 strain towards nitrogen starvation-induced chlorosis was investigated. We revealed that c-di-AMP is essential for entry into chlorosis and exit thereof. We found significant dysregulation in cellular glutamate and glutamine levels, indicating involvement of c-di-AMP in nitrogen metabolism. Moreover, a severe plasmolysis in later stages of chlorosis highlights the importance of c-di-AMP in maintaining osmotic balance during the chlorotic state.

Introduction:

Second messengers are small molecules and ions transmitting environmental and intracellular signals to receptor and effector proteins to tune cellular responses [1]. One large group of second messengers are cyclic nucleotides including the well-known cyclic adenosine monophosphate (cAMP). A different sub-group are the cyclic di-nucleotides, which gained interest in the last decades. One of them is cyclic di-adenosine monophosphate (3',5;-c-di-adenosine 5'-monophopshate; hereafter c-di-AMP). Since its discovery in *Bacillus subtilis* in 2008 [2], it has been found in various bacteria and archaea, but not in eukaryotes [3–5]. C-di-AMP is synthesised from two ATP molecules by diadenylate cyclases and degraded by phosphodiesterases [6,7]. In various genera of the firmicutes clade, mutants with deficient c-di-AMP synthesis or with increased c-di-AMP degradation are not viable in complex media. Diadenylate cyclase deficient mutants, however could be rescued in minimal media with low potassium supply [8–11].In contrast , mutants that overproduce c-di-AMP generally showed impairment [12–14]. Due to this tight requirement of limited amount of c-di-AMP, it was termed an "essential poison" [12]. In firmicutes, many interaction partners have been discovered through the analysis of suppressor mutations. In this manner, interaction partners of c-di-AMP that are involved in ion homeostasis and osmolyte uptake have been discovered [8–10,15–17].

As shown in firmicutes, c-di-AMP appears to play a central role in the potassium homeostasis as deduced from the number of mutations found in transporters thereof [8,10,15]. The immediate uptake of K^+ ions is the first response of many bacteria to hyperosmotic stress [18]. To circumvent long term ionic stress due to the charges of K^+ and the counter ion glutamate, bacteria will then replace these ions with compatible solutes and other osmolytes [18]. Since high levels of c-di-AMP inhibit the uptake of K^+ and increase its export [8,19,20], the concentration of c-di-AMP needs to decrease under hyperosmotic shock and needs to rise to export the K^+ ions again. Suppressor mutations were also found in osmolyte transporter encoding genes like *opuD* in *Staphylococcus aureus* [10] or the transcription repressor encoding gene *busR* [15]. BusR represses the expression of the glycine betaine uptake system BusAB actively when binding c-di-AMP.

Cyanobacteria are a ubiquitous group of bacteria owing to their unique ability in prokaryotes to perform oxygenic photosynthesis. In cyanobacteria, c-di-AMP has been reported to be necessary for diurnal growth, especially for night-time survival [21,22], and like in firmicutes, for ion homeostasis and osmoprotection [23]. In the model cyanobacterium *Synechocystis sp.* PCC 6803 (hereafter *Synechocystis*), a unicellular non-diazotrophic strain, only one diadenylate cyclase, termed DacA, is known [22,23]. Investigation of a Δ*dacA* knockout strain revealed reduced levels of glycogen, likely because the glycogen branching enzyme GlgB is activated by the PII-like signal transduction protein SbtB in complex with c-di-AMP [22]. Deprivation of combined nitrogen sources is a condition, which causes maximal glycogen accumulation. Prolonged nitrogen starvation causes reversible chlorosis and metabolic quiescence, whereby during this acclimation process, the cells prepare for rapid resuscitation from dormancy as soon as nitrogen becomes available again [24,25]. In a previous study, we observed that a Δ*dacA* mutant was unable to resuscitate from nitrogen starvation while a Δ*sbtB* mutant did not show an impairment in re-greening [22]. The metabolic recalibration necessary for the process of chlorosis follows a strictly organised program observable at different phenotypical levels. Upon nitrogen deprivation, the cells divide one last time before arresting growth [26] and the levels of ATP drop significantly [27]. The phycobilisomes, the thylakoid membrane-anchored light harvesting complexes , are degraded and the whole photosynthetic machinery is reduced until only a residual amount remains [24,25]. During the initial phase of the chlorosis process, the fixed CO2 is directed towards glycogen synthesis, which is the crucial energy reserve that fuels a subsequent resuscitation process [27–30].

The resuscitation process of chlorotic *Synechocystis* as a model for the awakening of a dormant bacterium has been studied in detail [27–29,31–34]. It starts with the addition of a usable nitrogen source. The cells immediately take up such a nitrogen compound and increase their ATP levels [27]. As the cells start to degrade glycogen to gain energy by respiration and to mobilise carbon skeletons for assimilatory reactions, they transiently switch off residual photosynthetic activity [27,28]. Following an initial reconstitution of the translational machinery and of central metabolic capacities, they rebuild the entire photosynthetic machinery. After about 24 hours, the thylakoid membranes and photosystems are rebuilt enough for the cells to switch into a mixotrophic phase [28]. After approximately 48 hours of resuscitation, the glycogen storages are largely degraded and the photosynthetic machinery is completely restored, allowing the cells to switch back to phototrophic lifestyle and resuming cell growth [28]. While this process proceeds in a highly reproducible manner, transcriptomic and proteomic studies showed that it is operated by a genetically encoded resuscitation program that executes the timing of differential gene expression. Among the genes, which were the first to be induced upon start of resuscitation, the *dacA* gene belonged to the most strongly induced genes [28,31], indicating a significant regulatory role of c-di-AMP for the recalibration of metabolism during resuscitation. The present study was carried out with the aim to reveal in more detail the role of c-di-AMP metabolism in cyanobacteria awakening from dormancy.

Material and Methods:

Cultivation, nitrogen stepdown and resuscitation, and colony PCR:

Cells were cultivated in BG_{11} medium in shaking flasks, shaking at 120 rpm and continuous white light between 30 – 70 µE at 28 °C. Nitrogen starvation was induced by washing cells with the BG_{11-0} medium, which contains all BG_{11} components except for $NaNO_3$. To induce resuscitation, 17.5 mM $NaNO_3$ was added to the culture. Cell density was measured in a photometer Heλios δ (Thermo Fisher Scientific, Waltham, MA, USA) at OD_{750}. The whole cell spectrum was measured in a spectrophotometer Specord 50 (Analytik Jena GmbH, Jena, TH, Germany). The adapted strains were checked by colony PCR.

Glycogen measurement:

Glycogen amounts were measured using an enzymatic assay according to Gründel et al (2012), with modifications established by Klotz et al (2015). Two ml samples were taken, washed with water, and incubated in 30% KOH for 2 h at 95 °C. Then, ice-cold ethanol was added to a final concentration of 75%, and glycogen precipitated overnight at −20 °C. Samples were then washed with 70 and 98% ethanol, spun down, the pellet dried, and the glycogen digested by the addition of a solution of 100mM sodium acetate and 4.4 U/µL amyloglucosidase (Sigma Aldrich, St. Louis, MO, USA) at pH 4.5 for 2 h. Then, 200 µL of the samples were mixed with 1 mL of 6 % O-toluidine in acetic acid and incubated for 10 min at 100 °C. Absorbance was then measured at 635 nm using a Tecan Spark 10M (Tecan, Männerdorf, ZH, Switzerland). A glucose calibration curve was used to determine the glycogen amount in the samples. At least three biological replicates were measured for every condition.

PS2 Yield with Pulse Amplitude Modulation (PAM)

The yield of Photosystem II (PSII) was measured in vivo using a WATER-PAM chlorophyll fluorometer (Walz GmbH, Effeltrich,BY, Germany). The maximum PSII quantum yield was determined by saturation pulse. At least three biological replicates were measured, and each one in three technical replicates.

ATP determination in the cells:

One ml samples were taken from each culture in cultivation conditions and immediately frozen in liquid nitrogen. Samples were then stored at −80 °C until further processing. Cells were lysed by three cycles of cooking at 99 °C and flash freezing in liquid nitrogen. Debris was spun down at 25.000 g at 4 °C for 1 min. The ATP content in the supernatant was measured according to the instructions of the "ATP determination kit'' (Molecular Probes (A22066), Eugene, OR, USA). A 50 µL reaction mix containing reaction buffer, luciferin, and firefly luciferase was mixed with a 10 µL sample supernatant and measured in a Sirius Luminometer (Berthold Detection Systems, Bad Wildbad, BW, Germany). An ATP calibration curve was used to determine the ATP amount in the samples. At least three biological replicates were measured for every condition.

Measurement of intracellular c-di-AMP concentration:

10 ml of cells with an OD_{750} 0.6 – 0.8 were harvested by vacuum filtration through glass microfibre membranes with a pore size of 1.2 µm (Whatman GF/C, Global Life Sciences Solutions Operations UK Ltd, Little Chalfont Buckinghamshire, UK, cat. no. 1822-025). The filter was transferred into a 2 ml reaction tube and frozen in liquid nitrogen. Samples were stored at – 80 °C until further processing. For that the filters were resuspended in 500 µl ice cold extraction solvent (acetonitrile/methanol/water 2/2/1, v/v/v), incubated on ice for 15 minutes and then heated for 10 min at 95 °C. After cooling the samples on ice, they were centrifuged at 20.800 g and 4 °C for 10 minutes, the supernatant was transferred into a new reaction tube. Filters were resuspended in extraction solvent, incubated on ice,

and spun down two more times; the supernatants were added to the reaction tube with the one from the first run. The tubes with the combined supernatants were then stored over night at -20 °C. Afterwards, samples were centrifuged at 20.800 g and 4 °C for 10 minutes again, and the supernatant transferred into a new tube. Supernatant was then evaporated using a vacuum exicator RVC 2-18(Martin Christ Gefriertrocknungsanlagen GmbH, Osterode, NI, Germany). Further sample preparation and measurement was done according to Selim et al, 2021.

Membrane potential determination:

Cells were stained using the dye Bis-(1,3-Dibutylbarbituric Acid)-trimethine axonol (DiBAC4(3)) (AAT Bioquest, Hamburg, HH, Germany, cat. no. 21411) dissolved in DMSO. Samples were taken in vegetative growth and at different times in chlorosis, cells were then stained with 10 µM DiBAC4(3) for 30 min in the dark. 10 µl of sample were then dropped onto an 1 % agarose-coated microscopy slide and imaged using a Leica DM5500 B (Wetzlar, HE, Germany) with an 100x/1.3 oil objective. A yellow fluorescent protein filter (excitation: 490 -510 nm, emission: 520 – 550 nm) was used for detection.

Transmission Electron Microscopy:

Samples for TEM were prepared, and images were taken as described in Watzer et al, 2015.

Metabolome:

For metabolome analysis, cells were cultivated and shifted as described above. For sampling, cells equating to an OD_{750} 4 were sampled by vacuum filtration through glass microfibre membranes with a 1.2 µm pore size (Whatman GF/C, Global Life Sciences Solutions Operations UK Ltd, Little Chalfont Buckinghamshire, UK) and washed with 10 ml BG_{11}^0 medium. Filters were transferred into 2 ml reaction tubes and frozen in liquid nitrogen. 630 µl Methanol with 1 µl carnitine standard (1mg/ml) were added to the tubes with the filters and mechanical breaking of the filters ensued. This was facilitated by vigorous mixing, 10 min incubation in a sonication bath and 15 min shaking. Afterwards 400 µl chloroform were added and samples incubated for 10 min at 37 °C. Then, 800 µl ultrapure water were added and samples again shaken for 15 min before incubating them for at least 2 h at – 20 °C. Cell debris and filters were removed by centrifugation at 20.000 g and 4 °C for 5 min. The upper polar phase was transferred into a new tube and dried in a vacuum concentrator (Concentrator plus, Eppendorf SE, Hamburg, HH, Germany). The extracts were then resuspended in 200 µl deionised water and filtrated through 0.2 µm filters (Omnifix, B. Braun SE, Melsungen, HE, Germany). Analysis was performed with the high-performance liquid chromatograph mass spectrometer LCMS-7050 system (Shimadzu Corporation, Nakagyo-ku, Kyõto, Japan). LC-MS data analysis was performed with the Lab solution software package (Shimadzu Corporation, Nakagyo-ku, Kyõto, Japan).

Recovery drop plate assay:

Chlorotic cells were dropped onto a BG_{11} agar plate in a dilution series. The highest concentration equated to an OD_{750} 1 with dilution steps of 1:10. 5 µl were dropped for each spot. Plates were then incubated at ~ 70 µE continuous white light at 28 °C for 7 days before imaging.

Results:

Physiological role of c-di-AMP upon nitrogen starvation:

Cyclic-di-AMP has been previously described as an important second messenger to enter and resuscitate from nitrogen depletion-induced chlorosis in *Synechocystis* [22] and in accord, the diadenylate cyclase gene *dacA* is strongly induced in the early phase of resuscitation [28]. Following these observations, we strived to identify the physiological relevance of c-di-AMP in chlorosis and resuscitation by characterising the c-di-AMP deficient Δ*dacA* knockout mutant. Therefore, we exposed both *Synechocystis* WT and Δ*dacA* to prolonged phases of nitrogen starvation before resuscitation was induced by the addition of nitrate. Measurement of the intracellular concentration of c-di-AMP showed that the levels of c-di-AMP in the wild-type peaked within the first day of chlorosis (fig. 1, A), indicating a higher requirement for the second messenger during metabolic recalibration. The c-di-AMP-deficient strain was incapable of producing measurable amounts thereof. During chlorosis, the cell colour changes from a green-blue to a yellow-orange pigmentation, because the photosynthetic machinery is mostly degraded and mainly carotenoids remain [25,26]. While the WT showed this typical colour change, the Δ*dacA* mutant turned completely white within 2 weeks of chlorosis, which is an indication of cell death (fig. 1, B). To quantify cell viability, we used the viability indicator dye bis-(1,3-dibutylbarbituric acid)-trimethine oxonol ($DiBAC_4(3)$), which stains depolarized cells. Within 3 weeks, approximately 75 % of the mutant cells were $DiBAC_4(3)$ positive indicating cell death (fig. 1, C, D). To find the reason for loss of viability, we investigated different physiological parameters. After nitrogen depletion the process of chlorosis begins with a final cell division, before growth arrest occurs [28,29]. Cultures of the Δ*dacA* mutant were unable to perform this last cell division upon nitrogen starvation (fig. 1, E), showing their inability to initiate a proper chlorosis response. The degradation of the photosynthetic machinery can be observed by pulse amplitude modulation (PAM) fluorometry as a proxy for photosystem II activity and by measuring phycobiliprotein absorbance at 625 nm. In both parameters, Δ*dacA* acts comparable to the WT (fig. 1, F, G). The quantification of intracellular ATP levels in WT cells showed a sudden drop to 20 % within 24 hours of nitrogen depletion reaching a plateau of approximately 40 % ATP as compared to vegetative growth. Strikingly, the sudden drop in ATP level did not occur in the Δ*dacA* mutant, further indicating its inability to adjust its metabolism to the onset of starvation (fig. 1, H). In fact, the ATP levels of Δ*dacA* even increased slightly during the first 2 days of chlorosis before dropping to lower levels after prolonged starvation. In agreement with previous studies, quantification of intracellular glycogen showed that glycogen levels in WT cells already peaked at maximum after one day of chlorosis with approximately. 120 $\mu g/10^8$ cells. By contrast, glycogen accumulation in the Δ*dacA* mutant was strongly retarded and diminished (fig.1, I), resembling the previously observed impairment in glycogen synthesis during diurnal growth [22]. To further characterize the morphological changes, which the cells undergo during chlorosis, we performed transmission electron microscopy (TEM) with WT and mutant cultures after 21 days of chlorosis (fig. 1, J). While WT cells showed the typical morphological characteristics of chlorotic cells like the accumulation of glycogen and polyhydroxybutyrate (PHB) granules, as well as a strongly reduced amount of thylakoid membranes, the cells in the Δ*dacA* cultures had a heterogenous appearance (fig. 1, J). Many of the Δ*dacA* cells showed indications of plasmolysis, marked by a shrinkage of the cytoplasmic space with retraction of the cytoplasmic membrane from the cell envelope, while some cells remained WT-like (fig. 1, J). In cells, which showed plasmolysis, less PHB granules were found, and the thylakoid membranes appeared to be completely degraded. The observed plasmolysis ranged from less shrinkage in some cells to a shrinkage of the cytoplasm up to half its original size in others. This phenotype indicates a failure to control cell turgor, which is in agreement with previously reported influence of c-di-AMP on ion homeostasis [7,15,17].

To reveal further metabolic consequences of the lack of c-di-AMP during chlorosis, different metabolites were quantified using LC-MS (fig. 2). Amino acid levels in the WT showed different profiles. Some amino acids showed increased levels, peaking in early stages of chlorosis, visible for example for lysine (fig. 2, B), likely due to proteolytic degradation of different cellular structures. A second group remained constant, as observed for glutamine (fig. 2, A). A third group declined immediately in response to nitrogen starvation, as observed for glutamate (fig. 2, A) or tryptophane (fig. 2, C). Several amino acids show greatly increased or reduced levels in the Δ*dacA* strain in comparison to the WT. Strikingly, glutamate levels increased in response to N-deprivation, as opposed to the wild-type. Glutamate is of particular relevance as it fulfills multiple roles in bacterial metabolism. It is the primary pivot point in nitrogen metabolism, it is/ as well as the precursor for many metabolites including tetrapyrroles and in maintaining intracellular pH and turgor [15]. In the WT, N-depletion causes a rapid drop in cellular glutamate levels whereas the glutamine levels remain at high levels. This pattern has been observed repeatedly in nitrogen starved *Synechocystis* cells [33,35]. It indicates a tight control of the GS-GOGAT cycle. Since the Δ*dacA* strain does not follow this pattern, it appears that the cells are unable to properly control the GS-GOGAT cycle.

Moreover, proline (fig. 2, A), aspartate, methionine (fig. 2, B) and tryptophane (fig. 2, C) show significantly increased levels in the Δ*dacA* mutant in the first week of chlorosis in comparison to the WT. The levels of aspartate and methionine (fig. 2, B) increase significantly within the first 3 days of chlorosis in the mutant. The overall increased level of proline in the mutant (fig. 2, A) is possibly coupled to its function as osmolyte, since c-di-AMP deficient strains are reportedly under osmotic stress [9,10,36]. For lysine and isoleucine, the mutant displayed lower levels as compared to the WT, indicating perturbation in amino acid turn-over. The massive increase in methionine levels in the mutant is striking. In the WT, the methionine levels remain low during vegetative growth as well as during N-starvation. Methionine has multiple roles in metabolism: As the initiating amino acid in protein synthesis as well as precursor for the methyl-group transfer factor S-adenosine-L-methionine (SAM) [37]. The strong deviation of methionine levels from equilibrium in the Δ*dacA* mutant could have detrimental metabolic consequences. At present, we cannot distinguish if the elevated methionine levels are causative or the consequence of metabolic perturbations.

Significance of c-di-AMP in resuscitation and the appearance of suppressor mutations:

Chlorosis and resuscitation from this dormant state are independent cellular processes, which, however, depend on each other. As we showed previously, c-di-AMP is essential for cell viability during nitrogen starvation. The fact that the *dacA* gene is early induced in the resuscitation process implies an important role of c-di-AMP in resuscitation. To investigate the role of c-di-AMP on resuscitation, we started the resuscitation of chlorotic cells by the addition of nitrate. Subsequently, we measured the c-di-AMP levels throughout resuscitation (fig. 3, A). In agreement with previous studies showing early expression of *dacA* [28,31], c-di-AMP levels peaked at approximately 25 µM/cell 8 hours after initiation of resuscitation, before dropping back to circa 5 µM/cell (fig. 3, A). No c-di-AMP was measurable in the mutant for the samples collected in the final stage of chlorosis. To investigate the overall ability to recover, samples were taken after 14 days of chlorosis, and dropped on BG_{11} plates in a dilution series and left to recover and grow for 7 days. The Δ*dacA* mutant, lacked behind the WT by 3 orders of magnitudes, thus showing a delayed resuscitation and growth thereafter in these recovery drop plate assays (fig. 3, D). This observation could be explained by the large number of dead cells in the culture (fig. 1, C, D). That the entire resuscitation program was heavily impaired in the *dacA* deficient strain was visible in all cellular parameters, such as the increase in ATP levels (fig. 3, B), reconstitution of

photosynthetic capacity as determined by PAM fluorometry (fig. 3, C) and the overall re-greening process [22].

Despite the fact that the Δ*dacA* mutant was heavily impaired in resuscitation, after prolonged time of resuscitation, viable cells of the Δ*dacA* mutant re-appeared. Thus, we checked the recovered cultures for presence of a functional *dacA* gene via colony PCR (fig. 3, E). We found that the recovered cells had regained the ability to synthesise c-di-AMP and accumulated even higher amounts of c-di-AMP, up to 70 % higher than in the WT. Analysis of the *dacA* gene by colony PCR showed reconstitution of the wild-type gene indicating that the interrupting resistance cassette has been excised from the *dacA* gene (fig. 3, F). Since these revertants retained the antibiotic resistance, the resistance cassette was presumably inserted in a different chromosomal locus. To check the original phenotype of the Δ*dacA* mutant, the cultures were subjected to a second chlorosis procedure. In the adapted strain, chlorosis proceeded as in the WT (fig. 3, G) and the adapted strain was also able to perform the typical last cell division at the entry of chlorosis (fig. 3, H). The frequent appearance of revertants highlights the selective pressure to maintain c-di-AMP synthesis during the process of chlorosis and resuscitation. However, the rapid appearance of revertants makes the interpretation of resuscitation experiments difficult, as the population becomes more and more heterogenous during resuscitation.

Discussion:

C-di-AMP has been previously described to play a significant role in osmotic stress and ion homeostasis in firmicutes [8–10,15–17], which was also highlighted for cyanobacteria in recent publications [21–23]. During standard vegetative growth under constant illumination, c-di-AMP regulation seemed dispensable. However, the role of c-di-AMP in various acclimation processes remained unknown so far. Here, we found that c-di-AMP is essential in the process of chlorosis, a switch to metabolic quiescence to survive times of nutrient limitation. Thus, in early chlorosis, when adaptation of the whole cell metabolism to nutrient starvation is in progress, an increased level of c-di-AMP appears to be necessary to tightly regulate osmotic/ionic homeostasis. Consequently, the lack of intracellular c-di-AMP causes cell death (fig. 1, B - D, fig. 3, G). Striking differences were observed between WT and Δ*dacA* mutant with respect to ATP and glycogen levels. In earlier publications [22], activation of the glycogen branching enzyme GlgB by a complex of c-di-AMP and the PII-like carbon regulator protein SbtB, has been reported [22]. However, the Δ*sbtB* knockout strain did not show a phenotype in chlorosis and produced WT-like levels of glycogen under these conditions. Thus, the involvement of c-di-AMP in glycogen synthesis during nitrogen starvation appears to be independent of SbtB. However, the synthesis of glycogen requires energy. Precursors for glycogen synthesis are derived from glycerate-3-phosphate, the product of carbon fixation by ribulose-1,5-bisphosphate carboxylase/oxygenase (RuBisCO). Conversion of glycerate-3-phosphate to ADP-Glucosem the building block of glycogen[38], requires 3 ATP. The higher ATP level in Δ*dacA* during the first days of chlorosis could be related to this missing synthesis. Another possible sink for ATP is amino acid and protein synthesis. The Δ*dacA* strain showed higher levels of several amino acids in chlorosis (fig. 2), which could be attributed to lacking protein synthesis, also consuming less ATP.

The impaired osmotic and ionic stress response of the Δ*dacA* mutant in chlorosis is also visible in TEM images (fig. 1, J). In a culture of the Δ*dacA* strain after 21 days of chlorosis, cells appeared heterogenous. Some cells were comparable to the WT, while others experienced plasmolysis to varying degrees, ranging from small spaces to a reduction of the cytoplasm to approximately 50 % (fig. 1, J). Starvation induced shrinkage of the cytoplasm has been reported for bacteria previously [39,40]. A reduction of the cytoplasmic volume can keep intracellular concentrations of metabolites and enzymes high to help move pathways along and reduce the amount of undesired intermediates in the cytoplasm, as the authors suggested. This explanation would need to be proven by live/dead staining and paying special care to cell form and fluorescent area. With the microscopic pictures taken for this study, distinguishing whether cells had a reduced cytoplasm or not and whether these cells were alive was not consistently possible. In firmicutes, it has been reported that cells with a high intracellular c-di-AMP concentration have their K^+-ion uptake inhibited [41] and thus loose water in this hypertonic condition. For the Δ*dacA* strain, a loss of water due to impaired ion homeostasis could also be possible. In a transcriptomic analysis of Δ*dacA*, it was found that the expression of sodium proton antiporter encoding genes *nhaS4* and *nhaS*6 is higher in the mutant [42]. When cells are shifted to nitrogen-deprived medium, the Na^+ concentration decreases from 22.5 mM to 5.5 mM. This reduction could lead the Na^+/H^+ antiporters NhaS4 and NhaS6 to export Na^+ ions together with water, leading to a shrinkage of the cytoplasm. In previous work, a Na^+ gradient has been described as essential for bioenergetics after the early stage of chlorosis [34]. The WT-like levels of ATP in the later stages of chlorosis (fig. 1, H) indicate that this gradient is still functioning in the living cells. The increased levels of ATP in the Δ*dacA* strain in comparison to the WT in early chlorosis are likely caused by different factors, like the missing glycogen synthesis, an ATP-consuming set of reactions.

In agreement with the assumption of ionic and osmotic stress, the levels of glutamate in the Δ*dacA* strain are elevated upon nitrogen starvation (fig. 2, A), which seems contradictory to the nitrogen starvation condition causing chlorosis. Nitrogen is assimilated and converted into glutamine and glutamate through the glutamine-synthetase-glutamate-synthase (GS-GOGAT) cycle. The GS reaction requires glutamate, ammonia and ATP. During nitrogen starvation, the supply of ammonia drops off, slowing down the GS reaction. The GOGAT reaction uses glutamine and 2-oxoglutarate as substrates, yielding 2 glutamate molecules per reaction. Subsequently, nitrogen is distributed in anabolic reactions mainly through aminotransferase reactions starting from glutamate. The rapid decline of glutamate levels in the WT indicates a reduced GOGAT turn-over. The inverse regulation in the Δ*dacA* mutant indicates involvement of c-di-AMP in regulating the GOGAT reaction. However, these effects appear to be mediated indirectly, as neither the GOGAT nor an associated protein has been found in previous c-di-AMP based pulldowns [22]. However, in those pulldowns, GS inhibition factors 7 and 17 (products of genes *gifA* and *gifB*) have been found. This points towards a so far unknown mechanism of regulation of the GS-GOGAT cycle by c-di-AMP. In a proteome analysis of the Δ*dacA* mutant in diurnal rhythm, a trend to a dysregulation of the global nitrogen regulator NtcA was observed (unpublished results). The increased glutamate levels might also be required to balance the rising intracellular cation concentrations. In firmicutes, K^+ homeostasis is regulated by c-di-AMP [7,41] and in cyanobacteria, multiple different ion transporters have been found to potentially bind c-di-AMP [22]. The metabolic switch from vegetative growth to nitrogen starvation induced quiescence reduces the levels of free glutamate and thus the buffering capabilities of the cytoplasm [43]. The intracellular accumulation of glutamate in the Δ*dacA* strain throughout the first week of chlorosis is unexpected but could counteract a dysregulation of cation homeostasis in the mutant. Supporting this hypothesis as well is the increased level of proline in the mutant throughout chlorosis. Proline can serve as an osmolyte in cells [44–46] and can stabilise osmotic stress without addition of a charge difference, as an increase in cations would. Proline synthesis requires glutamate, so the increasing levels of proline could be a spillover of the high glutamate level. This compares to the levels of aspartate, whose synthesis also requires glutamate, and which also shows increased levels in the mutant throughout the first week of chlorosis (fig. 2, B). In contrast, the level of lysine, which is significantly lower in the Δ*dacA* strain than in the WT (fig. 2, B), depends on glutamate in its synthesis as well. Methionine also shows a significantly higher level in the Δ*dacA* strain. After 7 days of nitrogen starvation, the amount of free methionine in the mutant is approximately 23 times higher than in vegetative growth (fig. 2, B). As it is the initiating amino acid in translation, this could indicate a disturbance in protein synthesis. Protein synthesis in early chlorosis of *Synechocystis* is directed to proteins essential for resuscitation, while the synthesis of other proteins is arrested [26,47]. A diminished synthesis of these essential proteins could easily turn lethal for cells.

Chlorosis is a severe stress condition in which the Δ*dacA* strain shows large phenotypical differences to the WT, culminating in a high cell death rate (fig. 1, G – I), but not total cell death. The observed heterogeneity of the Δ*dacA* strain after 21 days of chlorosis (fig. 1, J) can be attributed to the appearance of suppressor mutations under selective pressure. Similar appearances of suppressor mutations in c-di-AMP deficient strains have been previously reported for firmicutes upon conditions of elevated selective pressure [8–10,15–17]. Investigation of the recovered cultures revealed a restored *dacA* gene (fig. 3, E) and these cultures exhibited WT-like behaviour (fig. 3, D, G – I), underlining the essentiality of c-di-AMP to cope with stress conditions in a changing environment. It is likely that not all 25 % viable mutant cells after 21 days of chlorosis are sufficiently adapted, as resuscitation from a dormant state is a second selective pressure to survive. In the drop assay, the recovery of a first time chlorotic Δ*dacA* strain was 2 magnitudes lower than the WT (fig. 3, D), indicating a low amount of cells being able to resuscitate. Of these cells, approximately 1 %, were able to reconstitute the *dacA* gene and thus, the c-di-AMP production.

The ionic and osmotic stress caused by the change of cell metabolism resurfaces when chlorotic cells are presented with a source of fixed nitrogen. The expression of the *dacA* gene and the protein levels of DacA peak within the first 12 hours of resuscitation [28,31]. Consequently, c-di-AMP levels peak at 8 hours after addition of nitrate (fig. 3, A). A tight control of ion homeostasis is necessary, as the cell metabolism is re-established, and co-factors are required. Interpretation of the obtained results for the mutant is difficult, as the resuscitating cultures are adapted strains that survived both chlorosis and recovery due to their suppressor mutations. Interestingly, even the adapted cells were unable to produce c-di-AMP in resuscitation (fig. 3, A) but had to reach vegetative growth to have measurable amounts again (fig. 3, F). This means that the adapted mutants were able to survive chlorosis and resuscitation independent of the availability of c-di-AMP, due to secondary mutations. To identify those, additional research would be required, but overall and in regard to the literature, it can be assumed that ion transporters, osmolyte synthesising pathways and osmolyte uptake systems have to been changed.

In this study, we were able to show the importance of c-di-AMP in the adaption to fluctuating nitrogen levels, especially during the global cellular process of chlorosis. Cells lacking c-di-AMP were revealed to die under nitrogen limitation, leading to the occurrence of suppressor mutations. Although the mechanism how c—di-AMP influences nitrogen assimilation remains obscure, this study points towards a substantial influence of c-di-AMP in controlling nitrogen assimilation. Additionally, the influence of c-di-AMP on ion and osmolyte homeostasis was visualised in form of the observed plasmolysis. Knowledge about c-di-AMP is ever increasing and there appears to be no end to the global influence it has in bacterial cells.

References:

1. Newton, A.C.; Bootman, M.D.; Scott, J.D. Second Messengers. *Cold Spring Harb. Perspect. Biol.* **2016**, *8*, a005926, doi:10.1101/cshperspect.a005926.
2. Burnap, R.; Hagemann, M.; Kaplan, A. Regulation of CO2 Concentrating Mechanism in Cyanobacteria. *Life* **2015**, *5*, 348–371, doi:10.3390/life5010348.
3. Römling, U. Great Times for Small Molecules: C-Di-AMP, a Second Messenger Candidate in Bacteria and Archaea. *Sci. Signal.* **2008**, *1*, pe39–pe39, doi:10.1126/scisignal.133pe39.
4. Corrigan, R.M.; Gründling, A. Cyclic Di-AMP: Another Second Messenger Enters the Fray. *Nat. Rev. Microbiol.* **2013**, *11*, 513–524, doi:10.1038/nrmicro3069.
5. Braun, F.; Thomalla, L.; van der Does, C.; Quax, T.E.F.; Allers, T.; Kaever, V.; Albers, S.-V. Cyclic Nucleotides in Archaea: Cyclic Di-AMP in the Archaeon Haloferax Volcanii and Its Putative Role. *MicrobiologyOpen* **2019**, *0*, e829, doi:10.1002/mbo3.829.
6. Witte, G.; Hartung, S.; Büttner, K.; Hopfner, K.-P. Structural Biochemistry of a Bacterial Checkpoint Protein Reveals Diadenylate Cyclase Activity Regulated by DNA Recombination Intermediates. *Mol. Cell* **2008**, *30*, 167–178, doi:10.1016/j.molcel.2008.02.020.
7. Stülke, J.; Krüger, L. Cyclic Di-AMP Signaling in Bacteria. *Annu. Rev. Microbiol.* **2020**, *74*, 159–179, doi:10.1146/annurev-micro-020518-115943.
8. Gundlach, J.; Herzberg, C.; Kaever, V.; Gunka, K.; Hoffmann, T.; Weiß, M.; Gibhardt, J.; Thürmer, A.; Hertel, D.; Daniel, R.; et al. Control of Potassium Homeostasis Is an Essential Function of the Second Messenger Cyclic Di-AMP in *Bacillus Subtilis*. *Sci. Signal.* **2017**, *10*, eaal3011, doi:10.1126/scisignal.aal3011.
9. Whiteley, A.T.; Pollock, A.J.; Portnoy, D.A. The PAMP C-Di-AMP Is Essential for Listeria Monocytogenes Growth in Rich but Not Minimal Media Due to a Toxic Increase in (p)ppGpp. *Cell Host Microbe* **2015**, *17*, 788–798, doi:10.1016/j.chom.2015.05.006.
10. Zeden, M.S.; Schuster, C.F.; Bowman, L.; Zhong, Q.; Williams, H.D.; Gründling, A. Cyclic Di-Adenosine Monophosphate (c-Di-AMP) Is Required for Osmotic Regulation in Staphylococcus Aureus but Dispensable for Viability in Anaerobic Conditions. *J. Biol. Chem.* **2018**, *293*, 3180–3200, doi:10.1074/jbc.M117.818716.
11. Devaux, L.; Sleiman, D.; Mazzuoli, M.-V.; Gominet, M.; Lanotte, P.; Trieu-Cuot, P.; Kaminski, P.-A.; Firon, A. Cyclic Di-AMP Regulation of Osmotic Homeostasis Is Essential in Group B Streptococcus. *PLoS Genet.* **2018**, *14*, doi:10.1371/journal.pgen.1007342.
12. Gundlach, J.; Mehne, F.M.P.; Herzberg, C.; Kampf, J.; Valerius, O.; Kaever, V.; Stülke, J. An Essential Poison: Synthesis and Degradation of Cyclic Di-AMP in Bacillus Subtilis. *J. Bacteriol.* **2015**, *197*, 3265–3274, doi:10.1128/JB.00564-15.
13. Mehne, F.M.P.; Gunka, K.; Eilers, H.; Herzberg, C.; Kaever, V.; Stülke, J. Cyclic Di-AMP Homeostasis in Bacillus Subtilis. *J. Biol. Chem.* **2013**, *288*, 2004–2017, doi:10.1074/jbc.M112.395491.
14. Huynh, T.N.; Luo, S.; Pensinger, D.; Sauer, J.-D.; Tong, L.; Woodward, J.J. An HD-Domain Phosphodiesterase Mediates Cooperative Hydrolysis of c-Di-AMP to Affect Bacterial Growth and Virulence. *Proc. Natl. Acad. Sci. U. S. A.* **2015**, *112*, E747–E756, doi:10.1073/pnas.1416485112.
15. Gundlach, J.; Krüger, L.; Herzberg, C.; Turdiev, A.; Poehlein, A.; Tascón, I.; Weiß, M.; Hertel, D.; Daniel, R.; Hänelt, I.; et al. Sustained Sensing in Potassium Homeostasis: Cyclic Di-AMP Controls Potassium Uptake by KimA at the Levels of Expression and Activity. *J. Biol. Chem.* **2019**, doi:10.1074/jbc.RA119.008774.
16. Pham, H.T.; Nhiep, N.T.H.; Vu, T.N.M.; Huynh, T.N.; Zhu, Y.; Huynh, A.L.D.; Chakrabortti, A.; Marcellin, E.; Lo, R.; Howard, C.B.; et al. Enhanced Uptake of Potassium or Glycine Betaine or Export of Cyclic-Di-AMP Restores Osmoresistance in a High Cyclic-Di-AMP Lactococcus Lactis Mutant. *PLoS Genet.* **2018**, *14*, e1007574, doi:10.1371/journal.pgen.1007574.
17. Quintana, I.M.; Gibhardt, J.; Turdiev, A.; Hammer, E.; Commichau, F.M.; Lee, V.T.; Magni, C.; Stülke, J. The KupA and KupB Proteins of Lactococcus Lactis IL1403 Are Novel C-Di-AMP

Receptor Proteins Responsible for Potassium Uptake. *J. Bacteriol.* **2019**, JB.00028-19, doi:10.1128/JB.00028-19.
18. Bremer, E.; Krämer, R. Responses of Microorganisms to Osmotic Stress. *Annu. Rev. Microbiol.* **2019**, *73*, 313–334, doi:10.1146/annurev-micro-020518-115504.
19. Wang, X.; Cai, X.; Ma, H.; Yin, W.; Zhu, L.; Li, X.; Lim, H.M.; Chou, S.-H.; He, J. A C-Di-AMP Riboswitch Controlling kdpFABC Operon Transcription Regulates the Potassium Transporter System in Bacillus Thuringiensis. *Commun. Biol.* **2019**, *2*, doi:10.1038/s42003-019-0414-6.
20. Nelson, J.W.; Sudarsan, N.; Furukawa, K.; Weinberg, Z.; Wang, J.X.; Breaker, R.R. Riboswitches in Eubacteria Sense the Second Messenger C-Di-AMP. *Nat. Chem. Biol.* **2013**, *9*, 834–839, doi:10.1038/nchembio.1363.
21. Rubin, B.E.; Huynh, T.N.; Welkie, D.G.; Diamond, S.; Simkovsky, R.; Pierce, E.C.; Taton, A.; Lowe, L.C.; Lee, J.J.; Rifkin, S.A.; et al. High-Throughput Interaction Screens Illuminate the Role of c-Di-AMP in Cyanobacterial Nighttime Survival. *PLOS Genet.* **2018**, *14*, e1007301, doi:10.1371/journal.pgen.1007301.
22. Selim, K.A.; Haffner, M.; Burkhardt, M.; Mantovani, O.; Neumann, N.; Albrecht, R.; Seifert, R.; Krüger, L.; Stülke, J.; Hartmann, M.D.; et al. Diurnal Metabolic Control in Cyanobacteria Requires Perception of Second Messenger Signaling Molecule C-Di-AMP by the Carbon Control Protein SbtB. *Sci. Adv.* **2021**, *7*, eabk0568, doi:10.1126/sciadv.abk0568.
23. Agostoni, M.; Logan-Jackson, A.R.; Heinz, E.R.; Severin, G.B.; Bruger, E.L.; Waters, C.M.; Montgomery, B.L. Homeostasis of Second Messenger Cyclic-Di-AMP Is Critical for Cyanobacterial Fitness and Acclimation to Abiotic Stress. *Front. Microbiol.* **2018**, *9*, doi:10.3389/fmicb.2018.01121.
24. Görl, M.; Sauer, J.; Baier, T.; Forchhammer, K. Nitrogen-Starvation-Induced Chlorosis in Synechococcus PCC 7942: Adaptation to Long-Term Survival. *Microbiology* **1998**, *144*, 2449–2458.
25. Sauer, J.; Schreiber, U.; Schmid, R.; Völker, U.; Forchhammer, K. Nitrogen Starvation-Induced Chlorosis in Synechococcus Pcc 7942. Low-Level Photosynthesis as a Mechanism of Long-Term Survival. *Plant Physiol.* **2001**, *126*, 233–243.
26. Forchhammer, K.; Schwarz, R. Nitrogen Chlorosis in Unicellular Cyanobacteria – a Developmental Program for Surviving Nitrogen Deprivation. *Environ. Microbiol.* **2019**, *21*, 1173–1184, doi:10.1111/1462-2920.14447.
27. Doello, S.; Klotz, A.; Makowka, A.; Gutekunst, K.; Forchhammer, K. A Specific Glycogen Mobilization Strategy Enables Rapid Awakening of Dormant Cyanobacteria from Chlorosis. *Plant Physiol.* **2018**, *177*, 594–603, doi:10.1104/pp.18.00297.
28. Klotz, A.; Georg, J.; Bučinská, L.; Watanabe, S.; Reimann, V.; Januszewski, W.; Sobotka, R.; Jendrossek, D.; Hess, W.R.; Forchhammer, K. Awakening of a Dormant Cyanobacterium from Nitrogen Chlorosis Reveals a Genetically Determined Program. *Curr. Biol.* **2016**, *26*, 2862–2872, doi:10.1016/j.cub.2016.08.054.
29. Neumann, N.; Doello, S.; Forchhammer, K. Recovery of Unicellular Cyanobacteria from Nitrogen Chlorosis: A Model for Resuscitation of Dormant Bacteria. *Microb. Physiol.* **2021**, *31*, 1–10, doi:10.1159/000515742.
30. Díaz-Troya, S.; Roldán, M.; Mallén-Ponce, M.J.; Ortega-Martínez, P.; Florencio, F.J. Lethality Caused by ADP-Glucose Accumulation Is Suppressed by Salt-Induced Carbon Flux Redirection in Cyanobacteria. *J. Exp. Bot.* **2020**, *71*, 2005–2017, doi:10.1093/jxb/erz559.
31. Spät, P.; Klotz, A.; Rexroth, S.; Maček, B.; Forchhammer, K. Chlorosis as a Developmental Program in Cyanobacteria: The Proteomic Fundament for Survival and Awakening. *Mol. Cell. Proteomics MCP* **2018**, *17*, 1650–1669, doi:10.1074/mcp.RA118.000699.
32. Watzer, B.; Forchhammer, K. Cyanophycin Synthesis Optimizes Nitrogen Utilization in the Unicellular Cyanobacterium Synechocystis Sp. Strain PCC 6803. *Appl. Environ. Microbiol.* **2018**, *84*, e01298-18, doi:10.1128/AEM.01298-18.

33. Burkhardt, M.; Rapp, J.; Menzel, C.; Link, H.; Forchhammer, K. The Global Influence of Sodium on Cyanobacteria in Resuscitation from Nitrogen Starvation. *Biology* **2023**, *12*, 159, doi:10.3390/biology12020159.
34. Doello, S.; Burkhardt, M.; Forchhammer, K. The Essential Role of Sodium Bioenergetics and ATP Homeostasis in the Developmental Transitions of a Cyanobacterium. *Curr. Biol.* **2021**, S0960982221001305, doi:10.1016/j.cub.2021.01.065.
35. Krauspe, V.; Timm, S.; Hagemann, M.; Hess, W.R. Phycobilisome Breakdown Effector NblD Is Required To Maintain Cellular Amino Acid Composition during Nitrogen Starvation. *J. Bacteriol.* **2022**, *204*, e00158-21, doi:10.1128/jb.00158-21.
36. Commichau, F.M.; Stülke, J. Coping with an Essential Poison: A Genetic Suppressor Analysis Corroborates a Key Function of c-Di-AMP in Controlling Potassium Ion Homeostasis in Gram-Positive Bacteria. *J. Bacteriol.* **2018**, JB.00166-18, doi:10.1128/JB.00166-18.
37. Fontecave, M.; Atta, M.; Mulliez, E. S-Adenosylmethionine: Nothing Goes to Waste. *Trends Biochem. Sci.* **2004**, *29*, 243–249, doi:10.1016/j.tibs.2004.03.007.
38. Mills, L.A.; McCormick, A.J.; Lea-Smith, D.J. Current Knowledge and Recent Advances in Understanding Metabolism of the Model Cyanobacterium Synechocystis Sp. PCC 6803. *Biosci. Rep.* **2020**, *40*, doi:10.1042/BSR20193325.
39. Shi, H.; Westfall, C.S.; Kao, J.; Odermatt, P.D.; Anderson, S.E.; Cesar, S.; Sievert, M.; Moore, J.; Gonzalez, C.G.; Zhang, L.; et al. Starvation Induces Shrinkage of the Bacterial Cytoplasm. *Proc. Natl. Acad. Sci.* **2021**, *118*, e2104686118, doi:10.1073/pnas.2104686118.
40. Schink, S.; Polk, M.; Athaide, E.; Mukherjee, A.; Ammar, C.; Liu, X.; Oh, S.; Chang, Y.-F.; Basan, M. The Energy Requirements of Ion Homeostasis Determine the Lifespan of Starving Bacteria 2022, 2021.11.22.469587.
41. Commichau, F.M.; Gibhardt, J.; Halbedel, S.; Gundlach, J.; Stülke, J. A Delicate Connection: C-Di-AMP Affects Cell Integrity by Controlling Osmolyte Transport. *Trends Microbiol.* **2018**, *26*, 175–185, doi:10.1016/j.tim.2017.09.003.
42. Mantovani, O.; Reimann, V.; Haffner, M.; Herrmann, F.P.; Selim, K.A.; Forchhammer, K.; Hess, W.R.; Hagemann, M. The Impact of the Cyanobacterial Carbon-Regulator Protein SbtB and of the Second Messengers cAMP and c-Di-AMP on CO2-Dependent Gene Expression. *New Phytol.* **2022**, *234*, 1801–1816, doi:10.1111/nph.18094.
43. Cheng, X.; Guinn, E.J.; Buechel, E.; Wong, R.; Sengupta, R.; Shkel, I.A.; Record, M.T. Basis of Protein Stabilization by K Glutamate: Unfavorable Interactions with Carbon, Oxygen Groups. *Biophys. J.* **2016**, *111*, 1854–1865, doi:10.1016/j.bpj.2016.08.050.
44. Wood, J.M.; Bremer, E.; Csonka, L.N.; Kraemer, R.; Poolman, B.; van der Heide, T.; Smith, L.T. Osmosensing and Osmoregulatory Compatible Solute Accumulation by Bacteria. *Comp. Biochem. Physiol. A. Mol. Integr. Physiol.* **2001**, *130*, 437–460, doi:10.1016/S1095-6433(01)00442-1.
45. Götz, F.; Longnecker, K.; Soule, M.C.K.; Becker, K.W.; McNichol, J.; Kujawinski, E.B.; Sievert, S.M. Targeted Metabolomics Reveals Proline as a Major Osmolyte in the Chemolithoautotroph Sulfurimonas Denitrificans. *MicrobiologyOpen* **2018**, *7*, doi:10.1002/mbo3.586.
46. Sleator, R.D.; Hill, C. Bacterial Osmoadaptation: The Role of Osmolytes in Bacterial Stress and Virulence. *FEMS Microbiol. Rev.* **2002**, *26*, 49–71, doi:10.1111/j.1574-6976.2002.tb00598.x.
47. Rittershaus, E.S.C.; Baek, S.; Sassetti, C.M. The Normalcy of Dormancy. *Cell Host Microbe* **2013**, *13*, 643–651, doi:10.1016/j.chom.2013.05.012.

Supplementaries

Tab. S1: Metabolome data of *Synechocystis* WT and Δ*dacA* in early chlorosis.

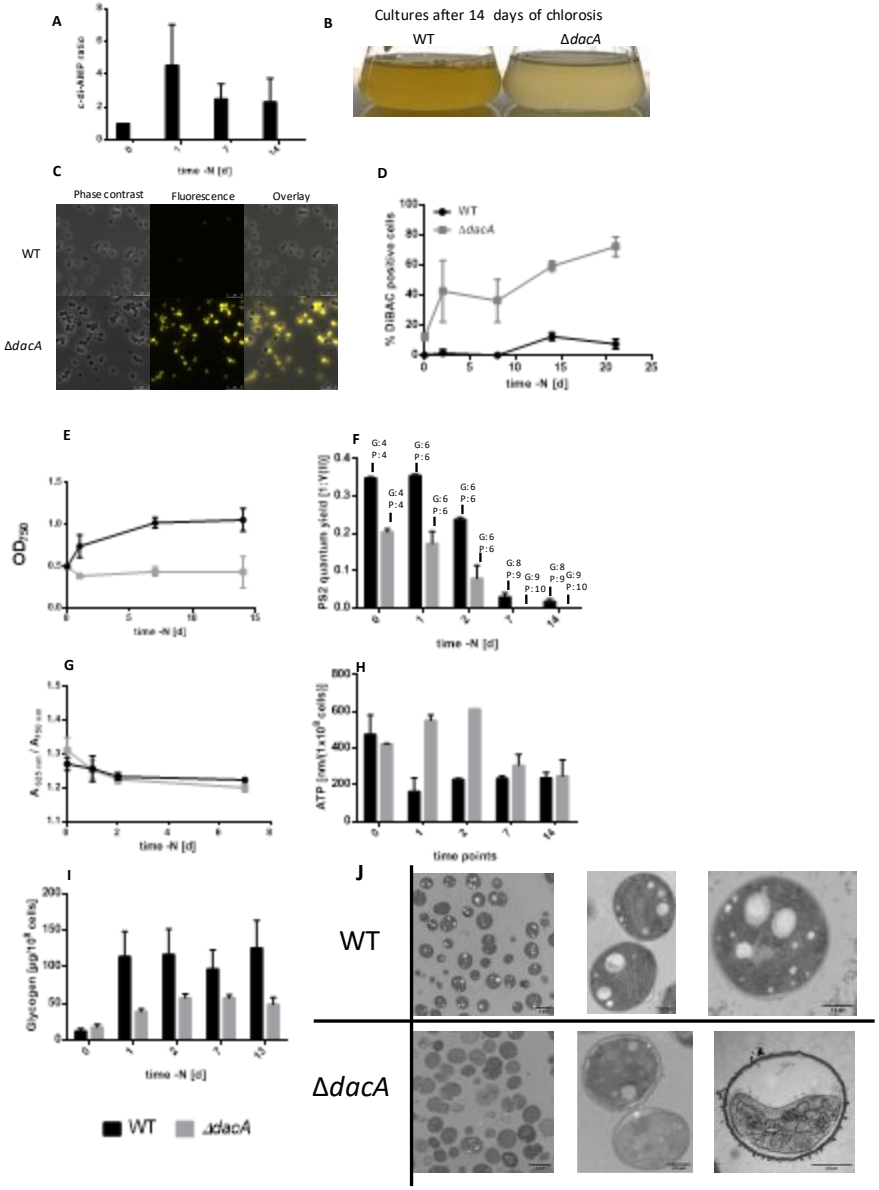
A
c-di-AMP ratio
time -N [d]
B
Cultures after 14 days of chlorosis
WT
ΔdacA
C
Phase contrast
Fluorescence
Overlay
WT
ΔdacA
D
WT
ΔdacA
% DiBAC positive cells
time -N [d]
E
OD750
time -N [d]
F
G:4 P:4
G:6 P:6
G:8 P:9
G:9 P:10
PS2 quantum yield [Y(II)]
time -N [d]
G
time -N [d]
H
ATP [nM]1x10^8 cells]
time points
I
Glycogen [pg/10^8 cells]
time -N [d]
WT
ΔdacA
J
WT
ΔdacA

Fig. 1: **Parameters during chlorosis .** (A) depicts the ratio of c-di-AMP during chlorosis , normalised to vegetative growth (timepoint 0). (B) shows a wildtype (WT) and Δ*dacA* culture after 2 weeks of chlorosis . (C) shows microscopic pictures of WT and Δ*dacA* after 21 days of chlorosis in phase contrast (left), fluorescence (middle) and the overlay (right). (D) depicts the amount of dead cells per culture in percent over 21 days of chlorosis . (E) shows the change in OD_{750} over time after initiation of chlorosis , indicating change in cell mass ; (F) the quantum yield of the photosystem 2 during chlorosis, G = Gain, P = PM-Gain; (G) the Absorbance at 685 nm normalised to the absorbanceat 750 nm over the first week of chlorosis , indicating the presence of phycobilisomes in relation to total cell mass ; (H) the amount of glycogen during chlorosis ; and (I) the levels of ATP throughout two weeks of chlorosis. (J) are pictures from transmission electron microscopy after 21 days of chlorosis. Top shows WT and bottom Δ*dacA*, on the left are overview pictures and to the right pictures of single cells. For all graphs, black colour signifies WT and grey Δ*dacA* . Each data-point represents measured triplicates. Error bars represent the SD.

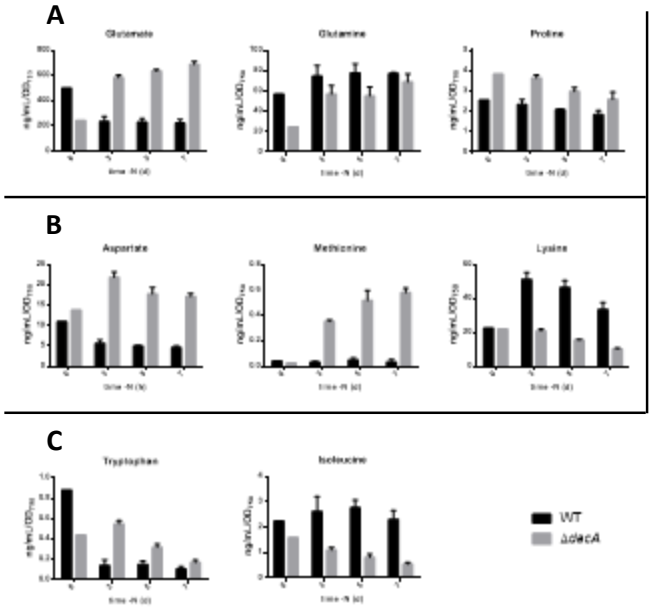

Fig. 2: **Metabolites during chlorosis.** (A-C) depict members of different amino acid families, members of the (A) glutamate based family, (B) oxaloacetatebased famil y and (C) tryptophan and isoleucine. Each data-point represents measured triplicates except for time point zero, which are unicates. Error bars represent the SD.

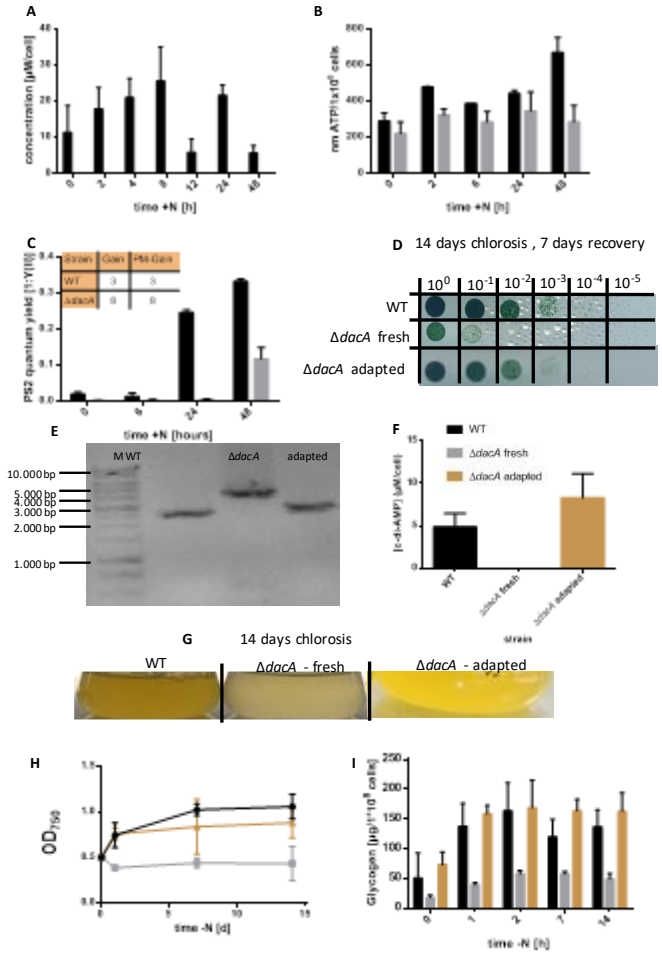
A
B
C
D
14 days chlorosis , 7 days recovery
WT
ΔdacA fresh
ΔdacA adapted
E
M WT
ΔdacA
adapted
10.000 bp
5.000 bp
4.000 bp
3.000 bp
2.000 bp
1.000 bp
F
WT
ΔdacA fresh
ΔdacA adapted
G
14 days chlorosis
WT
ΔdacA - fresh
ΔdacA - adapted
H
I

Fig. 3: **Overview of resuscitation and adaptation.** (A) depicts the levels of c-di-AMP during resuscitation, (B) the ATP levels in nm/10^8 cells and (C) the quantum yield of PS2 measured by PAM during resuscitation and the gain and PM-gain with which the measurement was done for each strain. (D) shows a recovery drop assays of WT, fresh Δ*dacA* and adapted Δ*dacA* cultures after 2 weeks of chlorosis. Dropped cultures were able to recover and grow for 7 days before picture was taken. (E) shows an agarose gel of a colony PCR to check for reconstitution of the *dacA* gene in the adapted strain. M = Marker, WT = wild type, adapted = adapted Δ*dacA* strain. (F) depicts the concentration of c-di-AMP in µM per cell in vegetative growth, (G) shows cultures of WT and mutant after 14 days of chlorosis (H) depicts the OD_{750} as an indication of cell mass and (I) the amount of glycogen throughout chlorosis. Each data-point represents measured triplicates. Error bars represent the SD. Δ*dacA* cultures were adapted by sending them through chlorosis and resuscitation and cultivation of the surviving cells.

Acknowledgements

I have to thank a lot of people who helped me and made my thesis possible.

Professionally, my gratitude is foremost to Prof. Dr. Forchhammer for allowing me to work in his lab and supporting me in my thesis. Always supportive and constructive, but calling me out when I was lazy, I feel I could not have been supervised better.

I also want to thank Prof. Dr. Schultz, my second supervisor, for his constructive criticism and Dr. Stegmann for evaluating this work.

My work in the lab was enriched by all the colleagues and friends in the groups of Forchhammer, Maldener and Mayer. I want to thank Sofia for her continued mentorship and Iris and Khaled for their counsel on scientific questions. I thank Anka, Johanna and Niels for challenging me, whenever I got lazy. Eva, Janette, and Tim, deserve my gratitude for their insights, ideas, help and jokes. I am also thankful to Nike and Michael, my friends in the night shift and Björn for always offering his expertise when I needed help from him. Also, the remaining staff, Heinz, my fellow early bird, Claudia, the TEM-expert, and Michaela, for always tanking bureaucracy. Big thanks are due also to Louisa and Matteo for their help in my attempt at genomics and all the rest of the lab for their support and occasional diversion.

Outside the lab, these people also helped me grow and I thank them with all my heart for it. Sofia and Anka, who got me to boulder and Nathan and Nathalie, who helped me pick it up again at the end of Covid. Tim, Janette, and Nike, who joined me in different Unisport activities and made me, for example, appreciate and improve my cooking. Also, the whole soup group pre-Covid, for increasing my palate.

Privat gilt mein Dank zuallererst meinen Eltern, die mich seit Beginn meines Bachelorstudiums unterstützt haben. Es war nicht immer einfach und verständlich, aber es hat zum Ende hin ja doch funktioniert. My friends, many of which also work in this group, for having my back, taking my mind off the lab in spare time and some bad decisions also deserve thanks. And, last but not least, Romina, who was always there in the late stages and a big pillar while writing this thesis.